UNIVERSIDAD COMPLUTENSE DE MADRID
FACULTAD DE CIENCIAS GEOLÓGICAS

TESIS DOCTORAL

Estudio sobre la emisión de ^{3}He y flujo de calor en sistemas volcánicos-hidrotermales: implicaciones para la exploración geotérmica

Emissions of ^{3}He and the heat flow studies in volcanic-hydrotermal systems: geothermal exploration implications

MEMORIA PARA OPTAR AL GRADO DE DOCTOR

PRESENTADA POR

Mar Alonso Cótchico

Directores

Nemesio Miguel Pérez Rodríguez
Eleazar Padrón González
Pedro Antonio Hernández Pérez

Madrid

UNIVERSIDAD COMPLUTENSE MADRID

FACULTAD DE CIENCIAS GEOLÓGICAS

ESTUDIO SOBRE LA EMISIÓN DE ^{3}He Y FLUJO DE CALOR EN SISTEMAS VOLCÁNICOS-HIDROTERMALES: IMPLICACIONES PARA LA EXPLORACIÓN GEOTÉRMICA

EMISSIONS OF ^{3}He AND HEAT FLOW STUDIES IN VOLCANIC-HYDROTHERMAL SYSTEMS: GEOTHERMAL EXPLORATION IMPLICATIONS

TESIS DOCTORAL
POR COMPENDIO DE PUBLICACIONES

Mar Alonso Cótchico

Nemesio Miguel Pérez Rodríguez
Director

Eleazar Padrón González
Co-director

Pedro Antonio Hernández Pérez
Co-director

Instituto Tecnológico y de Energías Renovables (ITER)
Instituto Volcanológico de Canarias (INVOLCAN)
Tenerife (Islas Canarias)

ITER Instituto Tecnológico y de Energías Renovables

INVOLCAN INSTITUTO VOLCANOLÓGICO DE CANARIAS

UNIVERSIDAD COMPLUTENSE DE MADRID
FACULTAD DE CIENCIAS GEOLÓGICAS

TESIS DOCTORAL

ESTUDIO SOBRE LA EMISIÓN DE 3He Y FLUJO DE CALOR EN SISTEMAS VOLCÁNICOS-HIDROTERMALES: IMPLICACIONES PARA LA EXPLORACIÓN GEOTÉRMICA

EMISSIONS OF 3He AND HEAT FLOW STUDIES IN VOLCANIC-HYDROTHERMAL SYSTEMS: GEOTHERMAL EXPLORATION IMPLICATIONS

MEMORIA PARA OPTAR AL GRADO DE DOCTORA

PRESENTADA POR

MAR ALONSO CÓTCHICO

DIRECTORES

NEMESIO MIGUEL PÉREZ RODRÍGUEZ
ELEAZAR PADRÓN GONZÁLEZ
PEDRO ANTONIO HERNÁNDEZ PÉREZ

ESTUDIO SOBRE LA EMISIÓN DE ^{3}He Y FLUJO DE CALOR EN SISTEMAS VOLCÁNICOS-HIDROTERMALES: IMPLICACIONES PARA LA EXPLORACIÓN GEOTÉRMICA

AUTOR DE LA TESIS:
Mar Alonso Cótchico
Licenciada en Geología
Instituto Tecnológico y de Energías Renovables (ITER)
Instituto Volcanológico de Canarias (INVOLCAN)
Tenerife, Islas Canarias

DIRECTORES:
Dr. Nemesio M. Pérez Rodríguez (ITER-INVOLCAN-AIET)
Dr. Pedro A. Hernández Pérez (ITER-INVOLCAN-AIET)
Dr. Eleazar Padrón González (ITER-INVOLCAN-AIET)

TUTOR:
Dra. María José Huertas Coronel (UCM)

TESIS DOCTORAL POR COMPENDIO DE PUBLICACIONES
REMITIDA PARA EL GRADO DE DOCTOR EN LA
UNIVERSIDAD COMPLUTENSE DE MADRID

Madrid
Diciembre, 2021

Proyectos que han ayudado a financiar la tesis doctoral: (i) MAKAVOL (MAC/3/C161) del programa de Cooperación Transnacional de la Unión Europea MAC 2007-2013, (ii) CABOVERDE (08-CAP2-1202) de la Agencia Española de Cooperación Internacional al Desarrollo, AECID, (iii) UNICV del Servicio de Acción Exterior del Cabildo Insular de Tenerife (Islas Canarias, España), (iv) VOLRISKMAC (MAC/3.5b/124) financiado por el programa INTERREG V A España-Portugal MAC 2014-2020 de la Comisión Europea, (v) TFassistance, TFinnova del Cabildo Insular de Tenerife.

Agradecimientos

En primer lugar, quiero agradecer al Dr. Nemesio Pérez, director de esta tesis, por darme la oportunidad de trabajar en su grupo de investigación, en el trabajo más bonito del mundo. Gracias por los ánimos y “empujones” para seguir hacia delante.

En segundo lugar agradecer a los co-directores de la tesis, Pedro Hernández y Eleazar Padrón, por su tiempo, asesoramiento y dedicación. Quiero incluir en este apartado a la Dra. Gladys Melián, que aunque no sea co-directora de la tesis me ha ayudado y dado ánimos como si lo fuera. Pedro, Eleazar y Gladys, ha sido un placer aprender de los mejores.

Gracias a María José Huertas, por tutorizarme la tesis y apoyarme en mi carrera científica desde mucho antes de que yo supiera que iba a tener una. Tu apoyo incondicional desde la distancia ha sido una gran ayuda.

Agradecer a todos los co-autores de los trabajos que forman parte de esta tesis doctoral y a las personas que colaboraron en el trabajo de campo, sin su granito de arena no habría sido posible.

Un millón de gracias, y me quedo corta, a todos mis compañeros del departamento de medioambiente del ITER, en especial a Germán, Pepe, María, Fátima, Iván, Monika, David, Claudia, Airam, Alba, Guille, Bev, Matt y Ana, por la ayuda y los ánimos en este largo proceso. Me quedo con un poco de cada uno para seguir creciendo como persona.

Cecilia, Tai y María, mil gracias por ser mi familia y estar ahí siempre.

Gracias a Amaia, Nagore, María y Natalia que a pesar de la distancia las he sentido siempre muy cerca, porque aunque nos veamos poco, nos pensamos mucho.

Agradecer a mi familia, pero en especial a mis padres, Jesús y Alicia, y a mis hermanas, Lur y Nagore, a quien les dedico esta tesis, por el cariño y el apoyo incondicional en cada paso por la vida.

Y por último, pero no menos importante, a Manolo, por enseñarme que el universo siempre está de nuestro lado, gracias por ser, estar y compartir.

Muchísimas gracias a todos,

Mar Alonso Cótchico

A mis padres y a mis
hermanas Lur y Nagore

ESTUDIO SOBRE LA EMISIÓN DE ^{3}He Y FLUJO DE CALOR EN SISTEMAS VOLCÁNICOS-HIDROTERMALES: IMPLICACIONES PARA LA EXPLORACIÓN GEOTÉRMICA

Emissions of ^{3}He and heat flow studies in volcanic-hydrothermal systems: Geothermal exploration implications

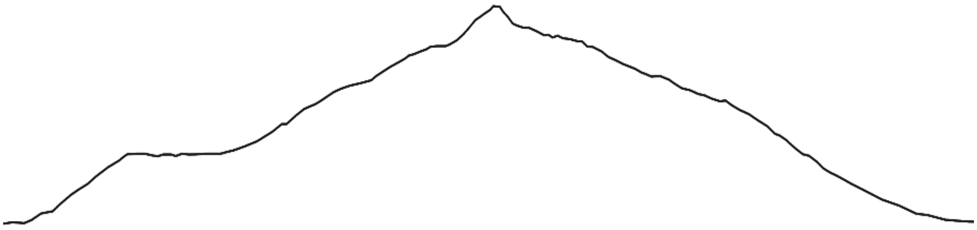

SUMMARY

CONTENTS

Alonso M, Padrón E, Sumino H, Hernández PA, Melián G.V, Asensio-Ramos M, Rodríguez F, Padilla G, García-Merino M, Amonte C and Pérez N.M (2019). Heat and Helium-3 fluxes from Teide Volcano, Canary Islands, Spain. Geofluids, ID 3983864.

Alonso M, Pérez NM, Padrón E, Hernández PA, Melián GV, Sumino H, Padilla GD, Barrancos J, Rodríguez F, Dionis S, Asensio-Ramos M, Amonte C, Silva S and Pereira JM (2021). Changes in the thermal energy and the diffuse 3He and 4He degassing prior to the 2014–2015 eruption of Pico do Fogo volcano, Cape Verde. Journal of Volcanology and Geothermal Research, 107271.

Alonso M, Pérez NM, Hernández PA, Padrón E, Melián G, Rodríguez F, Padilla G, Barrancos J, Asensio-Ramos M, Fridriksson T and Sumino H (2021b). Thermal energy and diffuse 4He and 3He degassing released in volcanic-geothermal systems. Renewable Energy 182, 17-31.

LIST OF FIGURES

LIST OF TABLES

ABSTRACT

In this Ph.D. Thesis "*Emissions of* ^{3}*He and heat flow studies in volcanic-hydrothermal systems: Geothermal exploration implications*", diffuse (not visible) emissions of helium-3 (^{3}He) and helium-4 (^{4}He) have been calculated, as well as the thermal energy released at various volcanic systems in order to determine the degree to which a relationship between the studied parameters may exist. In addition, a methodology has been proposed to estimate the diffuse ^{3}He and ^{4}He emissions into the atmosphere through two different approximations.

Volcanic areas emit large amounts of volatiles into the atmosphere as visible emanations (volcanic plumes, fumaroles, solfataras, bubblings) and non-visible emanations (diffuse degassing from the soil). The study of these endogenous gases provides important information about the movement of magma inside the Earth, helping to evaluate the activity of the volcanic system, and therefore, can act as early warning signals preceding eruptions. In the case of geothermal exploration, the study of soil gases can help to locate and delimit geothermal reservoirs at depth and study their physical-chemical conditions, by highlighting permeable areas connected with the hydrothermal system.

This work has focused on the geochemical study of diffuse He emissions in active volcanic systems. Due to its chemically conservative properties as a noble gas, helium is an excellent indicator of magmatic activity, which also makes it an ideal gas to investigate and delimit the extent of permeability areas and understand the ascent of fluids of deep origin towards the surface. Helium has two naturally occurring isotopes: ^{3}He and ^{4}He, with atmospheric ^{3}He/^{4}He ratio (R_A) of 1,384 × 10^{-6}. ^{4}He is produced as α

particles from the radioactive decay of ^{238}U, ^{235}U and ^{232}Th mainly in the crust. ^{3}He, by contrast, is primordial helium that was trapped inside the Earth during the planet formation and is derived from the deep reservoir of the Earth's mantle. Therefore, the ^{3}He emission measurement at the surface reflects areas connected to a deep mantle or magmatic sources.

In volcanic areas with no visible gas emanations, the detection of possible geothermal resources represents a higher level of complication. In this Ph.D. Thesis I propose that in areas with a high probability of finding deep geothermal resources where there are no visible manifestations, it is possible to make an estimation of the associated thermal energy of the reservoir by measuring the diffuse ^{4}He emission on the surface. Therefore, anomalous diffuse ^{4}He emission values suggest that there is a preferential degassing area from a deep source associated with a thermal anomaly, allowing the location of possible geothermal reservoirs. The great advantage of this geothermal exploration technique is that it reduces economic costs in the exploration phase, since the economic investment required in this phase is the greatest limitation that geothermal energy has compared to other renewable energies.

The geological setting of this study is located on some volcanic systems of the Macaronesia; Teide (Spain), Pico do Fogo (Cape Verde) and Furnas (Azores). In order to provide a global vision to the Ph.D. Thesis, the volcanic systems of Cerro Negro (Nicaragua), Poás (Costa Rica), Solfatara (Italy), Reykjanes and Hengill (Iceland), Mud Volcanoes in Yellowstone (USA), Caviahue-Copahue (Argentina), the volcanic systems of Ischia, Vesuvio, Vulcano and Pantelleria (Italy) and Nisysros (Greece) have been added. The study areas are active volcanic systems located in different geotectonic environments such as oceanic islands, volcanic arc zones, mid-oceanic ridges and intraplate volcanism.

In-situ measurement of the ambient and soil temperature at 15 and 40 cm depth and the diffuse carbon dioxide (CO_2) efflux had been carried out. Soil gases on the surface and visible emissions (fumaroles) present in each volcanic system had been sampled. In order to calculate the geochemical emission parameters of ^{3}He and ^{4}He as well as the thermal energy released, the collected samples were analysed in the laboratory of the Instituto Tecnológico y de Energías Renovables (ITER, Tenerife).

Through the studies presented in this Ph.D. Thesis, the following conclusions have been obtained:

- The study of the emissions of both He isotopes in volcanic systems contributes to the location of vertical permeability zones that may be related to the existence of deep geothermal reservoirs.
- Temporal evolution studies of the diffuse ^{3}He and ^{4}He emissions with the associated thermal energy released provide a powerful tool for monitoring volcanic activity that offers early warnings of reactivation processes or eruptive events.
- Diffuse ^{4}He emissions may be masked by a contribution of radiogenic ^{4}He from a crustal source, while the ^{3}He emission reflects the degree of connection of the system with the mantle source.
- These diffuse He emissions do not occur homogeneously throughout a volcanic system. In all study areas, a strong structural control is observed, by which preferential degassing zones are associated with faults or fractures.
- The highest diffuse ^{4}He fluxes are located in areas where visible anomalies are also observed, both in temperature and in the emission of other gases. This observation suggests that in volcanic areas in which there are no visible emanations, and therefore visible emission sampling or the calculation of the

diffuse ^{3}He emission is not possible, but there are anomalous values in the diffuse ^{4}He effluxes, the diffuse ^{4}He emission is associated with thermal anomaly at depth. Therefore, it is demonstrated that anomalous diffuse ^{4}He emissions suggest the existence of a preferential degassing zone for deep origin gases associated with a heat source at depth, facilitating the location of possible geothermal reservoirs.

- The low cost of geochemical surveys, which allow covering large sampling areas in a relatively short time period, together with the quality of the obtained data, demonstrate that helium emission studies are a valuable tool for the first stages of the location of possible geothermal reservoirs.

RESUMEN

En la presente tesis doctoral titulada *"Estudio sobre la emisión de ^{3}He y flujo de calor en sistemas volcánicos-hidrotermales: implicaciones para la exploración geotérmica"* se han calculado las emisiones difusas (no visibles) de helio-3 (^{3}He) y helio-4 (^{4}He), así como la energía térmica liberada en varios sistemas volcánicos con el objetivo de demostrar la existencia de una relación directa entre los parámetros estudiados. Además, se ha propuesto una metodología para estimar mediante dos aproximaciones diferentes la emisión difusa de ^{3}He y ^{4}He hacia la atmósfera.

Las áreas volcánicas emiten gran cantidad de volátiles a la atmosfera, en forma de emanaciones visibles (plumas volcánicas, fumarolas, solfataras, burbujeos) y emanaciones no visibles (desgasificación difusa). El estudio de estos gases de origen endógeno liberados en sistemas volcánicos activos nos da información sobre el

movimiento de magma en el interior de la Tierra, ayudando a evaluar el estado de actividad volcánica del sistema, y por tanto, como predicción de señales de alerta temprana ante episodios de reactivación volcánica. En el caso de la exploración geotérmica, el estudio de los gases en la superficie del suelo nos puede ayudar a localizar reservorios geotermales en profundidad y estudiar sus condiciones físico-químicas, detectando zonas permeables que conectan con el sistema hidrotermal.

Este trabajo se ha centrado en el estudio geoquímico de las emisiones difusas de He en sistemas volcánicos activos. Debido a sus propiedades como gas noble, el helio es un excelente indicador de la actividad magmática, lo que lo convierte en un gas ideal para investigar y delimitar la existencia de zonas de mayor permeabilidad y ascenso de fluidos de origen profundo hacia la superficie. Existen dos isótopos naturales del helio, el ^{3}He y el ^{4}He, con un ratio atmosférico ^{3}He/^{4}He (R_A) de 1.384×10^{-6}. El ^{4}He se produce como partículas α a partir de la desintegración radiactiva del ^{238}U, ^{235}U y ^{232}Th y se produce principalmente en la corteza. En cambio, el ^{3}He es primordial atrapado en el interior de la Tierra durante la formación del planeta y por lo tanto se encuentra acumulado en el manto terrestre. Por tanto, la medida de emisión de ^{3}He refleja áreas conectadas a una fuente mantélica profunda o a una fuente magmática.

En áreas volcánicas en las cuales no existen emanaciones de gases visibles, la detección de los posibles yacimientos geotérmicos presenta un mayor nivel de complicación. Por ello, en este trabajo se propone que en áreas con una alta probabilidad de encontrar recursos geotérmicos profundos donde no existan manifestaciones visibles, es posible realizar una estimación aproximada de la energía térmica asociada al reservorio mediante la medida del flujo difuso de ^{4}He medido en superficie. Por lo tanto, valores anómalos de flujo de ^{4}He sugieren que existe un área preferencial de desgasificación desde una fuente profunda asociada con una anomalía térmica que de esta manera permite la localización de posibles yacimientos geotérmicos. La gran ventaja que presenta esta técnica de exploración geotérmica es que permite reducir los costes económicos en la fase de exploración, pues la inversión económica necesaria en esta fase es la mayor limitación que tiene la energía geotérmica frente a otras energías renovables.

El marco de estudio de la presente tesis doctoral se centra principalmente en algunos sistemas volcánicos que conforman la Macaronesia; Teide (España), Pico do Fogo (Cabo Verde) y Furnas (Azores). Con el objetivo de proporcionar una visión global a la tesis doctoral, se han añadido los sistemas volcánicos de Cerro Negro (Nicaragua), Poás (Costa Rica), Solfatara (Italia), Reykjanes y Hengill (Islandia), Mud Volcanoes en Yellowstone (EEUU), Caviahue-Copahue (Argentina), los sistemas volcánicos de Ischia, Vesuvio, Vulcano y Pantelleria (Italia) y Nisysros (Grecia). Las áreas de estudio son sistemas volcánicos activos situados en diferentes contextos geotectónicos como son islas oceánicas, zonas de arco volcánico, dorsales centro-oceánicas y vulcanismo intraplaca.

Se ha realizado la medida *in-situ* de la temperatura ambiente y del suelo a 15 y 40 cm de profundidad y del flujo difuso de dióxido de carbono (CO_2). También se realizó un muestreo de gases en la superficie del suelo y de emisiones visibles (fumarolas) presentes en cada sistema volcánico. Posteriormente en el laboratorio del Instituto Tecnológico y de Energías Renovables (ITER, Tenerife) se analizaron las muestras recolectadas para así poder realizar el cálculo de los parámetros geoquímicos de emisión de ^3He y ^4He como de la energía térmica liberada.

A través de los estudios presentados en esta tesis doctoral se han obtenido las siguientes conclusiones:

- El estudio de emisión de ambos isótopos de He en sistemas volcánicos contribuye a la localización de zonas de permeabilidad vertical que pueden estar relacionadas con la existencia de reservorios geotermales profundos.
- Los estudios de evolución temporal de la emisión difusa de ^{3}He y ^{4}He conjuntamente con estudios de la energía térmica asociada proporcionan una poderosa herramienta de monitorización de la actividad volcánica que ofrece alertas tempranas de procesos de reactivación o eventos eruptivos.
- Las emisiones de ^{4}He pueden estar enmascaradas por una contribución de ^{4}He radiogénico de una fuente cortical, mientras que la emisión de ^{3}He refleja el grado de conexión del sistema con la fuente mantélica.
- Estas emisiones de He no se dan de forma homogénea por todo el sistema volcánico, sino que hay un fuerte control estructural, existiendo zonas de desgasificación preferencial asociada a fallas o fracturas.
- Los mayores flujos de ^{4}He se localizan en áreas donde se observan también anomalías visibles tanto de temperatura como de emisión de otros gases. Esta observación sugiere que en las zonas volcánicas en las cuales no existan emanaciones visibles, y por ello no sea posible su muestreo ni el cálculo de la emisión de ^{3}He, pero que sin embargo existan valores anómalos en el flujo de ^{4}He, la emisión de ^{4}He está asociada a una energía térmica en profundidad. Por ello, se deduce que concentraciones anómalas en el flujo de ^{4}He sugieren la existencia de una zona de desgasificación preferente para gases de origen profundo asociados a una fuente de calor en profundidad, facilitando la localización de posibles yacimientos geotérmicos.
- Debido al bajo coste de las campañas geoquímicas, que permiten cubrir grandes áreas de muestreo en relativamente poco tiempo, junto con la calidad de los

datos obtenidos, hacen de los estudios de la emisión de helio una excelente herramienta para las primeras etapas de localización de posibles yacimientos geotérmicos.

Introduction

1. INTRODUCTION

Geothermal energy has its origin in the heat produced within the Earth’s interior, manifesting convection cells, which cause a continuous heat flux to the surface. This heat flux is spatially heterogeneous, and regions of high flux may be economic to exploit as a source of energy. A good source of geothermal energy must have three basic requirements: a high thermal gradient, which translates into accessible hot rocks, a rechargeable fluid reservoir (water in most cases), and deep permeable pathways for the fluid to pass through the hot rocks. Volcanic-hydrothermal systems fulfil these basic requirements and as such are ideal areas for consideration.

The main limitation of geothermal energy, compared to other renewable energies, is that a high proportion of the investment is at high risk, since a significant expense is required in the initial exploration phase. Otherwise, production and maintenance costs per megawatt generated by geothermal energy are among the lowest of all renewables, hence the importance of investigating mechanisms that promote risk mitigation in the initial industrial phases. It follows that the development of research aimed at minimizing the associated risk of this phase makes it possible, through to technology and method improvement, for geothermal to become more competitive against other forms of energy generation.

The Earth's mantle is a major reservoir of gases and volatile compounds relevant to surface and atmospheric processes, such as water, carbon dioxide, sulfur, and, among the trace volatiles, noble gases. These are compounds captured during the Earth’s formation, in addition to others that were later joined by nuclear reactions or recycled from the surface. Consequently, these gaseous compounds provide an important key to understand the history of the Earth and its continuous evolution (Pepin et al., 2002). The plumbing system formed in response of the development of volcanoes at the surface represents preferential paths through which mantle gases escape to the atmosphere, so that volcanoes are huge emittors of gases and volatiles to the atmosphere, both during volcanic unrest and quiescent periods. Degassing in volcanic areas is associated with an important transport of thermal energy, which is released by condensation of water vapour of volcanic gas and is transferred to the atmosphere through soils that present thermal anomalies on the surface (Chiodini et al., 2001, Chiodini et al., 2005, Hernández et al., 2012, Dionis et al., 2015, Alonso et al., 2019). The heat transfer from the magmatic body to the atmosphere is sketched in Figure 1. The most important elements in this model are: i) a magmatic chamber acting as a heat source, ii) one or more aquifers located above the heat source, and iii) a fractured zone located above the aquifer occupied by a pure vapour phase, produced by boiling from the aquifer (Cioni et al., 1989, Chiodini et al., 2001). Fluids and heat rise from the magmatic chamber to the aquifer, where the heat dissipates by boiling.

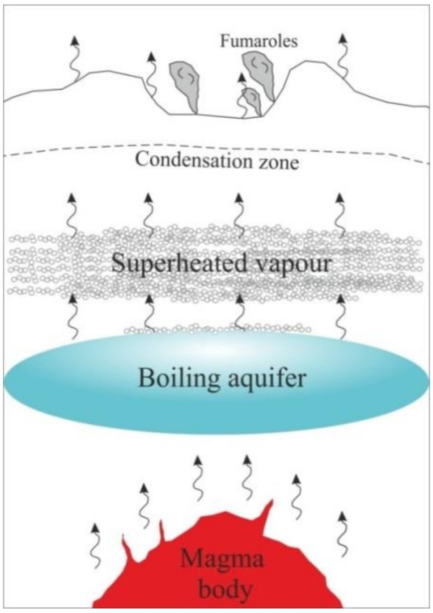

Figure 1. *Scheme of heat transfer from a magmatic body to the atmosphere .Modified from Cioni et al., 1989 and Chiodini et al., 2001.*

Degassing processes, coupled with thermal energy release from the volcanic-hydrothermal system, provide valuable information about volcanic systems' energy balance, activity, and the system's connection with the mantle.

Gaseous emissions at volcanoes occur in the form of visible emanations, through volcanic plumes, fumaroles, solfataras and bubbling gases, and through diffuse degassing (non-visible soil emanations) (Chiodini et al., 1996 and 2008, Hernández et al., 2012; Padrón et al., 2015). Both types of emissions are controlled by local volcano-tectonic structures as a result of transport via diffusion and advection (Hernández et al., 2012). Diffuse degassing refers to the non-visible emission of gases through the flanks of the volcanic edifice, through faults and/or fractures (Figure 2).

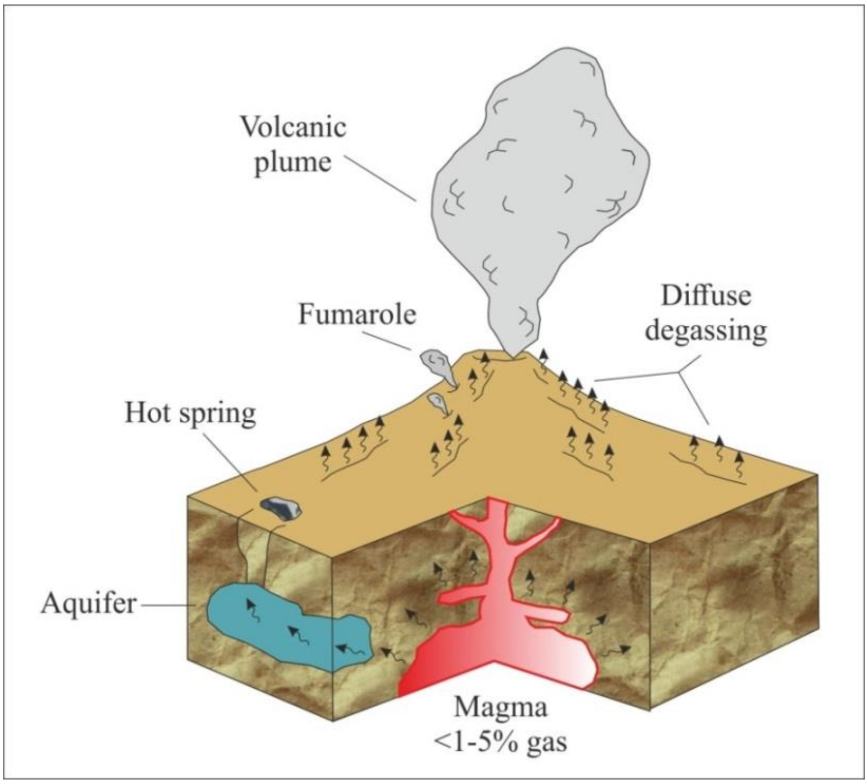

Figure 2. *Manifestations of volcanic gases.*

Non-visible degassing does not occur homogeneously along the whole volcanic edifice, but occurs preferentially through high permeability restrictive areas known as diffuse degassing structures (DDS) (Chiodini et al., 2005). Diffuse degassing represents the main form of degassing in many volcanic systems (Fridriksson et al., 2006, Pérez et al., 2011, Padrón et al., 2012a, Hernández et a., 2015) and the only one in others (Padrón et al., 2008 2015, Hernández et al., 2017). From the point of view of volcano monitoring, diffuse degassing studies allow to detect high permeability areas, changes in emission rates and changes in the conditions of the magmatic-hydrothermal system, where other methodologies such as thermal observation, geodesic, gravimetric or electromagnetic methods are not useful (Chiodini et al., 2012b, Inguaggiato et al., 2012, Liuzzo et al., 2015, Notsu et al., 2006). It has been demonstrated by several authors that diffuse emission of gases, e.g. CO_2 and He, increases during periods of volcanic unrest (Chiodini et al., 2002, Granieri et al., 2006, Hernández et al., 2001a, Hernández et al., 2017, Melián et al., 2014, Padrón et al., 2013, Tedesco et al., 1999).

Notsu et al., (2006) proposed a 5-stage evolution model in which diffuse degassing and visible emissions are observed (Figure 3). This model suggests that one mechanism of gas emission predominates over the other depending on the volcanic system's activity.

Studies of diffuse degassing in active volcanic areas may be of special interest in the exploration of geothermal resources since these gaseous emanations are generally associated with areas where there is a thermal gradient associated with a thermal source.

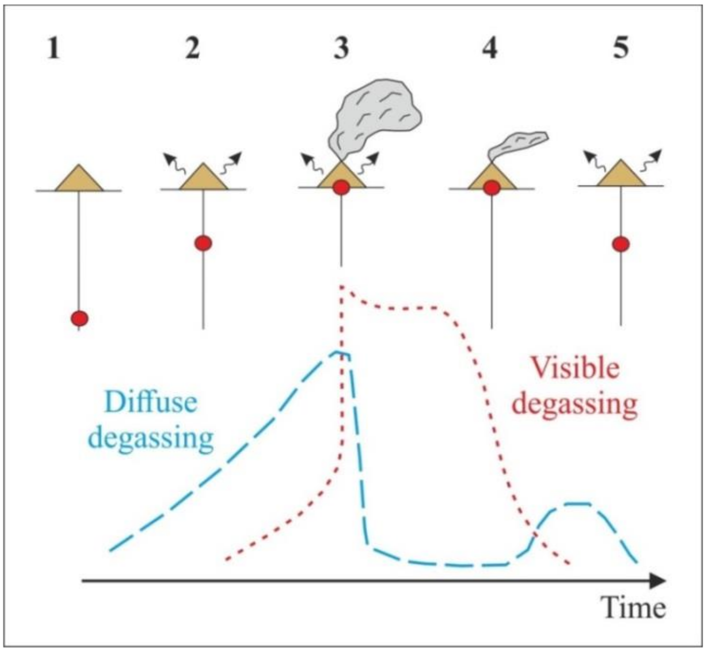

Figure 3. *Mechanism of gas release from volcanoes. (Modified from Notsu et al., 2006).*

Diffuse degassing studies are particularly useful to achieve the final objective of geothermal exploration: to locate, define, and characterize the geothermal resource(s) in a specific area. This type of study has the advantage of covering large areas, which represents a powerful tool for geothermal exploration. Detailed surveys of diffuse degassing allows the identification, from the surface, of permeable portions of deep-seated actively degassing geothermal reservoirs, drastically reducing the main risk in the geothermal exploration: the high cost of deep drilling (Rodríguez et al., 2015, 2021).

CO_2 has been traditionally one of the most studied gases in the soil atmosphere for geothermal exploration purposes (Mörner and Etiope 2002; Werner and Cardellini 2006). However, as a reactive gas, CO_2 is affected by the occurrence of interfering processes (gas scrubbing by ground-waters and interaction with rocks, decarbonization processes, biogenic production, etc.) during its ascent from hydrothermal systems toward the surface environment. This hinders the interpretation of their enrichment in the soil atmosphere and fluxes for geothermal exploration purposes (Marini and

Gambardella 2005, Agusto et al. 2013). Within the rest of the soil gases, particularly interest has been addressed to non-reactive (noble) gases. They offer important advantages for the detection of vertical permeability structures because their interaction with the surrounding rocks or fluids during the ascent toward the surface is minimal (Hernández et al. 2004; Padrón et al. 2012b; 2013).

Among the noble gases, helium (He) has been considered in recent years as an ideal geochemical tracer of magmatic and hydrothermal activity at depth: it is inert, physically stable, non-biogenic, sparingly soluble in water under ambient conditions, and highly mobile. There are two naturally isotopes of He: ^{4}He and ^{3}He. ^{4}He is produced as α-particles from the radioactive decay of ^{238}U, ^{235}U and ^{232}Th, while ^{3}He is primordial in origin and its most important source is the Earth interior (Graham, 2002). One of the most significant observations is the presence of ^{3}He enrichments in mantle-derived rocks from ocean ridges and islands, indicating that primordial volatiles are still escaping from the Earth's interior. The current atmospheric ^{3}He/^{4}He isotopic ratio is 1.384×10^{-6} (1 R_A) (Clarke et al., 1976). Mid-ocean ridge basalts (MORBs), formed by partial melting as the ascending mantle beneath spreading ridges reaches its solidus temperature, are generally accepted to represent a broad sampling of the convecting upper mantle (Graham, 2002) and is characterized by 8 ± 1 R_A. The highest ^{3}He/^{4}He values are observed at ocean islands that are thought to be produced by melting 'anomalies' that are generally related to lower mantle upwelling, that suggest that some portions of the mantle have remained relatively undegassed over geologic time. On the contrary, low ^{3}He/^{4}He isotopic ratios are indicative of contamination from crustal material (^{3}He/^{4}He in crustal gases ≤ 0.10 R_A). The presence of higher ^{4}He concentrations than that of the air (5.24 ppm, Sano et al., 1988) in the soil atmosphere can only be explained by a contribution of deep-seated ^{4}He. Unlike other gases, such as

CO_2 or H_2, He does not react in aquifer waters while rising to the surface and is not produced by a biogenic source.

Changes in diffuse ^{4}He emission and in the ^{3}He/^{4}He isotopic ratio have been observed before and after periods of volcanic unrest (Padrón et al., 2013, Sano et al., 2015, Kagoshima et al., 2016, Kagoshima et al., 2019, McMurtry et al., 2019, Alonso et al., 2021; Hernández et al., 2021; Melián et al., 2021). Temporal evolution of ^{3}He emission together with thermal energy release studies have proven to be a powerful tool that helps understanding mantle dynamics, and the link between the mantle and the atmosphere (Sano et al., 1984, Allard et al., 1992, Alonso et al., 2019, Alonso et al., 2021).

The main objective of this Ph.D. Thesis is to evaluate the relationship between the diffuse ^{4}He and ^{3}He emission and the thermal energy measured at the surface of volcanic systems. Since the source of heat and He isotopic character are the same, the central hypothesis tested is that there is a close relationship between these parameters, and thus if evidence supports the hypothesis, the potential to detect deep heat reservoirs through diffuse He emission surveys at the surface will be demonstrated. This objective implies innovative exploration techniques with the application and use of surface gas geochemistry in volcanic areas. To achieve the main objective of this study, the following specific objectives have been identified:

- Synthesis and analysis of the salient information in the literature regarding the investigation of geochemical and geophysical techniques applied to geothermal exploration, both in the study areas and in other places around the world where thermal anomalies are present.

- To evaluate the diffuse ^{4}He emissions from the volcanic-hydrothermal systems of Teide (Canary Islands, Spain), Fogo (Cape Verde) and Furnas (Azores, Portugal).
- To evaluate the diffuse ^{3}He emissions from the volcanic-hydrothermal systems of Teide (Canary Islands, Spain), Fogo (Cape Verde) and Furnas (Azores, Portugal) through the combined use of (a) the diffuse emission of ^{4}He and ^{3}He/^{4}He isotopic ratio; and (b) diffuse CO_2 emission and the CO_2/^{3}He ratio measured in the fumaroles of the hydrothermal volcanic systems.
- To evaluate the thermal energy released by the volcanic-hydrothermal systems of Teide (Canary Islands, Spain), Fogo (Cape Verde) and Furnas (Azores, Portugal) through (a) studies of spatial distribution of soil temperature at 15 cm depth; and (b) the combined use of diffuse CO_2 emission and the H_2O/CO_2 ratio in the vents of these hydrothermal volcanic systems.
- To evaluate of the relationship between the diffuse ^{3}He and ^{4}He emissions and thermal energy released by the volcanic-hydrothermal systems of Teide (Canary Islands, Spain), Fogo (Cape Verde) and Furnas (Azores, Portugal) in order to strengthen the studies of geothermal exploration in those volcanic systems.

Geological Settings

2. GEOLOGICAL SETTINGS

For this study, three volcanic systems have been selected to evaluate the relationship between He emissions and thermal energy released (Figure 4): Pico del Teide (Tenerife, Canary Islands), Pico do Fogo (Fogo, Cape Verde) and Furnas (São Miguel, Azores).

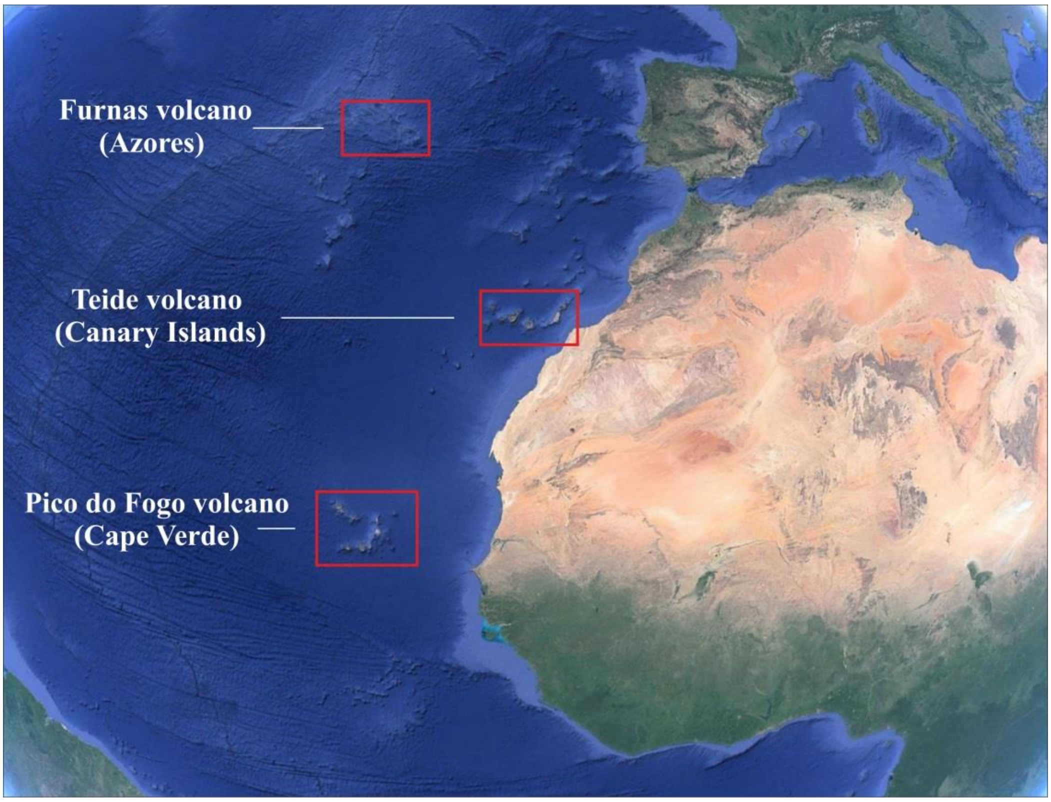

Figure 4. *Location of the studied volcanic-hydrothermal systems in this work. Image source Google Earth.*

The study areas are part of the group of Atlantic archipelagos that belong to Macaronesia. These archipelagos have several common geological characteristics, but the main one is their volcanic origin. The selected areas have a long history of active volcanism, formed by the rise of a thermal anomaly or hot spot from the Earth's mantle. Canary Islands and Cape Verde are hosted within the African plate, and the Azores are located at the triple junction between African, Eurasian and North American plates. Due to these characteristics, the Macaronesian archipelagos are ideal for this type of study, since all of them also present thermal anomalies on the surface, and therefore, with a high circulation of thermal energy under the surface.

2.1. Teide volcano

The Canary Islands are located north-western of Africa, near the coasts of southern Morocco and northern Western Sahara, between 27º 37' and 29º 25' N and 13º 20' and 18º 10' W and comprises eight main islands and some minor islets that rise over Jurassic oceanic lithosphere, decreasing ages from east to west (Carracedo et al., 2007) (Figure 5). The most widely accepted model for the formation of Canarian archipelago is the one that combines three different hypotheses: hot spot, propagating fracture, and uplifted block hypothesis. It means that the islands originate from a thermal anomaly in the mantle helped by regional fractures for the beginning of magmatism; meanwhile, the islands are in their present freeboard attitude due to the action of tectonic forces (Anguita and Hernán 2000).

Tenerife (2,034 km^2) is located at the centre of the archipelago and is the largest of the Canary Islands (Figure 5). The oldest subaerial rocks on Tenerife Island belong to the “Old Basaltic Series” (middle Miocene) and are composed of basaltic lavas and pyroclasts, with some silicic differentiates as dikes or domes. The “Old Basaltic Series” outcrops are not connected to each other and appear in the corners of the island in Anaga (North-East), Teno (North-West) and in Roque del Conde (South) (Acochea et al., 1990). Subsequently, a period of volcanic quiescence and erosion of 2-3 M.y. took place between the “Old Basaltic Series” and the eruptions that originated the younger volcanic series (Carracedo et al., 2007).

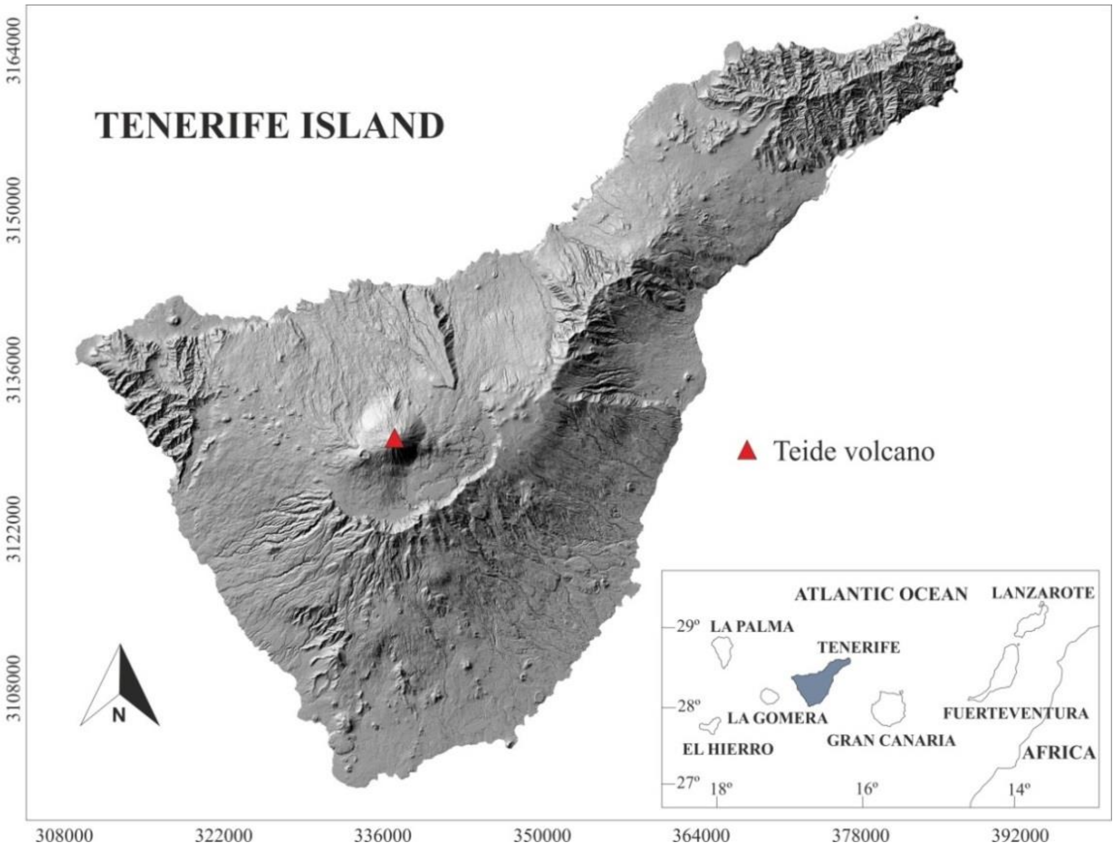

Figure 5. *Digital elevation model of Tenerife Island. Location of Pico del Teide is marked by a red triangle. Inset: Map of the Canarian archipelago highlighting Tenerife Island in grey.*

The Cañadas composite volcano filled the eroded area over the “Old Basaltic Series”, a complex succession of 2,700-3,000 m of basalts, trachybasalts, trachytes and phonolites with ages between 1.5 and 0.13 M.y. and an episode of silicic emissions ~0.6 M.y. (Acochea et al., 1990). The Cañadas edifice collapsed forming the 17 km long and 15 km wide depression of Las Cañadas caldera 200 k.y. ago. Two models have been proposed for the collapse of the Cañadas volcano: i) due to the emptying of the shallow magma chamber followed by explosive activity (Martí et al., 1994, 1997; Marty and Gudmundsson, 2000) and ii) due to a gravitational lateral collapse (Moore, 1964). Afterwards there was a massive filling of the caldera depression with the emission of trachybasalts, basalts, trachytes and phonolites forming the Teide-Pico Viejo volcanic complex, with its last eruption in 1798 through an adventive cone of Pico Viejo volcano. Las Cañadas caldera depression is located at the intersection of the island's three structural rifts, with NE, NW and NS directions and characterized by the alignment of cinder cones and fissure systems where five historical eruptions occurred.

The summit cone of Teide has been constructed during several phases, with phonolites and basaltic-trachybasaltic lavas as its main eruptive products (Ablay and Marti, 2000). Persistent degassing activity has taken place at the summit cone of the volcano since the last eruption, both visible as fumaroles and diffuse degassing. The fumaroles have an average temperature of 83.5 ºC and show chemical composition typical of hydrothermal fluids: H_2O vapour as the main gas compound followed by CO_2, N_2, H_2, H_2S, HCl, Ar, CH_4, He and CO. (Pérez et al., 1992, Melián et al., 2012). Some authors report $^3He/^4He$ isotopic values of 7.21 R_A (Pérez et al., 1994) and 6.72 R_A (Alonso et al., 2019) suggesting a magmatic contribution for the fumarolic gases. This assumption is supported by the $\delta^{13}C\text{-}CO_2$ isotopic values of the fumaroles discharges ranging from -3.7 to -8.1‰ (Pérez et al., 1994, 1996a).

2.2. Pico do Fogo volcano

The Cape Verde archipelago is located between 550-800 km west of the coast of Senegal, between 14º 40’ and 17º 30’ N and 21º 30’ and 25º 30’ W (Figure 6). The archipelago is built upon oceanic crust, located in the south-western part of the Cape Verde Rise, a ~2 km high and ~700 km in diameter hot spot swell formed by the activity of a Miocene mantle plume (Holm et al., 2008). It is formed by ten major islands and some islets arranged in a westward-opening horseshoe shape divided into two alignments: The Barlovento alignment, with SE-NW orientation, comprises the islands of Santo Antão, São Vicente, Santa Luzia, São Nicolau, Sal and Boa Vista, and the Sotavento alignment includes Maio, Santiago, Fogo and Brava defining an ENE-WSE orientation (Figure 6).

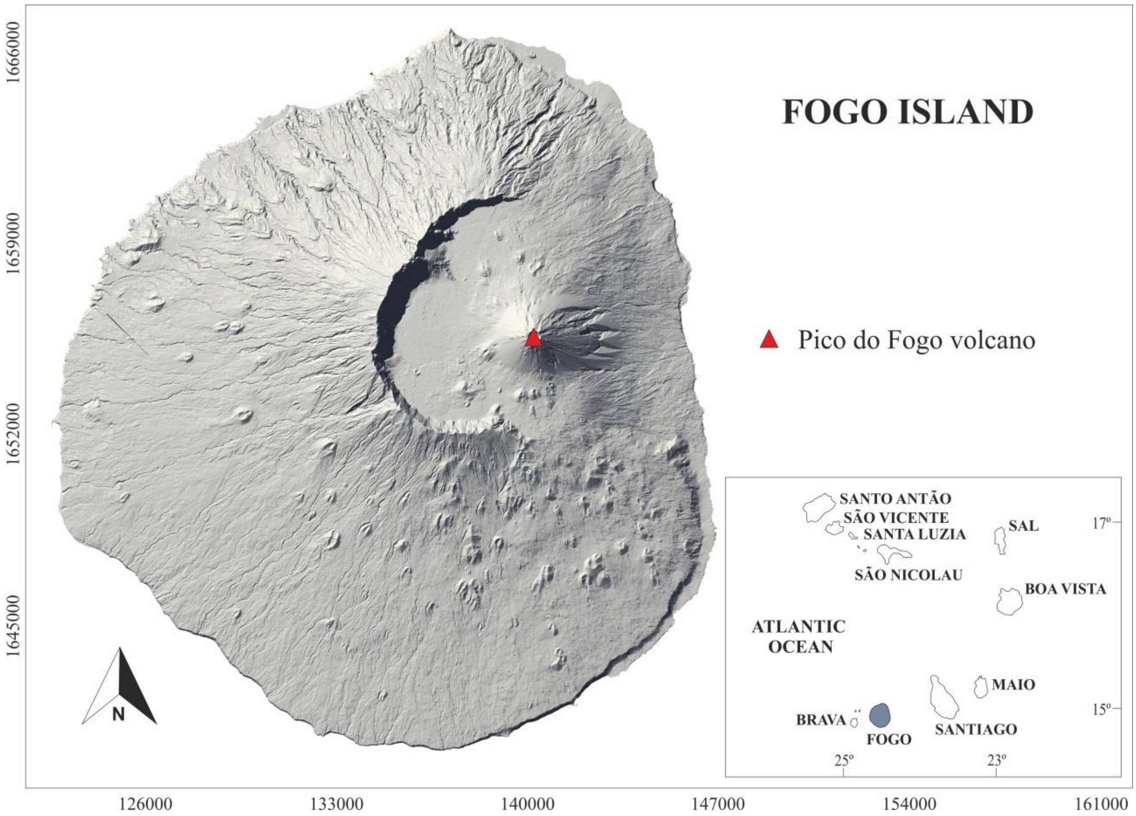

Figure 6. *Digital elevation model of Fogo Island. Location of Pico do Fogo is marked by a red triangle. Inset: Map of the Cape Verde archipelago highlighting Fogo Island in grey.*

Fogo Island (476 km^2) is located in the southwest of the archipelago (Figure 6), and it is characterized by a young volcanic morphology hosting the highest elevation of the archipelago: Pico do Fogo volcano with 2,829 m.a.s.l. Foeken et al., 2009 described four main volcanic periods for the evolution of Fogo Island: i) Ribeira de Almada Group (4.5 M.y.), composed of carbonatites and alkaline basalts from the uplifted Seamount Series, ii) Monte Barro Group, comprises the oldest subaerial lavas on the island. iii) Monte Amarello Group, period of intense volcanism with highly alkaline basic to intermediate lavas, several scoria and spatter cones, lapilli and epiclastic breccia units as the main volcanic products. This period ended with a giant landslide (123-62 k.a.) producing a lateral collapse caldera, Chã das Caldeiras, and iv) Chã das Caldeiras Group, a post-collapse sequence in which volcanic activity predominates within the caldera in which numerous cinder cones appear, culminating in the formation of the Pico do Fogo stratovolcano. Pico do Fogo, with 27 historical eruptions, is one of the world's most active volcanoes (Day et. al., 2000). Most of the historical eruptions have taken place in the summit crater area of the volcano, however, since 1785 the eruptive activity has migrated towards the flanks (Worsley, 2015). The last eruption took place in the lower flank between November 23, 2014 and February 7, 2015 (Barrancos et al., 2015; Capello et al., 2016; González et al., 2015; Pérez et al., 2015; Silva et al., 2015).

Several authors have studied the temporal evolutions of different geochemical parameters in Fogo volcanic system. Alonso et al., 2021 and Melián et al., 2021 studied the 2007-2018 and 2007-2016 periods respectively and observed significant changes in the parameters due to an input of magmatic derived gases. Both works present a model where they suggest the occurrence of a magmatic intrusion for the period 2008-2010 and a second increase in the parameters related to the 2014-2015 eruption.

The summit crater of Pico do Fogo is characterized by the existence of a fumarolic field located in the NW sector, composed of low and medium-temperature gas discharges, from 95ºC to ~315ºC, with an emission of ~1,060 tons/day of CO_2, being a considerable contribution of volatiles to the atmosphere (Aiuppa et al., 2020).

2.3. Furnas volcano

The Azores archipelago is a group of nine Portuguese islands located about 1,400 km west of Lisbon in the middle of the North Atlantic Ocean, in 30º 38' N and 28º 00' W (Figure 7). The volcanic activity of the archipelago is associated with the triple junction between the American, Eurasian and African plates. The islands are aligned along WNW-ESE direction, crossing the Mid-Atlantic ridge obliquely.

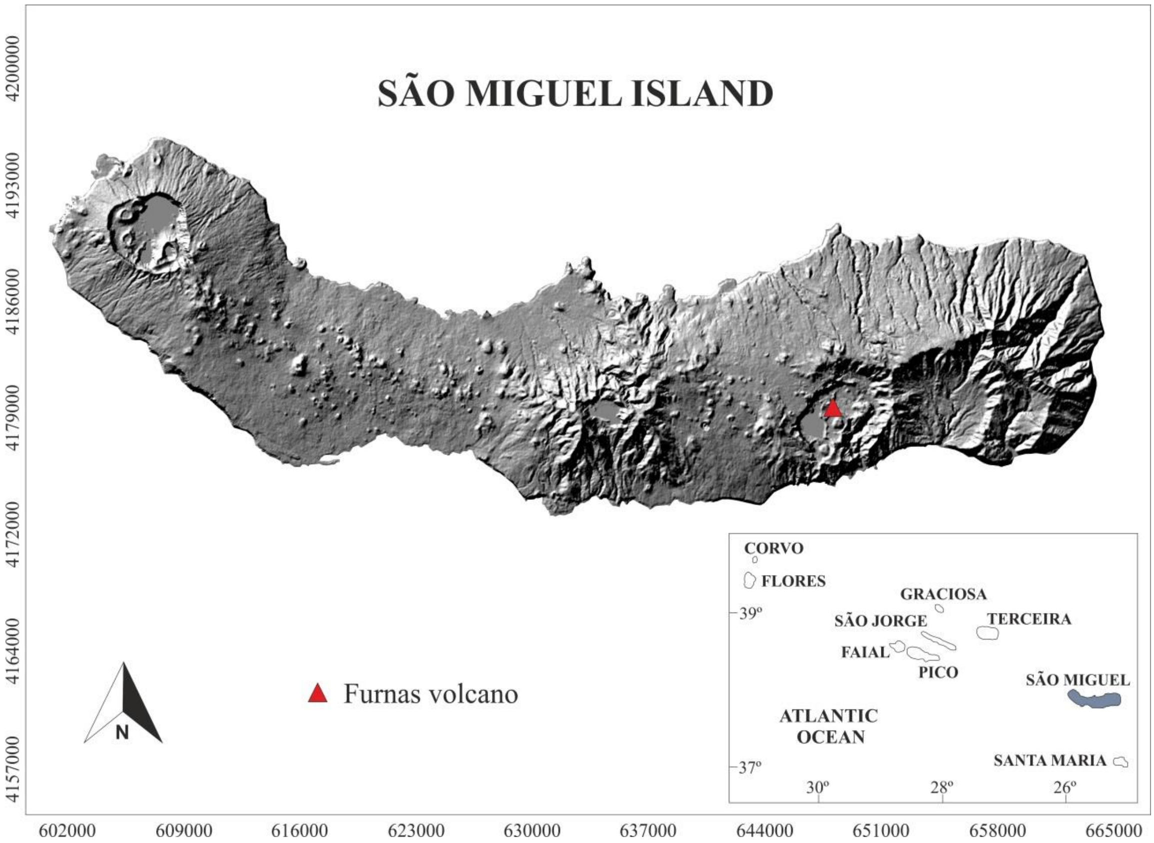

Figure 7. *Digital elevation model of São Miguel Island. Location of Furnas volcano is marked by a red triangle. Inset: Map of the Azores archipelago highlighting São Miguel Island in grey.*

The westernmost islands (Flores and Corvo) lie on the American plate, while the central islands (Terceira, Graciosa, São Jorge, Pico and Faial) and the eastern ones (São Miguel and Santa Maria) connect the Atlantic ridge with the Gloria fault zone (Madeira et al., 1990).

São Miguel Island (746.8 km^2) is the largest island of the archipelago and comprises three trachytic polygenetic volcanoes: Sete Cidades, Fogo, and Furnas. Furnas volcano, the youngest of the central trachytic volcanoes, unlike Sete Cidades and Fogo volcanoes, does not have a well-developed edifice, but consists of an 8 x 5 km across steep-sided caldera. The predominant activity in Furnas is explosive, producing plinian and sub-plinian pumice deposits, ignimbrites and surge deposits, phreatomagmatic ashes, blocks and ash deposits and dome materials (Guest et al., 1999).

Hydrothermal activity is present in the Furnas caldera as low temperature fumaroles (98.9 ºC) and hot springs controlled by the regional fault system, suggesting that a residual heat source is close to the surface (Guest et al., 1999, Viveiros et al., 2010). Although the fumaroles are the most visible surface manifestations they are not the biggest contributors of the total CO_2 output. The fumaroles CO_2 emission is larger than emitted by the hot springs, but far lower than the total soil diffuse CO_2 emission (Pedone et al., 2015).

2.4. Other volcanic systems to study

To obtain a more global point of view of this study, I have gathered new data from the following volcanic systems: Teide summit cone (Tenerife, Spain), Cerro Negro volcano cone and Cerro Negro volcano crater (Nicaragua), Poás volcano crater (Costa Rica), Solfatara (Campi Flegrei, Italy), Reykjanes geothermal area and Hengill volcano (Iceland), Mud volcanoes (Yellowstone, United States), Las Máquinas, Las Maquinitas, Termas and Anfiteatro (Caviahue-Copahue, Chile-Argentina), Ischia Island, Vesuvius volcano cone, Vulcano Island crater, Vulcano Island beach and Pantelleria volcano (Italy) and Nisyros volcano (Greece) (Figure 8). To do so, new literature data, where He isotopic data, He/CO_2 ratio and thermal energy measurements were available, have been added to construct relationships between He emissions and heat flow.

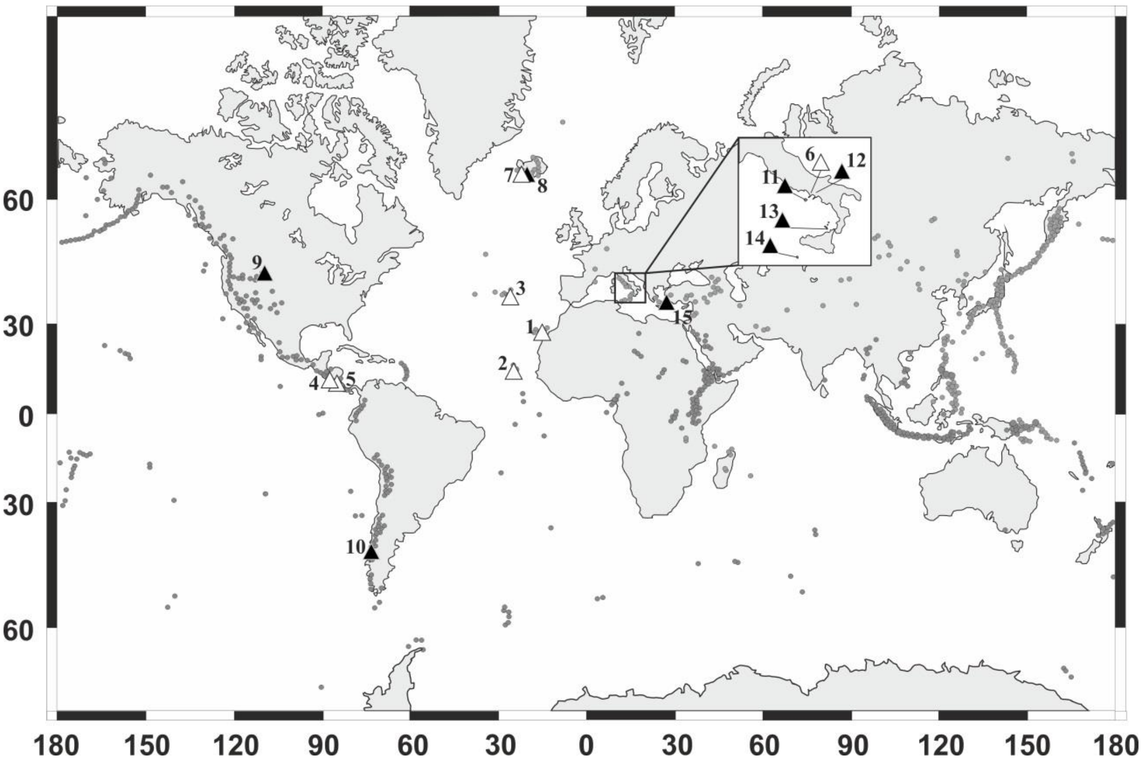

Figure 8. *Location of the studied volcanic systems. Grey dots indicates volcanic systems and black and white triangles the volcanic systems of this study: Teide volcano (1), Pico do Fogo volcano (2), Furnas caldera (3), Cerro Negro volcano (4), Poás volcano (5), Solfatara (6), Reykjanes geothermal area (7), Hengill volcano (8), Yellowstone (9), Copahue volcano (10), Ischia Island (11), Vesuvius volcano (12), Vulcano Island (13), Pantelleria volcano (14), Nysisros volcano (15).*

The volcanic systems of Teide, Pico de Fogo and Furnas, numbers (1), (2) and (3) in Figure 8 respectively, have already been described previously. Other volcanic systems included in this work are briefly described below:

- (4) Cerro Negro volcano is located in El Hoyo-Las Pilas volcanic complex, in Nicaragua, belonging to the Central American Volcanic Arc. It consists of a basaltic cinder cone formed in 1850 and has erupted 23 times since then, its last in 1999. Fumarolic activity is characterized by low-medium temperature discharges inside the main crater.
- (5) Poás volcano is a basaltic-andesitic stratovolcano located in Cordillera Central of Costa Rica in the Central American Volcanic Arc. The active crater typically hosts a super-acidic lake ($pH \leq 1.8$) in which frequent phreatic and phreatomagmatic

eruptions occur (de Moore et al., 2016). Since the last, between April-May 2017, the lake has not existed (Salvage et al., 2018).

- (6) Solfatara volcano is part of Campi Flegrei caldera located in Naples (Italy). Is a highly hydrothermally altered tuff cone where intense diffuse degassing is present. The highest temperatures are found in the Bocca Grande and Bocca Nuova fumaroles that exhibit temperatures between 145 and 165 ºC (Chiodini et al., 2001).
- (7) The Reykjanes geothermal field is located at the centre of Reykjanes volcanic system, in the southwestern of Reykjanes peninsula in Iceland. Is the subaereal continuation of the Reykjanes Ridge and is characterized by episodic fissure eruptions. The previous two eruptions were between 1900 and 2100 years ago (Sigurgeirsson 1995, 2004), being in eruptive activity at present.
- (8) Hengill volcano is located in the eastern part of the Reykjanes peninsula, on the boundary between the European and North American tectonic plates. The last eruption of Hengill volcano took place 2000 years ago (Ingólfsson et al., 2008). The temperature of the fumaroles are ~100ºC and mud pools and steaming ground are also present (Hernández et al., 2012).
- (9) Yellowstone geothermal area has one of the largest hydrothermal systems on the Earth, with up to 1000 km^2 (Rowley 1982). Volcanic activity has been active for the last 2.2 M.y. driven by a mantle hot spot beneath the North American plate (Werner and Brantley 2003), given mainly rhyolitic products with some minor basaltics. Several major caldera formation explosive eruptions ocurred 2, 1.3 and 0.6 M.y. ago (Fournier 1989). The last eruption is dated 70,000 years ago in rhyolitic lavas (Christiansen 2001).
- (10) Caviahue-Copahue volcanic complex is located in the southwestern sector of the Caviahue volcano-tectonic depression (Argentina-Chile). The volcanic complex

includes the Caviahue Caldera, an intra-arc extensional pull-apart basin, where hydrothermal areas are situated (Melnick et al., 2006). In the southwestern rim of the caldera Copahue volcano is located, where 23 phreatic and phreatomagmatic eruptions occurred in the last 250 years (Martini et al., 1997, Naramjo and Polanco 2004).

- (11) Ischia volcanic island is located in the southwest of Campi Flegrei, being the westernmost active volcanic field in the Napolitan volcanic region with it last eruption in 1302, the Arso eruption (Tedesco 1996). Its main morphological feature is the Mt. Epomeo volcano located in the centre of the Island. The volcanic-geothermal manifestations on the island consist of fumaroles and hot springs.
- (12) Vesuvius is a stratovolcano located about 9 km-southeast of Naples and belongs to the Somma-Vesuvio volcanic complex (Cioni et al., 1999). Eruptive activity is characterized by strombolian and plinian phases, with the last eruptive cycle between 1631 and 1944. Visible degassing consists of fumaroles on the crater slopes and bottom (Chiodini et al., 2005).
- (13) Vulcano volcanic island belongs to the Aeolian Islands archipelago formed by subduction beneath the Tyrrhenian Sea. The fumarolic activity on the island is located on Spiaggia di Levante beach, with temperatures of ~100ºC and in La Fossa volcanic edifice where the last eruption of the island took place in 1888-1890 (Mercalli 1891), hosting high-temperature fumaroles (up to 700ºC measured in 1993) (Chiodini et al., 2005, Nuccio et al., 1999).
- (14) Pantelleria volcanic island is a stratovolcano located on the axis of the Sicily Channel Rift Zone result of a transtensional tectonic. The subaerial outcrops are mainly formed by trachytes and peralkaline rhyolites (Pantellerites) (Parello et al., 2000). The last volcanic eruptions in the area took place in 1831 and 1891, both

being submarine eruptions (Civetta et al., 1988). The geothermal manifestations are widespread distributed and consist of hot springs, thermal wells and fumaroles (Parello et al., 2000).

- (15) Nisyros volcanic island is an stravolcano that formed in the last 100 k.a and belongs to the Aegean active Volcanic Arc. There has been no magmatic activity in historical times, but frequent phreatic eruptions occurred, the last in 1887 (Kavouridis et al., 1999). Surface geothermal manifestations are 40-50ºC-hot springs and ~100ºC-fumaroles (Kavouridis et al., 1999, Chiodini et al., 2002).

Methodology

3. METHODOLOGY

3.1. In–situ measurements and soil gas sampling

To achieve the objectives of this study, several field surveys were carried out at the selected volcanic areas. For each survey, a homogeneously distributed sampling points network was designed taking into account the geological and structural characteristics of the study areas, as well as accessibility criteria. Distances between planned sampling points were modified on-the-fly where anomalies in gas emissions were observed to more tightly constrain the areal extent of visible degassing anomalies and achieve more accurate overall estimates. Air temperature as well as soil temperature at 15 and 40 cm depth measurements, diffuse CO_2 efflux measurements and soil gas sampling were carried out at each measurement site. Additionally, a representative fumarolic discharge was sampled at each volcanic system. The field work was carried out during dry seasons to avoid the influence of meteorological conditions during the measurements.

3.1.1. In situ diffuse CO_2 efflux degassing measurements

To obtain the diffuse CO_2 efflux data, the “accumulation chamber method” (Parkinson, 1981, Chiodini et al., 1998) was used by means of West System portable non-dispersive infrared (NDIR) LICOR LI-820 and LI-840 CO_2 analysers equipped with a 20,000 ppm optical path. The portable CO_2 efflux meter was calibrated in the laboratory with different known concentrations of CO_2 before each survey. This method consists of placing the accumulation chamber on the soil surface, and sealing it to prevent the entry of atmospheric air. This allows circulation of the soil gas from the chamber to the detector and back to the chamber in a closed loop, helped by a pump (Figure 9). The accumulation chamber is equipped with a fan to ensure homogenization of the gas inside it. The obtained data is transmitted to a hand-size computer running Flux Manager-data-acquisition-software where the increase of CO_2 concentration as a function of time was recorded.

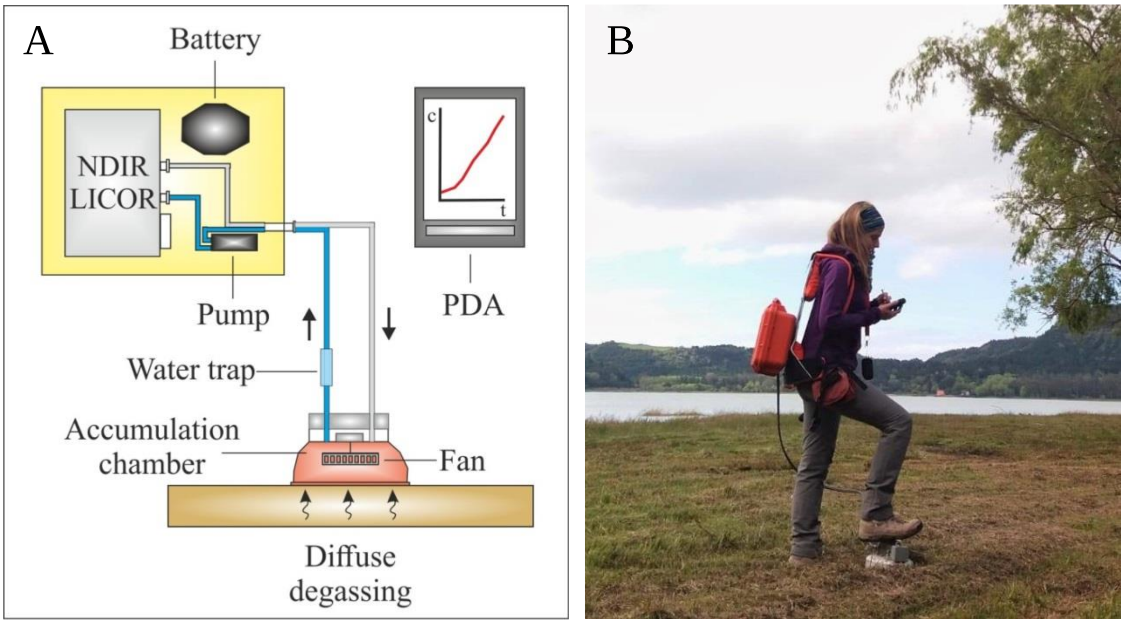

Figure 9. *A) In-situ measurement scheme of diffuse CO_2 efflux following the accumulation chamber method. B) Demonstration of in-situ CO_2 efflux measurement by means the accumulation chamber method.*

To calculate the CO_2 efflux, equations are used based on the geometry of the accumulation chamber and the mass balance within a known volume "control volume" (Figure 10).

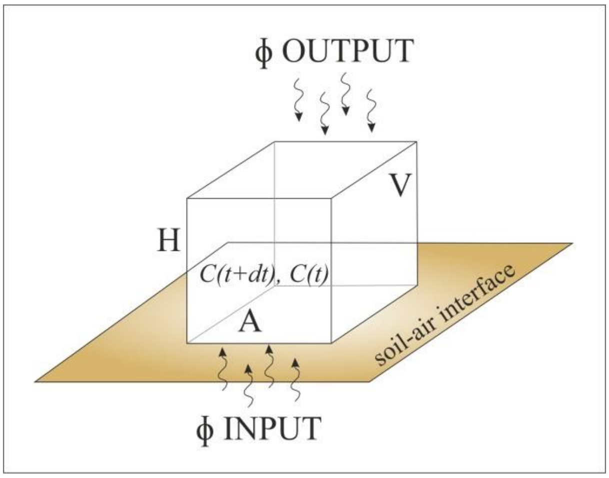

Figure 10. *Idealized scheme of the accumulation chamber, control volume of regular geometry.*

The mass of CO_2 inside the inverted chamber at time $t + dt$ is equal to the mass of CO_2 present at time t, plus the mass of CO_2 entering the chamber in the time interval dt, minus the mass of CO_2 leaving the chamber in the same time interval, as per the following equation:

$$V_c C_{CO2,t+dt} = V_c C_{CO2,t} + \phi_{input} A_c C_{soilCO2} dt - \phi_{output} A_c C_{CO2,t} dt \qquad (1)$$

where V_c and A_c represent the volume and the cross-sectional area of the chamber respectively. ϕ_{input} and ϕ_{output} the gas flow entering and leaving the chamber respectively.

For cylindrical chambers, the V_c/A_c ratio is equal to H_c, as follows:

$$\frac{dC_{CO2}}{C_{CO2,t} - C_{soilCO2}} = -\left(\frac{\phi_{input}}{H_c}\right) dt \qquad (2)$$

As shown by Schwarzenbach et al., (1993) and Baubron et al., (1991), the integration of the equation 2 leads to the following relation:

$$C_{CO2,t} = C_{soilCO2} + (C_{airCO2} - C_{soilCO2}) \exp(-t\, \phi_{input} H_c) \qquad (3)$$

Under initial conditions equation 2 can be written as:

$$\phi_{input}(C_{soilCO2} - C_{airCO2}) = \left(\frac{dC_{CO2}}{dt}\right)_{t\to 0} H_c \qquad (4)$$

If we assume $C_{soilCO2} >> C_{airCO2}$ as commonly observed in volcanic-geothermal systems, then:

$$\phi_{soilCO2} = \alpha H_c \qquad (5)$$

Equation 5 is the relationship to calculate $\phi_{soilCO2}$ based on the initial slope α of the $C_{CO2} - t$ line.

The accumulation chamber method allows large area coverage with a high sampling density in a relatively short time. Several authors have used this methodology to delimit areas with anomalous gas emissions in active volcanic systems (Arpa et al., 2013, Chiodini et al., 1996, 1998, 2001, 2005, Dionis et al., 2015b, Granieri et al., 2014, Hernández et al., 1998, 2001b, 2017, Pérez et al., 2013, Padrón et al., 2008, 2012a, 2015, Rodríguez et al., 2015, 2021).

3.1.2. In situ soil gas sampling

The methodology for soil gas sampling is shown in Figure 11. At each sampling site, a 50 cm metallic probe is inserted into the ground to reach 40 cm depth at its tip, and the gas is then extracted with a 60 cc hypodermic syringe connected to the probe and stored in a 12 cc pre-evacuated glass vial. Gas inside the probe is purged before sampling to be sure that all collected gas is from 40 cm depth. At each sampling point a total of three aliquots of soil gas are collected into vials, for the analysis of gas species concentration and isotopic analyses. Soil gas He, Ne, H_2, O_2, N_2, CO_2, CH_4 and H_2O concentrations are analysed by Micro-gas Chromatography, soil gas He and Ar isotopes concentrations are analysed with a Quadrupole Mass Spectrometer, and carbon isotopic signature with a Isotopic Ratio Mass Spectrometer.

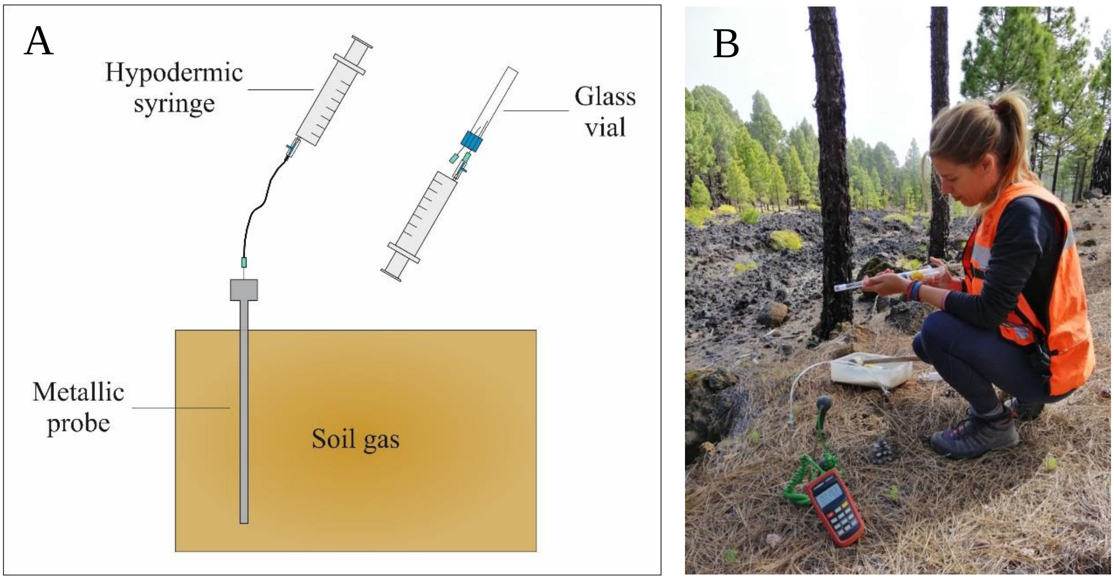

***Figure 11**. A) Scheme of the methodology for soil gas sampling. B) Demonstration of n-situ soil gas sampling.*

3.1.3. Soil and ambient temperature measurements

Air and ground (15 and 40 cm depth) temperatures were measured at each sampling site using a portable Type-K thermocouple (Figure 12).

Figure 12. *Soil 15 and 40 cm depth temperature measurements conducted in Teide volcano.*

3.1.4. Fumarole sampling

For each volcanic system selected in this study, at least one active fumarole was sampled and its gas composition analysed. To do so, a glass funnel or titanium tube is inserted into the fumarolic vent with its tip buried deep enough to avoid the atmospheric air from entering the sampling system. The funnel/tube is then connected to a pre-evacuated glass flask filled with 50 ml of 4N KOH following the method described by Giggenbach and Goguel (1989) (Figure 13). By this procedure H_2O vapour condenses, non-condensable gases (He, H_2, O_2, N_2, CH_4, CO) accumulate in the gas phase and acidic gases (CO_2, SO_2 and HCl) are dissolved in the alkaline solution.

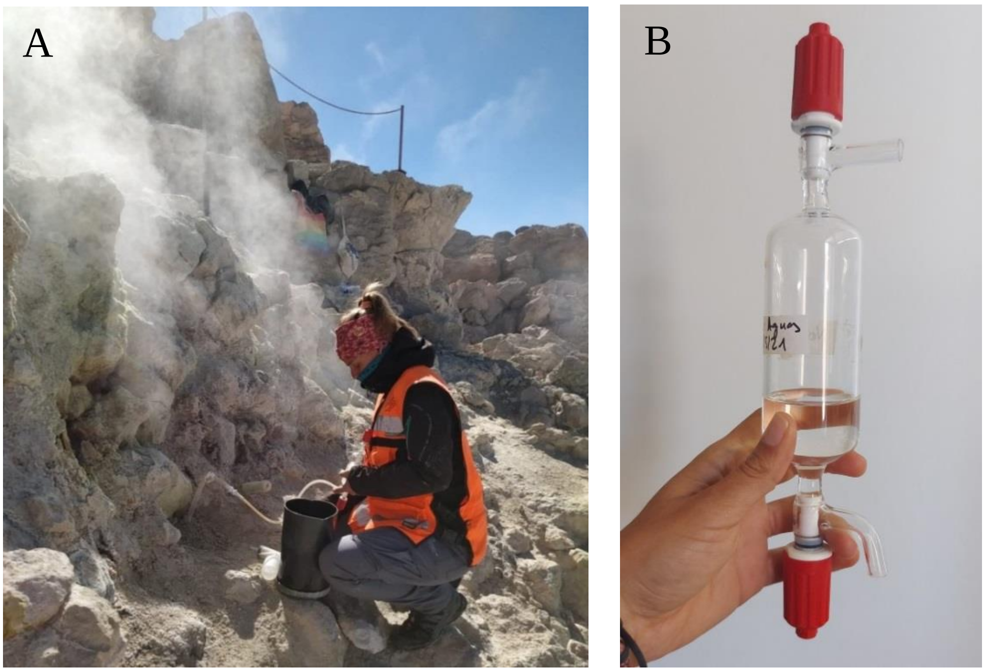

***Figure 13**. A) Fumarole sampling following the method described by Giggenbach and Goguel (1989) and B) Giggenbach bottle filled with 50 ml of 4N KOH.*

For the analysis of helium isotopes, the gas from the fumarolic discharge is conducted with a two-mouth syringe through a 50 cm^3 leaded glass bottle, and stored inside it (Figure 14).

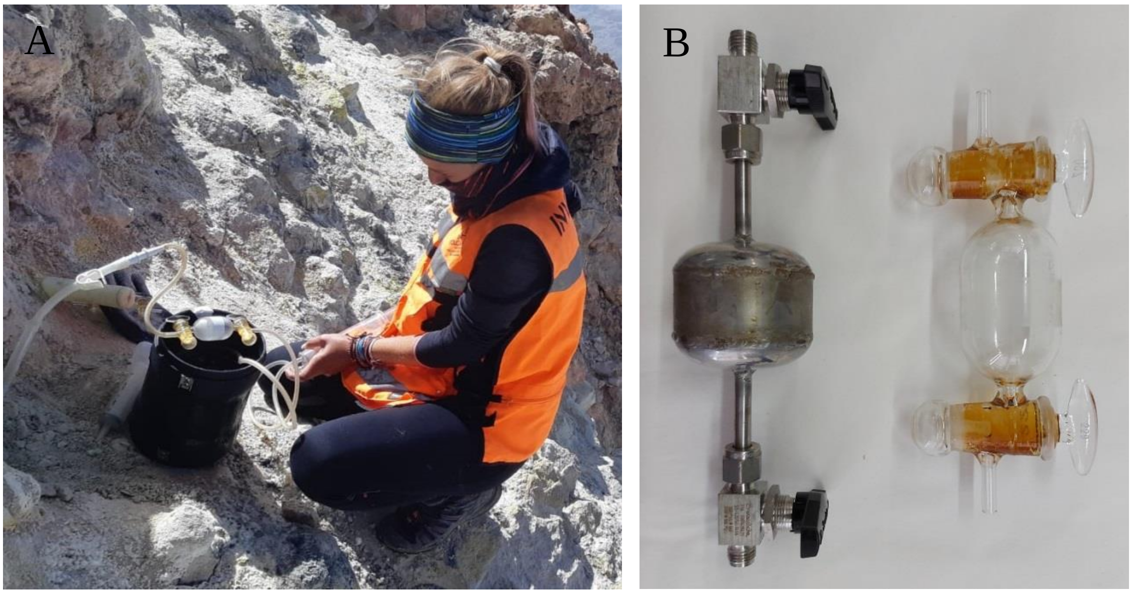

***Figure 14**. A) Demonstration of fumarole sampling for helium isotopes analysis and B) Steel and leaded-glass bottles for helium analysis.*

3.2. Laboratory analysis

3.2.1. Soil gas chemical analysis by micro-GC

One of the sample vials is analysed with an Agilent 490 micro-chromatography (µ-GC) system to obtain the chemical composition of the soil gas samples (Figure 15). The µ-GC system is equipped with two columns: a porous layer open tubular (PLOT) Mol Sieve 5A capillary column of 0.25 mm i.d. x 10 mm maintained at 80 ºC which is used for measuring He, Ne, H_2, O_2 and N_2 content. The second column is a PoraPLOT Q column of 0.25 mm i.d. x 10 m at 40 ºC, which is used to measure CH_4, CO_2 and H_2O. The carrier gas in both channels is Ar of high purity (>99.999%) and the detection system is based on a thermal conductivity (TCD) detector with a total runtime of 180 seconds. To calibrate the µ-GC system, certified gas standards with different concentrations of the species to be determined are used, bracketing the range of values estimated for the concentrations of our samples.

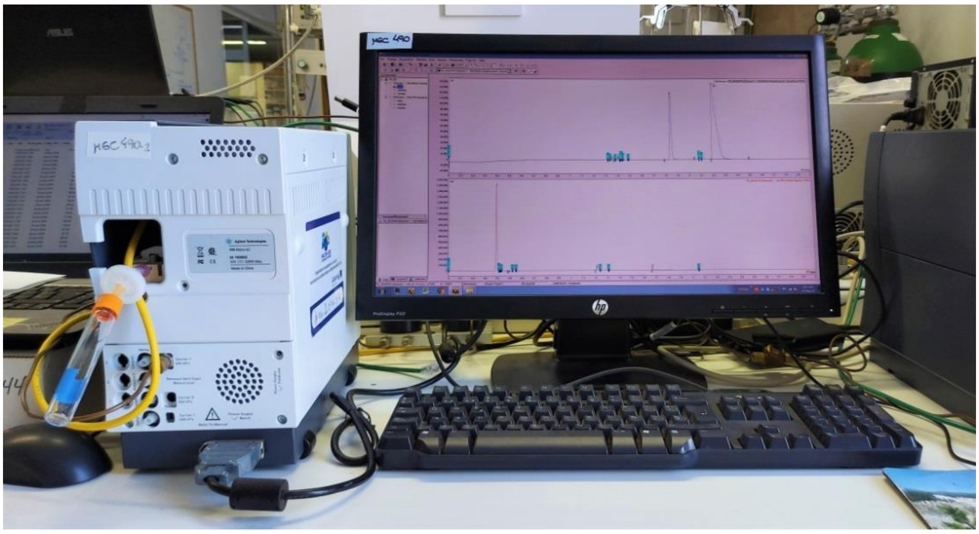

***Figure 15**. Agilent 490 micro-chromatography (µ-GC) system used for the analysis of soil gas composition.*

3.2.2. Soil gas chemical analysis by QMS

^{4}He, ^{40}Ar, ^{38}Ar and ^{36}Ar concentrations of each sample were analysed by means of a Quadrupole Mass Spectrometer (Pfeiffer Omnistar 422) (Figure 16) with precision of ±300 ppb. The sample is subjected to ionization and/or molecular fractionation process induced by a pair of filaments subjected to a variable voltage of between 50 and 70 eV (ionization source). External calibration is performed with an atmospheric air sample collected in a sealed vial prepared in the same way as the soil gas sample is taken.

***Figure 16**. Quadrupole Mass Spectrometer (Pfeiffer Omnistar 422 for the analysis of ^{4}He and $^{40, 38, 36}$Ar concentrations.*

3.2.3. Isotopic composition analysis of soil gases by IRMS

The C isotopic composition (^{13}C/^{12}C) of CO_2 (δ^{13}C-CO_2) was measured using a Thermo Finnigan MAT 253 isotope-ratio mass spectrometer (IRMS, Thermo Scientific) (Figure 17). The samples are injected in the IRMS using a dual inlet system that adds a flow rate of pure He of 0.5 $mL \cdot min^{-1}$ after injection in quadruplicate of the corresponding reference gas (CO_2). The results are reported in δ units per mil vs.

standard Vienna Pee Dee Belenmite (V-PDB) with a respective precision of ± 0.2‰ for $\delta^{13}C\text{-}CO_2$. Therefore, $\delta^{13}C\text{-}CO_2$ is calculated using the following equation:

$$\delta^{13}\mathrm{C}\ (‰) = \frac{(^{13}\mathrm{C}/^{12}\mathrm{C})\mathrm{sample} - (^{13}\mathrm{C}/^{12}\mathrm{C})\mathrm{std}}{(^{13}\mathrm{C}/^{12}\mathrm{C})\mathrm{std}} \times 1000 \qquad (6)$$

***Figure 17**. Thermo Finnigan MAT 253 for the analysis of isotopic composition ($^{13}C/^{12}C$) of CO_2 ($\delta^{13}C\text{-}CO_2$).*

3.2.4. Fumarole discharges analysis

3.2.4.1. Gas composition analysis

Non-condensable gases (He, H_2, O_2, N_2, CH_4, CO) stored in the head-space of the Giggenbach bottle are analysed by gas chromatography (GC) (Varian 3800). He, H_2, N_2 and O_2 are analysed by a TCD (thermal conductivity detector) and CH_4 and CO by a FID (flame ionization detector). The analytical errors are <5% and <10% for the main gas and for minor gas compounds, respectively. An aliquot of the alkaline liquid phase is oxidized with H_2O_2 under gentle heat for the determination of CO_2 and then analysed by titration with diluted HCl using an automatic titration system (Metrohm 716 DMS Titrino, Metrohm) with an analytical precision of <1 %.

3.2.4.2. $^{3}He/^{4}He$ isotopic ratio analysis by NGMS

Some of the ^{3}He/^{4}He isotopic ratio analyses of this study were carried out at the Geochemical Research Center of The University of Tokyo, Japan and others in the laboratory of the Instituto Tecnológico y de Energías Renovables (ITER) in Tenerife.

For the analysis of ^{3}He/^{4}He isotopic ratios at the University of Tokyo, we have followed the procedure of Sumino et al., (2001) using a high-precision Noble Gas Mass Spectrometer (NGMS) (Isotech modified VG-5400) (Figure 18) with an analytical error for R_A of <2 %. In ITER's laboratory the samples were analysed by means of a high-precision Noble Gas Mass Spectrometer (NGMS) (Thermo Fisher Scientific HELIX SFT) (Figure 19) with an analytical error for R_A of <2 %. The correction factor for ^{3}He/^{4}He isotopic ratio is determined by measurements of HESJ (inter-laboratory helium standard) with an established ^{3}He/^{4}He value of 20.63 ± 0.10 R_A (Matsuda et al., 2002) Atmospheric contamination is corrected using ^{4}He/^{20}Ne as a correction factor, assuming that all the Ne has an atmospheric origin (Craig and Lupton, 1976).

***Figure 18**. Noble Gas Mass Spectrometer (NGMS) (Isotech modified VG-5400).*

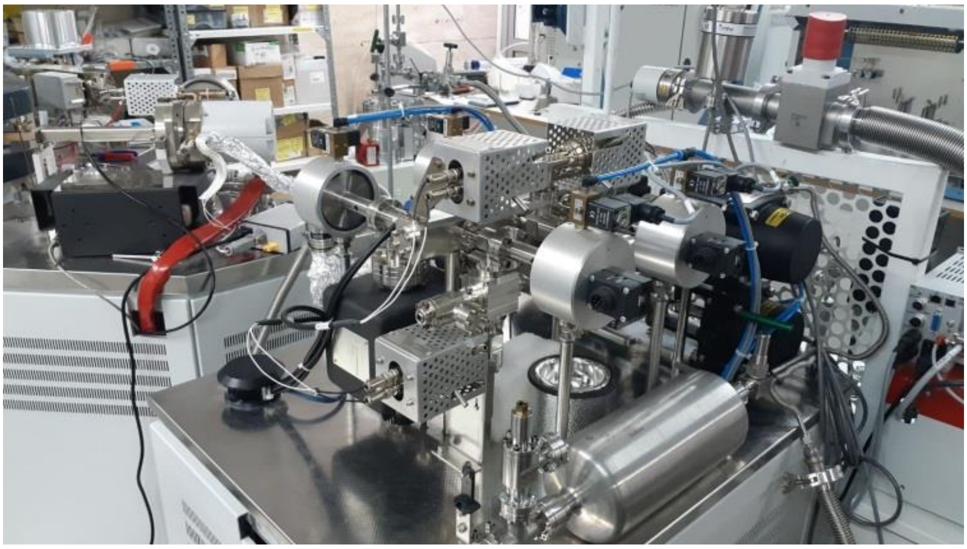

Figure 19*. Noble Gas Mass Spectrometer (NGMS) (Thermo Fisher Scientific HELIX SFT).*

3.3. Data processing

3.3.1. Diffuse helium isotopes emissions calculations

For this work the emissions of both ^{4}He and ^{3}He were calculated using two different methodologies that are explained below. Their relative utility depends upon the type of available data.

3.3.1.1. Diffuse ^{4}He emissions calculations

Circulation of gases at surface levels of volcanoes is governed by a combination of diffusive and advective mechanisms. For the calculation of ^{4}He emission using the first methodology, soil ^{4}He concentration data analysed by the QMS were used to estimate the diffusive and advective ^{4}He fluxes calculated by means of Fick’s and Darcy’s laws respectively, following the procedure described in Padrón et al., 2012, 2013, Dionis et al., 2015, Alonso et al., 2019, 2021, 2021b. The ^{4}He content at 40 cm depth was used to estimate the diffusive and advective gas fluxes (Φ), using the general equation of gas transport shown by Etiope and Martinelli (2002).

$$\Phi_i = -\mathrm{n}\mathrm{D}_m \frac{\mathrm{dC}}{\mathrm{dz}} + \nu C \qquad (7)$$

where n represents soils effective porosity; D_m the molecular diffusion coefficient (m^2/s); dC/dz the concentration gradient in one-dimensional form; νC gas velocity (m/s) and C the gas concentration (kg/m^3). According to Etiope and Martinelli (2002), the apparent diffusion coefficient (D) was used:

$$D = D_m \cdot n^2 \qquad (8)$$

The diffusive emission values ($-nD_m \cdot dC/dz$) for ^4He in equation (7) were calculated using a soil porosity value of 0.35, as has been used in similar volcanic areas (Carapezza et al., 2004), with a molecular diffusion coefficient of 7×10^{-3} (Craig and Lupton, 1976). Assuming that the advective component was mainly governed by convection (Dionis et al., 2015, Alonso et al., 2019), the following equation was used to calculate the convective component of the flux (F_i).

$$F_i = -C_i \frac{K_S \cdot P_{\mathrm{amb}}}{\rho \cdot g \cdot Z} \left(1 - \frac{T_{\mathrm{soil,40}}}{T_{\mathrm{air}}}\right) \qquad (9)$$

where C_i is the gas concentration ($kg \cdot m^{-3}$); K_s the hydraulic permeability ($m \cdot s^{-1}$); T_{soil} and T_{amb} the soil and ambient temperatures; P_{amb} the ambient pressure (Pa); ρ the gas density ($kg \cdot m^{-3}$); g the gravitational acceleration ($m \cdot s^{-2}$) and Z the depth of the soil gas sample (m). The hydraulic permeability was estimated by means of direct measurements of ambient and ground temperatures.

To obtain the diffuse ^{4}He emission by this methodology, sequential Gaussian simulation (sGs) by means of *sgsim* algorithm has been used (Deutsch and Journel, 1998, Cardellini et al., 2003). This method allowed us to interpolate the variable (in this case, diffuse ^{4}He flux) at non-sampled areas and obtain a final estimate of emission across the entire study area. 100 equiprobable simulations were performed to calculate the uncertainty of these results.

For the calculation of diffuse ^{4}He emission by the second methodology, the ^{4}He/CO$_2$ molar ratio measured in the fumarolic discharge of each volcanic system and the diffuse CO$_2$ emission obtained for the study area has been used as indicated by the following equation:

$$\phi^4\mathrm{He} = (^4\mathrm{He}/\mathrm{CO}_2)\times\phi\mathrm{CO}_2 \qquad (10)$$

3.3.1.2. Diffuse ^{3}He emissions calculations

Two methodologies have been used to calculate the diffuse ^{3}He output (Alonso et al. 2019, 2021, 2021b). The first assumes that the ^{3}He/^{4}He isotopic ratio measured in the fumarolic gases is representative of the entire volcanic-geothermal system, and that the source of all He is the same. Once the ^{4}He flux (ϕ^4He) is calculated by the first methodology at each sampling site following the procedure explained above, the ^{3}He flux (ϕ^3He) can be calculated as follows:

$$\phi^3\mathrm{He} = (^3\mathrm{He}/^4\mathrm{He}) \times \phi\, ^4\mathrm{He} \qquad (11)$$

The second methodology assumes that the CO$_2$ measured at the surface of the volcanic-geothermal-system derives from a deep-seated source, and travels along with

^{3}He during its ascent from the mantle source. The calculated CO_2 emission and $CO_2/^4He$ and $^3He/^4He$ ratios measured in the fumarole discharge can be used to estimate ^{3}He output using the following equations:

$$(CO_2/^4He)/(^3He/^4He) = CO_2/^3He$$

$$\phi^3He = \phi CO_2 / (CO_2/^3He) \qquad (12)$$

3.3.2. Thermal energy released calculations

In this work, thermal energy released has been calculated using two different methodologies explained below:

Firstly, CO_2 and H_2O measured in the fumaroles were used as a tracer of hydrothermal fluids to calculate the heat flow involved in the diffuse degassing process by the first methodology. Chiodini et al. (2001) reported this method under the assumption that the H_2O/CO_2 ratio is representative of the original fluids and is recorded, before steam condensation, by fumarolic effluents. These authors computed the heat flux adding the following contributions: (i) the heat released by H_2O gas moving from the hydrothermal reservoir to the steam condensation zone, (ii) the heat given off by CO_2 passing from the hydrothermal reservoir to atmospheric conditions, (iii) the enthalpy of steam condensation at 100°C given by the product of the total amount of steam condensed in one day by the enthalpy of evaporation at 100ºC, and (iv) the heat loss by liquid water on cooling from 100°C to the average seasonal value given by the product of the enthalpy lost by 1 g of water times the mass of the water.

Diffuse CO_2 emission values calculated before for the study areas, were used to estimate the emitted H_2O (steam condensed) considering H_2O/CO_2 ratio measured in the fumarole discharge. In addition, where the soil temperature is higher than the steam condensation temperature the enthalpy of the vapour must be considered.

Thermal energy released has been also calculated following the method described by Dawson 1964. This method uses the correlation between soil temperature at 15 cm depth (T_{15}) and surface heat flux by the following equation:

$$q = 5.2 \times 10^{-6} t_{15}^{4} \qquad (13)$$

By Dawson’s method a heat flux value for each sampling site is calculated. To compute the total heat flux released by the area, sequential Gaussian simulation (sGs) by means of *sgsim* algorithm has been used (Deutsch and Journel, 1998, Cardellini et al., 2003).

3.3.3. Geochemical mapping

Sequential Gaussian simulations (sGs) (Deutsch and Journel, 1998; Cardellini et al., 2003) have been used in recent years to estimate the soil diffuse degassing at volcanic and non-volcanic areas (Padrón et al., 2012 and 2013, Hernández et al., 2012, 2012b, 2017, Pérez et al., 2013, Rodríguez et al., 2015, 2021, Dionis et al., 2015, 2015b). In this work sGs was used to construct the diffuse CO_2 and ^4He degassing and thermal energy distribution maps and to obtain CO_2, ^4He and thermal energy emissions with its uncertainty by *WinGslib* software. The simulation is conditional and sequential, i.e., the variables (CO_2, ^4He and heat flux) are simulated at the non-sampled areas by random sampling of a Gaussian conditional cumulative distribution function defined on the basis of original data, and of previously simulated data within its neighbourhood (Cardellini et al., 2003). Soil CO_2 and ^4He fluxes are typically characterized by polymodal density distribution, generally consisting of a combination of low fluxes, connected to the biological activity in the soil and high flux populations generated by degassing processes of deeply derived gases. Heat fluxes are characterized also by polymodal density distribution with low and high fluxes corresponding with more diffuse or convective areas respectively. In this work, one hundred simulations were performed in order to quantify model uncertainty.

Results and Discussion

4. RESULTS AND DISCUSSION

This section is separated in four chapters depending on the volcanic system studied. Specific chapters have been dedicated to Teide, Pico do Fogo and Furnas volcanoes, and a chapter to the rest of the volcanic systems studied. All the results presented in this thesis are published in scientific journals except those specified in each case.

4.1. Teide volcano

In July 2016, a geochemical gas campaign was carried out at the summit cone of Teide volcano, covering an area of 0.5 km^2 (Figure 20). 170 measurement sites were selected with an average distance of 45 meters on the flanks and 10 meters inside the summit crater. At each sampling site, surface gas samples were collected and analysed later in the laboratory. In addition, the fumarolic gas discharge of an 83.3 ºC low temperature fumarole was sampled. The soil gas survey results are reported in Table 1 and the chemical composition of the fumarolic gas is reported in Table 2.

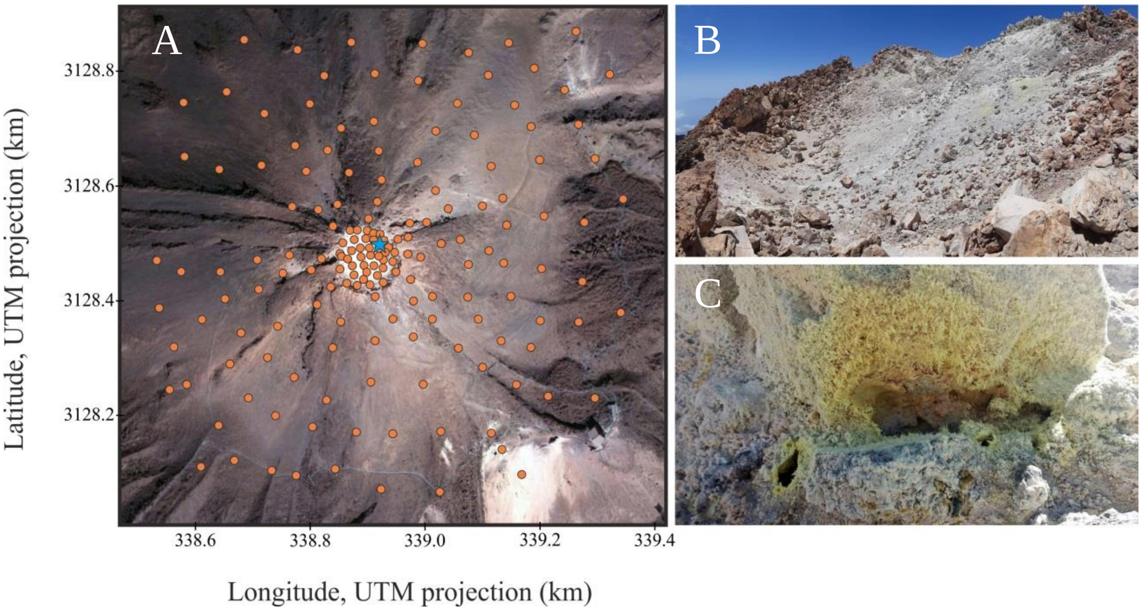

Figure 20: *A) The 170 measurement sites performed in each survey at the summit cone and crater of Teide volcano. Orange dots represent the measurement sites performed in each survey and the sampled fumarole is marked by a blue star. B) Image of Teide summit crater and C) Fumarole inside the summit crater of Teide volcano.*

4.1.1. Diffuse CO_2 efflux and temperature measurements

Diffuse CO_2 efflux values ranged from values below the detection limit of the instrument (<0.5 g m^{-2} d^{-1}) to 10,650 g m^{-2} d^{-1} with an average value of 879 g m^{-2} d^{-1}. Soil CO_2 efflux values in volcanic hydrothermal areas usually reflect the contribution of different CO_2 sources such as biogenic and endogenous, resulting in a bimodal distribution of CO_2 efflux values, which plot as a curve with an inflection point on a logarithmic probability plot (Cardellini, 2003). A probability plot technique (Sinclair, 1974) was applied to the entire CO_2 efflux values to check whether the Log of the data came from unimodal or polymodal distributions (Figure 21).

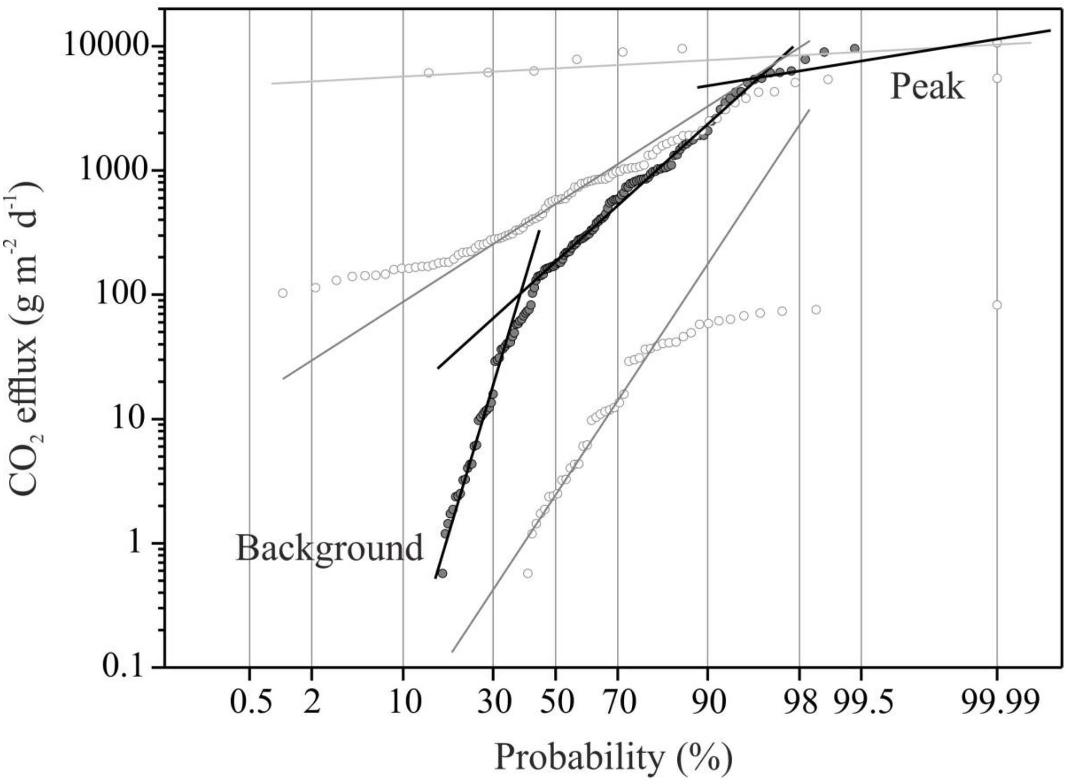

Figure 21. *Probability plot of the CO$_2$ efflux data measured at Teide summit cone and crater. Black lines indicate different log-normal geochemical population in the original data and grey lines indicate the separate background and peak populations.*

Diffuse CO$_2$ efflux values measured at Teide summit cone and crater depicted two Log-normal populations (background and peak). The background population had an average of 2.56 g m^{-2} d^{-1} and represented the 42% of the total data, while the peak population had an average of 6,665 g m^{-2} d^{-1} and represented the 4%. Peak population values were measured where fumarole degassing occurs, while background population values are likely indicative of a higher diffusive component. The contribution of biogenic CO$_2$ can be considered negligible, which is consistent with the very limited vegetation and its related biological activity in the summit cone of Teide volcano. The data regarding the probability plot technique (Sinclair, 1974) has not been previously published.

The diffuse CO_2 output released from the study area was estimated in 211 ± 20 t d^{-1}. Similar results were obtained by Pérez et al., 2013; where the authors computed a diffuse CO_2 emission of 180 ± 21 t d^{-1} in the 2009 survey for an area of 0.11 km^2. Diffuse CO_2 emission distribution map (Figure 22) shows higher values located inside the crater, along the crater rim mainly close to the fumarolic area and towards the north and north-east flanks. The flanks anomalies are probably related to radial fissures propagated from the volcanic axis. Lower values are observed at other sectors of the flanks of the cone.

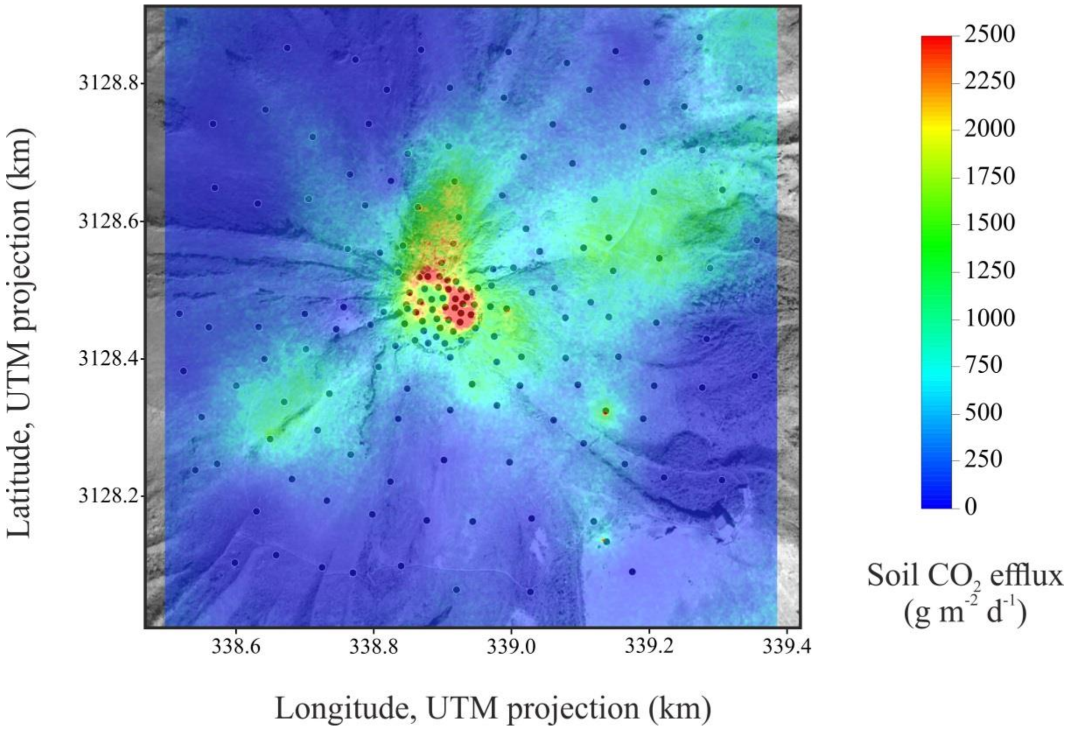

Figure 22. *Spatial distribution of diffuse CO_2 emission values at the summit cone and crater of Teide volcano.*

Areas showing higher CO_2 efflux values also showed relatively high soil temperatures (Figure 23) and are well correlated with surface geothermal areas, suggesting a strong convective degasification mechanism governing the gas emission regime at the study area. The spatial distribution of the soil temperature at 40 cm depth has not been previously published.

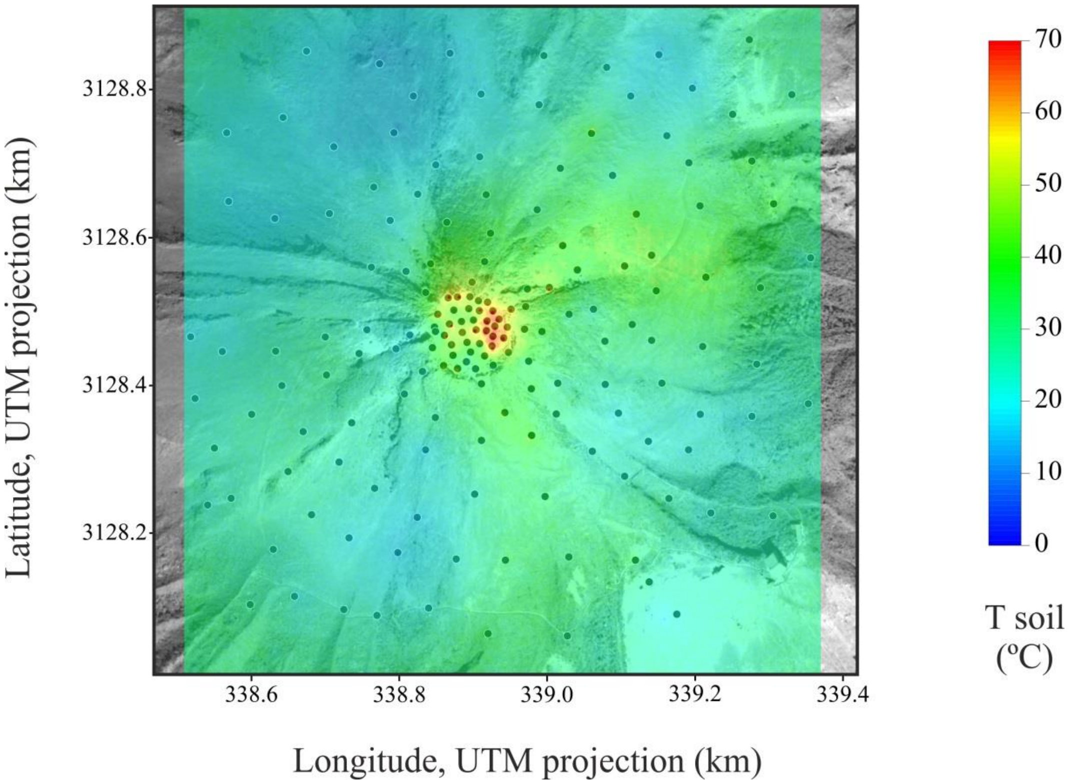

Figure 23. *Spatial distribution of the soil temperature at 40 cm depth at the summit cone and crater of Teide volcano.*

4.1.2. Origin of the CO_2

To investigate the origin of CO_2 in Teide volcanic system, a binary diagram of $\delta^{13}C(CO_2)$ vs. $1/[CO_2]$ ($ppmV^{-1}$) (Figure 24) was constructed, in which the three possible geochemical reservoirs are shown: atmospheric CO_2, characterized by $\delta^{13}C(CO_2)$ = -8‰ and $[CO_2]$ = 0.04%, deep-seated CO_2 with $\delta^{13}C(CO_2)$ = -3.1 ‰ and $[CO_2]$ = 100% and biogenic CO_2 with $\delta^{13}C(CO_2)$ = -20.6‰ and $[CO_2]$ = 100%. To determine the value of the biogenic end-member, Cerling et al. (1991) indicated that biogenic CO_2 in the soil can be +4.4‰ heavier than the soil-respired CO_2 produced by roots, owing to the fractionation of diffusion within the soil. Since the isotopic composition of soil organic matter is in the range -30‰ > $\delta^{13}C(CO_2)$ > -20‰ for plants using the C3 photosynthetic pathway, the isotopic composition for the soil CO_2 was defined by -25.6‰ > $\delta^{13}C(CO_2)$ > -15.6‰, vs. VPDB, with a mean value of -20.6. A $\delta^{13}C(CO_2)$ ~ - 3.1‰ value was measured by Melián et al., 2012 in the Teide fumaroles, corresponding to the average value measured for the hydrothermal system, with values between -2.3 and -4.2‰.

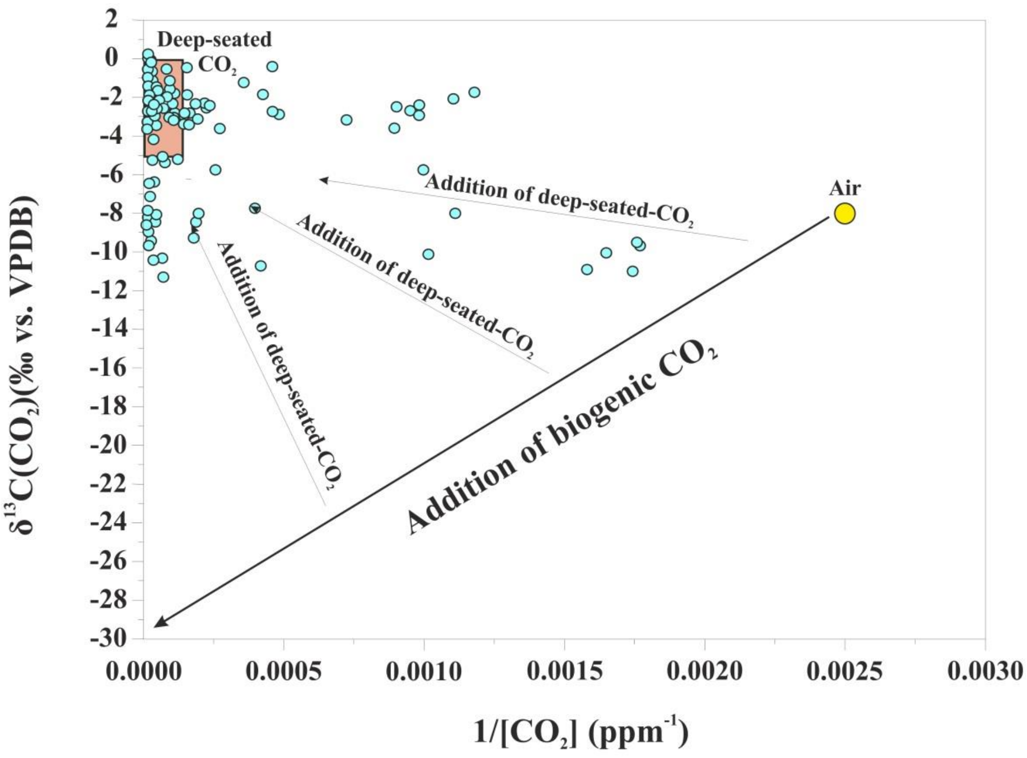

Figure 24. *Plot of* $\delta^{13}C(CO_2)$ *vs.* $1/[CO_2]$ *(ppmV*$^{-1}$*) data from Teide summit cone and crater in which possible geochemical reservoirs are shown. Mixing trend between biogenic, air-derived and deep-seated* CO_2 *is represented by straight lines.*

As shown in Figure 24, most of the analysed samples correspond to a deep-seated CO_2 source, with different degrees of atmospheric contributions. The heaviest $\delta^{13}C(CO_2)$ values, indicative of deep seated CO_2, were measured in and around the summit crater, where fumarolic activity and thermal anomalies occur. The contribution of biogenic CO_2 can be considered negligible, which is consistent with the absent of vegetation.

4.1.3. $^3He/^4He$ isotopic ratio in fumarolic gases

The measured $^3He/^4He$ isotopic ratio was 6.72 ± 0.06 R_A, suggesting a mixture of an upper mantle (MORB) He, radiogenic He and atmospheric sources feeding the Teide volcanic-hydrothermal system. This value is consistent with those measured by Perez et al., 1994, who obtained a value of 7.21 R_A.

4.1.4. Diffuse ^4He emission

The average value of the advective (convective) component exceeded the average value of the diffuse component by almost an order of magnitude: 4.2 vs. 0.44 mg m^{-2} d^{-1} respectively. Therefore, we can assume that most of the diffuse emission from the summit cone and crater of Teide volcano is governed by convective mechanisms. The total diffuse ^4He output from the studied area was estimated in 1.06 ± 0.2 kg d^{-1} (265.15 mol d^{-1}), with the highest values observed where fumarolic activity is present, along the crater rim and towards the north and north-east flanks, coinciding with the highest measured temperature and CO_2 efflux values (Figure 25).

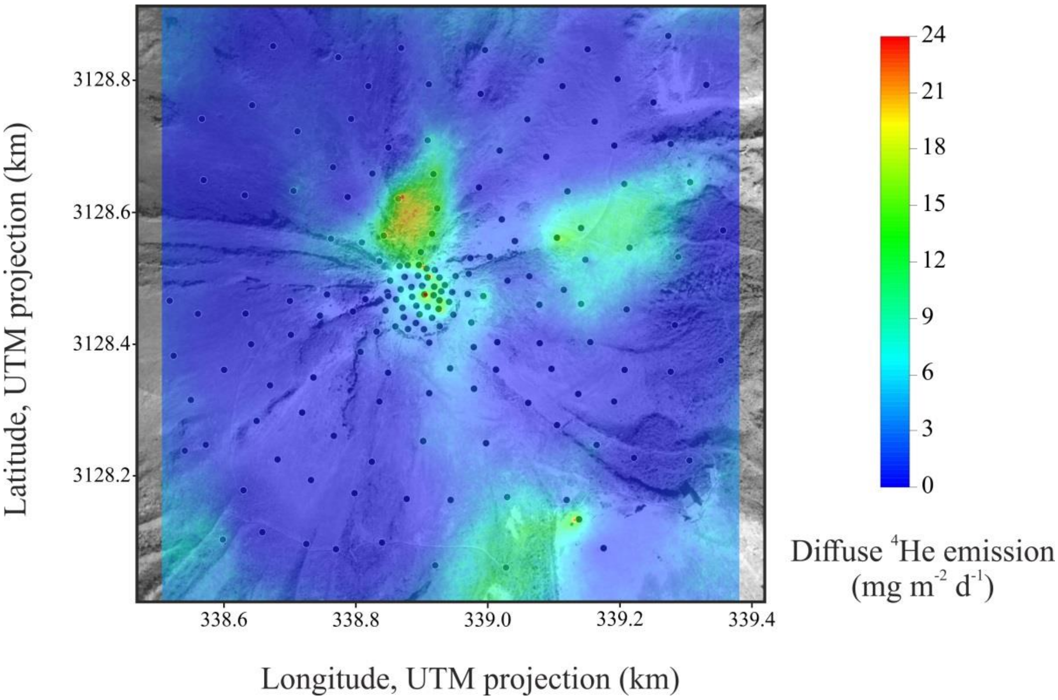

Figure 25. *Diffuse ^{4}He emission map for the summit cone and crater of Teide volcano.*

Other similar ^{4}He emission studies have been carried out in the Canary Islands, but only taking into account the diffusive component due to the lack of geothermal anomalies at the surface of the study areas. Padrón et al., 2012 estimated a diffuse ^{4}He emission that varied between 18 and 38 kg d^{-1} between 2002 and 2004 for an area of 220 km^2 in Cumbre Vieja on La Palma Island, and Padrón et al., 2013 estimated a diffuse emission of ^{4}He ranging from 9 to 38 kg d^{-1} in El Hierro Island prior and during the submarine eruption of 2011-2012 for an area of 278 km^2. If we normalize the emissions per unit area for our Teide survey, we obtain a value of 2.12 kg km^{-2} d^{-1} for the diffuse He emission, a value much higher than 0.17 and 0.14 kg km^{-2} d^{-1} calculated for Cumbre Vieja and El Hierro respectively, suggesting a much higher vertical permeability at the summit cone of Teide. The obtained value of the diffuse ^{4}He emission for the summit cone and crater of the Teide volcano is comparable to the 4.1

kg d^{-1} value for the 0.142 km^2 of the crater of Pico do Fogo volcano obtained by Dionis et al., 2015 calculated after considering an emission governed by convective mechanisms, with a normalized ^4He emission value of 28 kg km^2 d^{-1}. This emission value, higher than that obtained in our work for the Teide volcano, is likely due to the fact that Pico do Fogo volcano has experienced greater eruptive activity in historical times.

4.1.5. Diffuse ^3He emission

Chemical and isotopic composition of the fumarolic gases from the summit crater of Teide volcano is reported in Table 3. The diffuse ^3He emission was calculated using two methodologies explained in the "Methodology" section as follows:

- Assuming that the $^3He/^4He$ ratio analysed from the fumarole is the same for the whole hydrothermal system, the calculated diffuse ^3He emission by the first methodology is 2.48×10^{-3} mol d^{-1} (0.89 mol y^{-1}). Nevertheless, it must be taken into account that the estimated diffuse ^3He emission might be overestimated due to the addition of radiogenic (crustal) ^4He.
- Using the second methodology, we assume that the CO_2 efflux is wholly derived from a deep seated source and travels along with the ^3He from the mantle source to the surface. The calculated ^3He emission is 9.69×10^{-4} mol d^{-1} (0.35 mol y^{-1}). In this approximation, some amount of CO_2 derived from the deep-source would be trapped by water in soil or groundwater during its ascent, so the calculated diffuse ^3He emission might be underestimated. Marrero et al., 2008 estimated through a CO_2 mass balance, that 17.5×10^8 mol y^{-1} (211 t d^{-1}) of CO_2 is discharged by the groundwaters of Las Cañadas aquifer (144 km^2) (Figure 26).

That means a large amount of magmatic CO_2 is being trapped in the aquifer during its ascent to the atmosphere, suggesting that diffuse ^{3}He emission calculated using the second methodology is underestimated.

The obtained diffuse ^{3}He emission values for the summit crater and cone of Teide volcano are consistent with the value of 0.51 mol y^{-1} obtained by Hernandez et al.,1998 for the Teide crater in September 1996 (after correction of an error observed in the original calculation).

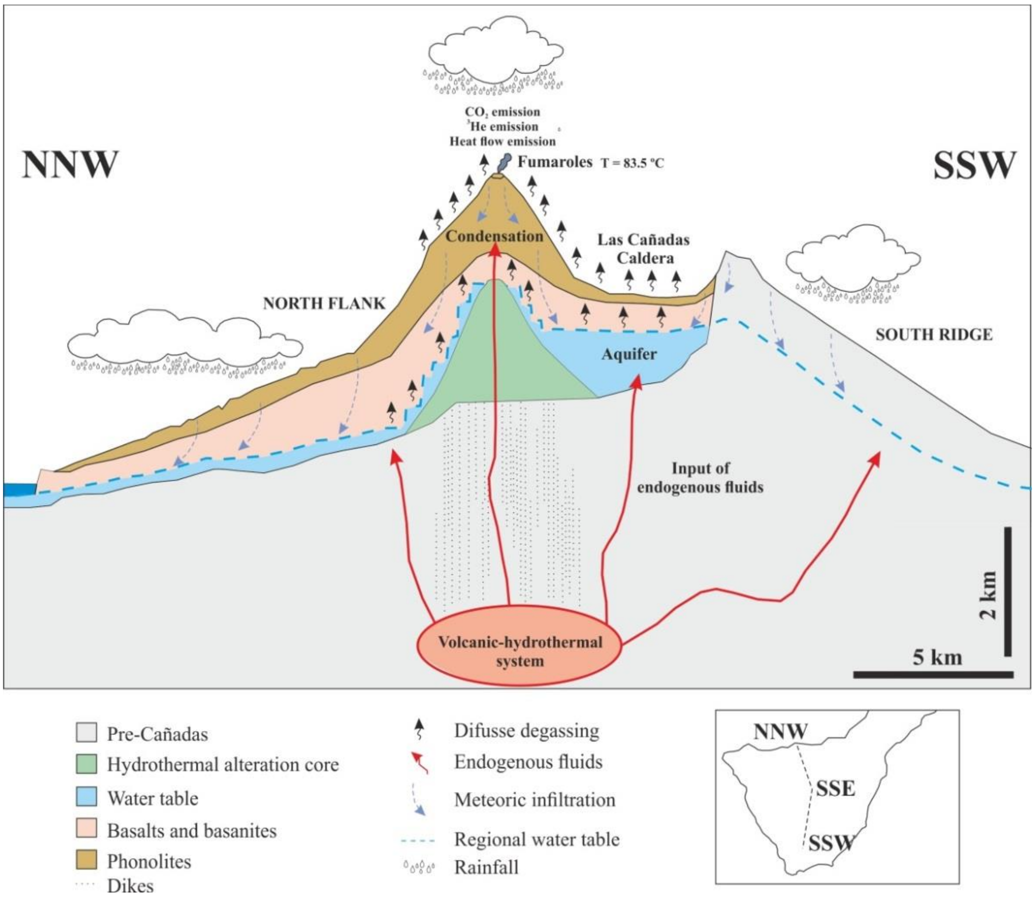

__Figure 26.__ Hydrogeological model of Las Cañadas aquifer in Tenerife Island. Fluid transport from the volcanic-hydrothermal system to the atmosphere is shown. Modified from Marrero et al., 2015.

Studies of diffuse ^3He emission in volcanic systems are scarce; herein we provide one more of the few values reported to date related to ^3He global emission. Other hot spot-type volcanic systems as Piton de la Fournaise in La Réunion Island and Kilauea in Hawaii show diffuse ^3He emission values of 1.1 mol y^{-1} and 9-14 mol y^{-1} respectively (Allard, 2015). Padrón et al., 2012 estimated a total output of ^3He in Cumbre Vieja volcano (La Palma, Canary Islands) of 0.6-0.7 mol y^{-1} considering a pure diffusive transport mechanism for an area of 220 km^2.

4.1.6. Thermal energy released

Following Chiodini et al., 2005, we have calculated a thermal energy released of 2.21 MW, while using the Dawson, 1964 method we calculated a thermal energy of 8.1 ± 0.97 MW. This difference among the heat emission calculations is likely caused by the approach used in the method proposed by Chiodini et al., 2001, as it assumes that H_2O/CO_2 molar ratio measured in the fumarolic discharges is the same for the whole hydrothermal system. In this study, we are comparing areas with higher convective component at the crater with areas showing mainly diffusive components at the flanks of the volcano.

In the heat flow distribution map, the areas with highest values are observed at the fumarolic area inside the crater and along the crater rim and NE flank (Figure 27).

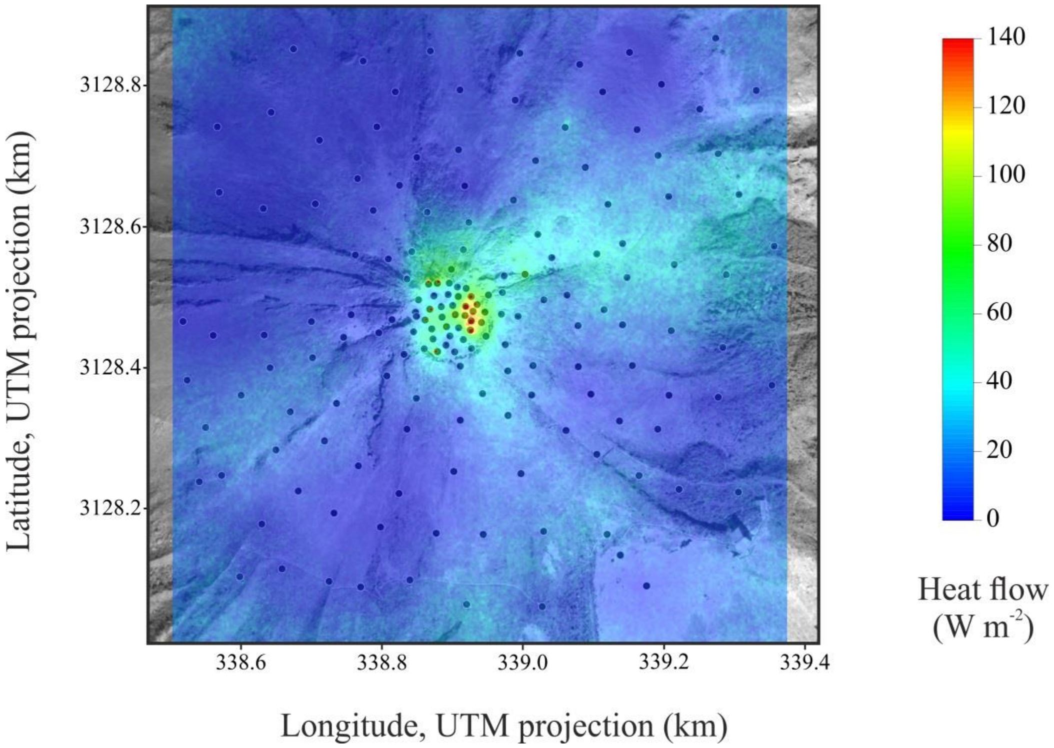

Figure 27. *Thermal energy emission map for the summit cone and crater of Teide volcano.*

Fumaroles in the crater of Teide volcano have an average temperature of 83.5 ºC. The main component of fumarole gas is water vapour originated from the vaporization of meteoric water, followed by CO_2, N_2, H_2, H_2S, Ar, CH_4 and CO, a typical chemical composition of hydrothermal fluids (Pérez et al., 1992 and Melián et al., 2012). These data suggest that the fumarolic effluents are made by endogenous gases which cross the aquifer located somewhere in the post-caldera structure close to the surface (Albert-Betrán et al., 1990). Most of the heat flow measured in Teide volcano is the result of the emitted heat by the phase change of water from gas to liquid in the condensation zone.

The heat flow calculated at Teide volcano summit cone is comparable to that at other volcanic systems. Hernandez et al., 2012 reported a total heat flow of 1.24 MW for Hengill volcanic system; Chiodini at al., 2005 reported the thermal energy released by other volcanic areas as Campi Flegrei 100.8 MW, Ischia 40.1 MW, Vesuvio cone 16.6 MW, Vulcano crater 21 MW, and Comalito cinder cone 0.9 MW, and Dionis et al., 2015 reported a values of 10.3 MW released from the summit crater of Pico do Fogo volcano.

4.1.7. ^{3}He/Heat ratio

We calculated a ^{3}He/heat ratio in the range from 0.117×10^{-12} to 0.764×10^{-12} cm^{3} STP J^{-1}, with an average value of 0.370×10^{-12} cm^{3} STP J^{-1}. This value is close to the 0.5×10^{-12} cm^{3} STP J^{-1} calculated for the ^{3}He/heat ratio for hydrothermal activity from the upper mantle (Figure 28) (Lupton et al., 1989 and Elderfield and Schultz, 1996).

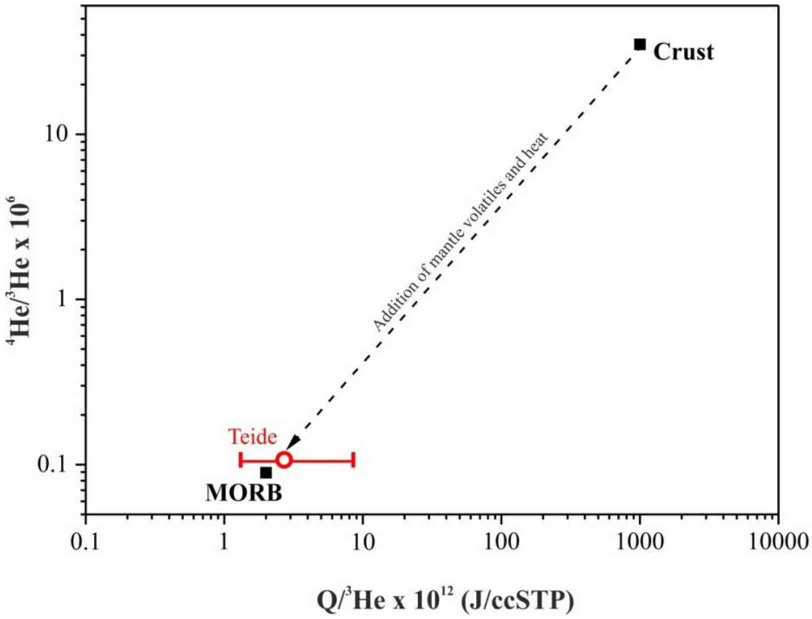

Figure 28. *Schematic representation of the coherence between heat and helium.*

4.2. Pico do Fogo volcano

We report the temporal evolutions of the isotopic composition of He measured in the fumarole gases of Pico do Fogo, as well as the temporal evolution of ^{4}He, ^{3}He and the thermal energy released from March 2007 to November 2018. Sixteen surveys were conducted inside the summit crater of Pico do Fogo volcano with sixty-three measurements performed in each survey, covering an area of 0.142 km^2 (Figure 29). The average distance between the sampling points was 30 meters. The measured data are reported in Table 4.

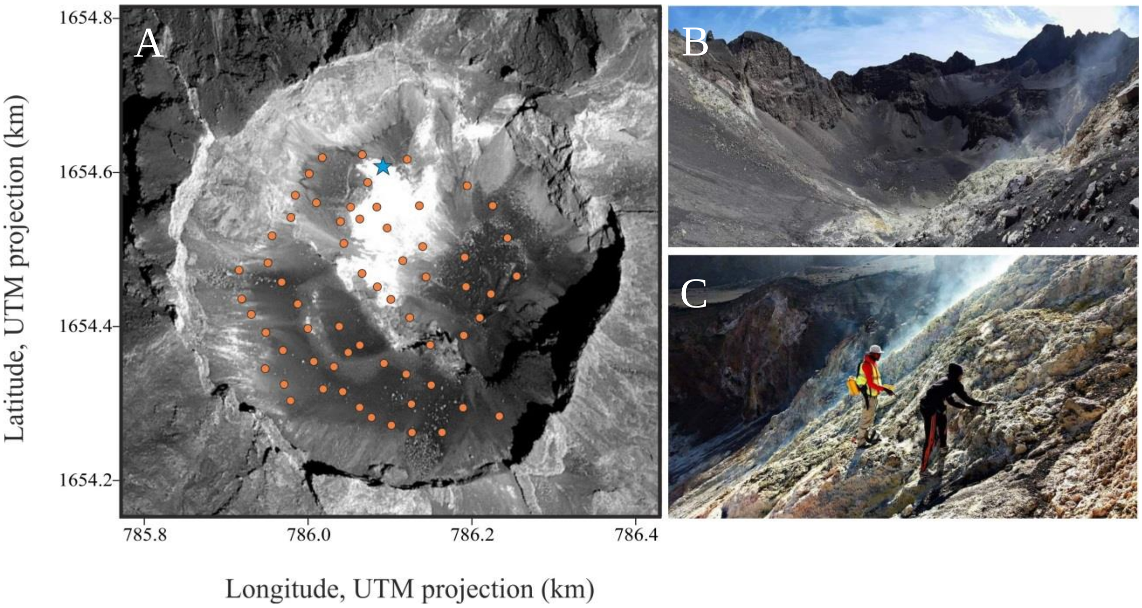

Figure 29. *A) Location of the 63 measurement sites performed in each survey at Pico do Fogo volcano. Orange dots represent the measurement sites performed in each survey and the location of the fumarole is marked by a blue star. B) Image of Pico do Fogo crater and C) Fumarolic field inside the crater of Pico do Fogo volcano.*

4.2.1. ^{3}He/^{4}He isotopic ratio

^{3}He/^{4}He isotopic ratios were measured in the same fumarole of Pico do Fogo volcano from March 2007 to November 2018. The air corrected ^{3}He/^{4}He $(R/R_A)_{\text{cor}}$ ratio ranged from 6.69 ± 0.04 to 8.63 ± 0.10 R_A, with an average value of 8.07 R_A. In the temporal evolution of the ^{3}He/^{4}He $(R/R_A)_{\mathrm{cor}}$ (Figure 30), two main peaks can be observed, one in February 2010 and other in November 2013, both with an increase of ~0.7 R_A in the isotopic ratio, and the latter followed by a continuous decrease in the isotopic ratio until the end of the study period. The decreasing slope represents degassing of the magmatic melts that were responsible of the 2014-2015 eruptive process.

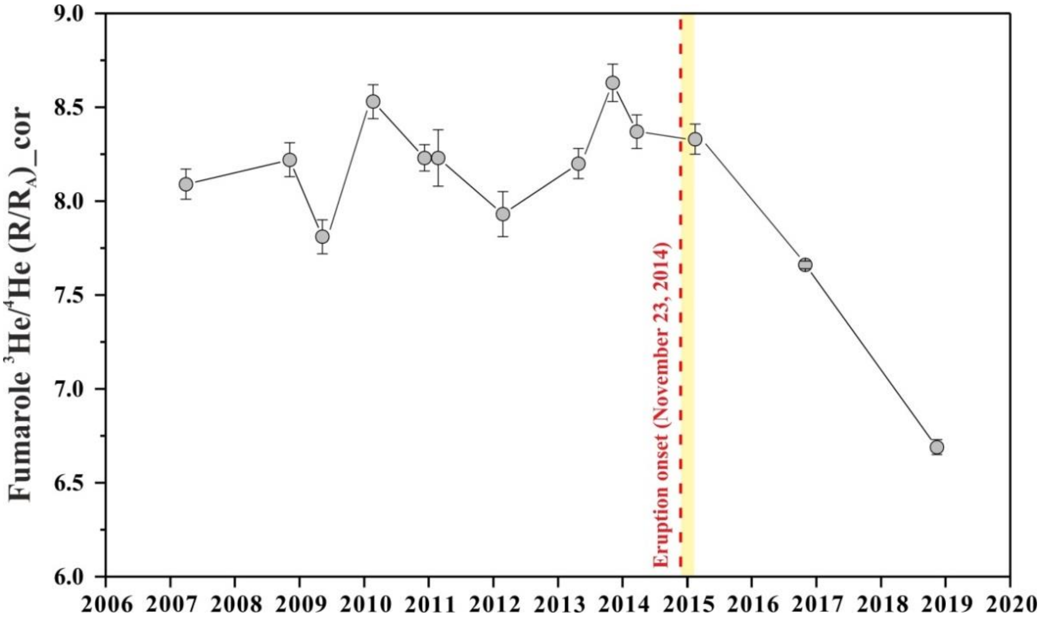

Figure 30. *Temporal evolution of the* ^{3}*He/*^{4}*He isotopic ratio measured in fumarolic gas from March 2007 to November 2018. The red dashed line indicates the eruption onset on November 23, 2014, and the yellow bar represents the eruptive period (November 23, 2014 to February, 7, 2015).*

Tedesco and Scarsi, 1999 studied long-term isotopic variations of ^{3}He/^{4}He isotopic ratios in Vulcano Island since 1987, obtaining values ranging between 4.9 to 6.0-6.2 R/R_A. The authors suggested that variations in the isotopic ratio were due to pressure variations in a deep gas reservoir, and therefore, these variations did not represent a volcanic unrest period. This explanation cannot be ruled out in the ^{3}He/^{4}He isotopic ratios variations observed in Pico do Fogo volcano during the 2009-2010 period. One observation supporting the statement of the presence of a magmatic intrusion during 2009-2010 period is that the variations of ~0.7 R_A are similar for both 2009-2010 and 2012-2014 periods, being the magmatic intrusion of the second period evident due to the occurrence of the subsequent volcanic eruption. Kagoshima et al. (2019) observed a rapid increase in the ^{3}He/^{4}He ratio at Mt. Hakone (Japan), from an average value of 6.37 R_A to a maximum value of 6.76 R_A, which was related to a small hydromagmatic eruption. After this episode of volcanic unrest, the ^{3}He/^{4}He isotopic ratio decreased gradually to 6.25 R_A. Measurements of the ^{3}He/^{4}He isotopic ratio of Turrialba volcano (Costa Rica), between 1999 to 2016 reveal several increases, suggesting deep degassing episodes of mafic magma and an arrival at the surface of magmatic gases, the last in October 2015 with a peak of 8.0 R_A (Rizzo et al. 2016). Decreases through the time series are due to a reduction in the degassing of the magmatic source. In addition to predicting future eruptive events, the ^{3}He/^{4}He isotopic ratio is also used to quantify the flow of magma that enters the reservoir beneath the volcano (Paonita et al 2016). These authors observed that in the 2010-2012 eruptive period of Etna volcano, the eruption began while the ^{3}He/^{4}He isotopic ratio was increasing due to a melt plus a deep gas input ascending toward shallow levels, reaching the highest 3He/4He values. When the deep input ceased, the ^{3}He/^{4}He isotopic ratio decrease rapidly, restoring background values, suggesting that the emitted volume was supplied by a single recharge event.

4.2.2. Diffuse ^{4}He emission

The diffuse (advective and diffusive) ^{4}He emission estimated during the study period, ranged from 249 ± 42 to 1997 ± 290 mol d^{-1}. Similar to ^{3}He/^{4}He $(R/R_A)_{cor}$

isotopic ratio, the temporal evolution of diffuse ^{4}He emission shows two main peaks (Figure 31). The first peak coincides with the ^{3}He/^{4}He increase observed in February 2010. The second peak in diffuse ^{4}He emission was measured in January 2015, with a continuous decrease in the emission after the eruptive period. Although the maximum value was measured in January 2015, the steepest increase in the diffuse ^{4}He emission was observed in March 2014.

Following the method described by Ballentine et al., 2002, the different contributions of diffuse ^{4}He emission, radiogenic (crustal) and magmatic (mantle), have been estimated. For this purpose, the ^{3}He/^{4}He isotopic ratio, the previously calculated diffuse ^{4}He emission for each survey and the air ^{3}He/^{4}He ratio (1.384×10^{-6}) have been considered. The magmatic end-member was supposed to be represented by the value 9.54 R_A (Doucelance et al., 2003). Although the highest He isotopic value measured in Fogo is 12.1 R_A (Christensen et al., 2001), we decided to use the second highest value of 9.54 R_A (Doucelance et al., 2003), because it is closer to the maximum values obtained in this work at Pico do Fogo volcanic system. The different contributions to the observed ^{3}He/^{4}He data are reported in Table 5 and represented in Figure 31. Our results suggest a low crustal contribution, with a mean value of ~ 100 mol d^{-1}, while mantle He is much higher, ranging between 200 and 1256 mol d^{-1}.

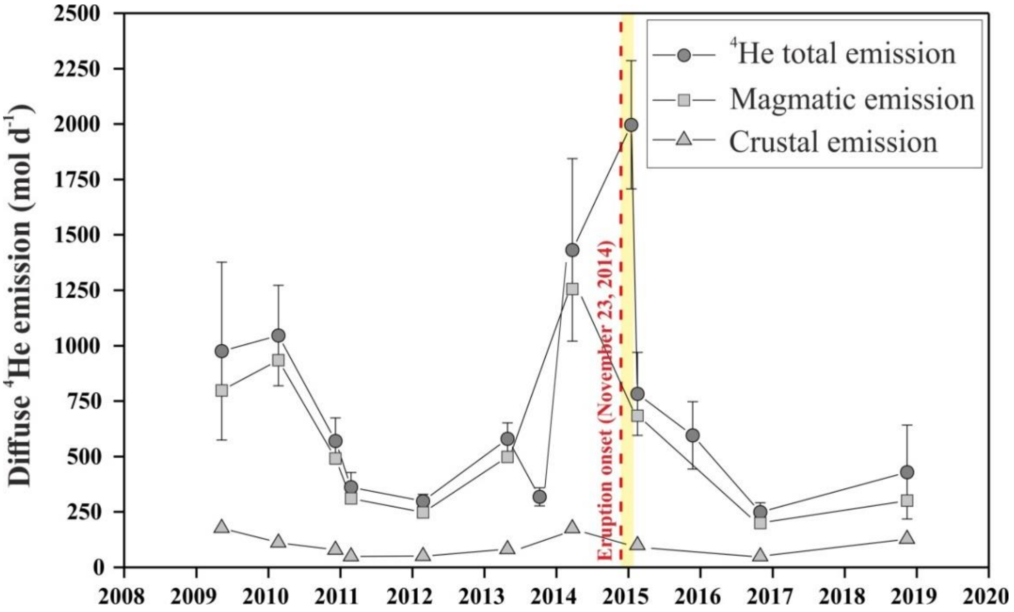

Figure 31. *Time series of diffuse ^{4}He output from March 2007 to November 2018 (dark grey circles). Estimated magmatic (light grey squares) and crustal (light grey triangles) helium emissions during the study period are also present. The red dashed line indicates the eruption onset on November 23, 2014, and the yellow bar represents the eruptive period (November 23, 2014 to February, 7, 2015).*

The spatial distribution of diffuse ^{4}He efflux inside the summit crater of Pico do Fogo volcano in each survey is shown in Figure 32. The maximum values of diffuse ^{4}He efflux are located in the fumarolic field inside the crater, well correlated with the hydrothermal alteration of the soil, highest temperatures and where anomalies of other gases such as CO_2 appear, suggesting convection as the main mechanism in the gas transport. The observed increase in the diffuse ^{4}He emission, warmer colours, can be considered as a clear precursory geochemical signal of the 2014-2015 eruption, in addition to a pulse in the emission in 2010, suggesting a magmatic intrusion towards shallower positions between the end of 2009 and early 2010.

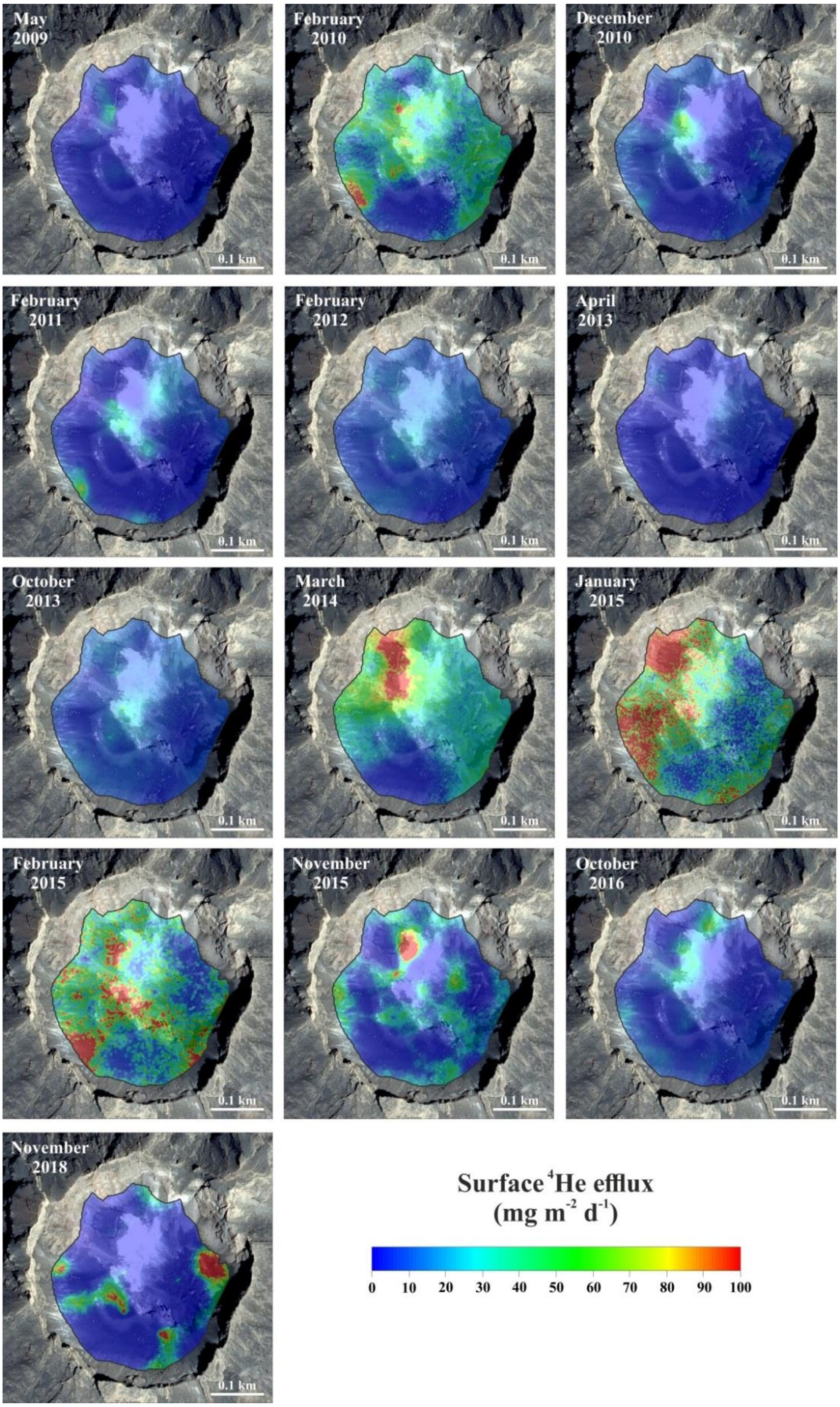

Figure 32. *Spatial distribution of diffuse ^{4}He emission inside the main crater of Pico do Fogo volcano from May 2009 to November 2018.*

4.2.3. Diffuse ^{3}He emission

The diffuse ^{3}He emission has been calculated using the two methodologies explained in the "Methodology" section and the obtained data are presented in Table 4. The values calculated by the first methodology ranged from 2.6×10^{-3} to 1.7×10^{-2} mol d^{-1} measured in October 2016 and March 2014 surveys respectively, with a mean diffuse ^{3}He emission value of 7.58×10^{-3} mol d^{-1}. Emission values calculated by the second methodology ranged from 4.5×10^{-6} to 1.5×10^{-3} mol d^{-1} for November 2008 and March 2014 surveys respectively, with a mean value of 3.5×10^{-4} mol d^{-1}. Both methodologies confirm that the highest emission value was measured seven months before the eruption onset, which can be interpreted as an early warning signal of the eruption. A difference of one order of magnitude is observed in the values obtained by the two methodologies, being higher the ones estimated by the first methodology. This difference is likely due to the fact that the total CO_2 emitted by the volcanic system, may be underestimated due to scrubbing processes that limit the amount of measured CO_2 released from deep sources to the atmosphere (Marini and Gambardella, 2005). Thus, the diffuse ^{3}He emission value obtained by the second methodology may be underestimated, as was observed in the case of the Teide volcanic system (Alonso et al., 2019).

The temporal evolutions of diffuse ^{3}He emission calculated by the two methodologies are depicted in Figure 33. Despite the different absolute values, there are similar trends in the temporal evolution, showing two peaks in the same periods, in February 2010 and March 2014, both following by a continuous decrease in the emissions.

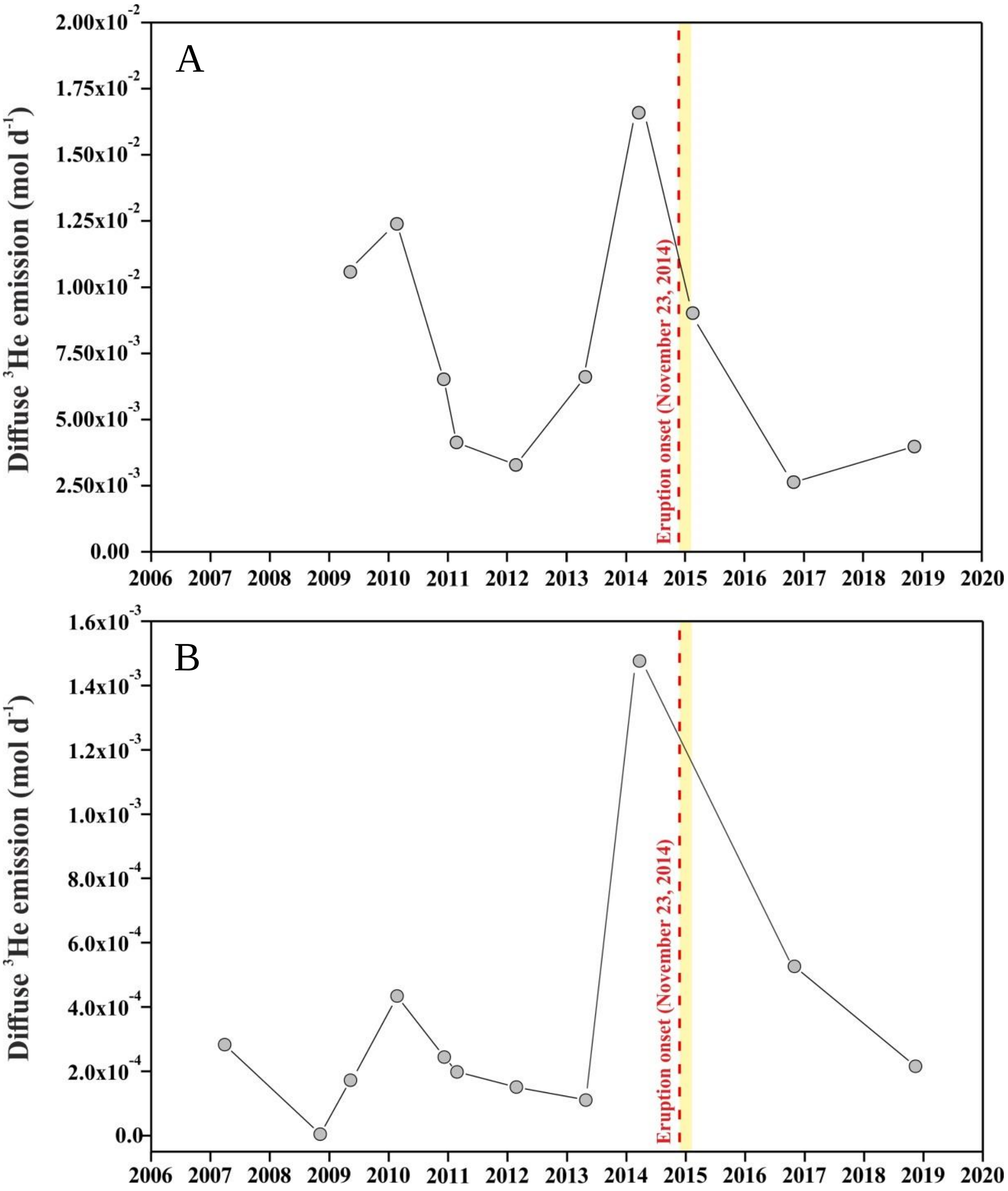

Figure 33. *A) Temporal evolution of ^{3}He emission calculated by multiplying the ^{4}He emission by ^{3}He/^{4}He molar ratio measured in the fumarole, and B) temporal evolution of ^{3}He emission calculated by multiplying the diffuse CO_2 emission by the ^{3}He/CO_2 ratio measured in the fumarole. The red dashed line indicates the eruption onset on November 23, 2014, and the yellow bar represents the eruptive period (November 23, 2014 to February, 7, 2015).*

The results obtained by the two methodologies confirm the occurrence of an increase in the mantle He released in the 2009-2010 period and another significant mantle contribution in 2014, several months before the eruption onset. These variations prior to the eruptive period are also supported by the changes observed in the chemical composition of the Pico do Fogo fumaroles studied by Melian et al, (2021), since the injection of deep-origin fluids is also reflected in the CO_2 content. , CH_4, CO and H_2 as well as in the isotopic signature of C from fumaroles. The rapid decrease in the emission after the eruptive event may be due to the drop in the gas pressure within the volcanic body, as a result, a decrease in the diffuse degassing through the volcanic edifice an in the magmatic component of the gas that feeds the fumarole activity (Notsu et al., 2006).

A good correlation was observed between the diffuse ^{4}He and ^{3}He emission values and the diffuse CO_2 emission as shown in Figure 34, as those periods when higher CO_2 emissions were measured, higher emission rates of both helium isotopes are also observed.

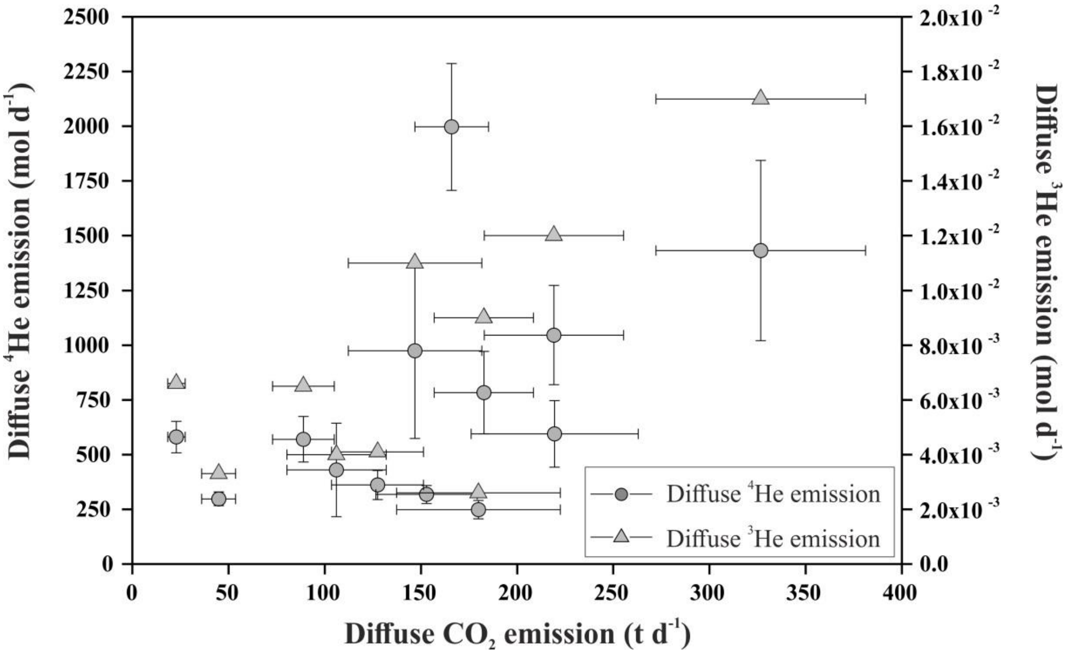

Figure 34. *Correlation between the diffuse CO_2 emission (t d^{-1}) and diffuse ^{4}He and ^{3}He emission rates measured at Pico do Fogo during the study period.*

4.2.4. Thermal energy released

The results of the thermal energy released estimated by the methodology pointed out by Chiodini et al., (2005) are reported in Table 4. The thermal energy release ranged from 1 MW, calculated in February 2011 period, to a maximum of 72 MW calculated in March 2014. Figure 35 depicts the temporal evolution of the thermal energy release and shows three peaks with 6, 8 and 72 MW values, corresponding to November 2008, February 2010 and March 2014 respectively. The drastic change in the trend from 4.8 MW calculated for April 2012 to 71.6 MW for March 2014 is likely due to the rise of magma to the surface, resulting in an increase in the heat released by the volcanic system.

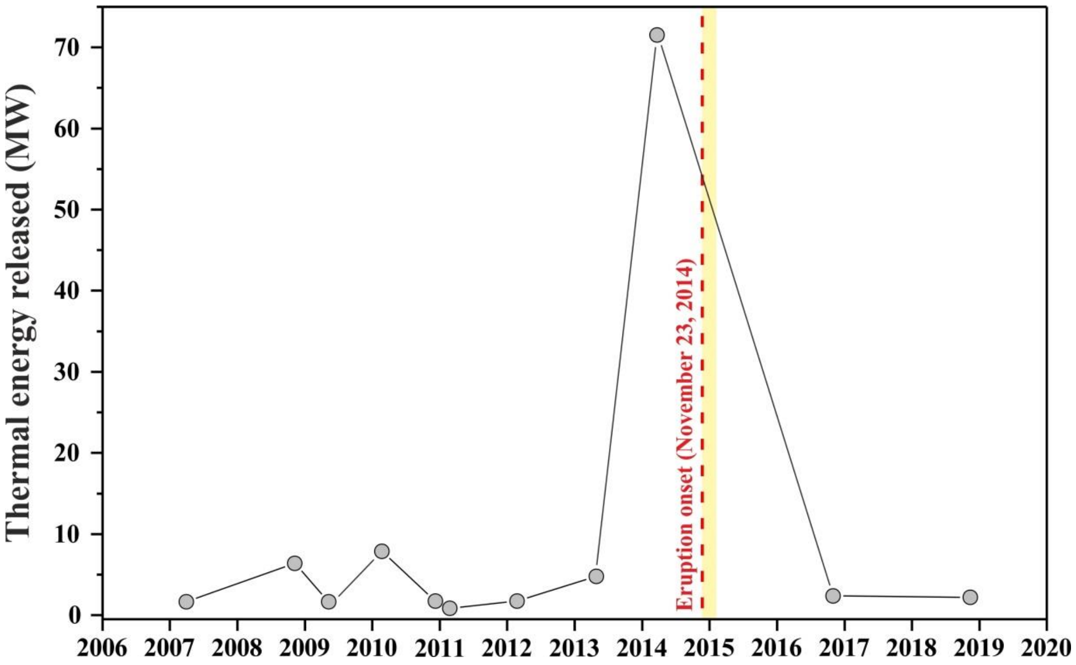

Figure 35. *Time series of thermal energy released (MW) from March 2007 to November 2018. The red dashed line indicates the eruption onset on November 23, 2014, and the yellow bar represents the eruptive period (November 23, 2014 to February, 7, 2015).*

Although coeval variations in the magmatic He emission and thermal energy output in 2010 and 2014 are shown, the magnitude of the precursory signals was different: while the obtained ^{3}He and magmatic ^{4}He emission rates in 2010 and 2014 were similar, there was a clear difference in one order of magnitude in the thermal energy released (8 and 72 MW for 2010 and 2014 periods respectively). This observation suggests the He/heat ratio could provide a discriminating indicator between magmatic intrusions capable to reach the surface and induce a volcanic eruption. Therefore, in volcanoes that present an active crater with surface volcanic-hydrothermal manifestations, precursory changes in ^{3}He emission should be accompanied by an increase in the thermal energy released, resulting in a volcanic eruption.

4.2.5. Model for He emission and thermal energy temporal evolutions in Fogo volcanic system

A conceptual model for the evolution of He and thermal energy in Pico do Fogo volcanic system during the study period has been presented in Figure 36. This model explains the observations in the years leading-up to, during and after the eruptive event:

1. To November 2008 Fogo volcanic system is in an inter-eruptive period during which no anomalous geochemical signals were observed. The magmatic source of the gas was located in a magma reservoir in the uppermost mantle at 24-30 km depth, according to geochemical data measured from erupted rocks by Klügel et al. 2020.
2. During November 2008-2010 period significant increases in ^{3}He/^{4}He isotopic ratio, diffuse ^{4}He and ^{3}He emissions and in the thermal energy released were observed. The geochemical signals suggest the reactivation of the volcanic system accompanied by a magmatic intrusion hosted close to the MOHO (~12-13 km depth) in the magma accumulation zone (Klügel et al. 2015).

3. During 2011-2010 period, a significant and simultaneous decrease in the parameters was observed, suggesting the magmatic intrusion of phase 2 ended.
4. During 2013-June 2015 period there is a resumption of primitive magma input, again accumulating close to the MOHO. During this second ascent the magma broke through a complex storage region, possibly an interconnected network of dikes/sills where part of the magma passed through, and part was stored (Klügel et al., 2020). The size of the MOHO-magma-accumulation zone had increased due to an increasing number of emplaced intrusions (Klügel et al., 2015). After breaking through the storage region, the magma rise rapidly through the crust and reached the surface on November 23, 2014. Prior to the eruptive period (November 23 to February 7) maximum values during the study period of 8.63 R_A, 1.7 × 10^{-2} mol d^{-1}, 1.5 × 10^{-3} mol d^{-1} and 71.6 MW were observed for $^3He/^4He$ isotopic ratio, diffuse ^3He emission and thermal energy released respectively. Although diffuse ^4He emission maximum value (1997 mol d^{-1}) was observed during the eruptive period, the biggest increase in the rate of change was observed prior to the eruptive event, in agreement with the other measured parameters.
5. From June 2015, after the eruptive event, a dramatic decrease was observed simultaneously in all the parameters, due to efficient degassing of the magma responsible for the eruption, beginning a new inter-eruptive period in Pico do Fogo volcanic system.

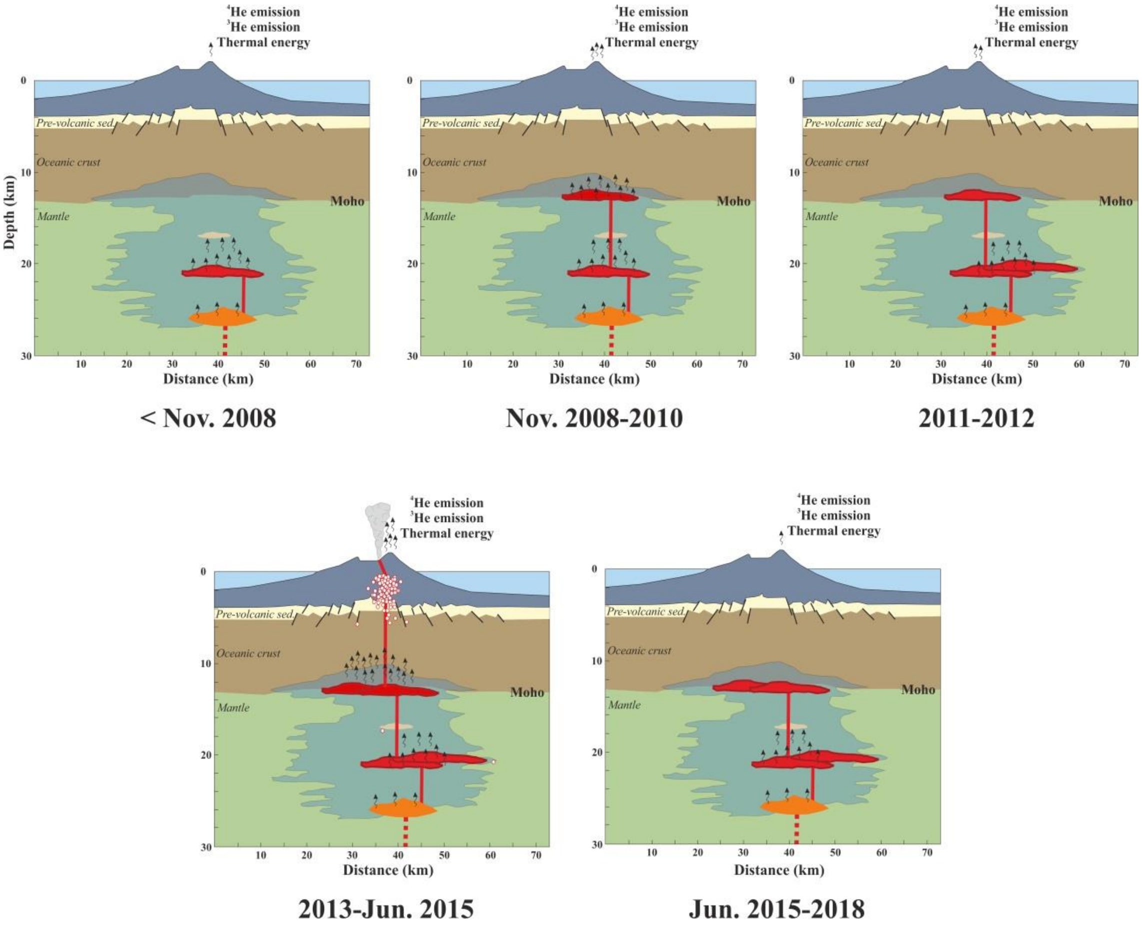

< Nov. 2008

Nov. 2008-2010

2011-2012

2013-Jun. 2015

Jun. 2015-2018

Figure 36. *Conceptual model of the observed changes in diffuse ^{3}He and ^{4}He emissions and thermal energy during the study period for Pico do Fogo volcanic system. Modified from Klugel et al., 2020.*

4.3. Furnas volcano

A soil gas emission survey of 272 measurement sites were selected at Furnas caldera (Azores) in May 2018, covering an area of 6.155 km^2. The average distance between points was 150 meters except in those areas where anomalies in soil temperature and degassing was observed. The distance between measurement points was 25 and 40 meters for the areas on Lagoa das Furnas lake shore and Caldeiras village respectively (Figure 37). This difference in spacing between the sites helps us to a better delimitation of the anomalies and thus to obtain a more accurate quantification of the degassing rate. In addition, gas samples were taken from two low-temperature fumaroles, one located in Caldeiras village with a temperature of 98.9ºC and the other on the shore of Lagoa das Furnas with a temperature of 98.6ºC.

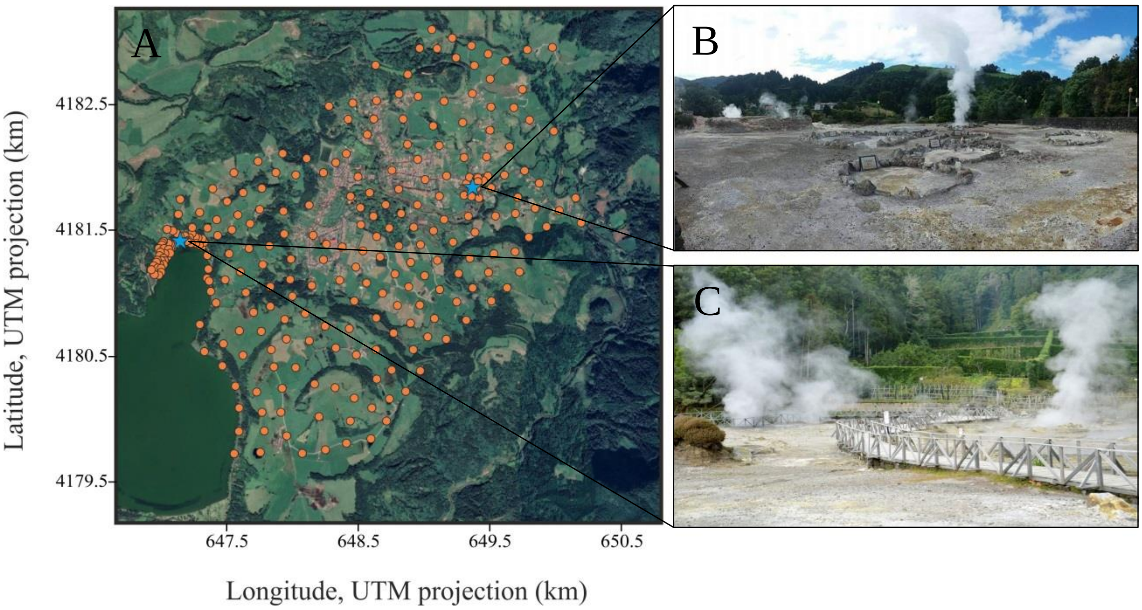

Figure 37. *A) The 272 measurement sites performed in each survey in Furnas volcano. Orange dots represent the measurement sites performed in each survey and the sampled fumaroles are marked by a blue star. B) Image of fumaroles in Caldeiras village and C) Image of the fumaroles located in the shore of Lagoa das Furnas.*

The data obtained during the Furnas caldera survey are reported in Table 6. At each sampling site, surface gas was collected and analysed later in the laboratory. The chemical composition of the soil gas is reported in Table 7.

4.3.1. Diffuse CO_2 efflux and soil temperature

Diffuse CO_2 efflux values in Furnas caldera ranged from 0.63 to 2,253.75 g m^{-2} d^{-1} with an average value of 63.62 g m^{-2} d^{-1} for the survey. A probability plot technique (Sinclair, 1974) has been applied to distinguish between the different sources feeding the CO_2 emission values at Furnas caldera (Figure 38).

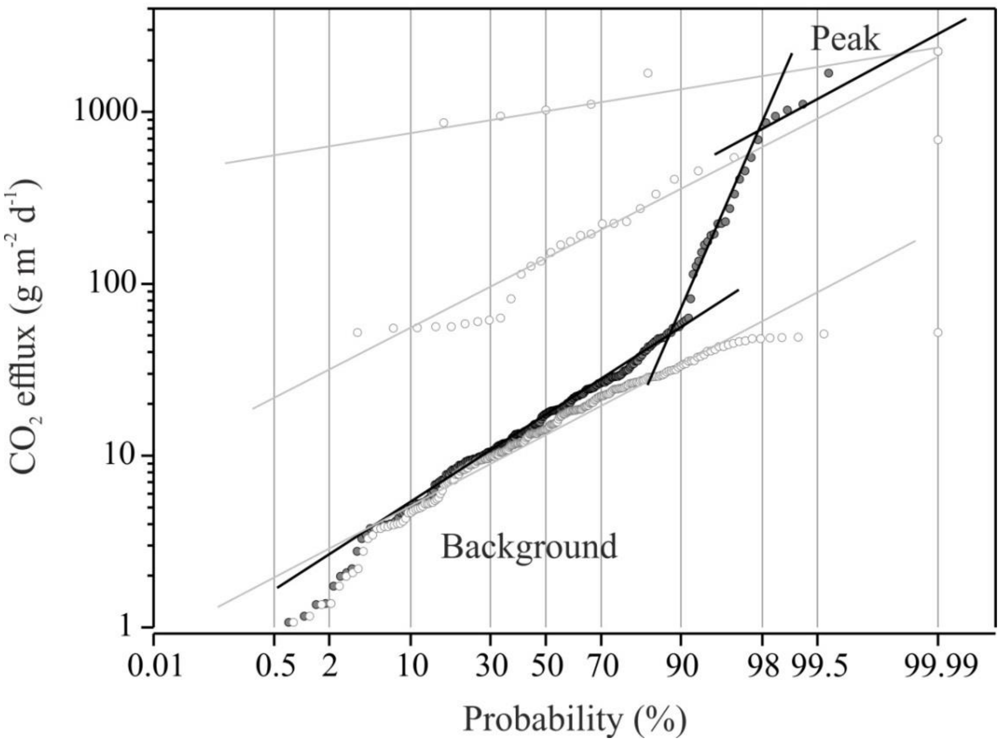

Figure 38. *Probability plot of the CO_2 efflux data measured at Furnas volcanic-hydrothermal system. Black lines indicate different log-normal geochemical population in the original data and grey lines indicate the separate background and peak populations.*

Two Log-normal populations have been found, background and peak, showing different contribution of shallow sources of CO_2 (i.e. biological activity) and an endogenous sources respectively. The background population has an average of 13.11 g m^{-2} d^{-1} and represents the 88% of the total data, while the peak population has an average of 1,019.52 g m^{-2} d^{-1} and represents the 2%. The data regarding the probability plot technique (Sinclair, 1974) has not been previously published.

The total diffuse CO_2 output released from Furnas caldera was calculated as 270 ± 29 t d^{-1} for an area of 6.16 km^2. Diffuse CO_2 emission map (Figure 39) shows higher values located both on the northern shore of Lagoa das Furnas lake and in the area of the town known as Caldeiras, where, in addition to the highest CO_2 emissions, hydrothermal alteration of the soil and visible gas emanations (fumaroles and bubbling gases) occur. The areas with high CO_2 effluxes are correlated with the areas where high soil temperatures are observed (Figure 40), suggesting a strong convective circulation of the gases. The spatial distribution of diffuse CO_2 emission and soil temperature at 40 cm depth have not been previously published.

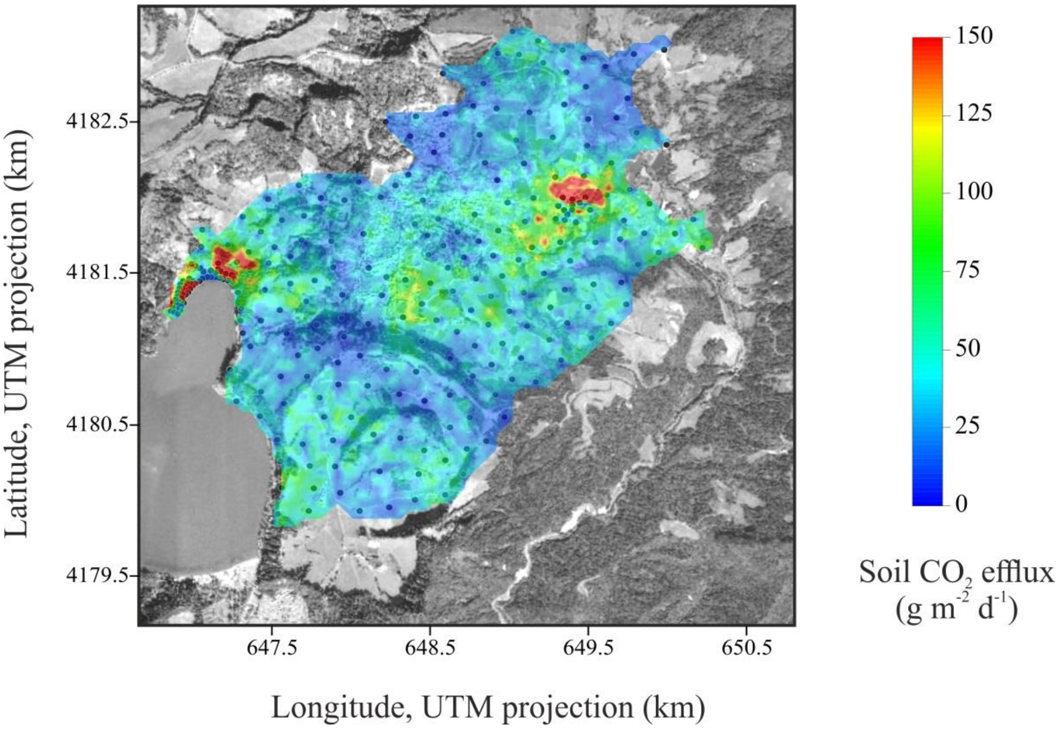

Figure 39. *Diffuse CO_2 emission map of Furnas caldera area.*

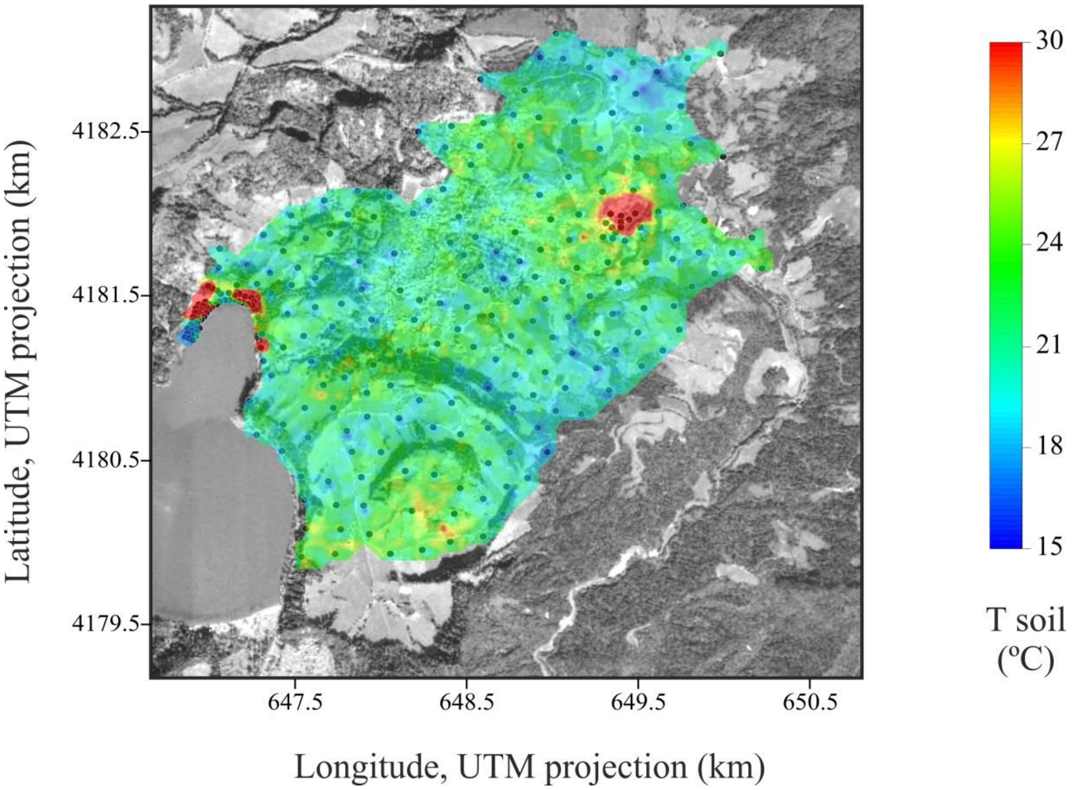

Figure 40. *Spatial distribution of the soil temperature at 40 cm depth in Furnas caldera area.*

4.3.2. Origin of the CO_2

A binary diagram has been constructed representing $\delta^{13}C(CO_2)$ vs. $1/[CO_2]$ ($ppmV^{-1}$) to investigate the contribution of the different CO_2 sources at Furnas caldera (Figure 41). The possible sources are as follows: atmospheric CO_2, characterized by $\delta^{13}C(CO_2)$ = -8‰ and $[CO_2]$ = 0.04%, deep-seated CO_2 with $\delta^{13}C(CO_2)$ = -4.05 ‰ (Ferreira and Óskarsson, 1999) and $[CO_2]$ = 100% and biogenic CO_2 with $\delta^{1}3C(CO_2)$ = -20.6‰ and $[CO_2]$ = 100%. The binary diagram representing $\delta^{13}C(CO_2)$ vs. $1/[CO_2]$ ($ppmV^{-1}$) has not been previously published.

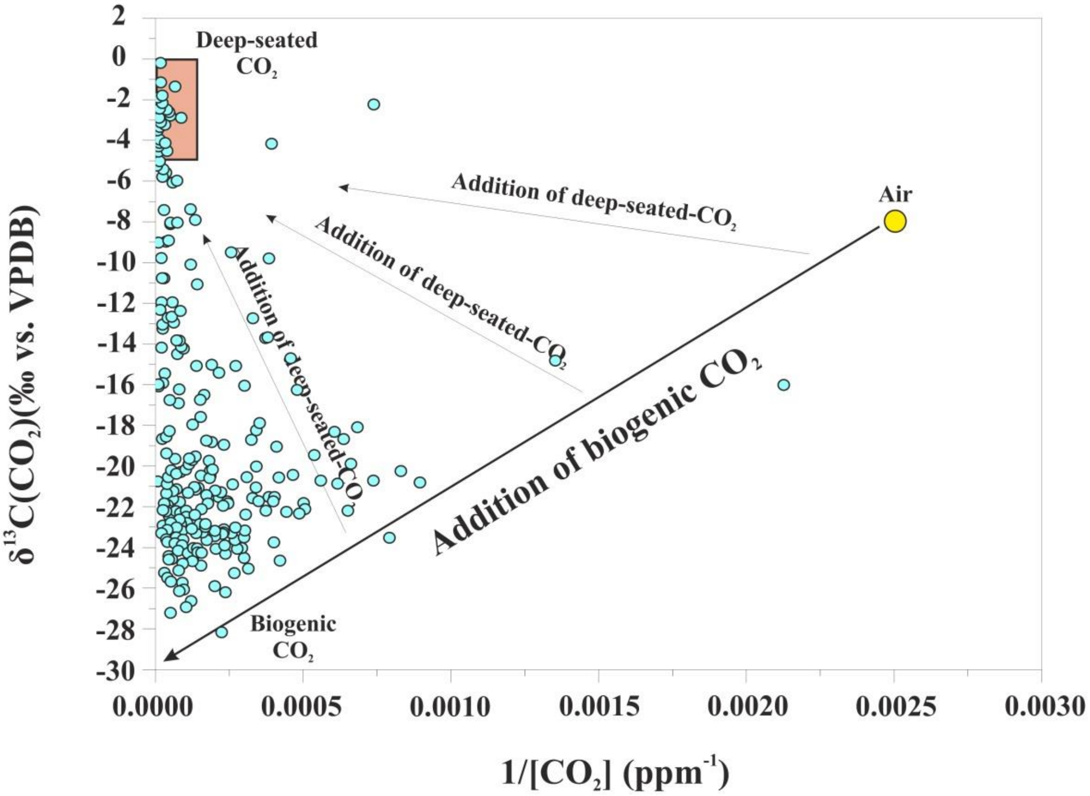

Figure 41. *Plot of $\delta^{13}C(CO_2)$ vs. 1/[CO_2] ($ppmV^{-1}$) data from Furnas caldera in which possible geochemical reservoirs are shown. Mixing trend between biogenic, air-derived and deep-seated CO_2 is represented by straight lines.*

Figure 41 depicts that most of the samples showed CO_2 composition reflecting different degrees of mixing between deep-seated CO_2 and biogenic CO_2, and with a minor mixture of atmospheric CO_2. The heaviest $\delta^{13}C(CO_2)$ values, indicatives of deep seated CO_2, were measured close to the fumarolic fields in the northern shore of Lagoa das Furnas lake and in the Caldeiras village. There is an important biogenic contribution due to the extensive vegetation and soil respiration in the vast majority of the study area. Viveiros et al. (2010) reported $\delta^{13}C(CO_2)$ values from -12.28‰ to -3.11‰ for Furnas volcano, confirming the hydrothermal system and the biological activity as sources of the CO_2.

4.3.3. $^3He/^4He$ isotopic ratio

$^3He/^4He$ isotopic values reported by other authors have been used. He isotopic data from Furnas volcanic system ranged from 5.23 to 6.07 R_A with an average of 5.59 R_A (Jean-Baptiste et al. 2009). This values represents a mixture between a plume-source, represented by high $^3He/^4He$ values measured on the island of Terceira (~9.6 R_A), and a crustal source with a contribution of approximately 45% of radiogenic helium (Caliro et al., 2015). The crustal component explains the $^3He/^4He$ isotopic ratio for Furnas samples, significantly lower than expected for a mantle origin. The spatial distribution of $^3He/^4He$ isotopic ratio indicates the mantle plume´s head underlies the central part of the Azores archipelago (Jean-Baptiste et al. 2009).

4.3.4. Diffuse ^4He emission

The diffuse ^4He emissions estimated at Furnas caldera area according to the first approach (see Methodology section) ranged from 0.63 to 2,253.75 g m^{-2} d^{-1}. The following data were used: ambient temperature ranging from 17.0 to 30.1 ºC, soil at 40 cm depth temperature ranging from 15.2 to 98.5 ºC, soil ^4He concentration ranging from 5.24 to 43.38 ppm, the hydraulic permeability ranging from 9.06×10^{-11} to 9.81×10^{-7} m s^{-1}, diffusion coefficient of 7×10^{-5} m^2 s^{-1} and soil porosity of 0.35 (Carapezza et al. 2004). Convective was the main gas movement mechanism governing the study area. The total diffuse ^4He output from the studied area was estimated in 1.37 ± 0.16 kg d^{-1} (342.79 mol d^{-1}), with the highest values observed where fumarolic activity is present, in the northern shore of Lagoa das Furnas lake, in Caldeiras village and in the southern section of the study area, in agreement with the highest soil temperatures and CO_2 efflux values (Figure 42).

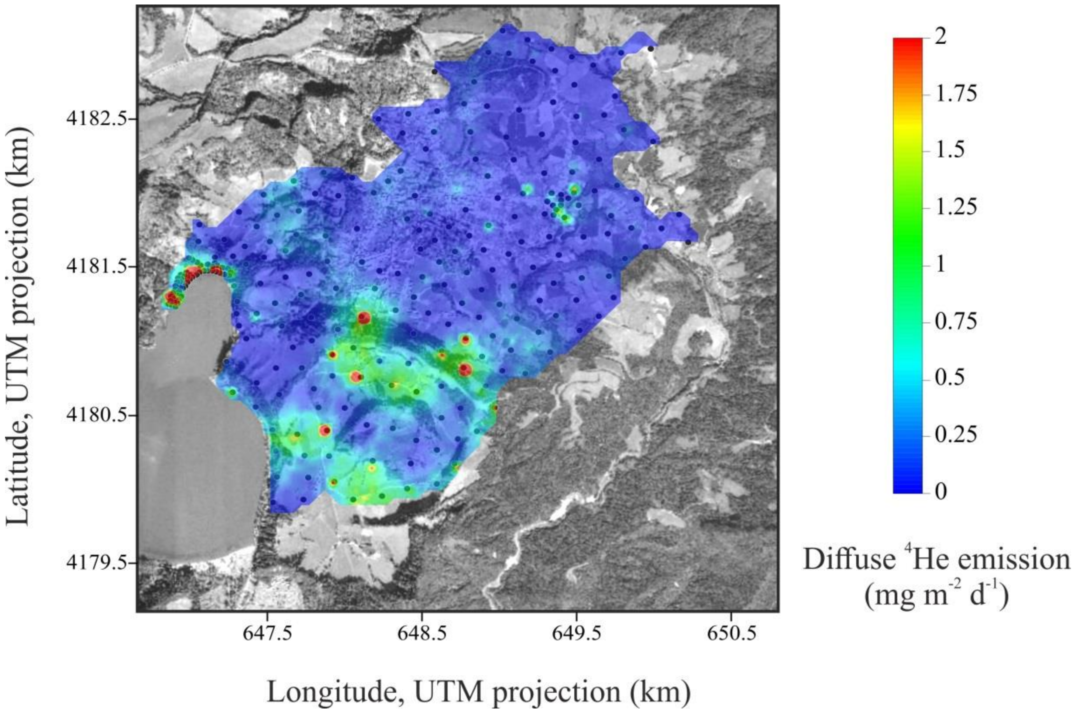

Figure 42. *Diffuse ^{4}He emission map for Furnas caldera.*

4.3.5. Diffuse ^{3}He emission

Diffuse ^{3}He emission has been calculated using the two methodologies explained in the “Methodology” section:

- Assuming the ^{3}He/^{4}He ratio measured in the fumarolic discharge is the same for the whole hydrothermal system and using the ^{4}He emission calculated before, the diffuse ^{3}He emission for Furnas caldera area was 2.65×10^{-3} mol d^{-1} (0.97 mol y^{-1}). As was explained before, the estimated diffuse ^{3}He emission might be overestimated due to the addition of radiogenic ^{4}He.
- Assuming that the CO_2 efflux is wholly derived from a deep seated source, diffuse ^{3}He emission for Furnas caldera area was estimated in 3.76×10^{-4} mol d^{-1} (0.14 mol y^{-1}). As was explained before, the diffuse ^{3}He estimated according to

the second approach, might underestimated due to some amount of that deep-seated CO_2 would have been trapped by ground water during its ascent to the surface.

4.3.6. Thermal energy released

The thermal energy released by Furnas caldera area was 141.9 MW using the Chiodini et al. (2005) method and 31.7 ± 6.5 MW using the Dawson (1964) method. As was explained before, the difference in the two estimations might be due to assumption that H_2O/CO_2 molar ratio measured in the fumarolic discharge is the same for the entire area studied within the volcanic system. As we are comparing areas with a strong convective component such as the northern area of Lagoa das Furnas Lake or Caldeiras village with purely diffusive areas in which no visible hydrothermal manifestation appears, the mentioned approach likely have important limitations. In the heat flow distribution map, the areas with highest values occurred in and around the fumarolic areas in Lagoa das Furnas Lake and Caldeiras village and in the southern part of the study area. (Figure 43). In a similar work, Viveiros et al., (2010), estimated a value of 118 MW by means of the Chiodini et al. (2005) method, close to the 141.9 MW obtained in this work. The calculated values following Dawson (1964) and the spatial distribution of the heat flow in Furnas caldera area have not been previously published.

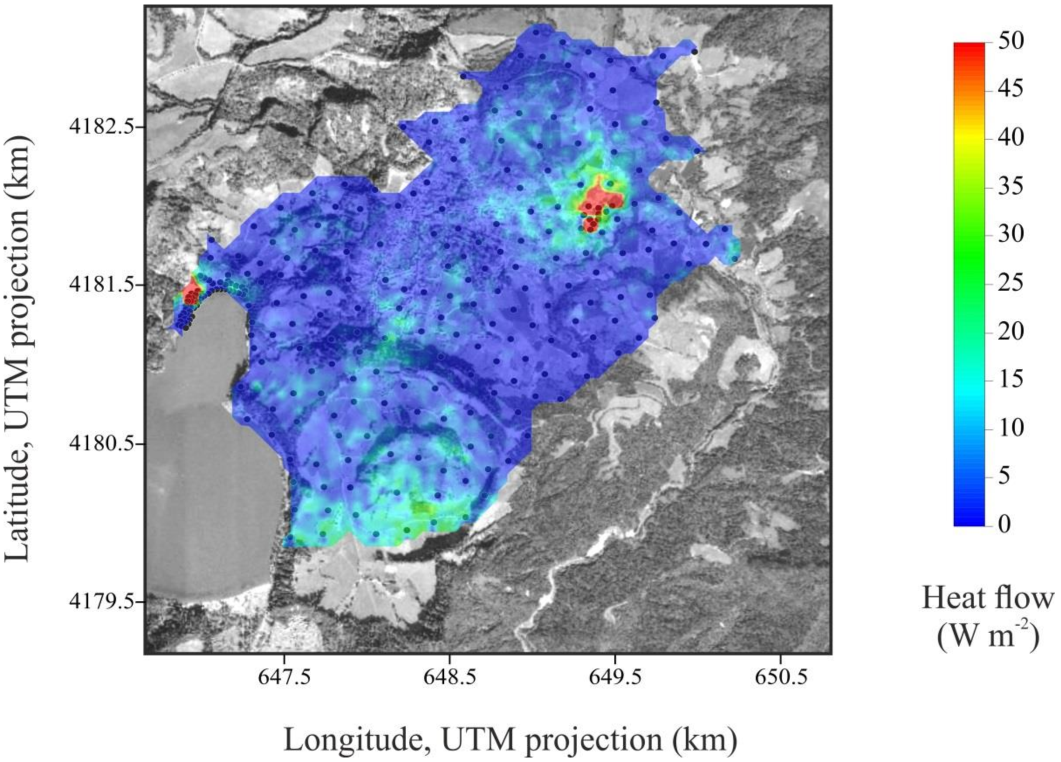

Figure 43. *Thermal energy emission map for Furnas caldera area.*

4.4. Other volcanic systems to study

In Table 8 shows a summary of data obtained from the literature in different volcanic systems around the world among the data previously reported in this work for the volcanic systems of Teide, Pico de Fogo and Furnas. The volcanic systems added in this study are Cerro Negro volcano (Nicaragua), Poás volcano (Costa Rica), Solfatara (Campi Flegrei, Italy), Reykjanes geothermal area and Hengill volcano (Iceland), Mud volcanoes (Yellowstone, United States), Las Máquinas, Las Maquinitas, Termas and Anfiteatro (Caviahue-Copahue volcanic system, Chile-Argentina), Ischia Island, Vesuvius volcano, Vulcano Island and Pantelleria volcano (Italy) and Nisyros volcano (Greece).

4.4.1. ^{3}He/^{4}He isotopic ratio

The ^{3}He/^{4}He isotopic ratios of the volcanic systems reported in Table 8 are described below.

- At Teide volcanic system, ^{3}He/^{4}He varies from 5.27 to 7.57 R_A, with a mean value of 6.91 R_A. These measured values are consistent with those measured by Perez et al. 1994, who obtained a value of 7.21 R_A from the summit crater fumarolic area. These values suggest a mixture of an upper mantle (MORB) and atmospheric sources for Teide volcanic system (Pérez et al., 1996), and probably with some minor contribution of radiogenic ^{4}He.
- ^{3}He/^{4}He isotopic ratios for Cerro Negro and Poás volcanoes ranged between 3.54 and 7.46 R_A and 7.14 R_A respectively. These values can be explained by a mixture of two components, MORB ~8.00 R_A and radiogenic ≤ 0.10 R_A. Other authors obtained ^{3}He/^{4}He isotopic values ranging from 6.7 to 7.6 R_A suggesting a proportion of mantle helium between 84 and 95% (Hilton et al., 2010) and ^{3}He/^{4}He values from 6.5 to 7.22 R_A (Fischer et al., 2015) at the fumaroles of Poás volcano. The high proportion of mantle-helium in Central America volcanoes is likely due to the rapid magma ascent from the mantle, limiting crustal ^{4}He contamination (Shaw et al., 2006, Battaglia et al., 2018).
- At Solfatara ^{3}He/^{4}He isotopic ratio values vary from 2.96 to 3.05 R_A. These ratios are higher than those of the atmospheric but significantly lower than that of the upper mantle, suggesting a mixing between upper mantle He (8.00 R_A) and crustal He ($\leq$ 0.10 R_A), with a proportion of mantle He of 40% at most (Tedesco et al., 1990). These lower ratios may be due both to a weak contribution of mantle He, a strong dilution of the mantle fluids with radiogenic ^{4}He from the crust, the radioactive

"aging" of an isolated magmatic chamber or to a particular characteristic of the local mantle (Tedesco et al., 1990). In contrast, Martelli et al. (2004) suggest that the low ^{3}He/^{4}He isotopic values reflect the composition of the mantle beneath the Roman Comagmatic Province. According to the authors, this mantle enriched in the radiogenic component has formed from the mixing of an astenospheric mantle source and the contribution of metasomatic fluids and postmetasomatic radiogenic growth in the wedge, suggesting that the last stages of subduction are fundamental in mantle domains production with a ^{3}He/^{4}He isotopic values lower than the MORB.

- At the Icelandic volcanic systems, ^{3}He/^{4}He isotopic ratio values are 14.42 and 13.73 R_A for Reykjanes and Hengill respectively. These values, much higher than MORB, indicate a mixture of two components, MORB He (8.00 R_A) and deep-mantle- plume He (> 29.00 R_A). The highest ^{3}He/^{4}He $(R/R_A)_{\mathrm{cor}}$ isotopic ratio measured in Iceland is located in the Köldukvislarbotnar fumaroles, with 26.00 R_A, indicating the centre of Icelandic mantle plume (Poreda et al., 1992).
- At Yellowstone Mud volcanoes, a maximum ^{3}He/^{4}He isotopic ratio of 16.5 R_A are reported by Chiodini et al., 2012. This value represents a mixture between two source components, the depleted upper mantle (MORB R_A = 8.00) and the less depleted lower mantle (Hawain-like R_A = 35) (Werner and Brantley 2003). 16.5 R_A from Mud Volcanoes is the highest value in this work.
- In Caviahue-Copahue volcanic system the ^{3}He/^{4}He isotopic ratio varies from 4.93 to 7.04 R_A (Chiodini et al., 2015). Agusto et al., 2013 also measured values of up to 7.94 R_A in this volcanic system. These values, close to that of MORB, are indicators of an ascent of the upper mantle due to the transtensional tectonism of the study area, which causes a thinning of the crust. The lowest ratios measured (≤ 5.00 R_A) are due

to contamination through local active fault systems from a shallow source (Agusto et al. 2013).

- In the west fumaroles of Ischia volcanic island the mean value of ^{3}He/^{4}He isotopic ratio is 3.63 R_A (Tedesco et al., 1996). This ratio is higher than the atmospheric (R_A ~ 1.00) and the crustal-He (≤ 0.10 R_A) and lower than the MORB value (R_A = 8.00) suggesting that although ~50% of the helium has a magmatic origin accompanied by contamination of radiogenic He (Tedesco et al., 1996). Other authors obtain a similar ^{3}He/^{4}He isotopic value of 3.36 R_A for Ischia island. However, as in the case of Solfatara, the radiogenic contamination occurs due to the enriched in the radiogenic component mantle beneath the Roman Comagmatic Province (Martelli et al., 2004).
- A mean value of 3.19 R_A are reported by Tedesco et al., 1998 for Vesuvius volcano. The authors suggest the following processes as responsible for the radiogenic ^{4}He enrichment: 1) radiogenic ^{4}He from the subduction of U-Th- rich continental sediments, 2) emplacement of the magma in the Mesozoic carbonate basement (3-5 km depth) before the eruption and 3) fractionation of the ^{3}He leaving a residual magma with a low ^{3}He/^{4}He due to magma aging. Martelli et al. (2004) report a ^{3}He/^{4}He value of 2.48 R_A for Vesuvius volcano, and propose, as in the case of other volcanic systems belonging to the Campanian magmatic province, that radiogenic contamination occurs due to the composition of the local mantle beneath central Italy.
- Tedesco and Scarsi, (1999) reported a ^{3}He/^{4}He isotopic value of 6.20 R_A for Vulcano volcanic Island. This value is similar to the range between 6.0-6.5 R_A proposed for the European Sub-Continental Mantle (ESCM) (Dunai and Baur, 1995), a value

lower than that proposed for the MORB (8.00 R_A) due to contamination by the radiogenic ^{4}He.

- On Pantelleria volcanic island, Parello et al., (2000) obtained a mean value of 7.33 R_A for the Favara fumarole, being the highest value measured in volcanic or hydrothermal gases in Italy. This value suggests a mixture of a magmatic source (8.00 R_A) as the origin of the fluids slightly contaminated by radiogenic ^{4}He ($\leq$ 0.10 R_A). Fourré et al. (2012) obtained a similar value of 7.6 R_A for ^{3}He/^{4}He isotopic ratio from Pantelleria island. As observed is the highest R_A value than the other volcanic systems in southern Italy due probably to the distensive tectonics existing in the Sicily Channel and a lower contamination by the regional subduction process (Parello et al., 2000).
- ^{3}He/^{4}He isotopic ratio measured in the fumaroles of Nisyros volcanic island is between 5.34-6.24 R_A, with a mean value of 5.88 R_A (Shimizu et al., 2005). The 6.24 R_A maximum value measured at Nisyros is slightly lower than that proposed for the MORB due to the existence of a subcontinental lithospheric mantle (SCLM) beneath the Aegean arc, where the ^{3}He/^{4}He ratio is more evolved towards more radiogenic values (Shimizu et al., 2005).

In all the volcanic systems studied in this work, ^{3}He/^{4}He isotopic ratios are above the atmospheric value (R_A = 1.00), which indicates a magmatic source as the origin of the fluids, accompanied by a greater or lesser radiogenic contribution depending on the volcanic system.

4.4.2. Diffuse He isotopes emissions and ^{4}He spatial distribution

The calculated diffuse ^{4}He and ^{3}He emissions for each studied volcanic system are reported in Table 8 and described as follows. Diffuse ^{4}He emissions and ^{4}He spatial distribution maps from Teide cone, Fogo crater and Furnas caldera have already been described in previous sections.

- At Teide summit cone in the study period from 2007 to 2013 the values varied between 57 ± 17 and 2,147 ± 536 mol/d and between 33 and 452 mol/d for diffuse ^{4}He emission by the first and the second approaches, respectively. Diffuse ^{3}He emission values ranged from 3.18×10^{-4} to 4.47×10^{-3} mol/d. The area of Teide summit crater contributed with values ranging from 8 ± 1 to 296 ± 88 mol/d of diffuse ^{4}He emission calculated by the first method and from 2 to 41 mol/d by the second method. Diffuse ^{3}He emission in the summit crater varied from 2.12×10^{-5} to 3.83×10^{-4} mol/d in the study period. Teide summit cone survey cover an area of 0.5 km^{2} while the area corresponding to Teide summit crater is 0.007 km^{2}. The spatial distribution of diffuse ^{4}He emission for Teide summit crater (Figure 44) shows that the ^{4}He flux anomalies are concentrated mainly inside the crater, close to the fumarolic fields.

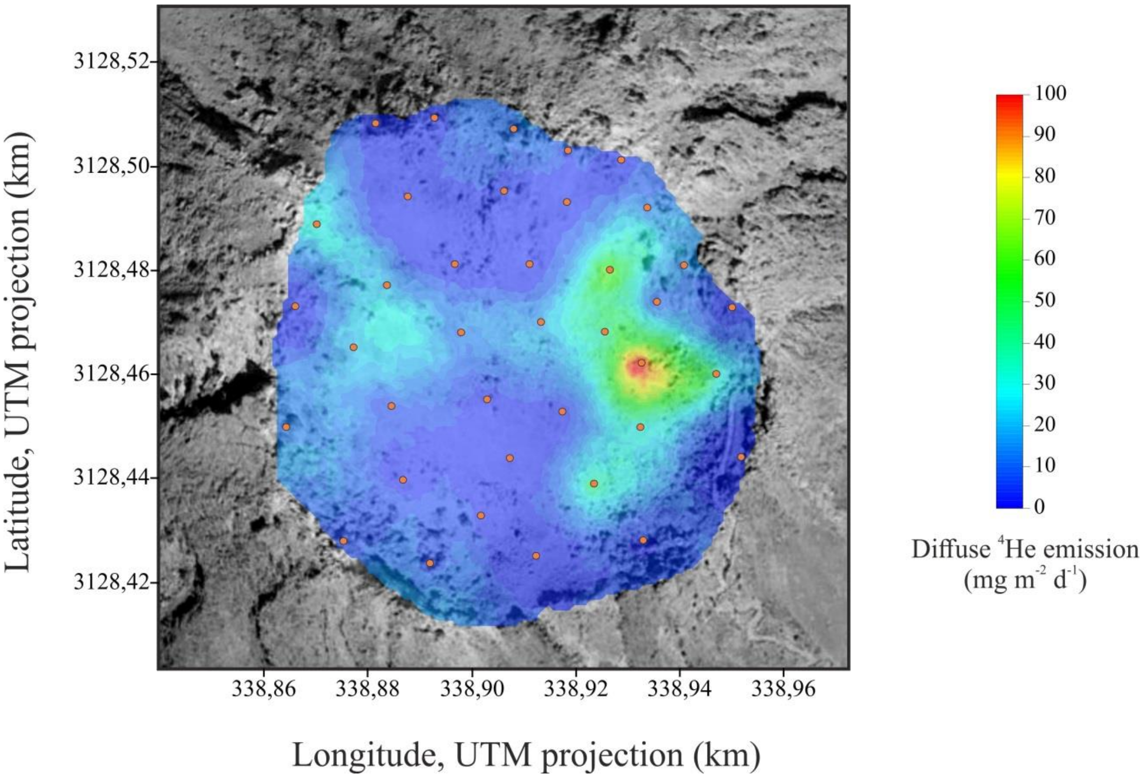

Figure 44. *Spatial distribution of diffuse* ^{4}*He emission of Teide summit crater. Orange dots indicate the sampling sites.*

- The emission values of diffuse ^{4}He emission calculated by the second approach and diffuse ^{3}He emission for Cerro Negro cone are 2 and 9 mol/d and 2.40×10^{-5} and 4.40×10^{-5} mol/d respectively, for an area of 0.6 km^2. Cerro Negro volcano crater released 4,848 ± 924 and 161 ± 31 mol/d of diffuse ^{4}He calculated by the first approach and 2 and 4 mol/d calculated by the second approach, respectively. Diffuse ^{3}He emissions values were estimated in 1.56×10^{-5} and 1.93×10^{-5} mol/d for an area of 0.14 km^2. The spatial distribution of ^{4}He emission shows that highest ^{4}He diffuse flux values occur along the walls inside the main crater of the volcano and in some sectors at the bottom of the crater, where fumarole activity is present (Figure 45).

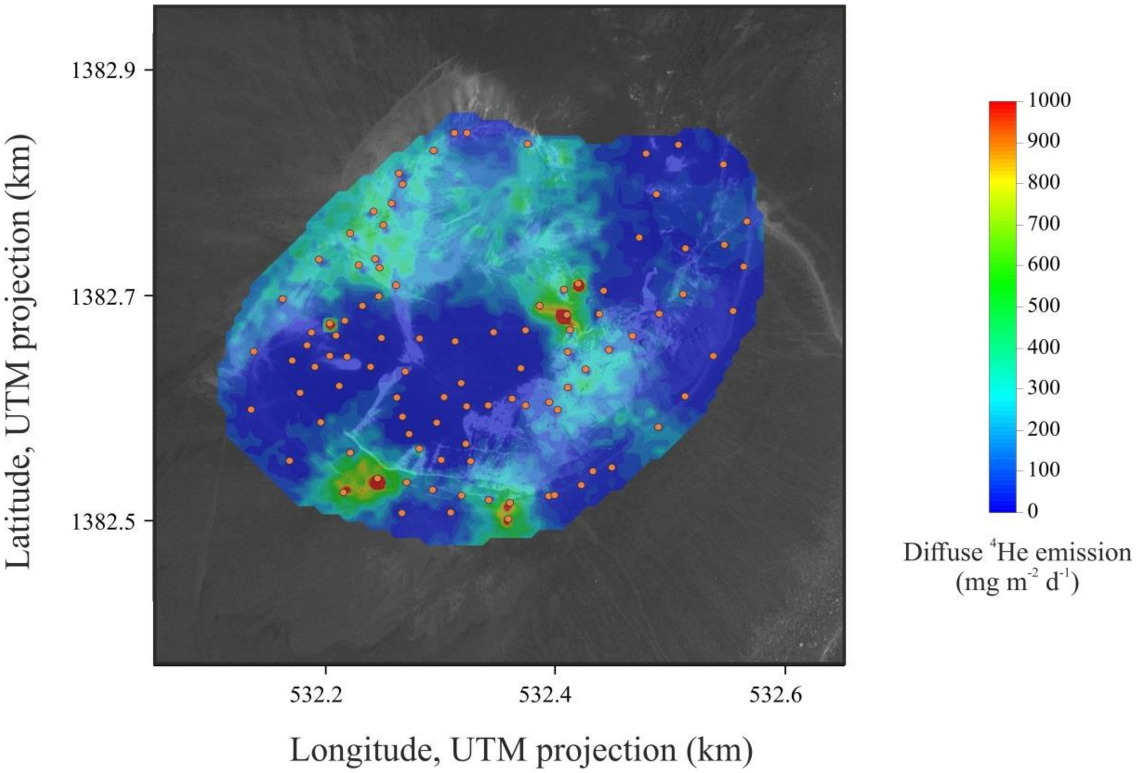

Figure 45. *Spatial distribution of diffuse ^{4}He emission of Cerro Negro crater. Orange dots indicate the sampling sites.*

- The diffuse ^{4}He emissions calculated for Poás volcano were 2,428 and 4 mol/d by the first and the second approach respectively. The diffuse ^{3}He emission was estimated in 3.58×10^{-5} mol/d for a study area of 0.86 km^2. According to the spatial distribution map (Figure 46), the highest ^{4}He diffuse emission values are located in the E zone of the crater, where the fumarolic activity is present and the highest temperatures and diffuse CO_2 fluxes are observed (Melián et al., 2019).

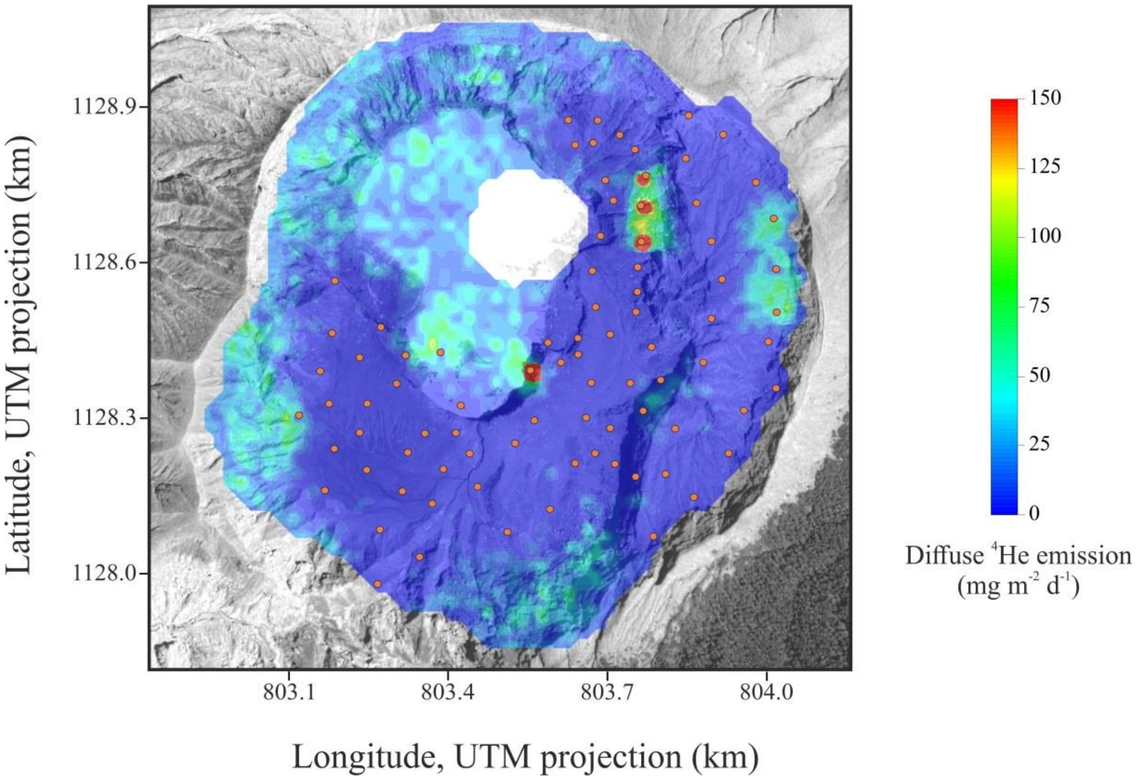

Figure 46. *Spatial distribution of diffuse* ^{4}*He emission of Poás crater. Orange dots indicate the sampling sites.*

- Diffuse ^{4}He emission for Solfatara calculated by the first approach yielded 2,799 ± 243 mol/d and 289, 60 and 285 mol/d by the second one. The obtained diffuse ^{3}He emissions were 1.22×10^{-3}, 2.46×10^{-4} and 1.20×10^{-3} mol/d for areas of 0.5, 0.1 and 0.62 km^2 respectively. The distribution map of diffuse ^{4}He in Solfatara (Figure 47) shows an anomaly in the NE area of study.

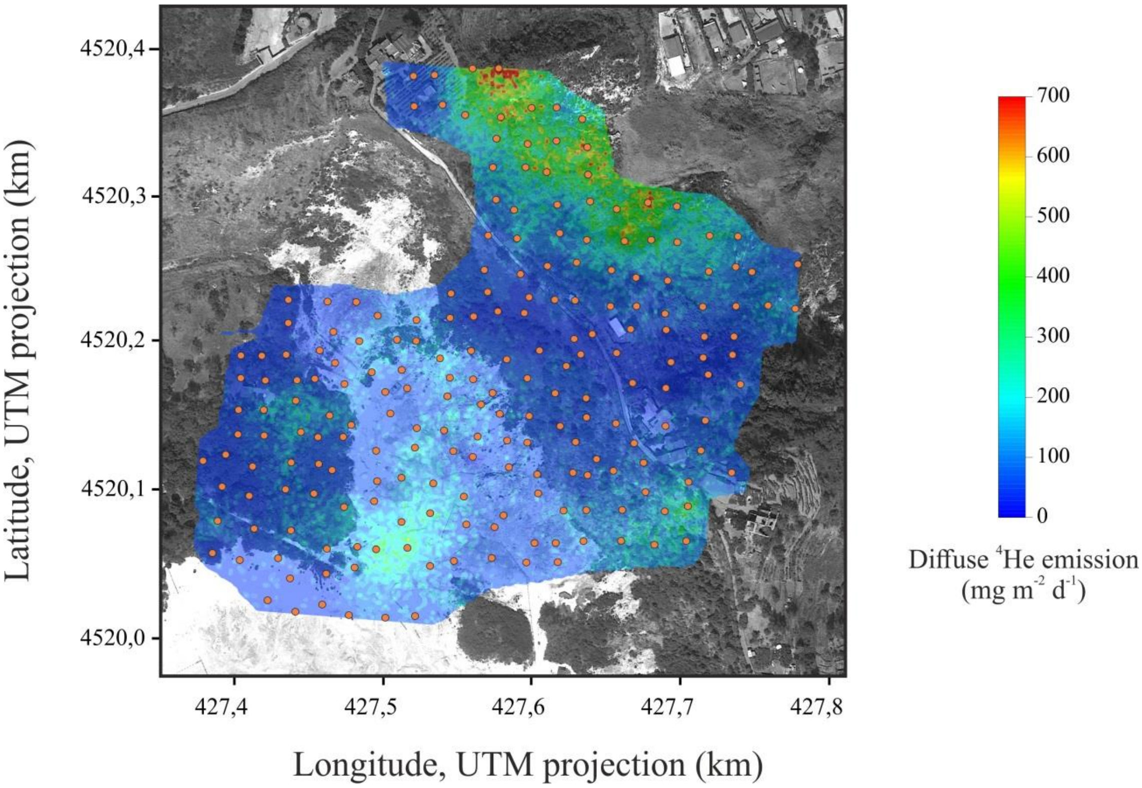

Figure 47. *Spatial distribution of diffuse ^{4}He emission of Solfatara. Orange dots indicate the sampling sites*

- The Reykjanes geothermal area (Iceland) showed a diffuse ^{4}He emission of 55 ± 11 mol/d and 21 mol/d calculated by the first and the second methods respectively, and a diffuse ^{3}He emission of 4.17×10^{-4} mol/d for an area of 0.225 km^2. In the distribution map of diffuse ^{4}He flux (Figure 48), the highest values are observed in the NW, centre and SE zone of the study area, in agreement with the anomalies in temperature, ^{4}He and CO_2 concentrations and diffuse CO_2 efflux observed by Fridriksson et al., (2016).

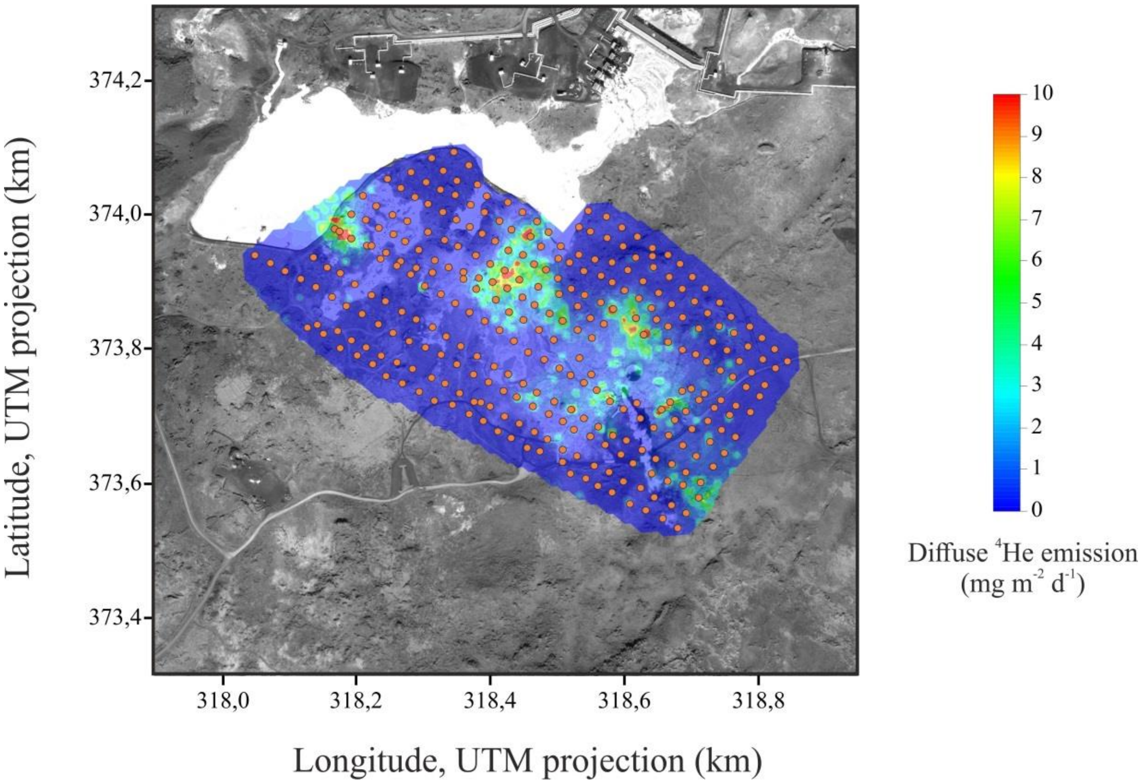

Figure 48. *Spatial distribution of diffuse ^{4}He emission of Reykjanes geothermal system. Orange dots indicate the sampling sites.*

- At Hengill geothermal area, diffuse ^{4}He and ^{3}He emission values were 500 mol/d calculated by the second approach and of 9.51×10^{-3} mol/, respectively, for a study area of 168.1 km^2.
- At Mud Volcanoes in Yellowstone, 1,554 and 3.55×10^{-2} mol/d of diffuse ^{4}He and ^{3}He were calculated respectively by the second approach.
- At Caviahue-Copahue volcanic system, diffuse ^{4}He and ^{3}He emissions in four different locations were calculated: Las Maquinas, Las Maquinitas, Termas and Anfiteatro, with areas of 0.321, 0.046, 0.033 and 0.576 km^2 respectively. The calculated diffuse ^{4}He emissions by the second approach are 14, 5, 34 and 25 mol/d respectively for the study areas with an average value of 19 mol/d and diffuse ^{3}He emission varies from to 4.86×10^{-5} mol/d released in Las Maquinitas area to the

maximum value of 3.27×10^{-4} mol/d released in Termas area. The average value of diffuse ^3He emission for the volcanic system is 1.7×10^{-4} mol/d.

- The calculated diffuse ^4He and ^3He emission values for Ischia volcanic island are 150 mol/d by the second approach and 7.56×10^{-4} mol/d respectively for 0.0576 km^2 of the study area.
- Vesuvius volcanic cone showed a diffuse ^4He calculated by the second approach and ^3He emissions of 15 and 6. $\times10^{-5}$ mol/d respectively calculated for an area of 0.331 km^2.
- At Vulcano volcanic Island the diffuse ^4He calculated by the second approach and ^3He emissions have been calculated for two areas: Vulcano crater with 437 and 3.75×10^{-3} mol/d and Spiaggia di Levante beach with 15 and 1.32×10^{-4} mol/d for areas of 0.415 and 0.0177 km^2 respectively.
- The calculated diffuse ^4He by the second approach and ^3He emissions for Pantelleria volcanic island are 31 and 3.10×10^{-4} mol/d respectively, for an area of 0.0577 km^2.
- In the case of the volcanic island of Nisyros, the diffuse ^4He calculated by the second approach and ^3He emissions were 28 and 2 $\times10^{-4}$ mol/d respectively.

4.4.3. Thermal energy released

Table 8 shows calculated thermal energy released by Chiodini et al., (2001) method described in “Methodology” section for each volcanic system.

4.5. Diffuse ^{4}He emission related to thermal energy released

The diffuse ^{4}He emissions calculated using the two methodologies have been plotted and notwithstanding there is a variation of approximately one order of magnitude between the diffuse ^{4}He emissions calculated by the two approaches, a good coherence is observed between them, where a direct relationship is observed (Figure 49). The difference may be due to the fact that diffuse CO_2 emission measured at each volcanic system was used for the calculation through the second approximation, which is likely underestimated. Since ^{3}He and ^{4}He emissions were based on the diffuse CO_2 emission, these values might also be underestimated.

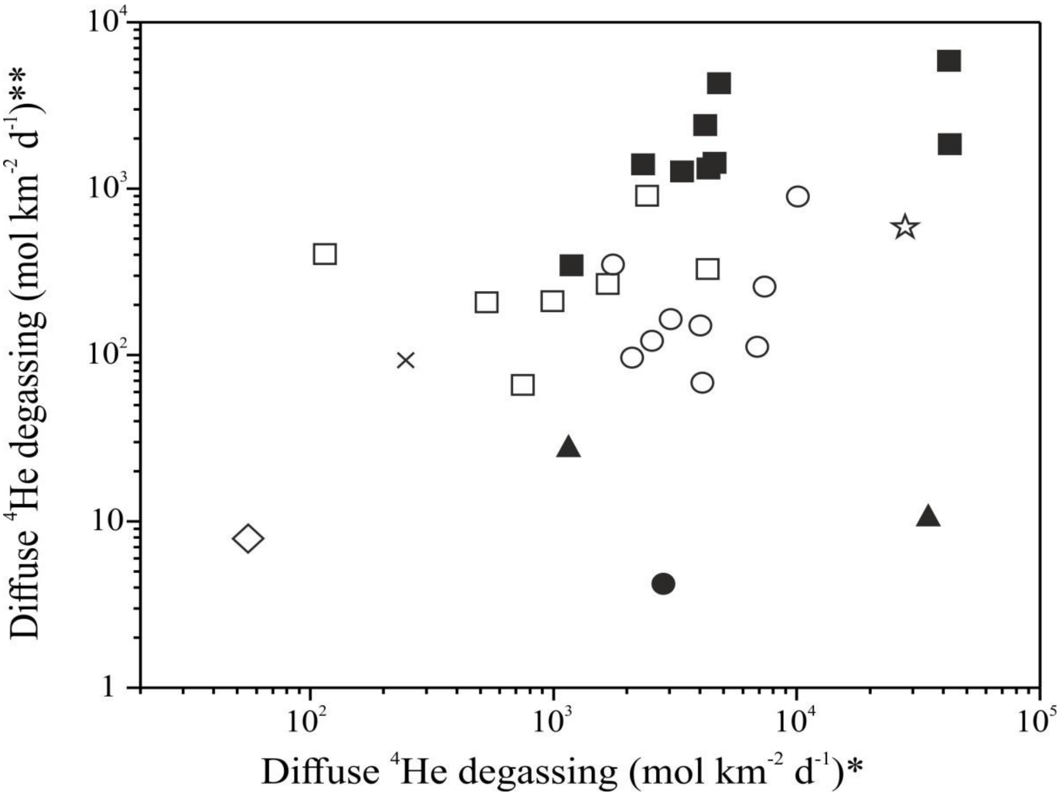

□ Teide summit cone, Tenerife, Canary Islands
■ Teide summit crater, Tenerife, Canary Islands
○ Fogo summit crater, Cape Verde
◇ Furnas caldera, São Miguel, Azores
▲ Cerro Negro volcano crater, Nicaragua
● Poás volcano crater, Costa Rica
☆ Solfatara, Campi Flegrei, Italy
× Reykjanes geothermal area, Iceland

Figure 49. **Diffuse ^{4}He degassing calculated by diffusive and advective ^{4}He fluxes vs. **Diffuse ^{4}He degassing calculated through CO_2 emission, and the $CO_2/^4$He and ^{3}He/^{4}He ratios measured in the fumarole vs. thermal energy released. The data are normalized by unit area.*

The ^{4}He diffuse emissions of the studied volcanic systems calculated by the first approach may be slightly overestimated due to a radiogenic contribution of crustal ^{4}He. This portion of crustal ^{4}He emission is almost negligible in the case of volcanic systems like Teide, Fogo, Reykjanes and Hengill, but is more important at Cerro Negro, Poás, Italian volcanic systems and Nisyros, where the lithosphere is thicker and/or crustal sediments may be supplied from the subducting slab. According to the obtained data in this study, those areas with relatively high diffuse ^{4}He emissions also show relatively high thermal energy released values (Figure 50), regardless of tectonic setting, data density or coverage area.

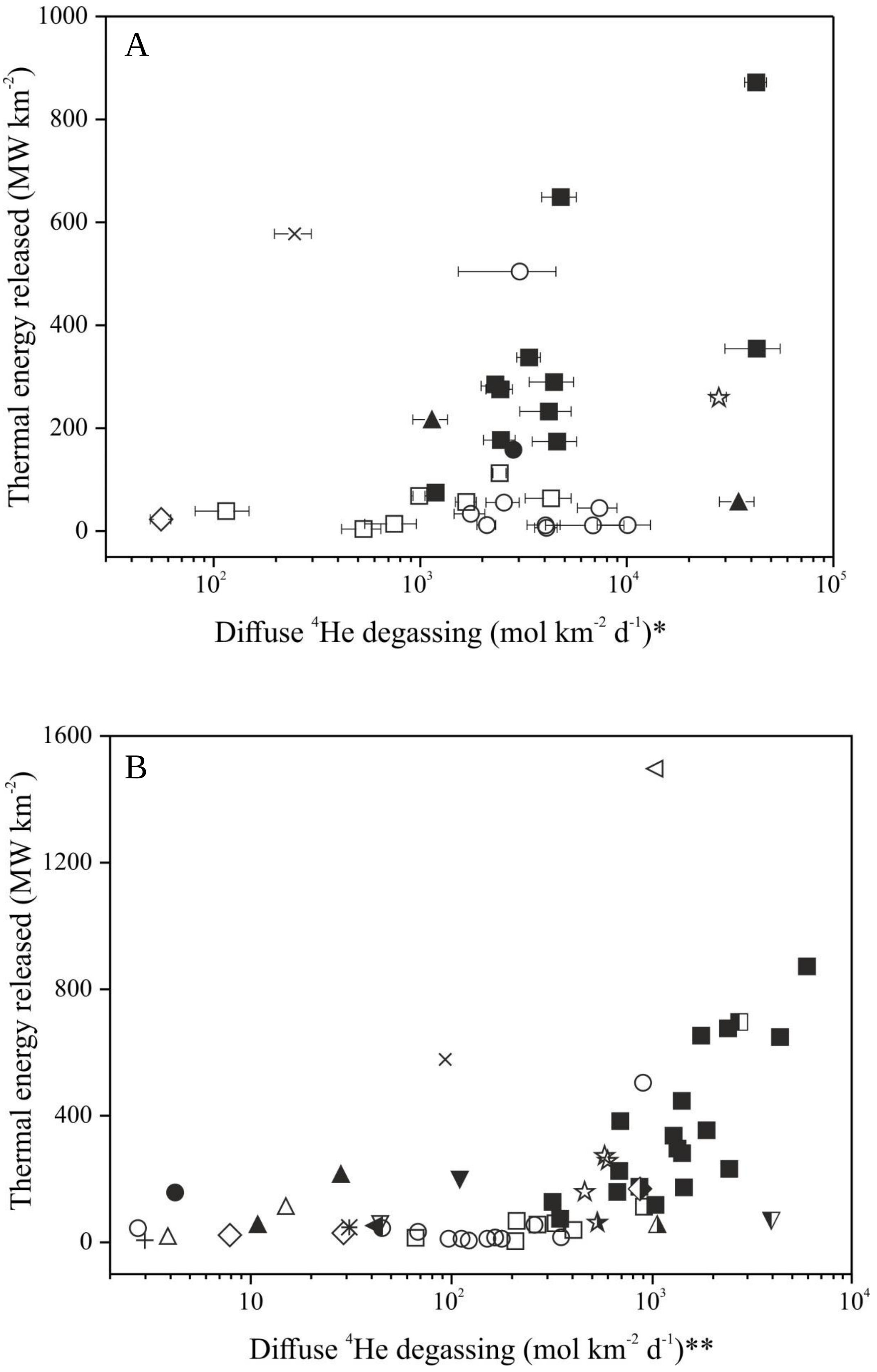
A
Thermal energy released (MW km^{-2})
1000
800
600
400
200
0
10^2
10^3
10^4
10^5
Diffuse ^{4}He degassing (mol km^{-2} d^{-1})*
B
Thermal energy released (MW km^{-2})
1600
1200
800
400
0
10
10^2
10^3
10^4
Diffuse ^{4}He degassing (mol km^{-2} d^{-1})**

□ Teide summit cone, Tenerife, Canary Islands
■ Teide summit crater, Tenerife, Canary Islands
○ Fogo summit crater, Cape Verde
◇ Furnas caldera, São Miguel, Azores
△ Cerro Negro volcano cone, Nicaragua
▲ Cerro Negro volcano crater, Nicaragua
● Poás volcano crater, Costa Rica
☆ Solfatara, Campi Flegrei, Italy
× Reykjanes geothermal area, Iceland
+ Hengill volcano, Iceland
▼ Mud volcanoes (Yellowstone), United States
▽ Copahue volcano (Las Máquinas), Chile-Argentina
▼ Copahue volcano (Las Maquinitas), Chile-Argentina
◁ Copahue volcano (Termas), Chile-Argentina
◀ Copahue volcano (Anfiteatro), Chile-Argentina
◧ Ischia Island, Italy
◐ Vesuvius volcano cone, Italy
▲ Vulcano Island crater, Italy
◆ Vulcano Island beach, Italy
★ Pantelleria volcano, Italy
✳ Nisyros volcano, Italy

Figure 50 *A) *Diffuse ^{4}He degassing calculated by diffusive and advective ^{4}He fluxes vs. thermal energy released and B)**Diffuse ^{4}He degassing through CO_2 emission, and the $CO_2/^4$He and ^{3}He/^{4}He ratios measured in the fumarole vs. thermal energy released. The data are normalized by unit area.*

Figure 50.A shows the diffuse ^{4}He degassing calculated by the first approach vs. the thermal energy released, both normalized per unit area. Noted that for those diffuse ^{4}He degassing values lower than 10^3 mol km^{-2} d^{-1}, the thermal energy remains approximately constant. Values higher than 10^3 mol km^{-2} d^{-1}, shows a proportional increase in the thermal energy with respect to the diffuse ^{4}He degassing. In Figure 50.B, where the diffuse ^{4}He degassing calculated by the second approximation vs. thermal energy released is plotted, a proportional increase in diffuse degassing and thermal energy can be observed. Despite the differences observed in the diffuse ^{4}He degassing values between the two approaches, there is a positive correlation of both with thermal energy released. This suggests that the two methods of calculus of the diffuse ^{4}He emission are valid to obtain an approximation of each volcanic system emission.

4.6. Diffuse ^{3}He emission related to thermal energy released

The correlation between diffuse ^{3}He degassing and thermal energy released by volcanic systems is showed in Figure 51.

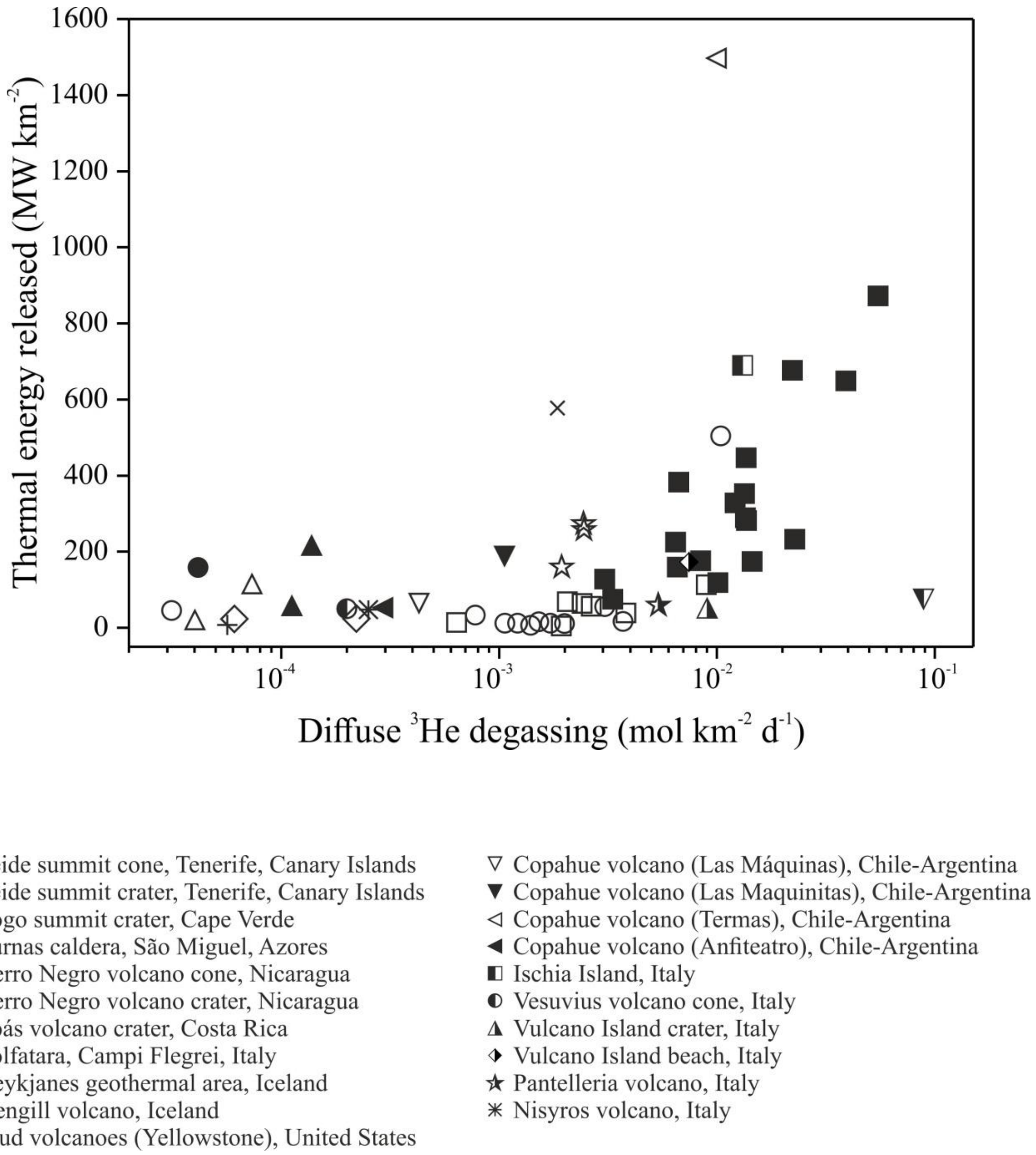

Figure 51. *Diffuse ^{3}He degassing vs. thermal energy released. The data are normalized by unit area.*

On the scale of the entire summarised dataset, and for those diffuse ^{3}He degassing values >2 × 10^{-3} mol km^{-2} d^{-1}, for every ~10-fold increase in ^{3}He emission there is a ~doubling in energy release. Across the entire dataset we observe that for ^{3}He emission values <2×10^{-3} mol km^{-2} d^{-1}the thermal energy released is similar despite a ~100 fold difference in diffuse ^{3}He degassing. This means that despite the measurable diffuse ^{3}He, degassing and overtly active volcanism, there is comparatively little heat emitted. Thus a magmatic-related heat source at depth exists, but not all the heat emitted at depth reaches the surface, due to the depth of the heat source or because it is very well sealed. In more detail, we observe that for each individual system represented by multiple measurements, a clear and positive relationship between diffuse ^{4}He and ^{3}He degassing and the thermal energy released exists. These observations are internally consistent and imply that 1) diffuse ^{3}He and ^{4}He emissions and thermal energy are indeed causatively linked and 2) this link is common across all volcanic systems studied, regardless of individual differences in ^{4}He/heat and ^{3}He/heat ratios. In addition, it has been observed that the anomalies of diffuse He isotopes effluxes and other gases anomalies such as CO_2 efflux, are related to the anomalies in the thermal energy, suggesting that the greater flows, both gas emission and thermal energy, mostly occurs in areas governed mainly by convective circulation of the fluids. These observations suggest that in volcanic areas where no visible geothermal emanations are observed and diffuse ^{3}He emission cannot be calculated (indicative of a mantle degassing), the existence of diffuse ^{4}He emission anomalies, would imply a deep thermal anomaly associated, and therefore, a possible geothermal reservoir.

Conclusions

5. CONCLUSIONS

This study provides the first estimation of ^{3}He/heat from the Teide volcanic system and supports theoretical estimates at a global scale. The calculation of ^{3}He and heat flux supports the presence of an important mantle source of volatiles and heat to the atmosphere. Most of the volcano-hydrothermal fluid discharges occurring at the summit cone of Teide volcano occur in the crater area, although other important emission rates are observed along the north and north-east flanks. These extra-crater emissions are suggestive of a strong structural control in the degassing process of Teide volcano.

Additionally, this study has shown a relationship between ^{3}He and released thermal energy that provides a robust discriminator for magmatic intrusions with the enough energy to produce a volcanic eruption. Thus, at those volcanoes with an active crater and established surface hydrothermal manifestations, changes in ^{3}He emissions should be accompanied by a significant increase in thermal output if the system is in an eruptive cycle. Long term gas emission and heat flux data may reveal patterns that allow a more thorough understanding of the timing of deep volatile release, and constitute a powerful tool to monitor the activity of volcanic areas around the world.

Finally, the use of helium isotopes in volcanic systems has proven to be a very useful geochemical tool to detect mantle degassing in different geotectonics environments as volcanic oceanic islands, volcanic arc zones, mid-ocean ridges and intraplate volcanism. Diffuse ^{4}He emission can be masked by a radiogenic contribution, ^{4}He from the crust, whereas the ^{3}He emission is primordial helium and reflects the degree of connection with the mantle source. Diffuse helium emissions do not occur homogeneously in the whole volcanic system, but there was a strong structural control in the degassing process. It means there are restricted areas with preferential fractures through gases and heat are preferentially emitted. This significant observation suggests that in volcanic areas where no visible geothermal emanations are observed, and therefore, the inability to be sampled, but anomalies in the diffuse ^{4}He emissions are present, there should be a deep thermal anomaly associated, and therefore, a possible geothermal reservoir. Due to the low cost of surface gas emission surveys, the possibility of covering large areas in a short time period, together with the reliability of the data, helium emissions studies at the surface are excellent tools during the first stages of location of the possible geothermal reservoir defining the best potential targets to exploit. The positive correlation between diffuse degassing levels of He and the associated thermal energy can be used to infer the associated thermal energy in those places where there are no obvious manifestations of geothermal activity on the surface.

References

6. REFERENCES

Ablay GJ and Martí J (2000). Stratigraphy, structure, and volcanic evolution of the Pico Teide–Pico Viejo formation, Tenerife, Canary Islands. Journal of Volcanology and Geothermal Research 103 (1-4), 175-208, https://doi.org/10.1016/S0377-0273(00)00224-9.

Agusto M, Tassi F, Caselli AT, Vaselli O, Rouwet D, Capaccioni B, Caliro S, Chiodini G and Darrah T (2013). Gas geochemistry of the magmatic-hydrothermal fluid reservoir in the Copahue–Caviahue Volcanic Complex (Argentina), Journal of Volcanology and Geothermal Research 257, 44-56, https://doi.org/10.1016/j.jvolgeores.2013.03.003.

Aiuppa A, Bitetto M, Rizzo A L, Viveiros F, Allard P, Frezzotti M L, Valenti V and Zanon V (2020). The fumarolic output from Pico do Fogo Volcano (Cape Verde). Italian Journal of Geosciences 139 (3), 325-340, https://doi.org/10.3301/IJG.2020.03.

Albert-Beltrán JF, Araña V, Diez JL and Valentin A (1990). Physical-chemical conditions of the Teide volcanic system (Tenerife, Canary Islands). Journal of Volcanology and Geothermal Research 43 (1-4), 321-332, https://doi.org/10.1016/0377-0273(90)90059-O.

Allard P (1992). Global emission of Helium-3 by subaereal volcanism. Geophysical Research Letters 19, 14, 1479-1481, https://doi.org/10.1029/92GL00974.

Alonso M, Padrón E, Sumino H, Hernández PA, Melián GV, Asensio-Ramos M, Rodríguez F, Padilla G, García-Merino M, Amonte C and Pérez NM (2019). Heat and Helium-3 fluxes from Teide Volcano, Canary Islands, Spain. Geofluids, ID 3983864, https://doi.org/10.1155/2019/3983864.

Alonso M, Pérez NM, Padrón E, Hernández PA, Melián GV, Sumino H, Padilla GD, Barrancos J, Rodríguez F, Dionis S, Asensio-Ramos M, Amonte C, Silva S and Pereira JM (2021). Changes in the thermal energy and the diffuse 3He and 4He degassing prior to the 2014–2015 eruption of Pico do Fogo volcano, Cape Verde. Journal of Volcanology and Geothermal Research, 107271, https://doi.org/10.1016/j.jvolgeores.2021.107271.

Alonso M, Pérez NM, Hernández PA, Padrón E, Melián G, Rodríguez F, Padilla G, Barrancos J, Asensio-Ramos M, Fridriksson T and Sumino H (2021b). Thermal energy and diffuse 4He and 3He degassing released in volcanic-geothermal systems. Renewable Energy 182, 17-31, https://doi.org/10.1016/j.renene.2021.10.016.

Ancochea E, Fuster JM, Ibarrola E, Cendrero A, Coello J, Hernan F, Cantagrel JM and Jamond C (1990). Volcanic evolution of the island of Tenerife (Canary Islands) in the light of new K-Ar data. Journal of Volcanology and Geothermal Research 44 (3-4), 231-249, https://doi.org/10.1016/0377-0273(90)90019-C.

Anguita F and Hernán F (2000). The Canary Islands origin: a unifying model. Journal of Volcanology and Geothermal Research 103 (1-4), 1-26, https://doi.org/10.1016/S0377-0273(00)00195-5.

Arpa MC, Hernández PA, Padrón E, Reniva P, Padilla GD, Bariso E, Melián GV, Barrancos J, Nolasco D, Calvo D, Pérez NM, Solidum Jr. RU (2013). Geochemical evidence of magma intrusion inferred from diffuse CO_2 emissions and fumarole plume chemistry: the 2010–2011 volcanic unrest at Taal Volcano, Philippines. Bulletin of Volcanology 75 (747), https://doi.org/10.1007/s00445-013-0747-9.

Ballentine CJ, Burgess R, and Marty B (2002). Tracing fluid origin, transport and interaction in the crust. Reviews in Mineralogy and Geochemistry 47 (1): 539–614, https://doi.org/10.2138/rmg.2002.47.13.

Barrancos J, Dionis S, Quevedo R, Fernandes P, Rodríguez F, Pérez NM, Silva SV, Cardoso N, Hernández PA, Melián GV, Padrón E, Padilla G, Asensio-Ramos M, Calvo D, Semedo H, AlfamaV (2015). Sulphur dioxide (SO_2) emissions during the 2014-15 Fogo eruption, Cape Verde. Geophysical Research Abstracts 17, EGU2015-11263, 2015.

Battaglia A, Bitetto M, Aiuppa A, Rizzo AL, Chigna G, Watson IM, D’Aleo R, Juárez Cacao FJ and de Moor MJ (2018). The magmatic gas signature of Pacaya Volcano, with implications for the volcanic CO_2 flux from Guatemala. Geochemistry, Geophysics, Geosystems 19, 667–692, https://doi.org/10.1002/2017GC007238.

Baubron J, Mathieu R and Miele G (1991). Measurement of gas flow from soils in volcanic areas: the accumulation method. Napoli'91 International Conference on active volcanoes and Risk Mitigation. Abstract, 27 August-1 September 1991, Napoli, Italy.

Caliro S, Viveiros F, Chiodini G and Ferreira T (2015). Gas geochemistry of hydrothermal fluids of the S. Miguel and Terceira Islands, Azores. Geochimica et Cosmochimica Acta 168, 43-57, https://doi.org/10.1016/j.gca.2015.07.009.

Capello A, Ganci G, Calvari S, Pérez NM, Hernández PA, Silva SV, Cabral J and Del Negro C (2016). Lava flow hazard modelling during the 2014–2015 Fogo eruption, Cape Verde. Journal of Geophysical Research: Solid Earth 121, 2290-2303, https://doi.org/10.1002/2015JB012666.

Carapezza ML and Granieri D (2004). CO_2 soil flux at Vulcano (Italy): comparison between active and passive methods. Applied Geochemistry 19 (1), 73–88. https://doi.org/10.1016/S0883-2927(03)00111-2.

Cardellini C, Chiodini G, Frondini F (2003). Application of stochastic simulation to CO_2 flux from soil: Mapping and quantification of gas release. Journal of Geophysical Research 108, 2425. https://doi.org/10.1029/2002JB002165.

Carracedo JC, Rodríguez Badiola E, Guillou H, Paterne M, Scaillet S, Pérez Torrado FJ, Paris R, Fra-Paleo U and Hansen A (2007). Eruptive and structural history of Teide Volcano and rift zones of Tenerife, Canary Islands. The Geological Society of America Bulletin 119 (9-10), 1027–1051, https://doi.org/10.1130/B26087.1.

Chiodini G, Frondini F and Raco B (1996). Diffuse emission of CO_2 from the Fossa crater, Vulcano Island (Italy). Bulletin of Volcanology 58, 41–50, https://doi.org/10.1007/s004450050124.

Chiodini G, Cioni R, Guidi M, Raco B and Marini L (1998). Soil CO_2 flux measurements in volcanic and geothermal areas. Applied Geochemistry. 13 (5), 543–552, https://doi.org/10.1016/S0883-2927(97)00076-0.

Chiodini G, Frondini F, Cardellini C, Granieri D, Marini L and Ventura G (2001). CO_2 degassing and energy release at Solfatara volcano, Campi Flegrei, Italy. Journal of Geophysical Research 106 (B8), 16213–16221, https://doi.org/10.1029/2001JB000246.

Chiodini G, Brombach T, Caliro S, Cardellini C, Marini L and Dietrich V (2002). Geochemical indicators of possible ongoing volcanic unrest at Nisyros Island

(Greece). Geophys. Res. Lett. 29 (16), https://doi.org/10.1029/2001GL014355,2002.

Chiodini G, Granieri D, Avino R, Caliro S, Costa A and Werner, C (2005). Carbon dioxide diffuse degassing and estimation of heat release from volcanic and hydrothermal systems. Journal of Geophysical Research 110, B08204, https://doi.org/10.1029/2004JB003542.

Chiodini G, Caliro S, Cardellini C, Avino R, Granieri D and Schmidt A (2008). Carbon isotopic composition of soil CO_2 efflux, a powerful method to discriminate different sources feeding soil CO_2 degassing in volcanic-hydrothermal areas. Earth and Planetary Science Letters 274 (3-4), 372-379, https://doi.org/10.1016/j.epsl.2008.07.051.

Chiodini G, Caliro S, Lowenstern JB, Evans WC, Bergfeld D, Tassi F and Tedesco D (2012). Insights from fumarole gas geochemistry on the origin of hydrothermal fluids on the Yellowstone Plateau. Geochimica et Cosmochimica Acta 89, 265-278, https://doi.org/10.1016/j.gca.2012.04.051.

Chiodini G, Caliro S, de Martino P, Avino R, Gherardi F (2012b). Early signals of new volcanic unrest at Campi Flegrei caldera? Insights from geochemical data and physical simulations. Geology 40 (10), 943–946, https://doi.org/10.1130/G33251.1

Chiodini G, Cardellini C, Lamberti MC, Agusto M, Caselli A, Liccioli C, Tamburello G, Tassi F, Vaselli O and Caliro S (2015). Carbon dioxide diffuse emission and thermal energy release from hydrothermal systems at Copahue–Caviahue Volcanic Complex (Argentina). Journal of Volcanology and Geothermal Research 304, 294-303, https://doi.org/10.1016/j.jvolgeores.2015.09.007.

Christensen BP, Holm PM, Jambon A, Wilson JR (2001). Helium, argon and lead isotopic composition of volcanics from Santo Antao and Fogo, Cape Verde Islands. Chemical Geology 178 (1-4), 127–142, https://doi.org/10.1016/S0009-2541(01)00261-3.

Cioni R, Corazza E and Marini L (1984). The gas/steam ratio as indicator of heat transfer at the Solfatara fumaroles, Phlegraean Fields (Italy). Bulletin of Volcanology 47, 295–302, https://doi.org/10.1007/BF01961560.

Civetta L, Cornette Y, Gillot PY and Orsi G (1988). The eruptive history of Pantelleria (Sicily Channel) in the last 50 ka, Bull. Volcanol. 50, 47–57. https://doi.org/10.1007/BF01047508.

Clarke WB, Jenkins WJ and Top Z (1976). Determination of tritium by mass spectrometric measurement of ^{3}He. International Journal of Applied Radiation and Isotopes 27, 515-522, https://doi.org/10.1016/0020-708X(76)90082-X.

Craig H and Lupton JE (1976). Primordial neon, helium and hydrogen in oceanic basalts. Earth and Planetary Science Letters 31 (3), 369–385. https://doi.org/10.1016/0012-821X(76)90118-7.

Christiansen RL (2001). The Quaternary and Pliocene Yellowstone Plateau volcanic field of Wyoming, Idaho, and Montana: U.S. Geological Survey Professional Paper 729, 144.

Cioni R, Santacroce R and Sbrana A (1999). Pyroclastic deposits as a guide for reconstructing the multi-stage evolution of the Somma-Vesuvius Caldera. Bull. Volcanol. 61, 207–222. https://doi.org/10.1007/s004450050272.

Day SJ, Carracedo JC, Guillou H, Pais Pais FJ, Badiola ER, Fonseca JFBD, Heleno SIN (2000). Comparison and cross-checking of historical, archaeological and geological evidence for the location and type of historical and sub-historical eruptions of multiple-vent oceanic island volcanoes. Geological Society of London, Spec Publ. 171 (1), 281–306.

Dawson GB (1964). The nature and assessment of heat flow from hydrothermal areas. New Zealand Journal of Geology and Geophysics 7, 1, 155–171.

Deutsch C and Journel A (1998). GSLIB: Geostatistical Software Library and Users Guide. 2nd edn. Oxford University Press, New York, p. 369.

Dionis SM, Melián G, Rodríguez F, Hernández PA, Padrón E, Pérez NM, Barrancos J, Padilla G, Sumino H, Fernandes P, Bandomo Z, Silva S, Pereira JM and Semendo H (2015). Diffuse volcanic gas emission and thermal energy release from the summit crater of Pico do Fogo, Cape Verde. Bulletin of Volcanology 77 (10), https://doi.org/10.1007/s00445-014-0897-4.

Dionis SM, Pérez NM, Hernández PA, Melián G, Rodríguez F, Padrón E, Sumino H, Barrancos J, Padilla GD, Fernandes P, Bandomo Z, Silva S, Pereira JM, Semedo H and Cabral J (2015b). Diffuse CO_2 degassing and volcanic activity at Cape Verde islands, West Africa. Earth, Planets and Space 67 (48) https://doi.org/10.1186/s40623-015-0219-x.

Doucelance R, Escrig, S, Moreira M, Gariépy C and Kurz MD (2003). Pb-Sr-He isotope and trace element geochemistry of the Cape Verde Archipelago. Geochimica et Cosmochimica Acta, 67 (19), 3717–3733, https://doi.org/10.1016/S0016-7037(03)00161-3.

Dunai TJ and Baur H (1995). Helium, neon, and argon systematics of the European subcontinental mantle: Implications for its geochemical evolution. Geochimica et Cosmochimica Acta 59 (13), 2767-2783, https://doi.org/10.1016/0016-7037(95)00172-V.

Elderfield H and Schultz A (1996). Mid-ocean ridge hydrothermal fluxes and the chemical composition of the ocean. Annual Review of Earth and Planetary Sciences 24 (1), 191–224.

Etiope G and Martinelli G (2002). Migration of carrier and trace gases in the geosphere: an overview. Physics of the Earth and Planetary Interiors 129 (3–4), 185–204. https://doi.org/10.1016/ S0031-9201(01)00292-8.

Ferreira T and Oskarsson N (1999). Chemistry and isotopic composition of fumarole discharges of Furnas caldera. Journal of Volcanology and Geothermal Research 92 (1-2), 169-179, https://doi.org/10.1016/S0377-0273(99)00074-8.

Fischer TP, Ramírez C, Mora-Amador RA, Hilton DR, Barnes JD, Sharp ZD, Le Brun M, de Moor JM, Barry PH, Füri E and Shaw AM (2015). Temporal variations in fumarole gas chemistry at Poás volcano, Costa Rica. Journal of Volcanology and Geothermal Research 294, 56-70, https://doi.org/10.1016/j.jvolgeores.2015.02.002.

Foeken JPT, Day S and Stuart FM (2009). Cosmogenic ^{3}He exposure dating of the Quaternary basalts from Fogo, Cape Verdes: Implications for rift zone and magmatic reorganisation. Quaternary Geochronology 4 (1), 37-49, https://doi.org/10.1016/j.quageo.2008.07.002.

Fournier RO (1989). Geochemistry and Dynamics of the Yellowstone National Park Hydrothermal System. Annual Review of Earth and Planetary Sciences 17, 13-53, https://doi.org/10.1146/annurev.ea.17.050189.000305.

Fourré E, Allard P, Jean-Baptiste P, Cellura D and Parello F (2012). ^{3}He/^{4}He Ratio in Olivines from Linosa, Ustica, and Pantelleria Islands (Southern Italy). Journal of Geological Research 2012, ID 723839, https://doi.org/10.1155/2012/723839.

Fridriksson T, Kristjánsson BR, Ármannsson H, Margrétardóttir E, Ólafsdóttir S and Chiodini G (2006). CO_2 emissions and heat flow through soil, fumaroles, and steam heated mud pools at the Reykjanes geothermal area, SW Iceland. Applied Geochemistry 21 (9), 1551-1569, https://doi.org/10.1016/j.apgeochem.2006.04.006.

Fridriksson T, Padrón E, Óskarsson F and Pérez NM (2016). Application of diffuse gas flux measurements and soil gas analysis to geothermal exploration and environmental monitoring: Example from the Reykjanes geothermal field, SW Iceland. Renewable Energy 86, 1295-1307, https://doi.org/10.1016/j.renene.2015.09.034.

Giggenbach WF and Goguel RL (1989) Collection and analysis of geothermal and volcanic water and gas discharges. Unpublished report, Chemistry Division, DSIR-Petone, New Zealand, p 81.

González PJ, Bagnardi M, Hooper A, Larsen Y, Marinkovic P, Samsonov SV and Wright TJ (2015). The 2014-2015 eruption of Fogo volcano: Geodetic modelling of Sentinel-1 TOPS Interferometry. Geophysical Research Letters 42, 9239-9246, https://doi.org/10.1002/2015GL066003.

Graham DW (2002). Noble gas isotope geochemistry of mid-ocean ridge and ocean island basalts: Characterization of mantle source reservoirs. Rev. Mineralogy and Geochemistry 47 (1), 247–317, https://doi.org/10.2138/rmg.2002.47.8.

Granieri D, Carapezza ML, Chiodini G, Avino R, Caliro S, Ranaldi M, Ricci T and Tarchini L (2006). Correlated increase in CO_2 fumarolic content and diffuse emission from La Fossa crater (Vulcano, Italy): Evidence of volcanic unrest or increasing gas release from a stationary deep magma body?. Geophysical Research Letters 33 (L13316), https://doi.org/10.1029/2006GL026460.

Granieri D, Chiodini G, Avino R and Caliro S (2014). Carbon dioxide emission and heat release estimation for Pantelleria Island (Sicily, Italy). Journal of Volcanology and Geothermal Research 275, 22-33, https://doi.org/10.1016/j.jvolgeores.2014.02.011.

Guest JE, Gaspar JL, Cole PD, Queiroz G, Duncan AM, Wallenstein N, Ferreira T and Pacheco JM (1999). Volcanic geology of Furnas Volcano, São Miguel, Azores. Journal of Volcanology and Geothermal Research 92, 1-29, https://doi.org/10.1016/S0377-0273(99)00064-5.

Hernández PA, Pérez NM, Salazar JM, Nakai S, Notsu K and Wakita H (1998). Diffuse emission of carbon dioxide, methane, and helium-3 from Teide Volcano, Tenerife, Canary Islands. Geophysical Research Letters 25 (17), 331-3314, https://doi.org/10.1029/98GL02561.

Hernández PA, Notsu K, Salazar JM, Mori T, Natale G, Okada H, Virgili G, Shimoike Y, Sato M, Pérez NM (2001a). Carbon dioxide degassing by advective flow from Usu volcano, Japan. Science 292 (5514), 83-86, https://doi.org/10.1126/science.1058450.

Hernández PA, Salazar JM, Shimoike Y, Mori T, Notsu K and Nemesio Pérez N (2001b). Diffuse emission of CO_2 from Miyakejima volcano, Japan. Chemical Geology 177 (1-2), 175-185, https://doi.org/10.1016/S0009-2541(00)00390-9.

Hernández P, Pérez N, Salazar J, Reimer M, Notsu K and Wakita H (2004). Radon and helium in soil gases at Cañadas caldera, Tenerife, Canary Islands, Spain. Journal of Volcanology and Geothermal Research 131 (1-2), 59-76, https://doi.org/10.1016/S0377-0273(03)00316-0.

Hernández PA, Pérez NM, Fridriksson T, Egbert J, Ilynskaya E, Thárhallsson A, Ívarsson G, Gíslason G, Gunnarsson I, Jónsson B, Padrón E, Melián G, Mori T and Notsu K (2012). Diffuse volcanic degassing and thermal energy release from Hengill volcanic system, Iceland. Bulletin of Volcanology 74, 2435-2448, https://doi.org/10.1007/s00445-012-0673-2.

Hernández PA, Padilla G, Padrón E, Pérez NM, Calvo D, Nolasco D, Melián G, Barrancos J, Dionis S, Rodríguez F and Sumino H (2012b). Analysis of long- and short-term temporal variations of the diffuse CO_2 emission from Timanfaya volcano, Lanzarote, Canary Islands. Applied Geochemistry 27 (12), 2486-2499, https://doi.org/10.1016/j.apgeochem.2012.08.008.

Hernández PA, Melián G, Giammanco S, Sortino F, Barrancos J, Pérez NM, Padrón E, López M, Donovan A, Mori T and Notsu K (2015). Contribution of CO_2 and H_2S emitted to the atmosphere by plume and diffuse degassing from volcanoes: the Etna volcano case study. Survey in Geophysics 36, 327–349, https://doi.org/10.1007/s10712-015-9321-7.

Hernández PA, Padilla G, Barrancos J, Melián G, Padrón E, Asensio-Ramos M, Rodríguez F, Pérez N, Alonso M and Calvo D (2017). Geochemical evidences of seismo-volcanic unrests at the NW rift zone of Tenerife, Canary Islands, inferred from diffuse CO_2 emission. Bulletin of Volcanology 79, 30, https://doi.org/10.1007/s00445-017-1109-9.

Hernández PA, Melián GV, Asensio-Ramos M, Padrón E, Sumino H, Pérez NM, Padilla GD, Barrancos J, Rodríguez F, Amonte C, Arcilla C and Lagmay M (2021). Geochemical and isotopic evidence of volcanic plumbing system processes from fumarolic gases of Taal volcano, Philippines, prior to the January 2020 eruption. Chemical Geology 574, 120216, https://doi.org/10.1016/j.chemgeo.2021.120216.

References

Hilton DR, Fischer TP and Marty B (2002) Noble gases and volatile recycling at subduction zones. Reviews in Mineralogy and Geochemistry 47, (1), 319-370, https://doi.org/10.2138/rmg.2002.47.9.

Hilton DR, Ramirez CJ, Mora-Amador R, Fischer TP, Furi E, Barry PH, Shaw AM (2010). Monitoring of temporal and spatial variations in fumarole helium and carbon dioxide characteristics at Poas and Turrialba volcanoes, Costa Rica (2001–2009).Geochemical Journal 44, 431–440, https://doi.org/10.2343/geochemj.1.0085.

Holm PM, Grandvuinet T, Friis J, Wilson JR, Barker AK and Plesner S (2008). An ^{40}Ar-^{39}Ar study of the Cape Verde hot spot: Temporal evolution in a semistationary plate environment. Journal of Geophysical Research 113, B08201, https://doi.org/10.1029/2007JB005339.

Ingólfsson Ó, Sigmarsson O, Sigmundsson F, Símonarson L (2008). The dynamic geology of Iceland. Jökull 58, 1–2.

Inguaggiato S, Calderone L, Inguaggiato C, Mazot A, Moriei S and Vita F (2012). Long-time variation of soil CO_2 fluxes at the summit crater of Vulcano (Italy). Bulletin of Volcanology 74, 1859–1863, https://doi.org/10.1007/s00445-012-0637-6.

Jean-Baptiste P, Allard P, Coutinho R, Ferreira T, Fourré E, Queiroz G and Gaspar JL (2009). Helium isotopes in hydrothermal volcanic fluids of the Azores archipelago. Earth and Planetary Science Letters 281 (1-2), 70-80, https://doi.org/10.1016/j.epsl.2009.02.009.

Kagoshima T, Sano Y, Takahata N, Ishida A, Tomonaga Y, Roulleau E, Pinti DL, Fischer TP, Lan T, Nishio Y, Tsunogai U, Guo Z (2016). Spatial and temporal variations of gas geochemistry at Mt. Ontake, Japan. Journal of Volcanology and

Geothermal Research 325, 179-188, https://doi.org/10.1016/j.jvolgeores.2016.06.013.

Kagoshima T, Sano Y, Takahata N, Lee H, Lan T and Ohba T (2019). Secular variations of helium and nitrogen isotopes related to the 2015 volcanic unrest of Mt. Hakone, Central Japan. Geochemistry, Geophysics, Geosystems 20, 4710-4722. https://doi.org/10.1029/2019GC008544.

Kavouridis T, Kuris D, Leonis C, Liberopoulou V, Leontiadis J, Panichi C, La Ruffa G and Caprai A (1999). Isotope and chemical studies for a geothermal assessment of the island of Nisyros (Greece). Geothermics 28 (2), 219-239, https://doi.org/10.1016/S0375-6505(99)00005-X.

Kennedy BM, Fischer TP, and Shuster DL (2000). Heat and helium in geothermal systems. Twenty-Fifth Workshop on Geothermal Reservoir Engineering Stanford University, 2000, Stanford, CA, USA, January 2000.

Klügel A, Longpré MA, García-Cañada L and Stix J (2015). Deep intrusions, lateral magma transport and related uplift at ocean island volcanoes. Earth and Planetary Science Letters 431, 140–149, https://doi.org/10.1016/j.epsl.2015.09.031.

Klügel A, Day S, Schmid M, Faria B (2020). Magma Plumbing During the 2014–2015 Eruption of Fogo (Cape Verde Islands). Frontiers in Earth Science 8, https://doi.org/10.3389/feart.2020.00157.

Liuzzo M, Di Muro A, Giudice G, Michon L, Ferrazzini V and Gurrieri S (2015). New evidence of CO_2 soil degassing anomalies on Piton de la Fournaise volcano and the link with volcano tectonic structures. Geochemistry. Geophysics. Geosystems 16, 4388– 4404, https://doi.org/10.1002/2015GC006032.

Lupton JE, Baker ET, and Massoth GJ (1989). Variable ^{3}He/heat ratios in submarine hydrothermal systems: evidence from two plumes over the Juan de Fuca ridge," Nature 337 (6203), 161–164, 1989.

Madeira J and Ribeiro A (1990). Geodynamic models for the Azores triple junction: A contribution from tectonics. Tectonophysics 184 (3-4), 405-415, https://doi.org/10.1016/0040-1951(90)90452-E.

Marini L and Gambardella B (2005). Geochemical modeling of magmatic gas scrubbing. Annals of Geophysics. 48, 739–753, https://doi.org/10.4401/ag-3230.

Marrero R. López DL, Hernández PA and Pérez NM (2008). Carbon dioxide discharged through the Las Cañadas aquifer, Tenerife, Canary Islands. Pure and Applied Geophysics 165, 147–172, https://doi.org/10.1007/s00024-007-0287-3.

Marrero-Díaz R, López D, Pérez N.M, Custodio E, Sumino H, Melián GV, Padrón E, Hernández PA, Calvo D, Barrancos J, Padilla G and Sortino F (2015). Carbon dioxide and helium dissolved gases in groundwater at central Tenerife Island, Canary Islands: chemical and isotopic characterization. Bulletin of Volcanology 77, 86, https://doi.org/10.1007/s00445-015-0969-0.

Martelli M, Nuccio PM, Stuart FM, Burgess R, Ellam RM and Italiano F (2004). Helium–strontium isotope constraints on mantle evolution beneath the Roman Comagmatic Province, Italy. Earth and Planetary Science Letters 224 (3-4), 295-308, https://doi.org/10.1016/j.epsl.2004.05.025.

Martí J, Mitjavila J and Araña V (1994). Stratigraphy, structure and geochronology of the Las Cañadas Caldera (Tenerife, Canary Islands). Geological Magazine 131 (6), 715–727.

Martí J and Gudmundsson A (2000). The Las Cañadas caldera (Tenerife, Canary Islands): An overlapping collapse caldera generated by magma-chamber migration. Journal of Volcanology and Geothermal Research 103 (1-4), 167–173.

Martí J, Hurlimann M, Ablay GJ and Gudmundsson A (1997). Vertical and lateral collapses on Tenerife (Canary Islands) and other volcanic ocean islands. Geology 25, 879–882, https://doi.org/10.1130/0091-7613(1997)025<0879:VALCOT>2.3.CO;2.

Martini M, Bermúdez A, Delfino D and Giannini L (1997). The thermal manifestation of Copahue volcano area. Final Proc. VIII Congreso Geológico Chileno, Antofagasta,Chile, 352–356.

Marty B, Gunnlaugsson E, Jambon A, Oskarsson N, Ozima M, Pineau F and Torssander P (1991). Gas geochemistry of geothermal fluids, the Hengill area, southweat rift zone of Iceland. Chemical Geology 91 (3), 207-225, https://doi.org/10.1016/0009-2541(91)90001-8.

Matsuda J, Matsumoto T, Sumino H, Nagao K, Yamamoto J, Miura Y, Kaneoka I, Takahata N and Sano Y (2002). The $^{3}He/^{4}He$ ratio of the new internal He Standard of Japan (HESJ). Geochemical Journal 36 (2), 191–195. https://doi.org/10.2343/geochemj.36.191.

McMurtry GM, Dasilveira LA, Horn EL, DeLuze JR and Blessing JE (2019). High $^{3}He/^{4}He$ ratios in lower East Rift Zone steaming vents precede a new phase of Kilauea 2018 eruption by 8 months. Scientific Repports 9, 11860, https://doi.org/10.1038/s41598-019-48268-0.

Melián G, Tassi F, Pérez NM, Hernández PA, Sortino F, Vasello O, Padrón E, Nolasco D, Barrancos J Padilla G, Rodríguez F, Dionis S, Calvo D, Notsu K and Sumino H (2012). A magmatic source for fumaroles and diffuse degassing from the summit crater of Teide Volcano (Tenerife, Canary Islands): a geochemical evidence for the 2004–2005 seismic–volcanic crisis. Bulletin of Volcanology 74, 1465–1483, https://doi.org/10.1007/s00445-012-0613-1.

Melián G, Hernández PA, Padrón E, Pérez NM, Barrancos J, Padilla G, Dionis S, Rodríguez F, Calvo D and Nolasco D (2014). Spatial and temporal variations of diffuse CO_2 degassing at El Hierro volcanic system: Relation to the 2011–2012 submarine eruption. Journal of Geophysics Research, Solid Earth 119, 6976–6991, https://doi.org/10.1002/2014JB011013.

Melián GV, Pérez NM, Mora Amador RA, Herández PA, Ramírez C, Sumino H, Alvarado GE and Fernández M (2019) Diffuse CO_2 degassing and thermal energy release from Poás volcano, Costa Rica. In: Tassi F, Vaselli O and Mora Amador R (eds) Poás volcano. Active volcanoes of the world. Springer, Cham, https://doi.org/10.1007/978-3-319-02156-0_6.

Melián GV, Hernández PA, Pérez NM, Asensio-Ramos M, Padrón E, Alonso M, Padilla GD, Barrancos J, Sortino F, Sumino H, Rodríguez F, Amonte C, Silva S, Cardoso N and Pereira JM (2021). Insights from fumarole gas geochemistry on the recent volcanic unrest of Pico do Fogo, Cape Verde. Frontiers in Earth Science 9, 599, https://www.frontiersin.org/article/10.3389/feart.2021.631190.

Melnick D, Folguera A and Ramos VA (2006). Structural control on arc volcanism: The Caviahue–Copahue complex, Central to Patagonian Andes transition (38°S). Journal of South American Earth Sciences 22 (1-2), 66-88, https://doi.org/10.1016/j.jsames.2006.08.008.

Mercalli G (1891). Cenni topografici–geologici dell’isola di Vulcano e storia delle sue eruzioni. Ann. Regio Uff. Centr. Di Meteor. e Geodinam. IV 10 (1891) 76–118.

Moore JG (1964). Giant submarine landslides on the Hawaiian Ridge: U.S. Geological Survey Professional Paper 501, 95–98.

de Moor JM, Aiuppa A, Pacheco J, Avard G, Kern C, Liuzzo M, Martínez M, Giudice G and Fischer TP (2016). Short-period volcanic gas precursors to phreatic eruptions: Insights from Poás Volcano, Costa Rica. Earth and Planetary Science Letters 442, 218-227. https://doi.org/10.1016/j.epsl.2016.02.056.

Mori T, Hernández PA, Salazar JML, Pérez NM and Notsu K (2001). An in situ method for measuring CO_2 flux from volcanic-hydrothermal fumaroles. Chemical Geology 177 (1-2), 85-99, https://doi.org/10.1016/S0009-2541(00)00384-3.

Mörner NA and Etiope G (2002). Carbon degassing from the lithosphere. Global and Planetary Change 33 (1-2), 185-203, https://doi.org/10.1016/S0921-8181(02)00070-X.

Naranjo JA and Polanco E (2004). The 2000 AD eruption of Copahue Volcano, Southern Andes. Revista Geológica de Chile 31 (2), 279–292, http://dx.doi.org/10.4067/S0716-02082004000200007.

Notsu K, Mori T, Do Vale S, Kagi H and Hito (2006). Monitoring quiescent volcanoes by diffuse CO_2 degassing: Case Study of Mt. Fuji, Japan. Pure and Applied Geophysics 163, 825–835, https://doi.org/10.1007/s00024-006-0051-0.

Nuccio PM, Paonita A and Sortino F (1999). Geochemical modeling of mixing between magmatic and hydrothermal gases: the case of Vulcano Island, Italy. Earth and Planetary Science Letters 167 (3-4), 321-333, https://doi.org/10.1016/S0012-821X(99)00037-0.

Padrón E, Melián G, Marrero R, Nolasco D, Barrancos J, Padilla G, Hernández PA and Pérez NM (2008). Changes in the diffuse CO_2 emission and relation to seismic activity in and around El Hierro, Canary Islands. Pure and Applied Geophysics 165, 95–114, https://doi.org/10.1007/s00024-007-0281-9.

Padrón E, Hernández PA, Pérez NM, Toulkeridis T, Melián G, Barrancos J, Virgili G, Sumino H and Notsu K (2012a). Fumarole/plume and diffuse CO_2 emission from Sierra Negra caldera, Galapagos archipelago. Bulletin if Volcanology 74, 1509-1519, https://doi.org/10.1007/s00445-012-0610-4.

Padrón E, Pérez NM, Hernández PA, Sumino H, Melián GV, Barrancos J, Nolasco D, Padilla G (2012b). Helium emission at Cumbre Vieja volcano, La Palma, Canary Islands. Chemical Geology 312-313, 138-147, https://doi.org/10.1016/j.chemgeo.2012.04.018.

Padrón E, Pérez NM, Hernández PA, Sumino H, Melián GV, Barrancos J, Nolasco D, Padilla G, Dionis S, Rodríguez F, Hernández I, Calvo D, Peraza MD and Nagao K (2013). Diffusive helium emissions as a precursory sign of volcanic unrest. Geology 41 (5), 539–542, https://doi.org/10.1130/G34027.1.

Padrón E, Pérez NM, Rodríguez F, Melián G, Hernández PA, Sumino H, Padilla G, Barrancos J, Dionis S, Notsu K and Calvo D (2015). Dynamics of diffuse carbon dioxide emissions from Cumbre Vieja volcano, La Palma, Canary Islands. Bulletin of Volcanology 77 (28), https://doi.org/10.1007/s00445-015-0914-2.

Paonita A, Caracausi A, Martelli M, Rizzo AL (2016). Temporal variations of helium isotopes in volcanic gases quantify pre-eruptive refill and pressurization in magma reservoirs: The Mount Etna case. Geology 44 (7), 499–502. https://doi.org/10.1130/G37807.1.

Parello F, Allard P, D’Alessandro W, Federico C, Jean-Baptiste P and Catani O (2000). Isotope geochemistry of Pantelleria volcanic fluids, Sicily Channel rift: a mantle volatile end-member for volcanism in southern Europe. Earth and Planetary

Science Letters 180 (3-4), 325-339, https://doi.org/10.1016/S0012-821X(00)00183-7.

Parkinson KJ (1981). An improved method for measuring soil respiration in the field. Journal of Applied Ecology 18, 221–228, https://doi.org/10.2307/2402491.

Pedone M, Viveiros F, Aiuppa A, Giudice G, Grassa F, Gagliano L, Francofonte V and Ferreira T (2015). Total (fumarolic + diffuse soil) CO_2 output from Furnas volcano. Earth Planet and Space 67, 174, https://doi.org/10.1186/s40623-015-0345-5.

Pepin RO and Porcelli D (2002). Origin of Noble Gases in the Terrestrial Planets. Reviews in Mineralogy and Geochemistry 47 (1), 191-246, https://doi.org/10.2138/rmg.2002.47.7.

Pérez NM, Sturchio NC, Williams SN, Carracedo JC and Coello J (1992). Geochemical characteristics of the volcanic hydrothermal gases in Teide, Timafaya, Taburiente, and Teneguia volcanoes, Canary Islands, Spain. In Proceedings of the Scientific Sessions: III Geological Congress of Spain 1, 1463–467, Graficas Varona, Salamanca.

Pérez N, Wakita H, Nakai S, Sano Y and Williams SN (1994). $^3He/^4He$ isotopic ratios in volcanic-hydrothermal discharges from the Canary Islands, Spain: implications on the origin of the volcanic activity. Goldschmidt Conference Edinburgh, Mineralogical Magazine 58A, 709-710.

Pérez NM, Nakai S, Wakita H, Hernández PA and Salazar JM (1996). Helium-3 emission in and around Teide Volcano, Tenerife, Canary Islands, Spain. Geophysical Research Letters 23 (24), 3531-3534, https://doi.org/10.1029/96GL03470.

Pérez NM, Sturchio NC, Arehart G, Hernández PA, Salazar JM and Wakita H (1996[a]). Short-term secular variations of carbon and radon isotopes of fumarolic discharges from Teide volcano, Tenerife, Canary Islands. Bulletin Earthquake Chem 7, 31-33.

Pérez NM, Hernández PA, Padilla G, Nolasco D, Barrancos J, Melían G, Padrón E, Dionis S, Calvo D, Rodríguez F, Notsu K, Mori T, Kusakabe M, Arpa MC, Reniva P, Ibarra M (2011). Global CO_2 emission from volcanic lakes. Geology 39 (3), 235–238, https://doi.org/10.1130/G31586.1

Pérez NM. Hernández PA, Padrón E, Melián G, Nolasco D, Barrancos J, Padilla G, Calvo D, Rodríguez F, Dionis S and Chiodini G (2013). An increasing trend of diffuse CO_2 emission from Teide volcano (Tenerife, Canary Islands): geochemical evidence of magma degassing episodes. Journal of the Geological Society 170, 585-592, https://doi.org/10.1144/jgs2012-125.

Perez NM, Dionis S, Fernandes P, Barrancos J, Rodríguez F, Bandomo Z, Hernández PA, Melián GV, Silva SV, Padilla G, Padrón E, Cabral J, Calvo D, Asensio-Ramos M, Pereira JM, Gonçalves AA, Barros I and Semedo H (2015). Precursory signals of the 2014-15 Fogo eruption (Cape Verde) detected by surface CO_2 emission and heat flow observations. Geophysical Research Abstracts, Vol. 17, EGU2015-10644, 2015.

Poreda R and Craig H (1989) Helium isotope ratios in circum-Pacific volcanic arcs. Nature 338, 473-478, https://doi.org/10.1038/338473a0

Poreda RJ, Craig H, Arnórsson S and Welhan JA (1992) Helium isotopes in Icelandic geotermal systems: I. ^{3}He, gas chemistry, and ^{13}C relations. Geochimica et Cosmochimica Acta 56 (12), 4221-4228, https://doi.org/10.1016/0016-7037(92)90262-H.

Rizzo AL, Di Piazza A, de Moor JM, Alvarado GE, Avard G, Carapezza ML and Mora MM (2016). Eruptive activity at Turrialbavolcano (Costa Rica): Inferences from ^{3}He/^{4}He in fumarole gases and chemistry of the products ejected during 2014 and 2015. Geochemistry, Geophysics. Geosystems 17, 4478–4494, https://doi.org/10.1002/2016GC006525

Rodríguez F, Pérez NM, Padrón E, Melián G, Piña-Varas P, Dionis S, Barrancos J, Padilla GD, Hernández PA, Marrero R, Ledo JJ, Bellmunt F, Queralt P, Marcuello A, Hidalgo R (2015). Surface geochemical and geophysical studies for geothermal exploration at the southern volcanic rift zone of Tenerife, Canary Islands, Spain. Geothermics 55, 195-206, https://doi.org/10.1016/j.geothermics.2015.02.007.

Rodríguez F, Pérez NM, Melián GV, Padrón E, Hernández PA, Asensio-Ramos M, Padilla GD, Barrancos J, D'Auria L (2021). Exploration of deep-seated geothermal reservoirs in the Canary Islands by means of soil CO_2 degassing surveys. Renewable Energy 164, 1017-1028, https://doi.org/10.1016/j.renene.2020.09.065.

Rowley JC (1982). Worldwide geothermal resources, in Handbook of Geothermal Energy, edited by W. H. Fertl, 44–176, Gulf, Houston, Tex.

Salazar JML, Hernández PA, Pérez NM, Melián G, Álvarez J, Segura F and Notsu K (2001). Diffuse emission of carbon dioxide from Cerro Negro Volcano, Nicaragua, Central America. Geophysical Research Letters 28 (22), 4275-4278, https://doi.org/10.1029/2001GL013709.

Salvage RO, Avard G, de Moor Jm, Pacheco JF., Brenes Marin J, Cascante M, Muller C and Martinez Cruz M (2018). Renewed Explosive Phreatomagmatic Activity at Poás Volcano, Costa Rica in April 2017. Frontiers in Earth Science 6, 160, https://doi.org/10.3389/feart.2018.00160.

Sano Y, Nakamura Y, Wakita H, Urabe A and Tominaga T (1984). Helium-3 emission related to volcanic activity. Science 224, 4645, 150-151,

Sano Y, Wakita H and Sheng X (1988). Atmospheric helium isotope ratio. Geochemical Journal 22, 177-181, https://doi.org/10.2343/geochemj.22.177,

Sano Y, Kagoshima T, Takahata N, Nishio Y, Roulleau E, Pinti DL and Fischer TP (2015). Ten-year helium anomaly prior to the 2014 Mt Ontake eruption. Scientific Reports 5, 13069, https://doi.org/10.1038/srep13069.

Schwarzenbach RP, Gschwend PM and Imboden DM (1993). Environmental Organic Chemistry. Wiley-Interscience, New York, 681 p.

Shaw AM, Hilton DR, Fischer TP, Walker JA, de Leeuw GAM (2006). Helium isotope variations in mineral separates from Costa Rica and Nicaragua: Assessing crustal contributions, timescale variations and diffusion-related mechanisms. Chemical Geology 230 (1-2), 124-139, https://doi.org/10.1016/j.chemgeo.2005.12.003.

Shimizu A, Sumino H, Nagao K, Notsu K and Mitropoulos P (2005). Variation in noble gas isotopic composition of gas samples from the Aegean arc, Greece. Journal of Volcanology and Geothermal Research 140 (4), 321-339, https://doi.org/10.1016/j.jvolgeores.2004.08.016.

Sigurgeirsson MA (1995). The younger Stampar eruption at Reykjanes. Náttúrufraedingurinn 64, 211-230 (in Icelandic).

Sigurgeirsson MA (2004). A chapter in the eruption history of Reykjanes: eruption episode two thousand years ago. Náttúrufraedingurinn 72, 21-28 (in Icelandic).

Silva S, Cardoso N, Alfama V, Cabral J, Semedo H, Pérez NM, Dionis S, Hernández PA, Barrancos J, Melián G, Pereira JM, Rodríguez F (2015). Chronology of the 2014 Volcanic Eruption on the Island of Fogo, Cape Verde. Geophysical Research Abstracts EGU General Assembly, Vienna, Austria ID13378.

Sinclair AJ (1974). Selection of threshold values in geochemical data using probability graphs. Journal of Geochemical Exploration 3 (2), 129-149, https://doi.org/10.1016/0375-6742(74)90030-2.

Sumino H, Nagao K and Notsu K (2001). Highly sensitive and precise measurement of helium isotopes using a mass spectrometer with double collector system. Journal of the Mass Spectrometry Society of Japan 49 (2), 61–68. https://doi.org/10.5702/massspec.49.61.

Tedesco D, Allard P, Sano Y, Wakita H and Pece R (1990) Helium-3 in subaereal and submarine fumaroles of Campi Flegrei cadera, Italy. Geochimica et Cosmochimica Acta 54 (4), 1105-1116, https://doi.org/10.1016/0016-7037(90)90442-N.

Tedesco D (1996). Chemical and isotopic investigations of fumarolic gases from Ischia island (southern Italy): Evidences of magmatic and crustal contribution. Journal of Volcanology and Geothermal Research 74 (3-4), 233-242, https://doi.org/10.1016/S0377-0273(96)00030-3.

Tedesco D (1996). Chemical and isotopic investigations of fumarolic gases from Ischia island (southern Italy): Evidences of magmatic and crustal contribution. Journal of Volcanology and Geothermal Research 74 (3-4), 233-242, https://doi.org/10.1016/S0377-0273(96)00030-3.

Tedesco D, Nagao K and Scarsi P (1998). Noble gas isotopic ratios from historical lavas and fumaroles at Mount Vesuvius (southern Italy): constraints for current and future volcanic activity. Earth and Planetary Science Letters 164 (1-2), 61-78, https://doi.org/10.1016/S0012-821X(98)00167-8.

Tedesco D and Scarsi P (1999). Intensive gas sampling of noble gases and carbon at Vulcano Island (sothern Italy). Journal of geophysical Research 104 (B5), 10499-10510. https://doi.org/10.1029/1998JB900066.

Tedesco D and Scarsi P (1999). Chemical (He, H_2, CH_4, Ne, Ar, N_2) and isotopic (He, Ne, Ar, C) variations at the Solfatara crater (southern Italy): mixing of different sources in relation to seismic activity. Earth and Planetary Science Letters 171 (3), 465-480, https://doi.org/10.1016/S0012-821X(99)00137-5.

Viveiros F, Cardellini C, Ferreira T, Caliro S, Chiodini G and Silva C (2010). Soil CO_2 emissions at Furnas volcano, São Miguel Island, Azores archipelago: Volcano monitoring perspectives, geomorphologic studies, and land use planning application, Journal of Geophysical Research 115, B12208, https://doi.org/10.1029/2010JB007555.

Werner C and Brantley S (2003). CO_2 emissions from the Yellowstone volcanic system. Geochem. Geophys. Geosyst. (4), 1061, https://doi.org/10.1029/2002GC000473.

Werner C and Cardellini C (2006). Comparison of carbon dioxide emissions with fluid upflow, chemistry, and geologic structures at the Rotorua geothermal system, New Zealand. Geothermics 35 (3), 221-238, https://doi.org/10.1016/j.geothermics.2006.02.006.

Worsley P (2015). Physical geology of the Fogo volcano (Cape Verde Islands) and its 2014-2015 eruption. Geology Today 31, 153-159, https://doi.org/10.1111/gto.12102.

Appendix I: Tables

7. APPENDIX I: Tables

Table 1. Obtained data from the summit cone and crater survey. T_{amb} is the ambient temperature, T_{15} and T_{40} the temperature at 15 and 40 cm depth. LOD indicates values lower than the limit of detection.

Waypoint	**Longitude (UTM, m)**	**Latitude (UTM, m)**	**Altitude (m)**	**T_{amb} (ºC)**	**T_{15} (ºC)**	**T_{40} (ºC)**	**CO_2 efflux (g m^{-2} d^{-1})**
1	338925	3128502	3723	20.4	44.3	61.2	253
2	338915	3128504	3723	12.0	28.4	38.7	1343
3	338905	3128508	3723	17.3	48.7	50.0	3086
4	338890	3128510	3720	14.3	81.7	81.7	6155
5	338879	3128509	3717	26.8	77.2	81.7	4278
6	338868	3128490	3720	31.3	64.0	72.6	3805
7	338885	3128495	3717	25.8	21.4	28.3	131
8	338903	3128496	3718	18.0	21.9	32.9	852
9	338915	3128494	3715	19.8	63.3	71.7	8986
10	338930	3128493	3713	16.7	78.8	82.2	1899
11	338937	3128482	3716	23.8	72.7	72.3	6109
12	338946	3128474	3716	25.1	59.6	63.8	666
13	338932	3128475	3716	16.8	65.9	71.1	310
14	338923	3128481	3709	17.6	82.3	81.9	9609
15	338908	3128482	3709	18.5	27.3	31.4	41
16	338894	3128482	3709	24.6	26.4	30.1	498
17	338881	3128478	3710	24.1	81.2	81.2	4293
18	338864	3128474	3715	23.2	20.2	21.6	1030
19	338862	3128451	3698	23.9	35.8	40.8	1727
20	338873	3128429	3701	25.8	41.9	53.8	937
21	338882	3128455	3705	28.5	40.1	54.1	1472
22	338875	3128466	3712	20.7	76.7	79.1	5538
23	338895	3128469	3708	18.1	49.2	55.5	812
24	338910	3128471	3700	29.3	73.6	81.5	5112
25	338922	3128469	3704	13.4	57.6	74.0	1772
26	338929	3128463	3709	14.6	82.4	82.8	10650
27	338943	3128461	3710	15.3	67.9	79.4	2622
28	338948	3128445	3712	14.0	45.4	37.4	114
29	338929	3128451	3699	17.3	81.9	82.1	7823
30	338914	3128454	3697	17.0	23.4	24.5	565
31	338900	3128456	3685	20.0	70.3	41.3	825
32	338884	3128441	3699	23.1	39.3	36.1	40
33	338899	3128434	3688	19.6	20.2	17.2	304
34	338889	3128425	3705	22.0	79.1	70.9	169

Waypoint	Longitude (UTM, m)	Latitude (UTM, m)	Altitude (m)	T_{amb} (ºC)	T_{15} (ºC)	T_{40} (ºC)	CO_2 efflux (g m^{-2} d^{-1})
35	338920	3128440	3692	25.7	44.4	34.1	857
36	338904	3128445	3698	19.7	30.3	27.2	1921
37	338909	3128426	3702	24.1	30.7	28.0	429
38	338929	3128429	3703	19.0	26.4	22.2	238
39	338907	3128526	3721	17.6	57.7	47.4	984
40	338921	3128552	3701	20.8	40.3	26.7	1922
41	338928	3128585	3681	20.8	36.8	31.6	1073
42	338878	3128598	3673	18.5	32.9	32.5	3513
43	338924	3128629	3654	21.0	4.9	37.3	2093
44	338918	3128675	3625	16.4	22.6	18.9	349
45	338920	3128751	3572	25.3	17.3	16.4	63
46	338987	3128738	3582	24.1	17.2	17.3	59
47	338994	3128797	3552	28.3	20.8	22.8	11
48	339067	3128782	3536	17.2	19.5	19.7	37
49	338916	3128408	3682	14.8	23.8	31.4	180
50	338942	3128374	3666	16.9	47.7	50.7	1636
51	338972	3128347	3644	17.7	42.3	54.0	289
52	338915	3128342	3646	18.6	19.4	24.7	10
53	338907	3128281	3617	18.1	18.1	20.9	LOD
54	338986	3128276	3611	21.6	22.8	27.1	166
55	339086	3128203	3561	23.3	30.9	33.8	253
56	339011	3128208	3579	22.2	24.5	26.4	LOD
57	338940	3128206	3572	23.1	23.7	31.2	174
58	338885	3128208	3571	22.1	20.2	20.2	LOD
59	338853	3128153	3541	22.2	21.2	19.0	LOD
60	338920	3128124	3541	22.6	32.4	32.9	182
61	339008	3128119	3541	20.6	22.1	25.2	LOD
62	339131	3128142	3654	19.7	16.4	14.3	LOD
63	338866	3128469	3708	26.8	20.8	22.7	219
64	338835	3128466	3694	24.9	18.2	14.9	220
65	338819	3128450	3674	28.6	21.1	15.2	30
66	338787	3128473	3659	29.3	15.9	18.9	LOD
67	338777	3128445	3650	30.6	23.6	23.3	2
68	338739	3128465	3630	26.6	21.3	24.1	16
69	338740	3128421	3619	28.6	27.9	26.3	580
70	338682	3128449	3600	29.8	18.5	23.3	14
71	338689	3128408	3594	26.6	25.3	21.9	50
72	338714	3128356	3590	26.0	25.3	21.9	735
73	338655	3128377	3564	24.8	29.5	24.0	277
74	338622	3128450	3556	30.7	16.0	19.0	3
75	338585	3128467	3532	35.7	14.4	15.1	0.6
76	338590	3128395	3532	31.8	22.1	21.2	LOD
77	338613	3128338	3532	33.6	25.3	21.6	12

Waypoint	**Longitude (UTM, m)**	**Latitude (UTM, m)**	**Altitude (m)**	**T_{amb} (ºC)**	**T_{15} (ºC)**	**T_{40} (ºC)**	**CO_2 efflux (g m^{-2} d^{-1})**
78	338966	3128471	3707	22.3	36.2	41.2	548
79	338986	3128468	3692	22.2	27.9	31.9	2499
80	339017	3128487	3674	25.8	24.3	22.3	147
81	339046	3128493	3652	24.3	22.8	20.3	46
82	339057	3128455	3650	24.1	27.4	27.4	331
83	339056	3128405	3635	21.0	20.2	20.2	183
84	339089	3128475	3629	22.3	32.7	32.7	163
85	339082	3128544	3658	21.3	44.9	44.9	1105
86	339111	3128456	3617	21.2	24.5	24.5	380
87	339121	3128406	3602	22.8	22.6	22.6	68
88	339169	3128447	3590	23.1	24.9	24.9	74
89	339164	3128369	3590	22.9	17.7	17.7	2
90	339230	3128427	3590	26.8	21.8	21.8	LOD
91	339222	3128366	3590	24.0	16.9	16.9	LOD
92	339286	3128380	3572	22.7	20.2	20.2	LOD
93	338853	3128516	3705	22.7	29.4	31.8	283
94	338860	3128549	3679	14.7	44.5	46.1	1326
95	338831	3128541	3672	15.6	16.3	19.9	6
96	338791	3128546	3651	16.1	22.6	21.7	413
97	338813	3128601	3641	18.4	16.3	17.3	170
98	338846	3128632	3636	17.6	18.5	19.0	LOD
99	338867	3128666	3621	18.5	16.7	17.1	1053
100	338796	3128640	3609	22.6	20.8	24.3	4
101	338744	3128610	3599	17.7	18.9	19.9	739
102	338680	3128606	3572	19.3	15.2	14.4	LOD
103	338627	3128626	3540	21.3	16.7	15.4	LOD
104	338749	3128691	3579	20.3	16.4	14.3	280
105	338819	3128705	3594	22.4	13.6	12.9	LOD
106	338842	3128749	3567	22.1	17.2	16.2	LOD
107	338692	3128726	3529	22.9	17.8	16.4	71
108	338625	3128709	3530	22.5	16.8	18.8	LOD
109	338719	3128806	3530	22.4	16.3	16.2	LOD
110	338802	3128789	3534	22.6	17.2	12.9	LOD
111	338884	3128801	3541	22.3	19.1	14.7	LOD
112	338970	3128434	3575	22.2	24.7	24.6	594
113	339003	3128407	3575	29.6	24.3	23.7	855
114	339001	3128372	3575	27.2	25.4	24.8	82
115	339071	3128372	3575	24.2	15.4	15.6	6
116	339040	3128329	3575	27.6	21.8	20.1	2
117	339076	3128300	3575	30.7	23.3	19.6	4
118	339105	3128339	3604	27.6	21.8	20.1	6330
119	339125	3128273	3580	21.2	32.1	33.6	261
120	339172	3128256	3561	22.5	19.2	19.2	LOD

Waypoint	Longitude (UTM, m)	Latitude (UTM, m)	Altitude (m)	T_{amb} (°C)	T_{15} (°C)	T_{40} (°C)	CO_2 efflux (g m^{-2} d^{-1})
121	339242	3128252	3575	27.2	21.9	21.9	LOD
122	338849	3128423	3693	20.7	21.3	19.6	141
123	338828	3128398	3674	14.7	20.4	23.6	449
124	338864	3128370	3665	19.8	30.3	27.2	4
125	338851	3128333	3645	20.4	14.9	13.6	10
126	338768	3128365	3634	22.7	24.6	22.0	636
127	338754	3128320	3600	23.6	22.3	20.6	194
128	338793	3128289	3589	24.9	21.3	21.5	332
129	338842	3128255	3580	28.5	13.6	14.0	2
130	338819	3128216	3564	28.8	14.6	13.7	1
131	338764	3128234	3557	26.9	15.7	17.8	76
132	338723	3128260	3552	29.8	20.9	22.0	36
133	338696	3128310	3570	28.6	27.7	25.7	1580
134	338632	3128280	3521	32.6	23.8	22.1	143
135	338606	3128273	3514	26.9	20.5	19.30	62
136	338679	3128221	3523	23.2	19.0	22.2	LOD
137	338654	3128159	3520	21.7	23.7	25.6	LOD
138	338703	3128168	3516	26.4	17.7	18.4	LOD
139	338759	3128152	3514	22.6	22.1	22.7	LOD
140	338795	3128145	3532	24.4	18.7	21.1	LOD
142	338951	3128494	3719	22.0	55.4	70.4	983
143	338967	3128498	3700	19.6	30.4	34.1	784
144	338970	3128519	3687	23.3	24.1	29.4	11
145	338995	3128520	3665	23.1	74.7	77.9	389
146	339029	3128540	3651	24.9	27.1	30.3	142
147	339011	3128568	3655	22.8	33.6	41.5	223
148	338983	3128612	3647	25.5	25.1	24.3	31
149	339011	3128660	3614	25.1	25.0	25.4	103
150	339047	3128702	3600	20.6	60.0	60.2	29
151	339071	3128651	3593	26.0	22.6	20.5	39
152	339096	3128604	3598	27.2	33.7	42.1	588
153	339113	3128556	3601	26.2	35.2	43.1	584
154	339118	3128514	3608	21.8	34.8	36.6	408
155	339175	3128529	3583	25.1	35.5	37.6	1053
156	339236	3128516	3570	30.5	32.3	33.1	878
157	339170	3128613	3562	25.6	24.4	26.9	1031
158	339159	3128664	3561	30.0	29.1	25.8	209
159	339135	3128699	3551	22.8	17.3	19.8	42
160	339095	3128746	3546	26.0	16.2	16.3	3
161	339128	3128796	3514	18.6	12.9	13.3	LOD
162	339166	3128756	3521	27.6	14.4	14.4	1
163	339212	3128722	3530	25.1	22.8	24.8	163
164	339233	3128812	3540	22.0	26.1	26.8	843

Waypoint	Longitude (UTM, m)	Latitude (UTM, m)	Altitude (m)	T_{amb} (ºC)	T_{15} (ºC)	T_{40} (ºC)	CO_2 efflux (g m^{-2} d^{-1})
165	339282	3128745	3540	29.4	22.2	22.5	58
166	339232	3128667	3550	29.6	31.2	30.3	159
167	339255	3128614	3555	28.6	38.3	37.3	793
168	339295	3128551	3562	26.8	25.6	19.9	3
112b	338973	3128401	3575	25.5	26.7	28.1	297
118b	339149	3128329	3604	26.1	21.1	18.1	12
62b	339101	3128179	3538	21.1	23.4	24.5	5427

Table 2. Chemical composition of the soil gas in Teide summit cone and crater survey.

Waypoint	**^{4}He (ppm)**	**Ne (ppm)**	**H_2 (ppm)**	**O_2 (ppm)**	**N_2 (ppm)**	**CH_4 (ppm)**	**CO_2 (ppm)**	**H_2S (ppm)**	**H_2O (ppm)**	**$\delta^{13}C\text{-}CO_2$ ‰ vs. VPDB**
1	12.9	9.2	2046.4	47560	179888	5.7	764700	0.0	854	-2.97
2	8.7	11.8	93.8	60436	238385	3.8	690326	0.0	949	-2.12
3	6.6	17.6	105.9	194198	730988	1.8	59723	0.0	788	-2.81
4	12.6	14.4	1093.1	102587	389963	4.0	477275	0.0	786	-3.13
5	14.3	7.0	2163.5	26839	117152	5.8	851479	0.0	1014	-3.05
6	9.7	13.5	873.6	103384	395542	4.0	479397	0.0	1033	-3.13
7	5.5	17.2	24.5	168772	635928	1.8	167147	0.0	1369	0.17
8	7.0	16.1	26.0	126317	477129	3.5	370528	0.0	1132	-1.17
9	6.8	16.9	51.9	169858	641069	2.5	166080	0.0	1073	-3.07
10	15.3	5.4	1719.2	27090	106858	5.7	861019	0.0	1021	-2.97
11	11.5	11.6	1152.0	81039	309843	4.3	588981	0.0	1030	-2.78
12	7.5	15.1	39.6	127037	484677	2.9	355857	0.0	1436	-2.85
13	15.4	6.3	2852.4	12803	49682	5.7	926115	437.6	1567	-2.87
14	9.5	10.3	2041.2	58225	219686	5.3	694730	0.0	1579	-2.92
15	5.5	17.8	61.6	196660	739357	5.0	34463	0.0	1461	-6.27
16	6.1	17.3	41.8	153685	578806	1.7	232693	0.0	1522	-1.19
17	10.7	11.4	1123.1	72167	278038	5.0	617452	0.0	1675	-2.90
18	6.6	16.5	54.1	157901	596659	1.7	210254	0.0	1537	-3.15
19	7.1	16.1	18.6	140600	534333	1.7	289213	0.0	1555	-3.01
20	6.6	17.3	5.8	178145	671421	1.8	120792	0.0	1376	-2.36
21	7.8	15.5	99.4	128572	489447	3.4	353415	0.0	1174	-2.95
22	11.9	10.9	821.7	72994	283422	4.0	617951	0.0	1298	-3.10
23	10.0	16.9	44.1	168392	633623	1.7	168320	0.0	1340	-0.49
24	8.8	17.4	215.6	188479	709254	1.7	77145	0.0	1177	-2.90

Waypoint	^{4}He (ppm)	Ne (ppm)	H_2 (ppm)	O_2 (ppm)	N_2 (ppm)	CH_4 (ppm)	CO_2 (ppm)	H_2S (ppm)	H_2O (ppm)	$\delta^{13}C$-CO_2 ‰ vs. VPDB
25	18.3	18.0	2964.5	18587	71350	5.9	911499	0.0	952	-2.90
26	10.6	10.5	1467.4	77203	292518	4.8	605279	0.0	1419	-2.81
27	12.4	11.4	1706.4	79642	304185	4.3	599212	66.7	935	-2.95
28	8.7	16.4	77.0	142232	538912	3.3	288820	0.0	1460	-2.68
29	19.4	13.1	1145.7	81767	311648	2.9	573008	0.0	1495	-2.78
30	12.8	16.0	69.6	128342	485544	2.1	355709	0.0	1452	-1.34
31	6.8	16.5	68.2	155726	589180	2.0	227154	0.0	1296	-3.01
32	7.5	16.2	20.9	136755	518796	1.7	315694	0.0	1322	-2.59
33	6.0	17.8	5.8	198501	745478	1.7	37688	0.0	1042	-5.53
34	15.9	10.2	1401.5	59667	227668	4.0	692758	0.0	1242	-2.84
35	12.2	13.5	78.8	57490	223078	4.8	695872	0.0	1568	-2.29
36	5.4	17.7	54.8	191534	720241	1.7	62815	0.0	1331	-3.12
37	6.9	16.8	17.9	168864	636157	1.7	172276	0.0	1088	-2.45
38	9.9	12.3	478.6	90772	349644	1.8	535417	0.0	1255	-1.79
39	7.2	17.0	15.3	184784	698711	1.7	101541	0.0	854	-2.92
40	6.1	17.6	5.6	191463	721072	1.7	74272	0.0	873	-3.00
41	11.0	17.1	4.4	190877	718471	1.7	74182	0.0	975	-3.05
42	7.2	17.6	8.0	191159	722194	1.7	74503	0.0	808	-3.24
43	6.0	17.9	33.4	191677	723981	1.7	67801	0.0	1018	-3.11
44	7.4	17.8	1.2	207013	776572	1.7	2076	0.0	965	-2.89
45	6.0	16.5	2.8	202213	758487	1.7	22497	0.0	1039	-1.58
46	5.6	17.9	3.5	205399	769736	1.7	8174	0.0	1065	-5.20
47	13.7	18.0	5.9	206123	774217	1.7	2346	0.0	1089	-1.85
48	6.1	18.0	2.2	204373	765643	1.7	9489	0.0	1258	-1.70
49	6.1	17.6	10.2	183291	689415	1.7	105168	0.0	1010	-0.96
50	7.3	17.3	30.6	136659	515343	1.8	322684	0.0	999	-2.02

Waypoint	^{4}He (ppm)	Ne (ppm)	H_2 (ppm)	O_2 (ppm)	N_2 (ppm)	CH_4 (ppm)	CO_2 (ppm)	H_2S (ppm)	H_2O (ppm)	δ^{13}C-CO_2 ‰ vs. VPDB
51	7.6	17.2	28.8	174878	659788	1.7	143844	0.0	932	-2.81
52	7.7	17.8	19.4	199425	750347	1.7	31491	0.0	938	-1.59
53	5.7	17.8	5.3	201736	758853	1.7	18781	0.0	1069	-2.12
54	5.7	17.6	0.9	189917	714181	1.7	79839	0.0	734	-2.20
55	6.2	17.1	3.9	158675	598506	2.1	219586	0.0	969	-0.01
56	5.3	17.9	1.0	202842	761669	1.7	14348	0.0	1090	-5.11
57	5.9	17.8	3.0	189248	712352	1.7	74494	0.0	1090	-2.15
58	5.2	17.9	1.1	204915	768816	1.7	5112	0.0	1089	-8.06
59	5.3	17.6	0.9	189917	714181	1.7	79839	0.0	734	-7.91
60	6.1	17.9	2.6	198470	746043	1.7	34384	0.0	1050	-1.65
61	8.5	17.4	0.9	204900	770035	2.1	2393	0.0	1111	-10.71
62	5.7	17.4	1.5	205747	772736	1.7	985	0.0	998	-10.11
63	6.2	17.9	1.6	197474	741019	1.7	50952	0.0	1178	-2.31
64	5.8	16.9	1.0	187061	702368	1.7	97787	0.0	1213	-3.31
65	5.3	18.1	0.7	205389	770183	1.7	14051	0.0	1147	-2.56
66	6.1	17.7	0.5	204450	765596	1.7	6540	0.0	1454	-3.38
67	15.5	17.8	1.2	207112	776136	1.7	3902	0.0	1272	-5.74
68	5.9	17.6	2.0	207193	776806	1.7	6395	0.0	1182	-1.87
69	5.6	17.4	2.1	195673	734122	1.7	55643	0.0	1251	-2.86
70	5.6	18.1	1.4	207236	775843	1.7	8697	0.0	1042	-2.75
71	5.5	17.4	2.4	200870	752677	1.7	31388	0.0	1238	-5.28
72	8.6	18.0	3.5	192317	721876	1.7	74971	0.0	1097	-1.26
73	5.5	16.8	2.0	197476	741129	1.7	49678	0.0	1154	-2.85
74	6.7	17.8	1.3	208602	781923	1.7	4459	0.0	1792	-2.56
75	6.2	17.8	1.8	207838	779388	2.1	1002	0.0	1179	-5.75
76	6.7	17.9	1.1	204794	768368	1.7	15379	0.0	1133	-10.32

Waypoint	^{4}He (ppm)	Ne (ppm)	H_2 (ppm)	O_2 (ppm)	N_2 (ppm)	CH_4 (ppm)	CO_2 (ppm)	H_2S (ppm)	H_2O (ppm)	δ^{13}C-CO_2 ‰ vs. VPDB
77	10.4	18.1	0.8	206499	774102	1.7	6985	0.0	1175	-3.36
78	6.6	17.2	13.2	171902	648048	2.0	156260	0.0	1148	-3.58
79	6.2	17.6	11.5	181964	685221	1.7	109962	0.0	1138	-2.84
80	5.8	17.1	2.1	195815	735448	1.7	48515	0.0	1052	-2.85
81	6.4	17.8	2.6	199161	747239	1.7	32601	0.0	1151	-2.59
82	5.8	17.6	3.1	193026	725711	1.7	59452	0.0	1108	-2.43
83	5.5	17.7	1.9	199120	747843	1.7	32259	0.0	1134	-2.94
84	6.6	17.6	6.1	194163	730046	1.7	54066	0.0	1148	-2.72
85	5.7	17.8	2.2	199302	748328	1.7	31762	0.0	1145	-2.89
86	5.9	18.0	2.5	200791	753813	1.7	20991	0.0	1290	-1.69
87	9.7	17.8	2.5	203446	763680	1.7	10867	0.0	1227	-2.97
88	5.7	17.7	3.2	201458	755839	1.7	21660	0.0	1180	-3.43
89	5.5	17.8	3.8	205458	769904	1.7	4511	0.0	1104	-2.30
90	5.6	18.0	1.4	204882	768868	1.7	3684	0.0	1240	-3.62
91	5.3	17.8	6.7	205536	771002	1.7	900	0.0	1168	-8.00
92	6.5	17.8	0.9	206054	772440	1.7	2513	0.0	1075	-7.73
93	5.8	17.5	1.3	197769	742649	1.7	51836	0.0	921	-9.70
94	17.8	17.5	1.8	185237	698604	1.7	106971	0.0	960	-3.03
95	28.9	17.8	1.0	203597	763451	1.7	26418	0.0	858	-3.04
96	5.9	17.8	1.1	200151	750637	1.7	41609	0.0	914	-0.59
97	5.4	18.0	3.9	201903	760335	1.7	42121	0.0	817	-2.94
98	5.8	17.9	3.5	203166	765981	1.7	30492	0.0	935	-1.15
99	5.3	18.0	2.2	208151	783656	1.7	9357	0.0	836	-3.17
100	5.9	17.9	2.1	202234	762046	1.7	35761	0.0	811	-1.63
101	5.9	17.9	6.1	191910	723352	1.7	81332	0.0	896	-3.19
102	5.4	18.0	1.6	207380	779695	1.7	9340	0.0	956	-2.99

Waypoint	^{4}He (ppm)	Ne (ppm)	H_2 (ppm)	O_2 (ppm)	N_2 (ppm)	CH_4 (ppm)	CO_2 (ppm)	H_2S (ppm)	H_2O (ppm)	δ^{13}C-CO_2 ‰ vs. VPDB
103	5.4	17.9	1.8	208980	785813	1.7	1109	0.0	932	-2.50
104	9.7	17.8	3.6	204704	770389	1.7	21918	0.0	854	-8.07
105	6.0	18.0	2.3	208602	783964	1.7	1381	0.0	886	-3.14
106	5.3	18.0	1.6	209075	786442	1.8	568	0.0	891	-9.53
107	6.0	18.0	3.2	207837	781836	1.7	5306	0.0	907	-8.44
108	6.0	18.0	1.9	207857	781993	1.7	7120	0.0	847	-2.89
109	5.7	18.0	1.6	208815	785409	1.8	848	0.0	973	-1.74
110	8.3	18.0	1.9	208844	786021	1.7	574	0.0	949	-11.00
111	6.7	18.0	1.5	208409	783890	1.8	607	0.0	1040	-10.03
112	6.8	18.0	3.4	196968	740917	1.7	52349	0.0	1135	-14.18
113	5.7	17.3	12.6	193235	725979	1.7	55244	0.0	1292	-0.06
114	5.7	17.8	5.9	199242	748040	1.7	29059	0.0	1223	-2.50
115	5.7	17.9	2.6	204423	766093	1.7	6184	0.0	1220	-2.83
116	5.2	18.1	4.6	207403	780902	1.7	7308	0.0	988	-2.94
117	5.9	18.0	2.4	207747	781486	1.7	2795	0.0	1183	-1.23
118	5.6	17.7	4.6	203972	764635	1.7	13181	0.0	1029	-5.34
119	5.7	17.7	4.7	198313	745211	1.7	40857	0.0	1088	-7.14
120	5.2	17.5	0.7	206166	773238	1.7	906	0.0	1057	-2.08
121	7.2	17.1	1.2	204147	765926	2.0	4246	0.0	1408	-2.43
122	7.5	18.0	2.2	203078	764472	1.7	28612	0.0	944	-1.67
123	6.0	17.7	3.1	185318	699297	1.7	113152	0.0	868	-7.84
124	5.3	18.0	2.6	205726	774293	1.7	14278	0.0	1093	-11.29
125	5.6	18.0	2.0	207767	781931	1.7	5384	0.0	1086	-2.34
126	5.6	17.9	2.5	199270	750245	1.7	45148	0.0	1108	-2.31
127	5.4	18.0	2.4	201488	758836	1.7	35512	0.0	1115	-9.40
128	8.1	17.9	2.4	203542	766897	1.7	27820	0.0	984	-4.18

Waypoint	^{4}He (ppm)	Ne (ppm)	H_2 (ppm)	O_2 (ppm)	N_2 (ppm)	CH_4 (ppm)	CO_2 (ppm)	H_2S (ppm)	H_2O (ppm)	$\delta^{13}C$-CO_2 ‰ vs. VPDB
129	5.7	18.0	1.7	209208	786857	1.7	2178	0.0	1038	-0.41
130	5.5	18.0	1.7	208701	785220	1.7	1017	0.0	1183	-2.41
131	5.8	18.0	1.6	207046	779693	1.7	9587	0.0	1114	-2.37
132	5.5	18.0	2.6	207802	782441	1.7	5602	0.0	1122	-9.27
133	7.7	17.9	3.4	198483	747994	1.7	52112	0.0	1025	-6.38
134	6.2	18.0	2.6	206759	778795	1.7	12044	0.0	1057	-1.98
135	6.1	18.0	5.8	206444	777282	1.7	9238	0.0	1217	-1.78
136	5.8	18.0	2.0	208749	786083	1.7	1017	0.0	1139	-2.91
137	6.1	17.9	2.0	205182	771122	1.7	5137	0.0	987	-3.10
138	5.2	18.0	0.7	205271	770233	1.7	1119	0.0	1182	-3.60
139	6.7	17.8	0.6	205961	772480	1.7	633	0.0	1066	-10.89
140	5.2	18.0	0.9	206428	775039	1.8	565	0.0	989	-9.69
142	8.1	17.1	9.1	150496	569937	3.1	277073	0.0	898	-8.41
143	7.2	17.2	11.6	145766	551518	3.0	298922	0.0	961	-8.79
144	5.3	18.0	2.5	204563	770252	1.7	24649	0.0	978	-8.46
145	10.3	15.7	9.1	118254	450350	3.9	425922	0.0	1088	-2.40
146	6.5	17.6	3.9	164638	622538	1.9	207110	0.0	1088	-1.51
147	7.3	17.0	14.3	162665	618669	1.8	215616	0.0	919	-1.57
148	5.6	18.0	4.9	203213	765467	1.7	28651	0.0	1072	-2.66
149	5.5	18.0	5.0	203103	765516	1.7	28994	0.0	1064	-1.69
150	5.5	18.0	1.9	204677	767657	1.7	8880	0.0	1131	-2.83
151	5.3	17.9	2.7	207156	779781	1.7	11917	0.0	1016	-0.54
152	6.6	17.7	8.8	187911	710840	1.7	96856	0.0	1050	-2.62
153	16.0	17.7	7.5	178813	675037	2.0	141108	0.0	1133	-2.31
154	6.7	17.3	9.5	181130	685170	1.9	130174	0.0	1058	-1.50
155	6.0	17.6	4.4	188658	712510	2.0	92945	0.0	1171	-2.70

Waypoint	^{4}He (ppm)	Ne (ppm)	H_2 (ppm)	O_2 (ppm)	N_2 (ppm)	CH_4 (ppm)	CO_2 (ppm)	H_2S (ppm)	H_2O (ppm)	δ^{13}C-CO_2 ‰ vs. VPDB
156	6.0	18.0	5.6	192284	725625	1.8	76272	0.0	1261	-2.84
157	5.6	17.7	3.8	197966	745740	1.7	45542	0.0	1235	-2.83
158	5.6	17.9	4.4	199304	750866	1.7	39707	0.0	1267	-2.71
159	5.4	17.7	3.0	203900	764413	1.7	9860	0.0	1301	-2.89
160	5.4	17.6	2.0	206171	772110	1.7	2171	0.0	1173	-2.73
161	5.3	17.4	0.5	206193	772384	1.7	1051	0.0	1211	-2.69
162	7.2	17.8	1.5	204718	766842	1.7	10518	0.0	1089	-1.19
163	5.6	17.9	2.6	195991	737746	1.7	63805	0.0	1091	-0.40
164	6.3	16.8	4.4	164496	619324	1.7	191648	0.0	1254	-8.59
165	5.4	17.9	2.4	203610	766752	1.7	27743	0.0	1145	-10.41
166	5.5	17.9	2.9	199796	752168	1.7	44412	0.0	1149	-1.89
167	8.1	17.9	2.7	196723	740296	1.7	55892	0.0	1182	-0.43
168	5.4	17.2	1.7	205591	774325	1.8	17726	0.0	1098	-2.15
112b	5.9	17.8	12.4	189523	712234	1.7	71798	0.0	1354	-0.54
118b	9.4	17.7	3.5	205856	771918	1.7	6466	0.0	1123	-0.46
62b	6.0	17.6	17.4	184809	696752	1.7	95334	0.0	1052	-2.75

Table 3. Outlet temperature, chemical and isotopic composition of fumarolic gases from the summit crater of Teide volcano.

	T (ºC)	$^{4}He/^{20}Ne$	$^{3}He/^{4}He$ (R/R_A)	$\delta^{13}C-CO_2$ (‰)	CO_2 (%)	Gas/steam ratio
Teide fumarole	83.3	33.6	6.72 ± 0.06	-3.13 ± 0.01	98.2	0.25

Table 4. Corrected $^{3}He/^{4}He$ (R/R$_A$), $^{4}He/^{20}Ne$, calculated ^{4}He emission (mol d^{-1}), ^{3}He emissions (mol d^{-1}) by the different approaches:*^{3}He emission calculated by multiplying the ^{4}He emission by $^{3}He/^{4}He$ molar ratio measured in the fumarole, **^{3}He emission calculated by multiplying the diffuse CO_2 emission by the $^{3}He/CO_2$ ratio measured in the fumarolic gas, H_2O/CO_2 mass ratio measured in the fumarolic gas and thermal energy released (MW). One sigma error in the corrected $^{3}He/^{4}He$ ratios is reported. n.m.: not measured

Date	**$(^{3}He/^{4}He)_{cor}$ (R/R$_A$)**	**$^{4}He/^{20}Ne$**	**^{4}He emission (mol/d)**	**^{3}He emission* (mol/d)**	**^{3}He emission** (mol/d)**	**H_2O/CO_2 mass ratio**	**Diffuse CO_2 emission (t/d)**	**Thermal energy released (MW)**
30/03/2007	8.09 ± 0.08	123	n.m.	n.m.	2.8×10^{-4}	0.8	71.1 ± 19.3	1.6
06/11/2008	8.22 ± 0.09	362	n.m.	n.m.	4.5×10^{-6}	5	41.8 ± 10.6	6.4
10/05/2009	7.81 ± 0.09	23	975 ± 401	$1.1\times10^{-2} \pm 4.5\times10^{-5}$	1.7×10^{-4}	0.4	146.9 ± 34.7	1.7
21/02/2010	8.53 ± 0.09	228	1046 ± 227	$1.2\times10^{-2} \pm 2.8\times10^{-5}$	4.3×10^{-4}	1.2	219.1 ± 36.2	7.9
08/12/2010	8.23 ± 0.07	94	570 ± 104	$6.5\times10^{-3} \pm 1.3\times10^{-5}$	2.4×10^{-4}	0.6	88. 9 ± 16.0	1.7
24/02/2011	8.23 ± 0.15	42	361 ± 66	$4.1\times10^{-3} \pm 8.3\times10^{-6}$	2.0×10^{-4}	0.2	127.5 ± 23.9	0.9
24/02/2012	7.93 ± 0.12	194	298 ± 31	$3.3\times10^{-3} \pm 3.9\times10^{-6}$	1.5×10^{-4}	1.2	44.9 ± 8.8	1.7
27/04/2013	8.20 ± 0.08	18	580 ± 72	$6.6\times10^{-3} \pm 9.0\times10^{-6}$	1.1×10^{-4}	7.6	22.9 ± 4.5	4.8
07/10/2013	n.m.	n.m.	318 ± 41	n.m.	n.m.	n.m.	152.9 ± 26.4	n.m.
06/11/2013	8.63 ± 0.10	406	n.m.	n.m.	n.m.	5.1	n.m.	n.m.
22/03/2014	8.37 ± 0.09	110	1432 ± 412	$1.7\times10^{-2} \pm 5.0\times10^{-5}$	1.5×10^{-3}	7.1	326.6 ± 54.5	71.6
14/01/2015	n.m.	n.m.	1997 ± 290	n.m.	n.m.	0.3	166.0 ± 19.1	n.m.
16/02/2015	8.33 ± 0.08	36	783 ± 188	$9.0\times10^{-3} \pm 2.2\times10^{-5}$	n.m.	n.m.	182.7 ± 25.8	n.m.
22/11/2015	n.m.	n.m.	595 ± 152	n.m.	n.m.	n.m.	219.5 ± 43.4	n.m.
30/10/2016	7.66 ± 0.02	106	249 ± 42	$2.6\times10^{-3} \pm 4.4\times10^{-6}$	5.3×10^{-4}	0.3	179.9 ± 42.6	2.4
13/11/2018	6.69 ± 0.04	16	430 ± 213	$4.0\times10^{-3} \pm 2.0\times10^{-5}$	2.2×10^{-4}	0.6	106.1 ± 25.8	2.2

Table 5. Percentage of total diffuse ^{4}He emission corresponding to a crustal or magmatic contribution and the amount of mantelic and crustal diffuse ^{4}He emission in mol d^{-1}. n.m.: not measured.

Data	**Crustal ^{4}He (%)**	**Magmatic ^{4}He (%)**	**Magmatic emission (mol d^{-1})**	**Crustal emission (mol d^{-1})**
30/03/2007	15	85	n.m	n.m
06/11/2008	14	86	n.m	n.m
10/05/2009	18	82	798.1	176.9
21/02/2010	11	89	935.2	110.8
08/12/2010	14	86	491.7	78.3
24/02/2011	14	86	311.4	49.6
24/02/2012	17	83	247.7	50.3
27/04/2013	14	86	498.5	81.5
07/10/2013	n.m	n.m	n.m	n.m
06/11/2013	10	90	n.m	n.m
22/03/2014	12	88	1256.2	175.8
14/01/2015	n.m	n.m	n.m	n.m
16/02/2015	13	87	683.6	99.4
22/11/2015	n.m	n.m	n.m	n.m
30/10/2016	20	80	199.9	49.1
13/11/2018	30	70	301.4	128.6

Table 6. Summary of soil gas survey data at Furnas caldera. T_{amb} is the ambient temperature, T_{15} and T_{40} the temperature at 15 and 40 cm depth, respectively.

Waypoint	**Longitude (UTM, m)**	**Latitude (UTM, m)**	**Altitude (m)**	**T_{amb} (ºC)**	**T_{15} (ºC)**	**T_{40} (ºC)**	**CO_2 efflux (g m^{-2} d^{-1})**
1	646902	4181239	259	19.8	16.5	17.0	20.4
2	646878	4181250	260	21.8	16.0	16.5	20.3
3	646854	4181256	260	22.0	16.3	16.8	19.6
4	646868	4181278	259	20.3	17.0	17.8	81.9
5	646893	4181270	258	19.8	16.7	17.1	5.7
6	646916	4181261	257	19.8	16.4	16.7	35.6
7	646921	4181286	257	18.5	17.4	17.9	17.0
8	646897	4181295	258	18.8	16.7	17.0	60.2
9	646874	4181307	258	19.1	16.2	16.4	224.7
10	646889	4181330	258	18.6	16.6	16.7	947.1
11	646914	4181318	256	18.7	17.2	17.4	18.8
12	646936	4181306	255	18.7	16.7	17.1	17.8
13	646928	4181342	255	19.1	17.3	18.2	55.6
14	646947	4181360	255	19.9	18.1	18.6	453.3
15	646967	4181382	256	20.3	42.5	47.6	46.6
16	646980	4181400	255	20.2	46.1	66.2	866.0
17	646994	4181422	255	20.6	42.8	55.9	1108.5
18	647014	4181440	255	20.9	20.2	21.3	40.6
19	646998	4181457	257	21.5	19.9	21.9	48.4
20	646977	4181442	258	21.4	32.8	38.0	48.0
21	646959	4181419	259	21.7	28.4	34.6	195.1
22	646900	4181359	261	21.2	18.7	18.9	41.4
23	646904	4181378	263	21.1	22.5	26.5	40.4
24	646907	4181406	263	20.7	20.8	22.1	9.3
25	646918	4181430	263	21.4	33.6	37.6	542.4
26	646931	4181407	262	21.6	38.5	39.4	38.8
27	646919	4181413	262	20.2	67.8	91.8	43.2
28	646937	4181424	262	21.5	41.1	48.8	333.7
29	646947	4181444	262	21.8	98.0	98.1	175.9
30	646925	4181453	264	21.5	28.4	28.9	19.5
31	646935	4181466	263	19.7	91.9	98.0	230.6
32	646975	4181469	265	20.9	67.2	83.9	113.7
33	646951	4181391	264	20.2	29.1	32.9	26.7
34	646935	4181372	264	19.4	19.5	19.6	4.2
35	647038	4181454	262	19.7	21.6	22.5	48.6
36	647055	4181473	262	18.6	22.6	23.9	9.6
37	647086	4181477	261	19.6	20.4	21.6	3.8
38	647113	4181481	261	19.8	17.3	17.6	13.4
39	647140	4181483	262	20.1	17.0	17.2	26.7
40	647165	4181472	262	19.9	17.0	17.1	0.6
41	647192	4181466	262	20.1	19.4	19.3	1.2

Waypoint	**Longitude (UTM, m)**	**Latitude (UTM, m)**	**Altitude (m)**	**T_{amb} (ºC)**	**T_{15} (ºC)**	**T_{40} (ºC)**	**CO_2 efflux (g m^{-2} d^{-1})**
42	647218	4181456	262	20.4	19.2	19.6	1.4
43	647247	4181445	261	20.9	19.3	19.9	2.8
44	647257	4181475	264	20.1	34.1	40.8	135.3
45	647239	4181496	264	19.6	46.3	56.8	191.2
46	647207	4181506	264	20.5	45.2	52.5	406.5
47	647176	4181515	264	19.5	28.7	32.7	51.1
48	647156	4181536	268	19.6	33.8	37.0	126.7
49	647156	4181574	275	20.7	23.0	24.2	274.1
50	647142	4181513	263	17.2	16.2	17.2	32.6
51	647108	4181522	263	17.8	17.4	18.2	15.5
52	647061	4181517	263	17.3	19.7	20.0	24.5
53	647042	4181540	264	17.1	23.2	24.7	12.9
54	647012	4181555	265	23.3	37.0	44.7	152.6
55	646990	4181567	266	22.0	38.5	46.4	224.0
56	648344	4181461	208	17.6	16.0	16.6	56.3
57	648283	4182088	195	18.4	16.0	16.7	25.0
58	648458	4181987	192	18.5	17.8	18.4	18.4
59	648728	4182044	192	18.6	18.4	18.8	7.2
60	648579	4182423	193	18.5	17.3	17.9	10.7
61	648600	4182563	203	18.7	17.2	19.5	6.3
62	648522	4182304	190	19.8	18.8	20.6	3.5
63	648373	4182414	203	23.5	16.8	18.7	4.0
64	648220	4182511	223	18.8	15.3	15.5	3.8
65	648362	4182157	192	21.4	17.6	18.2	9.8
66	648185	4182010	197	20.9	17.3	18.4	11.7
67	648049	4182115	222	19.7	15.6	17.5	5.2
68	647861	4182148	236	22.0	16.2	17.4	8.5
69	647668	4182087	245	24.5	16.5	16.9	13.5
70	647474	4181997	247	22.1	16.7	17.7	11.2
71	647314	4181879	259	21.1	16.8	17.3	18.3
72	647514	4181682	254	24.2	17.2	17.6	14.5
73	647687	4181727	244	21.3	17.1	17.7	6.8
74	647875	4181719	225	21.7	16.3	16.7	22.5
75	647885	4181552	229	19.6	16.8	16.3	3.9
76	647944	4181363	239	20.1	16.3	16.8	11.4
77	647719	4181316	256	20.9	17.4	17.8	29.5
78	647362	4181026	270	19.8	16.7	17.4	11.4
79	647295	4181196	268	19.8	89.2	95.1	63.3
80	647282	4181378	270	19.5	21.5	22.8	23.0
81	647234	4180865	273	19.9	17.6	17.8	20.3
82	647275	4180662	274	20.8	17.9	17.8	24.8
83	647424	4180556	273	20.1	17.5	17.4	21.2
84	647530	4180409	273	21.5	17.7	17.8	7.1

Waypoint	**Longitude (UTM, m)**	**Latitude (UTM, m)**	**Altitude (m)**	**T_{amb} (ºC)**	**T_{15} (ºC)**	**T_{40} (ºC)**	**CO_2 efflux (g m^{-2} d^{-1})**
85	647555	4180257	274	27.7	18.4	17.9	27.9
86	647692	4180373	280	20.9	17.2	16.6	15.7
87	647829	4180552	277	22.4	18.6	18.2	19.2
88	647888	4180400	279	23.1	19.3	18.8	9.5
89	647900	4180224	279	21.4	16.8	16.0	8.5
90	647932	4180052	281	21.8	21.8	21.0	7.8
91	648058	4179924	283	21.7	19.7	18.5	8.9
92	648241	4179951	283	25.4	22.1	18.9	2.0
93	648405	4180002	284	22.4	21.5	20.6	18.6
94	648601	4180036	282	23.3	21.0	20.1	25.7
95	648717	4180172	285	24.1	19.8	17.4	8.3
96	648735	4180337	285	22.1	19.3	17.2	11.9
97	648633	4180481	287	21.8	19.6	17.7	10.5
98	648470	4180659	299	19.6	21.7	20.0	2.1
99	648304	4180704	294	21.9	17.3	17.4	4.8
100	648100	4180760	280	23.4	18.1	16.9	28.9
101	647915	4180770	280	21.5	17.7	17.4	9.9
102	647797	4180687	281	22.5	16.7	16.0	24.4
103	647913	4180914	314	23.5	20.0	20.3	9.4
104	648057	4180958	334	25.2	21.2	20.1	9.9
105	647958	4181083	295	23.3	21.4	20.2	2.2
106	648108	4181168	242	20.9	20.7	20.0	8.1
107	648197	4181363	214	23.8	20.4	19.2	14.0
108	648331	4181213	218	26.1	20.1	19.3	45.0
109	648448	4181056	244	20.6	16.6	17.3	22.0
110	648626	4180940	265	19.3	16.1	15.9	4.0
111	648765	4180824	278	19.2	17.1	17.0	9.3
112	648919	4180709	293	19.4	17.5	17.0	15.3
113	648860	4180394	311	21.8	19.5	18.1	14.8
114	648974	4180549	320	20.9	15.9	15.5	1.1
115	648785	4181897	191	22.1	20.1	20.6	31.3
116	648933	4181788	187	21.7	21.5	22.7	58.6
117	649145	4181681	184	21.1	21.7	23.1	26.6
118	649330	4181708	182	21.8	20.3	21.1	52.1
119	649424	4181845	184	21.2	19.6	19.6	18.5
120	649341	4182003	190	22.2	84.0	96.5	1025.6
121	649313	4181952	193	23.3	22.0	23.9	19.4
122	649298	4181868	203	23.7	18.9	19.5	27.4
123	649406	4181998	186	23.8	61.5	80.2	690.7
124	649403	4181960	195	23.4	24.7	26.0	33.3
125	649450	4181977	193	25.0	30.7	36.6	4.3
126	649487	4182013	193	27.3	96.8	98.0	1684.4
127	649351	4181925	190	26.4	24.5	27.4	12.9
128	649358	4181862	187	26.7	18.8	19.7	48.8

Waypoint	Longitude (UTM, m)	Latitude (UTM, m)	Altitude (m)	T_{amb} (ºC)	T_{15} (ºC)	T_{40} (ºC)	CO_2 efflux (g m^{-2} d^{-1})
129	649370	4181895	181	25.4	97.3	98.5	2253.7
130	649402	4181925	181	26.5	50.7	56.4	168.6
131	649158	4182005	204	24.7	20.1	19.5	55.2
132	649101	4181851	199	22.2	17.7	17.0	12.3
133	648992	4181975	200	24.1	21.5	21.9	28.8
134	648928	4182125	201	23.1	19.2	18.3	4.6
135	648847	4182239	217	20.2	16.6	16.6	11.7
136	649132	4182572	247	21.7	19.0	19.2	13.4
137	649353	4182628	247	23.2	19.5	18.6	11.8
138	649492	4182747	241	22.0	15.6	15.2	10.8
139	649614	4182877	216	22.6	15.8	15.6	7.2
140	649789	4182961	220	22.2	17.5	16.8	3.9
141	649987	4182990	242	21.3	19.2	18.4	3.3
142	649366	4182841	250	23.4	16.0	15.5	10.1
143	649476	4182931	225	25.0	19.4	20.2	5.2
144	649341	4182990	236	23.5	20.1	18	17.6
145	649506	4182527	239	26.4	18.0	17.3	9.9
146	649681	4182535	232	28.1	19.1	18.8	1.4
147	649755	4182667	219	26.4	17.7	17.9	5.6
148	649812	4182440	215	29.5	17.6	17.5	10.2
149	650002	4182357	195	28.0	19.2	18.2	8.8
150	649498	4182353	232	26.1	21.8	20.6	4.0
151	649475	4182152	218	28.6	21.6	19.8	11.9
152	649298	4182147	203	27.5	19.8	18.3	24.3
153	649095	4182234	231	28.9	19.2	18.6	5.1
154	649047	4182388	227	30.1	18.6	17.8	17.4
155	648927	4182598	251	25.5	20.6	20.0	9.6
156	648773	4182615	260	22.0	18.1	18.4	5.3
157	648813	4182426	240	26.2	22.5	21.7	16.8
158	648600	4180268	350	21.5	18.1	17.9	56.2
159	648464	4180336	378	20.3	18.8	18.6	24.7
160	648311	4180413	368	21.3	18.8	19.0	8.8
161	648145	4180439	368	21.5	20.3	20.3	13.3
162	648183	4180198	376	21.0	21.2	21.4	11.8
163	648429	4180173	365	21.0	20.8	20.0	26.4
164	648751	4180554	305	23.0	19.1	18.3	14.3
165	648626	4180703	312	23.8	20.4	20.0	13.8
166	648413	4180851	314	24.4	19.5	19.3	27.3
167	648223	4180869	305	24.3	18.2	17.9	8.3
168	647998	4180555	308	26.2	20.7	19.9	43.0
169	647594	4181109	286	18.6	17.6	17.2	4.9
170	647783	4181160	263	18.4	16.1	17.0	7.2
171	647938	4181208	248	21.6	19.3	18.7	7.0

Waypoint	Longitude (UTM, m)	Latitude (UTM, m)	Altitude (m)	T_{amb} (ºC)	T_{15} (ºC)	T_{40} (ºC)	CO_2 efflux (g m^{-2} d^{-1})
172	647787	4181008	291	23.2	18.0	18.7	10.1
173	647658	4180959	298	23.6	20.9	20.3	14.2
174	647551	4180821	314	23.0	20.1	19.4	6.8
175	647427	4180723	342	23.3	19.8	18.7	21.0
176	647578	4180641	345	21.3	19.0	18.4	10.5
177	647720	4180822	323	20.7	21.0	20.1	13.4
178	647217	4181696	301	26.5	17.0	16.3	31.7
179	647060	4181794	344	25.7	19.3	18.4	19.3
180	647051	4181681	351	22.6	16.0	15.7	4.7
181	647425	4181784	291	23.8	21.3	19.9	7.8
182	647558	4181855	288	24.4	22.3	20.3	25.3
183	647702	4181886	284	26.4	21.5	20.6	23.5
184	647809	4182004	277	24.0	20.3	19.6	8.3
185	647959	4181991	291	24.4	23.8	21.7	22.8
186	648454	4181309	267	24.6	19.2	19.1	26.3
187	648644	4181389	265	24.1	20.1	20.0	18.6
188	648793	4181472	260	23.8	18.6	19.0	14.7
189	648903	4181623	254	25.0	19.4	19.7	10.5
190	648488	4181628	255	24.3	20.0	19.2	9.9
191	648615	4181543	258	24.3	21.0	20.5	25.8
192	648507	4181437	265	22.3	20.2	20.0	30.6
193	648078	4181768	267	22.6	17.2	16.9	9.6
194	648113	4181542	261	23.2	21.1	21.0	13.7
195	648222	4181479	263	19.5	19.2	19.3	28.7
196	647558	4180079	345	25.8	20.3	19.8	17.4
197	647739	4180228	350	23.0	21.2	21.3	46.1
198	647759	4180079	353	22.6	20.2	19.1	26.3
199	647734	4179928	352	23.6	20.9	20.7	44.1
200	647529	4179913	347	23.4	20.8	19.9	13.9
201	648413	4182545	278	23.3	22.0	20.7	18.3
202	648838	4182762	378	19.8	19.3	18.4	5.5
203	649215	4182901	329	20.7	20.0	18.2	23.9
204	649188	4183047	294	20.0	17.8	17.0	3.9
205	648961	4181487	250	18.7	16.2	18.4	37.9
206	648888	4181354	247	18.8	17.5	18.8	28.6
207	648761	4181265	252	19.5	17.7	19.0	24.6
208	648877	4181167	252	19.7	18.2	19.4	28.9
209	649003	4181253	250	19.8	15.8	17.9	9.4
210	649120	4181158	249	21.8	14.1	16.2	17.1
211	649081	4180943	260	19.5	18.5	18.2	17.9
212	649027	4180803	280	20.1	17.5	18.3	18.2
213	649175	4180783	292	19.7	16.4	17.4	15.2
214	648960	4181038	253	17.8	16.4	17.6	18.5
215	648894	4180900	263	18.3	17.3	18.8	18.1

Waypoint	Longitude (UTM, m)	Latitude (UTM, m)	Altitude (m)	T_{amb} (ºC)	T_{15} (ºC)	T_{40} (ºC)	CO_2 efflux (g m^{-2} d^{-1})
216	648788	4181034	248	18.9	16.5	17.2	10.7
217	649258	4181066	254	19.3	15.5	16.5	22.3
218	649331	4180932	278	19.5	15.5	16.9	5.0
219	649376	4181175	273	19.3	15.8	17.0	4.9
220	649264	4181277	304	21.8	19.2	20.7	27.6
221	649355	4181397	312	20.2	16.5	17.1	15.3
222	649095	4181376	246	19.4	15.9	16.6	9.6
223	648541	4181193	240	20.7	20.0	19.5	14.3
224	648668	4181119	251	21.1	17.3	17.9	11.9
225	649220	4181506	232	21.8	18.5	19.3	15.2
226	647351	4181646	320	17.0	15.9	16.7	61.3
227	647277	4181582	349	17.8	16.4	17.2	34.0
228	647361	4181525	315	18.1	16.8	17.7	52.2
229	647475	4181573	306	17.4	18	18.5	24.4
230	647618	4181620	295	17.7	17.8	18.2	11.8
231	647772	4181459	318	18.5	18.7	18.9	29.3
232	647617	4181439	314	20.9	16.9	18.1	20.1
233	647454	4181394	334	22.0	16.5	17.3	13.4
234	647547	4181260	310	21.3	17.9	19.0	18.3
235	649392	4181586	233	22.9	15.6	17.2	1.7
236	649552	4181712	242	22.1	17.2	17.9	10.9
237	649707	4181735	231	21.5	17.1	17.5	5.3
238	649860	4181773	217	22.4	17.4	17.6	28.6
239	650054	4181765	210	22.5	15.9	17.1	18.6
240	649890	4181966	220	21.8	25.6	29.7	22.2
241	649517	4181925	225	21.5	16.9	15.8	26.8
242	649771	4182058	228	21.6	17.5	17.7	11.6
243	649621	4182024	227	21.4	18.2	18.1	35.7
244	649727	4181856	235	20.5	18.3	18.1	22.8
245	649066	4182958	272	20.3	18.1	17.9	31.2
246	648930	4182962	269	19.7	15.7	15.7	14.0
247	649027	4183107	267	19.4	18.2	18.6	21.7
248	649650	4182238	214	21.5	17.7	17.7	37.4
249	648402	4181838	210	22.9	18.4	18.9	28.6
250	648553	4181864	208	22.1	18.0	18.6	22.8
251	648677	4181778	215	21.9	16.3	16.2	11.5
252	648806	4181720	213	21.3	16.1	15.9	7.8
253	648714	4181612	222	20.8	16.4	16.0	9.4
254	648585	4181690	220	21.0	20.3	19.5	10.6
255	648484	4181754	212	22.5	20.2	20.1	13.3
256	649063	4181594	205	21.4	18.7	19.0	34.4
257	649954	4181644	203	21.3	18.0	18.6	31.6
258	649816	4181562	222	22.3	19.2	19.8	22.3

Waypoint	Longitude (UTM, m)	Latitude (UTM, m)	Altitude (m)	T_{amb} (ºC)	T_{15} (ºC)	T_{40} (ºC)	CO_2 efflux (g m^{-2} d^{-1})
259	649527	4181079	253	22.1	18.3	19.3	35.7
260	649649	4181180	311	19.4	16.5	16.9	13.4
261	649501	4181287	303	19.8	18.1	18.0	18.2
262	649744	4181298	343	21.4	17.8	18.2	9.0
263	649712	4181447	320	21.5	19.6	19.2	6.0
264	649540	4181431	299	21.6	18.3	18.6	30.0
265	649281	4182407	223	24.6	18.5	18.1	21.6
266	648583	4182832	334	24.1	15.5	15.6	12.7
267	647305	4181273	279	22.3	19.6	18.8	16.3
268	647300	4181186	280	21.9	18.6	18.2	8.9
269	647311	4181110	280	21.4	17.5	16.5	11.9
270	647428	4181195	298	23.0	19.5	18.6	5.3
271	650229	4181672	179	21.6	21.2	21.6	47.9
272	650173	4181863	179	20.6	20.8	20.0	15.7

Table 7. Chemical composition of the soil gas in Furnas caldera survey.

Waypoint	^{4}He (ppm)	Ne (ppm)	H_2 (ppm)	O_2 (ppm)	N_2 (ppm)	CH_4 (ppm)	CO_2 (ppm)	H_2S (ppm)	H_2O (ppm)	$\delta^{13}C\text{-}CO_2$ ‰ vs. VPDB
1	5.6	17.5	9.7	184544	790794	13569.3	20408	0.0	566	-12.67
2	9.6	18.8	11.2	82929	843746	14561.8	71367	0.0	590	-23.31
3	21.3	16.9	1.0	163566	765293	7.6	67586	0.0	723	-11.95
4	12.1	17.1	6.2	179305	685929	1.7	134463	0.0	618	-0.20
5	18.3	18.0	3.7	176601	772938	1.7	53519	0.0	549	-13.08
6	6.0	18.4	5.2	165100	804193	1.7	41680	0.0	535	-22.14
7	14.0	18.9	7.4	151450	810462	34.1	48183	0.0	592	-10.77
8	23.5	19.2	11.3	186355	724421	2.8	90132	0.0	578	-1.86
9	19.2	16.0	3.0	121306	459560	1.7	408998	0.0	586	-2.50
10	17.5	15.9	5.3	137929	520142	1.7	323910	0.0	564	-2.94
11	11.1	18.4	4.2	198925	784966	1.7	27240	0.0	589	-12.75
12	6.5	18.5	10.5	145462	787062	1.7	78898	0.0	564	-9.77
13	9.5	18.0	16.8	15672	104351	2177.3	925314	0.0	618	-3.98
14	18.6	15.2	11.0	72126	273249	4.5	657019	0.0	857	-2.81
15	5.7	18.7	5.7	190999	725011	8.0	89310	0.0	511	-2.15
16	18.2	18.0	710.3	13081	52731	1493.7	964440	0.0	1988	-4.80
17	6.5	18.0	1140.0	12597	48333	196.0	1003269	591.6	556	-4.26
18	43.0	18.5	6.2	194953	778049	1.7	34408	0.0	629	-2.56
19	41.6	18.0	5.9	175068	675373	1.7	143472	0.0	607	-2.59
20	6.4	18.9	4.3	200643	761244	1.7	47554	0.0	551	-3.18
21	5.7	15.9	8.8	113766	450187	4.7	425650	0.0	589	-2.61
22	5.2	18.0	3.1	185792	706780	1.7	108270	0.0	569	-1.15
23	5.9	17.3	4.8	197226	749787	1.7	49227	0.0	541	-4.15
24	10.6	18.1	3.4	206230	790038	1.7	14709	0.0	687	-8.05

Waypoint	^{4}He (ppm)	Ne (ppm)	H_2 (ppm)	O_2 (ppm)	N_2 (ppm)	CH_4 (ppm)	CO_2 (ppm)	H_2S (ppm)	H_2O (ppm)	δ^{13}C-CO_2 ‰ vs. VPDB
25	5.5	17.1	6.8	99213	375463	1.7	519971	0.0	590	-2.44
26	5.7	18.2	23.5	204296	769723	1.7	16633	0.0	1513	-1.34
27	7.3	18.0	1286.4	28970	113899	42.2	888104	5.0	1575	-4.94
28	5.9	14.5	14.0	92319	354189	7.1	537719	0.0	1503	-3.80
29	6.1	14.9	205.2	101806	394200	6.3	496184	0.0	609	-3.33
30	6.3	11.8	16.2	54942	208694	11.9	753748	0.0	607	-4.16
31	7.1	18.0	179.4	23207	86432	35.1	932213	0.0	1348	-5.02
32	7.9	16.3	156.7	105052	403985	9.7	475678	0.0	632	-4.94
33	6.3	12.8	6.6	61968	285422	5.4	647421	0.0	1518	-4.12
34	6.3	17.9	7.2	195143	753516	1.7	51569	0.0	641	-5.77
35	26.5	18.6	7.0	116325	803145	1.7	93684	0.0	542	-12.32
36	28.2	18.0	6.8	165203	782826	1.7	55475	0.0	568	-13.24
37	13.8	18.5	6.2	183285	788507	1.7	38424	0.0	538	-15.45
38	43.4	17.9	4.1	202187	791651	1.7	14509	0.0	593	-14.50
39	6.1	17.5	2.3	205555	789493	1.7	5571	0.0	571	-20.19
40	38.8	18.2	2.2	209987	794740	1.7	2672	0.0	708	-13.68
41	8.4	17.7	3.8	208418	790313	1.7	3091	0.0	534	-12.74
42	5.7	18.2	3.8	191214	793557	1.7	19543	0.0	587	-11.96
43	5.8	16.6	5.3	90622	393329	1.7	504412	0.0	566	-2.00
44	10.4	18.0	3.5	33911	132843	9.2	865273	0.0	560	-4.25
45	17.4	18.0	33.5	31962	124057	36.3	888758	0.0	560	-4.76
46	6.2	13.6	14.4	78344	300046	20.9	625152	0.0	507	-3.95
47	6.1	16.4	8.9	161116	619809	1.7	204268	0.0	539	-2.77
48	18.4	12.3	6.9	69166	267097	3.4	670733	0.0	606	-4.14
49	5.7	15.7	5.2	106098	406394	1.7	483313	0.0	571	-2.89
50	6.1	18.2	2.3	204741	784475	1.7	22258	0.0	499	-8.12

Waypoint	**^{4}He (ppm)**	**Ne (ppm)**	**H_2 (ppm)**	**O_2 (ppm)**	**N_2 (ppm)**	**CH_4 (ppm)**	**CO_2 (ppm)**	**H_2S (ppm)**	**H_2O (ppm)**	**δ^{13}C-CO_2 ‰ vs. VPDB**
51	5.9	18.2	2.5	197558	765866	1.7	42223	0.0	627	-7.43
52	7.1	18.7	3.7	196119	794178	1.7	23778	0.0	525	-21.71
53	6.0	18.3	1.6	196555	770653	1.7	42086	0.0	499	-10.76
54	6.5	18.0	10.4	166295	630241	4.0	198265	0.0	577	-2.34
55	5.2	9.9	60.3	29087	134374	16.6	880241	0.0	567	-4.51
56	5.8	18.7	0.5	204123	796639	2.3	9366	0.0	492	-24.11
57	6.2	18.4	1.9	210345	802306	1.7	2404	0.0	459	-24.65
58	5.8	18.2	2.5	208568	797173	1.9	4831	0.0	414	-21.29
59	6.6	18.5	1.5	205628	786247	1.7	25996	0.0	452	-8.92
60	6.0	18.8	3.1	204935	794586	1.7	7595	0.0	536	-23.29
61	5.8	17.7	2.5	208647	797486	1.7	2732	0.0	512	-13.68
62	5.8	19.1	2.4	202234	801522	1.7	11348	0.0	471	-23.61
63	5.7	18.5	1.3	210627	793527	1.7	2212	0.0	596	-14.69
64	5.8	19.0	0.7	210725	795746	1.7	1124	0.0	535	-20.81
65	5.8	18.0	2.7	209967	794084	1.7	2023	0.0	573	-21.86
66	5.9	18.9	2.2	205042	799280	1.7	9055	0.0	498	-19.66
67	5.6	18.1	7.5	204925	795359	1.7	8308	0.0	589	-24.56
68	6.1	19.0	1.0	205150	801907	1.7	5134	0.0	557	-25.90
69	8.1	18.5	8.6	200617	799049	1.7	12585	0.0	606	-21.35
70	5.9	18.5	5.3	175380	800598	1.7	33662	0.0	607	-22.21
71	5.7	18.5	2.8	194523	799373	1.7	23610	0.0	457	-22.21
72	5.9	19.7	3.7	186271	758058	1.7	55256	0.0	609	-5.80
73	5.9	17.7	0.8	200594	794921	1.7	12943	0.0	634	-22.79
74	6.4	18.6	3.8	193124	793363	1.7	20612	0.0	742	-23.75
75	6.1	18.3	3.1	207124	788919	1.7	12702	0.0	612	-12.37
76	5.8	18.3	2.1	210439	794609	1.7	2476	0.0	527	-19.05

Waypoint	**^{4}He (ppm)**	**Ne (ppm)**	**H_2 (ppm)**	**O_2 (ppm)**	**N_2 (ppm)**	**CH_4 (ppm)**	**CO_2 (ppm)**	**H_2S (ppm)**	**H_2O (ppm)**	**δ^{13}C-CO_2 ‰ vs. VPDB**
77	6.1	18.7	3.8	201954	799492	1.7	13867	26.9	512	-16.92
78	5.8	18.1	2.8	206402	794464	1.7	5943	0.0	619	-23.64
79	6.5	11.3	165.9	61908	238328	73.4	711821	0.0	618	-4.31
80	6.1	18.2	9.2	205386	781907	1.7	22108	0.0	643	-8.03
81	6.0	18.7	3.0	206870	795168	1.7	7802	0.0	664	-19.54
82	10.6	18.0	1.9	205751	794312	1.7	7557	0.0	552	-15.07
83	5.9	18.3	1.5	209030	794334	1.7	3131	0.0	590	-18.72
84	6.5	18.5	6.7	207145	792428	1.7	4782	0.0	771	-15.41
85	6.2	18.5	1.6	209391	798029	1.7	3386	0.0	648	-16.05
86	11.4	18.4	3.8	207875	794588	1.7	4266	0.0	671	-21.80
87	6.0	18.5	1.2	207473	793018	1.7	4369	0.0	648	-23.17
88	24.4	18.3	1.7	206900	795222	1.7	5674	0.0	555	-20.51
89	6.3	18.8	3.1	207795	802006	1.7	5127	0.0	536	-23.27
90	12.4	17.7	2.5	209369	793505	1.7	2177	0.0	695	-20.44
91	11.4	18.1	9.4	201406	791803	1.7	13080	0.0	686	-21.67
92	8.7	17.8	2.7	204329	790674	1.7	7841	0.0	739	-21.09
93	9.8	16.3	2.9	210606	792953	1.7	742	0.0	712	-14.81
94	5.9	18.1	6.5	163376	789482	1.7	50696	0.0	800	-15.91
95	12.2	18.0	1.3	207615	794602	6.4	5088	0.0	650	-21.20
96	5.8	18.8	2.3	209132	794062	1.7	2864	0.0	635	-17.89
97	6.0	18.1	3.0	204387	793767	1.7	6760	7.0	727	-20.46
98	6.6	18.4	2.7	209806	790347	1.7	1477	0.0	813	-18.09
99	11.3	18.3	3.1	211113	798487	1.7	1584	0.0	606	-18.68
100	19.3	17.6	0.7	204375	789971	1.7	7965	0.0	751	-22.48
101	5.9	18.5	1.5	210186	794729	1.7	1664	0.0	650	-18.32
102	5.8	18.1	1.8	209666	794628	1.7	2113	0.0	713	-16.25

Waypoint	**^{4}He (ppm)**	**Ne (ppm)**	**H_2 (ppm)**	**O_2 (ppm)**	**N_2 (ppm)**	**CH_4 (ppm)**	**CO_2 (ppm)**	**H_2S (ppm)**	**H_2O (ppm)**	**δ^{13}C-CO_2 ‰ vs. VPDB**
103	15.3	18.2	0.8	206700	795473	1.7	4575	0.0	562	-28.17
104	8.6	17.4	3.1	207653	793678	1.7	4322	0.0	634	-24.31
105	5.9	18.8	1.0	206042	796771	1.7	6174	0.0	658	-22.89
106	27.1	18.6	2.6	210950	799143	1.7	1526	0.0	555	-19.89
107	7.3	18.5	11.3	212176	800604	1.7	471	0.0	472	-16.01
108	6.7	18.4	1.5	208240	793184	1.7	3298	0.0	674	-20.54
109	5.7	18.9	1.9	210413	796041	1.7	1366	0.0	571	-20.72
110	12.6	19.5	3.1	209951	796296	1.7	2717	0.0	556	-22.19
111	27.9	18.9	8.1	210297	800246	1.7	2996	0.0	458	-21.05
112	6.0	18.7	3.8	209163	794953	1.7	3093	0.0	571	-21.57
113	8.1	19.5	2.6	207446	793625	1.7	5916	0.0	574	-21.53
114	13.2	18.6	3.3	210373	798521	1.7	2432	0.0	561	-20.57
115	5.8	18.3	1.0	211024	798187	1.7	3998	0.0	543	-9.50
116	6.1	18.4	4.1	164793	785748	1.7	56924	0.0	599	-18.65
117	5.7	18.4	3.6	192610	780983	1.7	24562	0.0	1365	-18.27
118	5.8	18.4	10.8	198243	783667	1.7	28293	0.0	641	-21.35
119	10.5	18.5	3.7	195999	782971	1.7	18034	0.0	1453	-12.94
120	5.2	18.0	1826.1	27897	109929	149.2	900002	501.9	718	-20.75
121	5.8	18.4	3.7	198932	764989	1.7	25222	0.0	1652	-2.61
122	5.6	18.1	9.0	204817	794338	1.7	8938	0.0	591	-7.39
123	6.0	18.2	8.1	162639	616897	7.6	210676	0.0	659	-16.06
124	5.7	18.5	1.7	207777	787923	1.7	12336	0.0	635	-2.88
125	5.8	18.2	2.3	207432	784344	1.7	14969	0.0	672	-5.97
126	6.9	14.1	306.9	50617	212001	43.5	753086	0.0	781	-1.94
127	5.6	17.5	5.0	204724	773996	2.6	29600	0.0	636	-4.52
128	5.7	17.9	2.4	198929	759253	1.7	48130	0.0	571	-5.41

Waypoint	^{4}He (ppm)	Ne (ppm)	H_2 (ppm)	O_2 (ppm)	N_2 (ppm)	CH_4 (ppm)	CO_2 (ppm)	H_2S (ppm)	H_2O (ppm)	$\delta^{13}C\text{-}CO_2$ ‰ vs. VPDB
129	6.2	18.0	4074.4	23664	90810	50.7	913198	481.0	1703	-5.24
130	6.1	16.2	60.7	111764	444807	16.0	428351	0.0	935	-4.56
131	9.7	18.1	10.3	202030	766617	1.7	24546	0.0	1564	-2.80
132	5.8	18.0	2.0	210279	795874	1.7	2581	0.0	632	-4.15
133	5.7	17.3	7.3	191643	736639	1.7	72230	0.0	715	-14.17
134	5.8	17.4	14.3	154946	618489	1.7	208815	0.0	1378	-9.04
135	5.8	18.4	5.5	210627	796765	1.7	1365	0.0	675	-2.24
136	5.6	17.9	1.7	209824	796015	1.7	2644	0.0	605	-9.80
137	5.5	18.2	14.4	206901	794672	1.7	5434	0.0	734	-18.82
138	5.6	18.1	3.7	209913	796203	1.9	1805	0.0	642	-20.71
139	5.5	18.3	2.5	204038	784857	1.7	4975	0.0	1518	-21.53
140	5.9	18.5	7.2	172569	810102	1.7	29087	0.0	636	-23.72
141	5.7	18.2	7.1	210606	797535	1.7	1550	0.0	630	-22.18
142	5.6	18.6	2.3	206176	797226	1.7	6879	0.0	557	-16.74
143	5.8	18.5	14.2	202805	796843	1.7	8975	0.0	690	-24.54
144	5.8	18.5	9.1	209688	799562	1.7	4321	0.0	646	-26.20
145	5.8	18.3	2.6	208741	792414	1.7	2016	0.0	811	-22.13
146	5.7	18.7	5.6	201613	793039	1.7	10324	0.0	753	-20.17
147	5.7	18.5	3.4	202249	791437	1.7	10212	0.0	879	-22.19
148	6.4	18.4	1.3	201250	802159	1.7	7660	0.0	691	-21.16
149	5.7	18.2	3.8	207186	793261	1.7	4473	0.0	828	-21.94
150	5.5	18.3	2.6	206860	784948	1.7	2546	0.0	1468	-21.56
151	6.7	18.0	1.3	203462	791440	1.7	8450	0.0	850	-19.71
152	5.6	18.7	3.6	205374	784659	1.7	15849	0.0	714	-21.81
153	5.6	18.4	2.3	203898	797182	1.7	7718	0.0	652	-7.90
154	5.7	18.5	7.3	208720	796284	1.7	3418	0.0	661	-23.50

Waypoint	^{4}He (ppm)	Ne (ppm)	H_2 (ppm)	O_2 (ppm)	N_2 (ppm)	CH_4 (ppm)	CO_2 (ppm)	H_2S (ppm)	H_2O (ppm)	δ^{13}C-CO_2 ‰ vs. VPDB
155	5.7	18.5	1.6	195001	796396	1.7	17939	0.0	692	-21.24
156	5.9	18.6	1.9	207030	796863	1.7	5693	0.0	591	-19.74
157	5.9	18.4	2.4	207002	792080	1.7	6651	0.0	650	-24.26
158	6.3	18.3	2.2	208027	795153	1.7	3906	0.0	605	-20.90
159	5.6	18.2	14.1	203242	799376	1.7	12660	0.0	539	-23.91
160	6.4	18.5	4.6	204580	801672	1.7	11505	0.0	547	-25.77
161	5.8	18.5	3.8	203161	795843	1.7	8632	0.0	610	-24.49
162	6.0	18.8	3.3	208778	796490	1.7	3392	0.0	562	-24.51
163	5.6	18.4	6.0	201009	798275	1.7	17702	0.0	570	-21.86
164	5.8	18.6	2.8	207414	795122	1.7	5108	0.0	601	-23.42
165	5.9	18.5	8.8	204208	794445	1.7	9005	0.0	623	-22.98
166	6.1	18.3	2.4	206721	795335	1.7	5920	0.0	622	-21.86
167	6.1	18.2	1.2	211210	798662	1.7	1272	0.0	615	-23.53
168	5.7	18.6	0.9	181798	787952	1.7	37774	0.0	663	-18.59
169	6.0	18.3	1.5	206500	793144	1.7	6744	0.0	610	-24.89
170	5.6	18.3	3.4	207438	794098	1.7	4439	0.0	643	-18.96
171	5.9	18.6	2.2	208443	795174	1.7	3495	0.0	693	-24.03
172	5.6	18.1	3.3	208624	797495	1.7	4158	0.0	572	-21.83
173	5.6	18.5	7.1	178341	788807	1.7	39541	0.0	662	-21.88
174	5.7	18.8	3.3	188709	793380	1.7	28519	0.0	622	-20.68
175	5.7	18.5	13.6	195593	791930	1.7	21665	0.0	649	-25.67
176	5.9	18.6	3.4	192617	797388	1.7	26003	0.0	511	-22.69
177	5.9	18.6	6.7	193852	794462	1.7	22804	0.0	547	-24.42
178	5.5	19.7	2.5	198206	763599	1.7	40640	0.0	655	-25.25
179	5.6	18.1	4.5	189690	782701	1.7	33322	0.0	798	-5.58
180	5.9	18.3	2.5	198556	793928	1.7	14685	0.0	652	-21.97

Waypoint	^{4}He (ppm)	Ne (ppm)	H_2 (ppm)	O_2 (ppm)	N_2 (ppm)	CH_4 (ppm)	CO_2 (ppm)	H_2S (ppm)	H_2O (ppm)	δ^{13}C-CO_2 ‰ vs. VPDB
181	5.8	18.3	2.4	205300	792383	1.7	10140	0.0	634	-26.92
182	6.0	18.5	13.7	207383	795553	1.7	6310	0.0	591	-16.50
183	5.8	18.6	15.3	202345	796091	1.7	10497	0.0	634	-22.47
184	5.7	18.8	11.0	186841	787252	1.7	32426	0.0	632	-19.38
185	5.6	18.5	3.3	200631	802919	1.7	13937	0.0	477	-13.87
186	5.9	18.0	1.1	209359	796167	1.7	2531	0.0	587	-23.74
187	5.6	18.4	3.6	208257	793246	1.7	2978	0.0	667	-20.02
188	5.9	18.5	1.2	194960	801713	1.7	16232	0.0	687	-20.34
189	5.6	18.2	3.7	207530	795221	1.7	4382	0.0	614	-23.90
190	5.8	18.7	1.5	205271	794785	1.7	6689	0.0	637	-22.12
191	6.0	18.6	5.3	199915	791151	1.7	18913	0.0	651	-21.61
192	6.6	18.1	6.5	207231	792487	1.7	5026	0.0	674	-24.06
193	5.7	17.6	3.7	209420	797324	1.7	2916	0.0	576	-21.73
194	5.8	18.2	1.8	207784	791997	1.7	7187	0.0	602	-21.08
195	5.7	18.5	4.3	204192	792283	1.7	8815	0.0	665	-10.10
196	6.3	18.5	4.1	210281	801221	1.7	3336	0.0	535	-22.38
197	6.0	18.5	2.4	200841	790519	1.7	13271	0.0	752	-16.24
198	5.6	18.4	9.9	165388	790040	1.7	51575	0.0	687	-22.92
199	5.7	18.1	4.2	192633	785272	1.7	29918	0.0	631	-20.87
200	5.7	18.5	4.7	209516	794870	1.7	2283	0.0	626	-22.24
201	5.9	18.8	20.6	207737	796828	1.7	5419	0.0	601	-15.02
202	5.9	18.5	1.7	197799	797938	1.7	13795	0.0	565	-22.12
203	5.9	18.3	6.0	201965	790447	1.7	15880	0.0	619	-22.27
204	5.8	18.5	1.6	177573	805500	1.7	29083	0.0	578	-25.48
205	5.7	18.7	2.9	208097	796827	1.7	4087	0.0	562	-23.27
206	5.8	18.4	3.5	191598	798150	1.7	22085	0.0	563	-24.47

Waypoint	^{4}He (ppm)	Ne (ppm)	H_2 (ppm)	O_2 (ppm)	N_2 (ppm)	CH_4 (ppm)	CO_2 (ppm)	H_2S (ppm)	H_2O (ppm)	$\delta^{13}C-CO_2$ ‰ vs. VPDB
207	5.9	18.3	4.1	202538	794353	1.7	11658	0.0	682	-26.04
208	5.8	18.4	5.6	206362	797813	1.7	7846	0.0	544	-24.23
209	6.1	18.7	3.6	205410	796264	1.7	11407	0.0	539	-14.21
210	6.0	18.6	3.7	199102	794970	1.7	15321	0.0	570	-23.70
211	6.0	18.3	5.7	205529	797590	1.7	9212	0.0	538	-19.93
212	5.8	18.4	1.9	203778	798547	1.7	13184	0.0	533	-21.77
213	5.9	19.1	9.0	208647	794790	1.9	3362	0.0	586	-23.17
214	5.8	18.7	3.9	206049	793083	1.7	6098	0.0	668	-23.01
215	5.9	18.8	7.5	193535	792322	1.7	24409	0.0	518	-23.45
216	16.6	18.6	3.8	208797	796769	1.7	3692	0.0	503	-24.07
217	5.9	18.7	4.8	203291	794414	1.7	9578	0.0	597	-21.31
218	5.8	18.8	5.9	207480	793859	1.7	3835	0.0	625	-25.25
219	6.1	18.5	2.6	205131	794944	1.7	7369	0.0	643	-24.04
220	5.8	18.6	6.0	188218	794093	1.7	26437	0.0	612	-20.55
221	5.7	18.5	3.5	208203	796570	1.7	3239	0.0	557	-25.04
222	5.8	18.6	1.6	207901	796415	1.7	4523	0.0	548	-23.33
223	5.6	18.7	1.4	207069	797508	1.7	5833	0.0	634	-21.54
224	5.7	18.4	0.7	207850	795862	1.7	4808	0.0	604	-21.52
225	5.6	18.5	1.5	204353	792444	1.7	8174	0.0	781	-24.03
226	5.5	17.5	1.5	207529	790668	1.7	2643	0.0	517	-21.52
227	5.6	18.7	4.9	199095	786919	1.7	20677	0.0	573	-20.20
228	5.9	18.2	3.5	187665	792851	1.7	26118	0.0	578	-23.27
229	5.8	18.4	12.3	205568	791892	1.7	6916	0.0	549	-22.85
230	5.8	18.4	7.5	198858	789275	1.7	15521	0.0	540	-23.51
231	5.6	18.8	10.0	205081	791339	1.7	6787	0.0	582	-17.59
232	5.8	18.3	12.6	204606	796468	1.7	9462	0.0	551	-24.31

Waypoint	^{4}He (ppm)	Ne (ppm)	H_2 (ppm)	O_2 (ppm)	N_2 (ppm)	CH_4 (ppm)	CO_2 (ppm)	H_2S (ppm)	H_2O (ppm)	δ^{13}C-CO_2 ‰ vs. VPDB
233	5.6	18.6	5.1	202728	789491	1.7	8324	0.0	653	-24.50
234	5.8	18.3	5.9	189479	784677	1.7	28824	0.0	602	-21.90
235	5.4	18.5	1.0	208464	793043	1.7	3774	0.0	622	-23.02
236	5.5	18.0	8.2	203654	788362	1.7	9951	0.0	699	-22.79
237	5.7	18.1	2.7	209920	790184	1.7	1212	0.0	633	-20.25
238	5.8	16.1	8.1	122480	462632	1.7	396726	0.0	913	-1.96
239	5.7	17.9	7.6	197541	784718	1.7	22982	0.0	587	-16.75
240	5.5	18.7	6.3	205442	788330	1.7	5988	0.0	688	-18.74
241	5.8	18.5	0.8	209155	791222	1.7	1880	0.0	618	-19.46
242	6.1	18.3	3.2	208046	792711	1.7	3762	0.0	537	-15.08
243	5.7	18.8	2.3	204202	782336	1.7	18913	0.0	598	-6.08
244	5.9	17.7	9.3	205373	786816	1.7	8373	0.0	627	-17.97
245	5.8	18.2	3.7	198929	789597	1.7	16445	0.0	567	-19.65
246	5.9	18.5	1.6	188568	799013	1.7	21897	0.0	539	-27.20
247	5.7	18.3	10.5	200085	789941	1.7	14501	0.0	620	-22.98
248	5.6	18.6	11.4	201253	788081	1.7	14814	0.0	595	-21.14
249	6.0	18.1	1.5	184451	791578	1.7	29459	0.0	610	-22.20
250	6.5	18.4	3.7	192980	794675	1.7	25087	0.0	546	-22.43
251	5.5	18.4	3.1	202548	793874	1.7	11607	0.0	542	-24.79
252	5.7	18.2	1.9	208154	793661	1.7	4456	0.0	553	-23.20
253	5.9	18.5	8.7	207806	796199	1.7	3797	0.0	526	-23.64
254	5.7	18.2	3.1	201693	794814	1.7	12657	0.0	539	-22.30
255	5.6	18.1	3.7	199587	797852	1.7	12586	0.0	590	-22.85
256	5.7	18.4	6.1	198836	793142	1.7	12644	0.0	585	-20.29
257	5.5	18.3	15.0	203680	795545	1.7	8727	0.0	604	-26.63
258	5.8	18.9	18.3	192741	788989	1.7	24909	0.0	596	-24.46

Waypoint	^{4}He (ppm)	Ne (ppm)	H_2 (ppm)	O_2 (ppm)	N_2 (ppm)	CH_4 (ppm)	CO_2 (ppm)	H_2S (ppm)	H_2O (ppm)	δ^{13}C-CO_2 ‰ vs. VPDB
259	5.6	18.5	7.4	207914	792890	1.7	3966	0.0	613	-23.30
260	5.7	18.5	19.6	199005	791797	1.7	14137	0.0	576	-24.16
261	5.5	18.5	7.6	199509	791289	1.7	13852	0.0	618	-25.12
262	5.4	17.9	1.4	205622	789493	1.7	6507	0.0	631	-23.26
263	6.0	17.9	0.7	198796	790571	1.7	13335	0.0	619	-26.15
264	5.9	18.5	12.6	208812	792676	1.7	2069	0.0	599	-22.32
265	5.6	18.3	6.1	182208	785818	1.7	32960	0.0	696	-23.59
266	5.6	18.2	3.1	211119	796272	1.7	1636	0.0	504	-20.87
267	5.8	18.0	1.6	206380	786206	1.7	7353	0.0	721	-11.07
268	5.6	18.1	4.6	199147	767459	1.7	33546	0.0	652	-8.96
269	5.7	18.2	1.8	209595	791301	1.7	2979	0.0	579	-18.24
270	8.3	18.0	2.9	202141	793592	1.7	11749	0.0	604	-23.12
271	5.8	10.3	26.6	46620	175332	73.2	801450	0.0	617	-3.61
272	5.7	19.3	5.8	204306	791274	1.7	12229	0.0	585	-14.16

Table 8. Data of ^{3}He/^{4}He (R/Ra)$_c$, diffuse ^{4}He emission (mol/d)*, diffuse ^{4}He emission (mol/d)**, diffuse ^{3}He emission (mol/d) and thermal energy released (MW) from studied areas. n.c.: not calculated. * diffuse ^{4}He emission (mol/d) calculated by the first methodology. ** diffuse ^{4}He emission (mol/d) calculated by the second methodology. Data sources: this study in addition to (a) Alonso et al., 2019, (b) Alonso et al., 2021, (c) Jean-Baptiste et al., 2009, (d) Viveiros et al., 2010), (e) Fischer et al., 2015, (f) Melián et al., 2019, (g) Tedesco and Scarsi, 1999, (h) Chiodini et al., 2001, (i) Chiodini et al., 2005, (j) Poreda et al., 1992, (k) [13] Fridriksson et al., 2006, (l) Marty et al., 1991, _(m) Hernandez et al., 2012, (n) Chiodini et al., 2012, (o) Chiodini et al., 2005, (p) Tedesco 1996, (q) Tedesco et al., 1998, (r) Tedesco and Scarsi 1999, (s) Parello et al., 2000, (t) Shimizu et al., 2005.

Volcano-Geothermal System	**Region**	**Study área** (km^2)	^{3}**He/**^{4}**He** (R/Ra)$_c$	**Diffuse** ^{4}**He*** (mol·d^{-1})	**Diffuse** ^{4}**He**** (mol·d^{-1})	**Diffuse** ^{3}**He** (mol·d^{-1})	**Thermal energy** (MW)
Teide summit cone	Tenerife, Canary Islands	0.500	7.16 ± 0.08	836 ± 98	134	1.32×10^{-3}	28.4
			7.05 ± 0.08	494 ± 32	105	1.03×10^{-3}	34.2
			6.95 ± 0.07	374 ± 105	33	3.18×10^{-4}	7.2
			6.72 ± 0.06 (a)	265 ± 57 (a)	104	9.66×10^{-4} (a)	2.2 (a)
			7.15 ± 0.05	1213 ± 88	452	4.47×10^{-3}	56.4
			5.27 ± 0.05	2147 ± 536	165	1.20×10^{-3}	32.0
			6.8 ± 0.1	57 ± 17	202	1.91×10^{-3}	19.5
Teide summit crater	Tenerife, Canary Islands	0.007	7.16 ± 0.08	31 ± 8	10	9.43×10^{-5}	2.0
			7.04 ± 0.06	n.c	10	9.48×10^{-5}	3.1
			7.0 ± 0.1	n.c	5	4.66×10^{-5}	2.7
			7.11 ± 0.08	n.c	5	4.58×10^{-5}	1.1
			7.05 ± 0.08	16 ± 3	10	9.52×10^{-5}	2.0
			7.07 ± 0.06	n.c	7	7.05×10^{-5}	0.8
			7.09 ± 0.07	n.c	6	5.87×10^{-5}	1.2
			6.92 ± 0.08	n.c	2	2.12×10^{-5}	0.9
			6.95 ± 0.07	8 ± 1	2	2.32×10^{-5}	0.5
			6.87 ± 0.08	n.c	5	4.51×10^{-5}	1.6
			6.72 ± 0.06	17 ± 3	n.c	n.c	1.9
			7.57 ± 0.04	17 ± 3	n.c	n.c	1.2
			6.77 ± 0.44	295 ± 35	41	3.83×10^{-4}	6.1
			7.15 ± 0.05	24 ± 3	9	8.77×10^{-5}	2.4

			6.76 ± 0.44	n.c	17	1.55×10^{-4}	4.7
			7.32 ± 0.04	32 ± 8	10	1.01×10^{-4}	1.2
			5.27 ± 0.05	296 ± 88	13	9.43×10^{-5}	2.5
			6.56 ± 0.05	33 ± 6	30	2.72×10^{-4}	4.5
			6.85 ± 0.11	29 ± 8	17	1.59×10^{-4}	1.6
Fogo summit cráter	Fogo, Cape Verde	0.142	8.09 ± 0.08 (b)	n.c	25	2.83×10^{-4} (b)	1.6 (b)
			8.22 ± 0.09 (b)	n.c	0.4	4.46×10^{-6} (b)	6.4 (b)
			7.81 ± 0.09 (b)	975 ± 401 (b)	16	1.73×10^{-4} (b)	1.7 (b)
			8.53 ± 0.09 (b)	1046 ± 227 (b)	37	4.34×10^{-4} (b)	7.9 (b)
			8.23 ± 0.07 (b)	570 ± 104 (b)	21	2.44×10^{-4} (b)	1.7 (b)
			8.23 ± 0.15 (b)	361 ± 66 (b)	17	1.98×10^{-4} (b)	0.9 (b)
			7.93 ± 0.12 (b)	298 ± 31 (b)	14	1.51×10^{-4} (b)	1.7 (b)
			8.20 ± 0.08 (b)	580 ± 72 (b)	10	1.10×10^{-4} (b)	4.8 (b)
			8.37 ± 0.09 (b)	1432 ± 412 (b)	127	1.48×10^{-3} (b)	71.6 (b)
			7.66 ± 0.02 (b)	249 ± 42 (b)	50	5.26×10^{-4} (b)	2.4 (b)
			6.69 ± 0.04 (b)	430 ± 213 (b)	23	2.16×10^{-4} (b)	2.2 (b)
Furnas caldera	São Miguel, Azores	6.175	5.59 (c)	343 ± 39	49	3.76×10^{-4}	141.9
		4.800	5.59 (c)	n.c	138	1.06×10^{-3}	118.0 (d)
Cerro Negro cone	Nicaragua	0.600	7.46 ± 0.15	n.c	2	2.40×10^{-5}	12.4
			3.54 ± 0.17	n.c	9	4.40×10^{-5}	68.9
Cerro Negro crater	Nicaragua	0.140	7.46 ± 0.15	4848 ± 924	2	1.56×10^{-5}	8.0
			3.54 ± 0.17	161 ± 31	4	1.93×10^{-5}	30.1
Poás crater	Costa Rica	0.860	7.14 ± 0.1 (e)	2824	4	3.58×10^{-5}	136.0 (f)
Solfatara	Italy	0.500	3.05 (g)	n.c	289	1.22×10^{-3}	138.0 (h)
		0.100	2.96 ± 0.026	2799 ± 243	60	2.46×10^{-4}	26.2
		0.620	3.05 (g)	n.c	285	1.20×10^{-3}	100.8 (i)
Reykjanes	Iceland	0.225	14.42 (j)	55 ± 11	21	4.17×10^{-4}	130.0 (k)
Hengill	Iceland	168.1	13.73 (l)	n.c	500	9.51×10^{-3}	1237.0 (m)
Mud Volcanoes	Yellowstone, United States	0.400	16.50 (n)	n.c	1554	3.55×10^{-2}	30.4 (i)
Copahue (Máquinas)	Chile-Argentina	0.321	7.04 (o)	n.c	14	1.38×10^{-4}	18.9 (o)
Copahue (Maquinitas)		0.046	6.97 (o)	n.c	5	4.86×10^{-5}	9.1 (o)
Copahue (Termas)		0.033	7.01 (o)	n.c	34	3.27×10^{-4}	49.1 (o)

Copahue (Anfiteatro)		0.576	4.93 (o)	n.c	25	1.69×10^{-4}	30.4 (o)
Ischia Island	Italy	0.0576	3.63 (p)	n.c	150	7.56×10^{-4}	40.1 (i)
Vesuvius cone	Italy	0.331	3.19 (q)	n.c	15	6.50×10^{-5}	16.6 (i)
Vulcano cráter	Italy	0.415	6.20 (r)	n.c	437	3.75×10^{-3}	21 (i)
Vulcano PL beach		0.0177	6.20 (r)	n.c	15	1.32×10^{-4}	3 (i)
Pantelleria	Italy	0.0577	7.33 (s)	n.c	31	3.10×10^{-4}	3.6 (i)
Nisyros	Greece	0.903	5.88 (t)	n.c	28	2.27×10^{-4}	42.6 (i)

Appendix II: Research papers published

8. APPENDIX II: Research papers published

Alonso M, Padrón E, Sumino H, Hernández PA, Melián GV, Asensio-Ramos M, Rodríguez F, Padilla G, García-Merino M, Amonte C and Pérez NM (2019). Heat and Helium-3 fluxes from Teide Volcano, Canary Islands, Spain. Geofluids, ID 3983864, https://doi.org/10.1155/2019/3983864.

Alonso M, Pérez NM, Padrón E, Hernández PA, Melián GV, Sumino H, Padilla GD, Barrancos J, Rodríguez F, Dionis S, Asensio-Ramos M, Amonte C, Silva S and Pereira JM (2021). Changes in the thermal energy and the diffuse 3He and 4He degassing prior to the 2014–2015 eruption of Pico do Fogo volcano, Cape Verde. Journal of Volcanology and Geothermal Research, 107271, https://doi.org/10.1016/j.jvolgeores.2021.107271.

Alonso M, Pérez NM, Hernández PA, Padrón E, Melián G, Rodríguez F, Padilla G, Barrancos J, Asensio-Ramos M, Fridriksson T and Sumino H (2021b). Thermal energy and diffuse 4He and 3He degassing released in volcanic-geothermal systems. Renewable Energy 182, 17-31, https://doi.org/10.1016/j.renene. 2021.10. 016.

Hindawi
Geofluids
Volume 2019, Article ID 3983864, 12 pages
https://doi.org/10.1155/2019/3983864

Research Article

Heat and Helium-3 Fluxes from Teide Volcano, Canary Islands, Spain

Mar Alonso,[1,2] **Eleazar Padrón**,[1,2,3] **Hirochika Sumino**,[4] **Pedro A. Hernández**,[1,2,3] **Gladys V. Melián**,[1,2,3] **María Asensio-Ramos**,[1] **Fátima Rodríguez**,[1] **Germán Padilla**,[1,2] **Marta García-Merino**,[2] **Cecilia Amonte**,[1] **and Nemesio M. Pérez**[1,2,3]

[1]*Instituto Volcanológico de Canarias (INVOLCAN), 38320, San Cristóbal de La Laguna, Tenerife, Canary Islands, Spain*
[2]*Instituto Tecnológico y de Energías Renovables (ITER), 38600 Granadilla de Abona, Tenerife, Canary Islands, Spain*
[3]*Agencia Insular de la Energía de Tenerife (AIET), 38600 Granadilla de Abona, Tenerife, Canary Islands, Spain*
[4]*Department of Basic Science, Graduate School of Arts and Sciences, The University of Tokyo, 3-8-1 Komaba, Meguro-ku, Tokyo 153-0041, Japan*

Correspondence should be addressed to Mar Alonso; mar@iter.es

Received 11 February 2019; Revised 22 April 2019; Accepted 14 May 2019; Published 23 June 2019

Guest Editor: Guodong Zheng

During July 2016, the first integrated heat flow, CO_2, and ^3He emission survey was conducted across 0.5 km^2 of the summit cone and crater of Teide volcano, Tenerife, Canary Islands, Spain. The thermal energy released from Teide summit cone by diffuse degassing was 2.2 MW, and the heat flux calculated through Dawson's method was 8.1 MW, difference due to the comparison of purely convective areas as the crater with diffusive areas as the flanks of the volcano. Diffuse CO_2 output was 211 ± 20 t d^{-1}, and ^3He emission was estimated to be within a range between 0.35 and 0.89 mol y^{-1}. The obtained values of diffuse degassing and heat fluxes are close to others obtained for similar volcanic areas. The calculation of ^3He/heat ratio for the first time in this volcanic system supports the presence of an important mantle source for the degassing of Teide volcano.

1. Introduction

The Earth's mantle is an important reservoir for compounds pertinent to surface and atmospheric processes such as water, carbon dioxide, sulphur, and noble gases. Advection of heat to the atmosphere via transportation of these gases remains an understudied phenomenon despite its potential importance [1, 2]. Volcanic activity represents focussed conduits for these fluxes and, as such, represents a key connection between the mantle and the atmosphere. Accurate measurements of both heat and gas flux from active volcanoes, and appraisal of their various sources, has contributed to a better understanding of the mantle-atmosphere link. In this study, we present the first data about the relationship between ^3He and heat flux in the Teide volcanic system. This work is a new contribution to ^3He global emission estimates.

Volcanoes emit large amounts of gases and volatiles to the atmosphere. These take the form of visible emanations through volcanic plumes, fumaroles, and solfataras and through diffuse degassing (nonvisible emanations). Both types of gas emissions are controlled by local volcano-tectonic structures as a result of transport via diffusion and advection [3].

Among volcanic gases, helium has been considered as a useful tool in the geochemists' toolbox [4]. Helium is chemically inert, physically stable, nonbiogenic, sparingly soluble in water under ambient conditions, almost nonadsorbable, and, consequently, highly mobile. Due to these properties and its deep origin, helium is considered a tracer of magmatic activity and its speed of traversing the crust makes it an excellent precursor of volcanic eruptions [5–7].

There are two naturally occurring isotopes of helium: ^4He and ^3He, with an atmospheric $^3He/^4He$ ratio (R_A) of $1.384 \cdot 10^{-6}$ [8]. ^4He is produced mainly in the crust as α-particles from the radioactive decay of ^{238}U, ^{235}U, and ^{232}Th, while nearly all of the ^3He is primordial in origin and, by far, its most important source is the Earth's interior. The $^3He/^4He$ ratio varies from high values ($>10^{-5}$) in mantle-derived lavas and fluids to low values ($\sim 10^{-8}$) in continental regions [9]. Helium production and the degree of tortuosity are the main parameters that control the uprising mantle-derived helium from the source to the atmosphere, showing a decreasing trend of the $^3He/^4He$ ratio with the distance in and around stratovolcanoes [6, 10]. However, in the case of Tenerife Island, Pérez et al. [11] demonstrated that the $^3He/^4He$ ratio remained constant regardless of the distance to Teide volcano.

In the case of the Canary Islands, the geographical distribution of the $^3He/^4He$ ratios shows the highest values on the westernmost islands (La Palma and El Hierro), which implies the existence of a helium source derived from the deep mantle [12–14]. Mass transfer of mantle helium to a fluid is accompanied by transfer of heat [15]. The presence of magmatic helium in a hydrothermal fluid therefore implies direct transport of heat from that magma to the fluid [15]. Previous studies have demonstrated a positive relation between helium isotopic composition and heat flux [16–18].

The calculated ^3He/heat production ratio in the upper mantle of the Earth is $\sim 0.5 \times 10^{-12}$ cm^3 STP/J [19] (where STP is $P = 1$ atm and $T = 25°C$) and is spatially heterogeneous. For instance, the ^3He/heat production ratio associated with hot-spot volcanism is typically $\sim 24 \times 10^{-12}$ cm^3 STP/J [19, 20]. These values are much higher than that estimated for crustal regimes, $\sim 1 \times 10^{-15}$ cm^3 STP/J, which are also dominated by radiogenic ^4He production [20]. Therefore, ^3He emission and heat flux studies at volcano-geothermal systems improve understanding not only of those systems but also the connection between mantle and atmosphere.

The measurement of the total thermal energy flux through the surface in volcanic areas is used to determinate changes in the magmatic activity and detecting changes in the energy balance of the volcanic system as a result of magmatic and tectonic processes [3, 21, 22].

The main objectives of this work are to compare ^3He emission estimated through different approaches, describe those estimates' relationship with heat flux, and calculate an indicative ^3He/heat production ratio at Teide volcano. It is important to highlight that it is the first study about the relationship between ^3He and heat flux in the Teide volcanic system. As such, this work is a new contributing value to ^3He global emission estimates.

2. Geological Setting

The Canarian archipelago is located in the Atlantic ocean about 100 km west of the African coast between 27°37′ and 29°25′N and between 13°20′ and 18°10′W (offshore Morocco). It consists of 7 main islands, decreasing ages from east to west, with the western islands still in the shield stage and the eastern-most in the erosional phase [23]. Their genesis continues to attract debate discussed below.

The most widely accepted "working" model is the one that combines three different hypotheses: hot spot, propagating fracture, and uplifted block hypothesis. It means that the islands originate from a thermal anomaly in the mantle helped by regional fractures for the beginning of magmatism; meanwhile, the islands are in their present freeboard attitude due to the action of tectonic forces [24].

Tenerife (2,034 km^2) (Figure 1), the central and largest island of the archipelago, is currently at the zenith of its volcanic development [23, 25]. The structure of Tenerife is controlled by a volcano-tectonic rift system with NW, NE, and NS directions. The oldest visible geological unit on Tenerife is called the "old basaltic series," from central Miocene, and its forms by three strongly eroded edifices distributed in the corners of the island: Anaga (north-east), Teno (north-west), and Roque del Conde (south). This unit is formed by basaltic lavas and pyroclastics with some trachytes and phonolites [26]. A period of 2-3 M.y. of volcanic quiescence and erosion took place between "old basaltic series" and the eruptions which formed the younger volcanic series. Las Cañadas volcano grew on the eroded remains of the "old basaltic series" reaching about 40 km in diameter and 2,700-3,000 m of a complex succession of basalts, trachybasalts, trachytes, and phonolites that then collapsed 200 ky ago to form Las Cañadas caldera depression [23]. The caldera is located in the intersection of the three rifts, and the vertical collapse was associated with emptying of shallow magma chambers [27–29]. Other authors suggest the combination of vertical and lateral collapse for the formation of Las Cañadas caldera [30]. The youngest activity of the island is represented by basalts, trachytes, and phonolites of Teide-Pico Viejo volcanic complex and some individual basaltic cones scattered around the island, mainly located on the structural rift systems (NW, NE, and NS directions), characterized by the alignment of cinder cones and fissure systems, where historical eruptions occurred. Those monogenetic cones represent the most common eruptive activity during the last 1 M.y., and it is possible to easily recognize 297 of these cones in the island [31].

The 17 km long and 10 km wide caldera is the salient geomorphological feature of Tenerife partly because it hosts the highest stratovolcano in the Atlantic Ocean: Teide volcano (3,718 m.a.s.l.), a portion of Teide-Pico Viejo volcanic complex. Teide and Pico Viejo volcanoes overlap to form an elongate double cone. This volcanic complex was formed through different eruptive styles, ranging from strombolian to phreatomagmatic eruptions to cryptodome formation and dome extrusions [28, 32] forming basaltic, trachytic, and phonolitic products. The last eruption in this complex, Chahorra, occurred in 1798 through an adventive cone of Pico Viejo volcano.

Teide summit cone has been constructed during several phases. Its eruptive products are mainly phonolitic and basaltic-trachybasaltic lavas [32]. Persistent degassing activity has taken place at the summit of the volcano since the last eruption [33, 34].

Visible degassing in the summit cone of Teide volcano consists in low temperature fumaroles (around 83°C). Water is the major component of these fumaroles, followed by CO_2, N_2, H_2, H_2S, Ar, CH_4, and CO, a composition typical of hydrothermal fluids [34, 35]. Diffuse degassing is the principle degassing mechanism of Teide volcano, with the highest

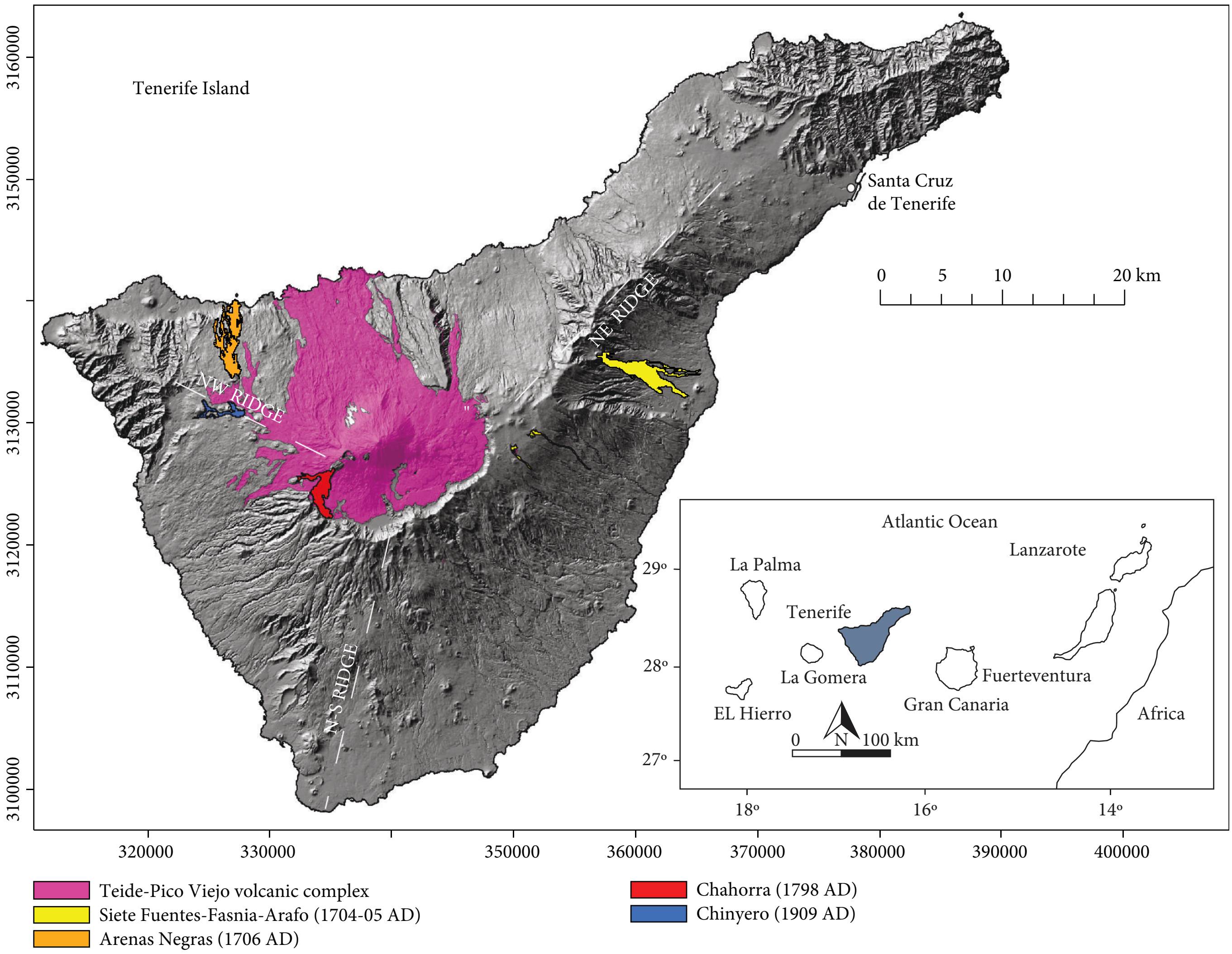

Figure 1: Tenerife Island marked with the location of the volcanic system studied, locations of historical eruptions and the three rifts. Inset: map of the Canarian archipelago highlighting Tenerife Island in grey.

rates emanated from the summit cone and crater of Teide volcano [36, 37].

3. Sampling Procedures, Analytical Methods, and Data Reduction

During July 2016, a soil gas survey comprised of 170 measurement sites was conducted at the summit cone of Teide volcano covering an area of 0.5 km^2 (Figure 2). The field work was carried out in the summer in order to minimize meteorological influences. The average distance between points of the summit cone was 45 meters on the slopes and 10 meters inside the crater, designed to tightly constrain the areal extent of visible degassing anomalies and arrive at more accurate overall estimates, while also achieving an evenly spaced distribution per domain.

3.1. Soil CO_2 Efflux and Temperature Measurements. Measurements of diffuse CO_2 were conducted at the soil surface using the accumulation chamber method [38] by means of West Systems portable CO_2 efflux meters equipped with a nondispersive infrared CO_2 analyzer LICOR-820. This system is composed of a double beam infrared carbon dioxide sensor compensated for temperature and atmospheric pressure and an optical bench of 20,000 ppm of resolution. The gas flux meter was interfaced to a handheld computer running data acquisition software.

Soil temperature was determined by inserting a Type K thermocouple at each sampling site at 15 and 40 cm depth.

3.2. Soil Gas Sampling. At each measurement site, soil gas was collected in 20 cc glass vials. This was achieved by inserting a 50 cm stainless probe 40 cm depth into the ground connected to a hypodermic syringe. Residual gas inside the probe was purged before sampling.

Gaseous species as Ne, H_2, O_2, N_2, CH_4, CO_2, and H_2O were analyzed by microchromatrography with a VARIAN model 4900 (Agilent Technologies, USA), using a thermal conductivity detector and a 20 m PoraPLOT Q column using argon (Ar) as carrier gas. The temperature of the column and injector was 40°C and 80°C, respectively, and the injection time was 20 ms. The detection limit for CO_2 was

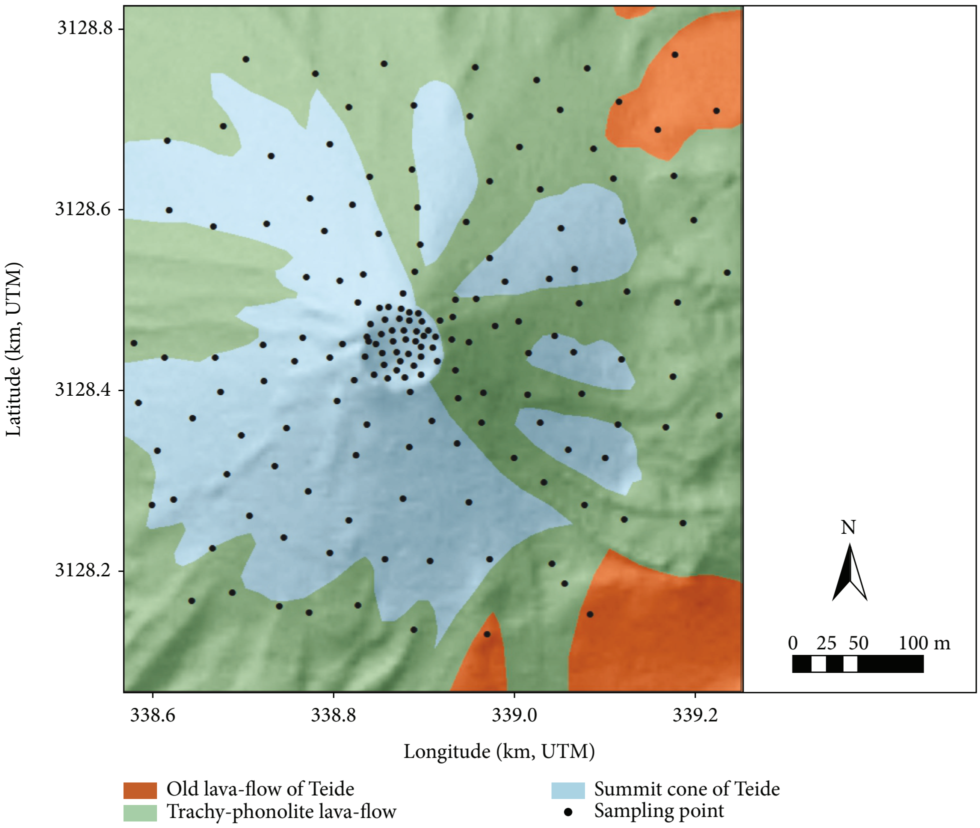

FIGURE 2: Geological map of Teide volcano summit cone and crater marked with the 170 measurement sites performed in the survey.

estimated to be about 10 ppmV, and the accuracy of the measurements was about 2.5% on the basis of standard sample measurements.

Helium was analyzed by a quadrupole mass spectrometer Pfeiffer Omnistar 422. The instrument accuracy of helium concentration was estimated to be ±300 ppb, and the detection limit for helium is 1 ppm. Atmospheric gas was used periodically to calibrate the instrument.

The isotopic ratio expressed as δ^{13}C-CO$_2$‰ vs. VPDB was measured by means of a Thermo Finnigan MAT 253 mass spectrometer. The analytical error for δ^{13}C values is of ±0.1‰.

3.3. Fumarole Sampling. Fumarolic gas samples were also collected in July 2016. Teide fumarolic activity consists of fluids discharged at approximately 83.5°C, close to the boiling point of water at 3,718 m.a.s.l. (87.5°C). A vent located inside the rim of the summit crater in the NE sector was the focus of the sampling effort.

A glass funnel was inserted into the vent and buried to prevent atmospheric air entering into the sampling system. The funnel was connected to a preevacuated glass flask filled with 50 ml of an alkaline solution (4 N KOH). H_2O vapour condenses and acidic gases as CO_2, SO_2, and HCl dissolve into the alkaline solution, while noncondensable gases (N_2, O_2, He, H_2, CH_4, etc.) are concentrated in the gas phase of the sampling flask [35]. CO_2 concentration and CO_2/H_2O molar ratio were analyzed by titration following the method described by Giggenbach and Goguel [39].

For the analysis of helium isotopes, lead-glass containers were filled with the fumarolic gas discharge. Helium concentration and ^{3}He/^{4}He isotopic ratios are expressed as $R_A = R/R_{\text{air}}$, where R is the measured ^{3}He/^{4}He ratio and R_{air} is that of the air; 1.384×10^{-6} [8] were analyzed using a high-precision noble gas mass spectrometer (modified-VG5400), following the procedure of Sumino et al. [40]. The correction factor for the helium isotope ratio was determined by measurements of interlaboratory helium standard named HESJ, with an established ^{3}He/^{4}He value of $20.63 \pm 0.10R_A$ [41]. The analytical error for R_A was <2%. The measured ^{3}He/^{4}He ratios were corrected for air contamination based on the ^{4}He/^{20}Ne ratios measured with the mass spectrometer, assuming that all the neon has an atmospheric origin [16, 42].

3.4. Data Reduction and Spatial Interpolation

3.4.1. ^{4}He Flux Determination. The circulation of gases at superficial levels of volcanoes is governed by a combination of diffusive and advective mechanisms. Flows and velocities of gas moving by advective mechanisms, however, are much higher than those produced by diffusion. Diffusive and advective emission values were estimated at each sampling site as follows.

Diffusion is described by Fick's law:

$$F_i = -D_m \frac{dC}{dz}, \tag{1}$$

where D_m is the molecular diffusion coefficient (m^2 s^{-1}) and dC is the variation of gas concentration ($kg\,m^{-3}$) along dz (m).

The apparent diffusion coefficient (D) includes the effect of porosity (n) and tortuosity (τ) of the environment. For soils, Etiope and Martinelli [43] define this coefficient as

$$D = D_m n^2 = D_m \frac{n}{\tau}. \tag{2}$$

Advection is described by Darcy's law:

$$F_i = -C_i \frac{k \nabla P}{\mu Z}, \tag{3}$$

where C_i is the soil gas concentration ($kg\,m^{-3}$), k the permeability (m^2), μ the dynamic viscosity of the gas ($kg\,m^{-1}$ s^{-1}), and ∇P the pressure difference ($kg\,m^{-1}$ s^{-2}) between two points spaced at distance Z (m) [43].

Soil intrinsic permeability (k) is a key factor to estimate the theoretical emission of gases via Darcy's law. It depends on the hydraulic permeability (K_s) following Schaap and Lebron [44]:

$$k = \frac{\mu}{\rho g} K_s, \tag{4}$$

where μ is the gas viscosity ($kg\,m^{-1}$ s^{-1}), ρ the gas density ($kg\,m^{-3}$), and g the gravitational constant ($m\,s^{-2}$).

In case of Teide volcano, pressure gradients are mostly generated by the geothermal gradient, which manifests by convection. We assume in this study, therefore, that the advective component of gas flux from the deep interior to the atmosphere is mainly governed by the efficiency of convection at the soil scale. Under this assumption, the pressure gradient is obtained from:

$$\nabla P = P_{\text{amb}} - P_{\text{soil}} = P_{\text{amb}} \left(1 - \frac{T_{\text{soil}}}{T_{\text{amb}}}\right), \tag{5}$$

where P_{soil} and P_{amb} are soil and ambient pressure and T_{soil} and T_{amb} are soil and ambient temperatures, respectively.

By combining equations (3), (4), and (5), we obtain the following expression for the convective flux:

$$F_i = -C_i \frac{K_s P_{\text{amb}}}{\rho g Z} \left(1 - \frac{T_{\text{soil}}}{T_{\text{amb}}}\right). \tag{6}$$

Direct measurements of diffuse CO_2 emission ($F_{CO2)}$), soil CO_2 concentration (C_{CO2}), air temperature (T_{amb}), and soil temperature at 40 cm depth (T_{soil}) were used to estimate the hydraulic permeability (K_s) from equation (6) at each sampling site. These values were used later to estimate the convective flux of ^{4}He. To calculate the diffusive emission component for ^{4}He, we used a 7×10^{-5} as diffusion coefficient [43] and a value of 0.35 for porosity, as have been used in similar volcanic areas [45].

3.4.2. ^{3}He Flux Determinations. ^{3}He generally has low abundance, which leads to high analytical uncertainty for most gas samples. To arrive at an accurate estimate of flux across the study area, we must interpolate from ^{3}He measurements with high certainty using robust relationships with other gas fluxes. The ^{3}He output released to the atmosphere from the summit cone of Teide volcano can be estimated to be within the limits calculated by two end-member assumptions:

(1) The $^3He/^4He$ ratio in the fumarolic gases (9.34×10^{-6}) is the same across the whole hydrothermal system, which is to assume the source of all helium is the same. In this case, ^{3}He emission (mol d^{-1}) is simply calculated using the $^3He/^4He$ ratio and the ^{4}He emission (mol d^{-1}) using the relationship:

$$\Phi_{3\text{He}} = \left({}^3\text{He}/{}^4\text{He}\right) \times \Phi_{4\text{He}} \tag{7}$$

(2) The ^{3}He flux is wholly derived from deep-seated source and therefore can be tied to the nonbiogenic component of the CO_2 flux. The estimated diffuse CO_2 emission, the $CO_2/^4He$ molar ratio, and the $^3He/^4He$ isotopic ratio measured in the fumarolic discharges of Teide can be used to estimate ^{3}He output using the relationships:

$$\begin{aligned} \left(\text{CO}_2/{}^4\text{He}\right)/\left({}^3\text{He}/{}^4\text{He}\right) &= \text{CO}_2/{}^3\text{He}\,; \\ \Phi_{3\text{He}} &= \Phi_{\text{CO2}}/\left(\text{CO}_2/{}^3\text{He}\right) \end{aligned} \tag{8}$$

3.4.3. Heat Flow. CO_2 was used as a tracer of hydrothermal fluids to calculate the heat flow involved in the diffuse degassing process. Chiodini et al. [46] first demonstrated this method that rests on the assumption that the H_2O/CO_2 ratio is recorded, before steam condensation, by fumarolic effluents. These authors computed the heat flux adding the following contributions: (1) the heat released by H_2O gas moving from the hydrothermal reservoir to the steam condensation zone, (2) the heat given off by CO_2 passing from the hydrothermal reservoir to atmospheric conditions, (3) the enthalpy of steam condensation at 100°C, and (4) the heat loss by liquid water on cooling from 100°C to the average seasonal value.

In the July 2016 survey, the measured H_2O/CO_2 ratio was 2.24. On the basis of this ratio, we computed that 473 t d^{-1} of steam are condensed to produce the hydrothermal CO_2 output of 211 t d^{-1} following the procedure described by Frondini et al. [47]. The released thermal energy associated with the condensation of 473 t d^{-1} of steam was estimated on 1.26×10^{12} J d^{-1}.

This value was obtained following two contributions. The enthalpy of steam condensation at 100°C (1.07×10^{12} J d^{-1}) is given by the product of the total amount of steam condensed in one day (4.73×10^8 g) times the enthalpy of evaporation at 100°C (2,257 J g^{-1}) [48]. The heat loss by liquid water on cooling from 100°C to the average seasonal value of 3.2°C (1.89×10^{11} J d^{-1}) is given by the product of the enthalpy lost

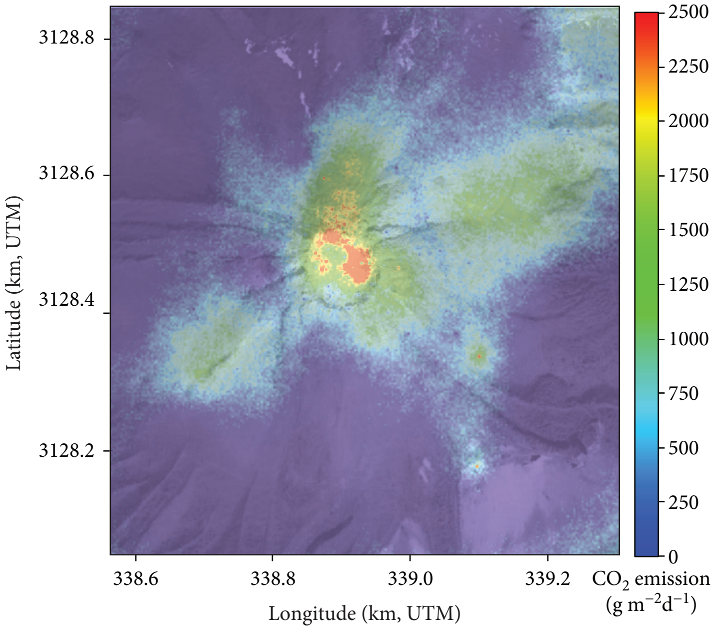

FIGURE 3: Diffuse CO_2 emission map of the summit cone and crater of Teide volcano.

by 1 g of water ($\Delta H = 398.7\ J\ g^{-1}$) times the mass of water (4.73×10^8 g).

The heat flux was also calculated following the method described by Dawson [49]. The method is based on correlation between soil temperature at 15 cm depth (t_{15}) and surface heat flux (q) by the following equation:

$$q = 5.2 \times 10^{-6} t_{15}^{4}, \tag{9}$$

where t_{15} was measured by a portable calorimeter at each point.

Sequential Gaussian simulation (sGs) using the sGsim program [50] was used to construct spatial distribution maps of CO_2, ^{4}He, and heat fluxes. The sGs procedure allowed us to interpolate the different parameters at a nonsampled area between the sampling points and obtain the uncertainty of emissions. Emission of the entire area of study was estimated using these maps.

4. Results and Discussion

4.1. CO_2 Fluxes and Isotopic Signatures. Diffuse CO_2 efflux values ranged from below detection to 10,650 g m^{-2}d^{-1} with an average value of 879 g m^{-2}d^{-1}. The spatially interpolated total diffuse CO_2 output released from the summit cone of Teide volcano was calculated as 211 ± 20 t d^{-1}. Similar results were obtained by Pérez et al. [37]; an emission value of 180 ± 21 was calculated for the 2009 survey for an area of 0.11 km^2.

The diffuse CO_2 emission map (Figure 3) shows higher values located inside the crater, along the crater rim mainly close to the fumarolic area and towards the north and north-east flanks. The areas with higher CO_2 efflux values also show relatively high temperatures and appear correlated to hydrothermal alteration at the surface, suggesting a mainly advective degasification mechanism governing the gas emission regime at the study area. The north and north-east anomalies are probably related to radial fissures propagated from the volcanic axis [37]. Lower values are observed at other sectors of the flanks of the cone.

The total diffuse CO_2 output is comparable with the 219 ± 36 t d^{-1} released by Pico do Fogo volcano, Cape Verde, a similar volcanic system in a similar volcano-tectonic environment, measured during a survey in February 2010 [21].

Figure 4 summarizes the CO_2 isotopic composition and indicates that most of the analyzed samples correspond to a deep-seated source of CO_2, with different degrees of atmospheric contributions. The heaviest $\delta^{13}C(CO_2)$ values, indicatives of deep-seated CO_2, were measured in soil gases in and around the summit crater, where fumarolic activity and thermal anomalies occur. The contribution of biogenic CO_2 can be considered negligible, which is consistent with the very limited vegetation and its related biological activity in the summit cone of Teide volcano.

4.2. ^{4}He Emission. The total output of ^{4}He from the studied area was estimated in 1.06 ± 0.2 kg d^{-1} (265.15 mol d^{-1}) with the highest values observed where fumarolic activity is present, along the crater rim, and towards the north and north-east flanks, coinciding with the highest temperature and CO_2 efflux values measured (Figure 5). The average value of the convective component exceeded the average value of the diffusive component by almost an order of magnitude (4.2 vs. 0.44 mg m^{-2} d^{-1}, respectively). For this reason, we can assume that most of the diffuse gas emission from the summit cone of Teide volcano is governed by convection.

Similar studies carried out in other volcanic systems of the Canary Islands have taken into account only the diffusive component due to the lack of geothermal anomalies in the surface environment of the study areas. Padrón et al.

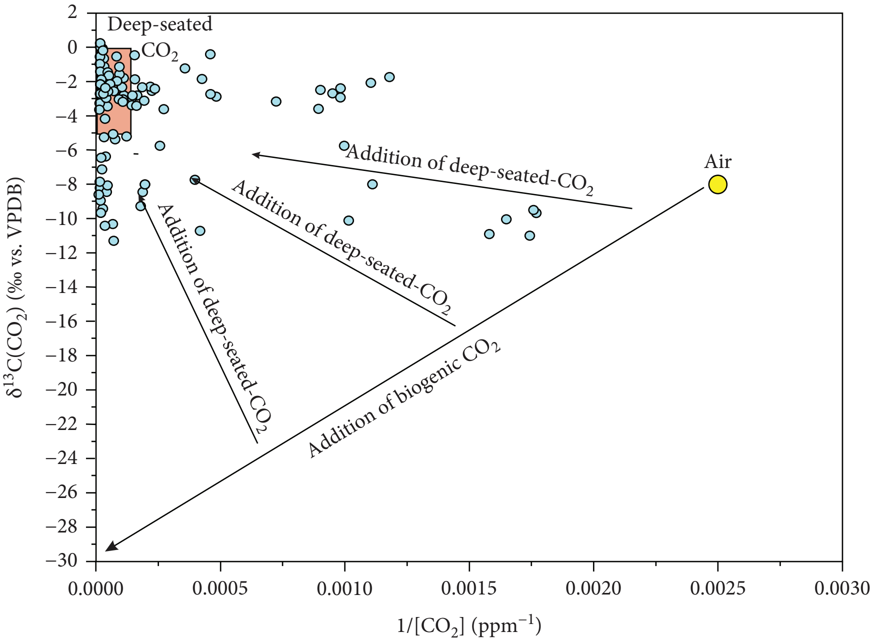

Figure 4: A plot of $^{13}\delta$C(CO$_2$) versus 1/[CO$_2$] (ppmV^{-1}) data from the Teide summit cone and crater. This figure depicts three possible geochemical reservoirs: air, characterized by a δ^{13}C(CO$_2$) = −8‰ and [CO$_2$] = 0.04%, deep-seated CO$_2$ with δ^{13}C(CO$_2$) = −3.1‰ and [CO$_2$] = 100%, and biogenic CO$_2$ with δ^{13}C(CO$_2$) = −27.5‰ and [CO$_2$] = 100%. Mixing trend between biogenic, air-derived, and deep-seated CO$_2$ is represented by straight lines.

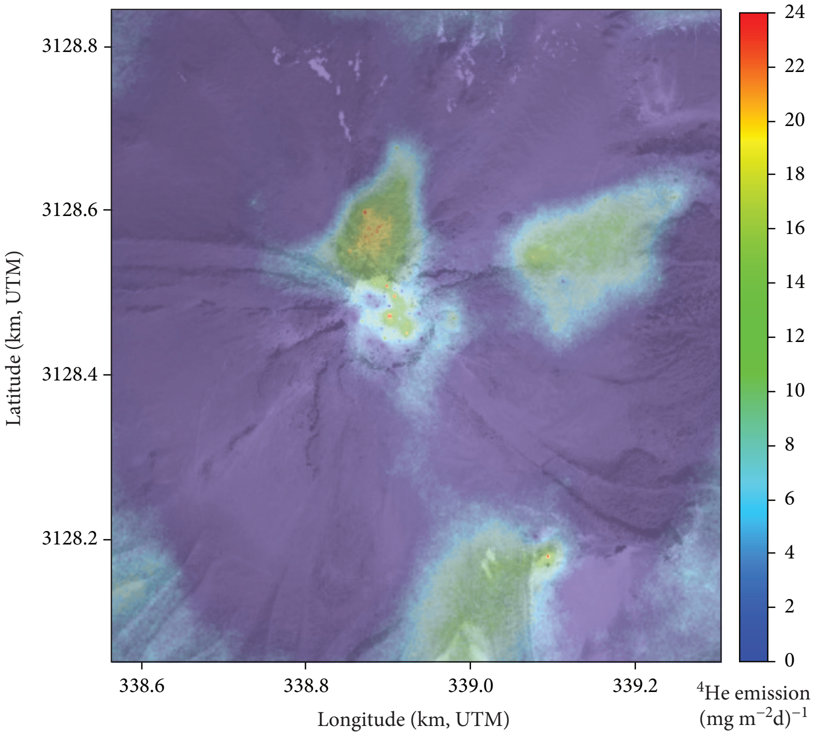

Figure 5: Diffuse ^{4}He emission map for the summit cone and crater of Teide volcano.

[51] estimate a ^{4}He emission between 15 and 38 kg d^{-1} from Cumbre Vieja volcano (La Palma) for an area of 220 km^2. Padrón et al. [7] observed an increase in the diffusive component of ^{4}He emission from 9 to 38 kg d^{-1} of the whole El Hierro island (278 km^2) prior to and during the 2011-2012 submarine eruption that took place 2 km off the southern coast of the island. In the case of the summit cone of Teide, with an area of 0.5 km^2, the normalized ^{4}He emission rate is

Table 1: Outlet temperature, chemical, and isotopic composition of fumarolic gases from the summit crater of Teide volcano.

	T (°C)	^{4}He/^{20}Ne	^{3}He/^{4}He (R/R_A)	δ^{13}C-CO$_2$ (‰)	CO$_2$ (%)	Gas steam
Teide fumarole	83.3	33.613	6.723 ± 0.056	−3.13 ± 0.01	98.15	0.251

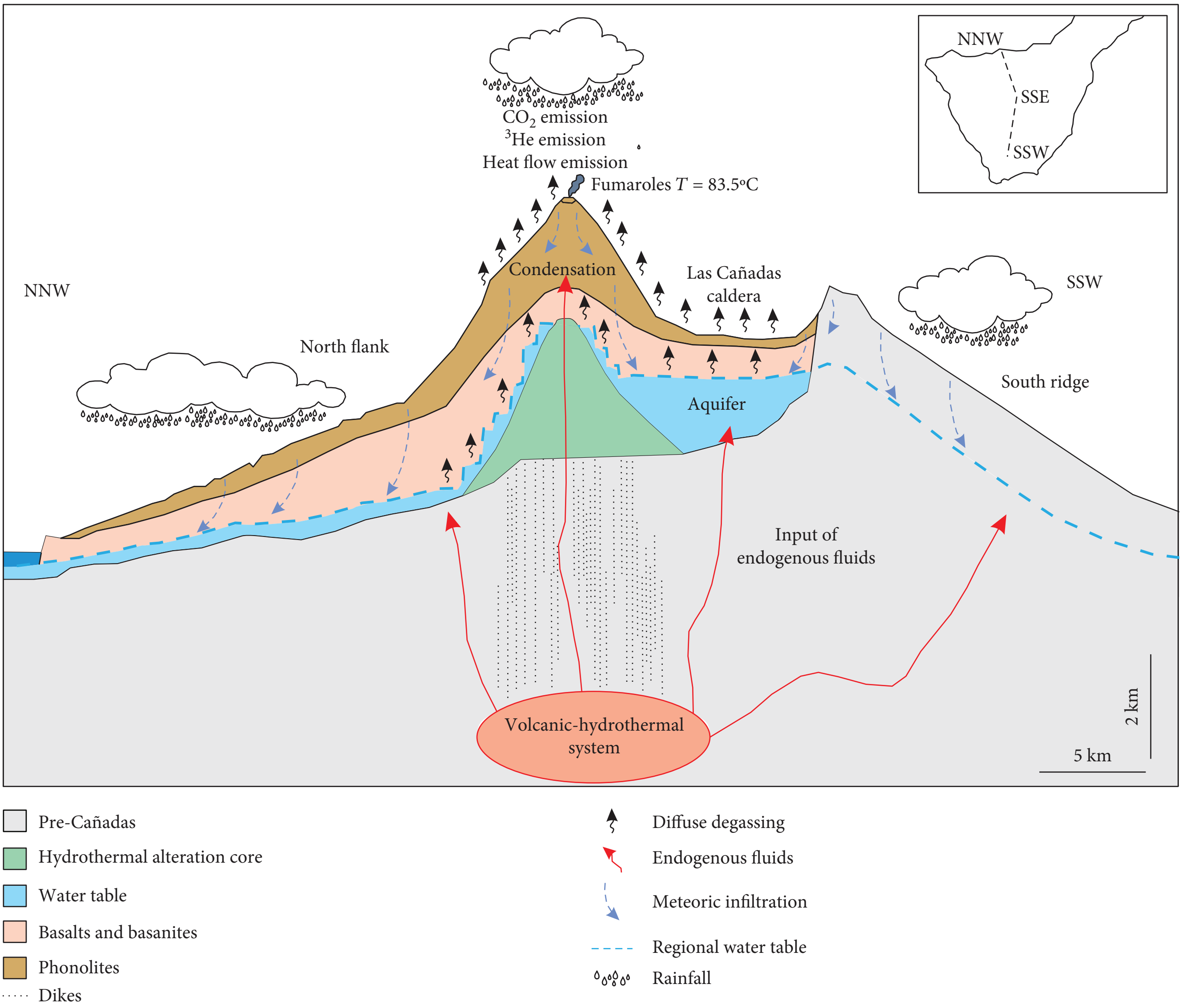

Figure 6: Hydrogeological model of Las Cañadas aquifer in the island of Tenerife. Fluid transport from the volcanic-hydrothermal system to the atmosphere is shown. Modified from Marrero-Díaz et al. [55].

2.12 kg km^{-2} d^{-1}, which represents a much higher value than that calculated for Cumbre Vieja and El Hierro (0.17 and 0.14 kg km^{-2} d^{-1}, respectively).

The summit cone of Teide value for ^{4}He is comparable to Pico do Fogo volcano in Cape Verde. Dionis et al. [21] estimated a helium emission of 4.1 kg d^{-1} from the crater that has an area of 0.142 km^{2} by considering a pure convective emission and a normalized emission rate of 28 kg km^{-2} d^{-1}. It is worth noting that Pico do Fogo volcano has experienced a higher eruptive activity in the historical times (last 500 years) than Teide. This observation might suggest a more general relationship between ^{4}He emission and volcanic activity than that demonstrated at the scale of the Cape Verde archipelago by Dionis et al. [21] using CO$_2$ and ^{3}He emission.

4.3. ^{3}He Emission. Chemical and isotopic composition of fumarolic gases from the summit crater of Teide volcano are summarized in Table 1.

Assuming that the ^{3}He/^{4}He ratio analyzed from the fumaroles is the same for the whole hydrothermal system, the calculated diffuse ^{3}He emission for the first assumption is 2.48×10^{-3} mol d^{-1} (0.89 mol y^{-1}). Nevertheless, because

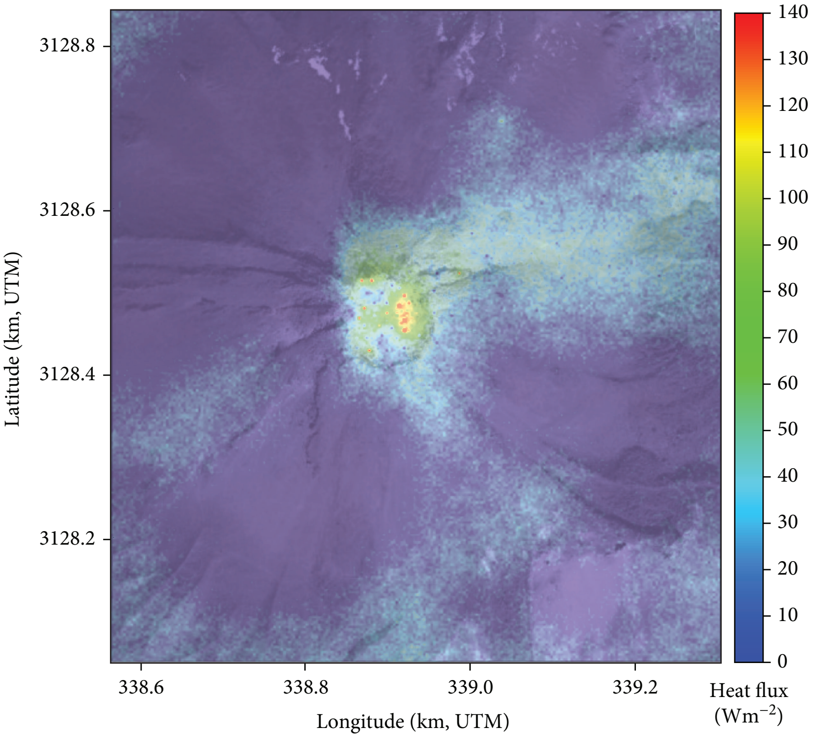

Figure 7: Heat flux emission map for the summit cone and crater of Teide volcano.

we have used the ^{4}He flux calculated before for our estimation, the ^{3}He emission could be overestimated because there must be some radiogenic ^{4}He from the crust. Anyway, that amount of ^{4}He from the crust is almost negligible for polygenetic volcanoes at oceanic islands as Tenerife [11]. For the second assumption, we use the CO_2 flux calculated before because we assume that the ^{3}He flux is wholly derived from deep-seated source. The calculated ^{3}He emission is 9.69×10^{-4} mol d^{-1} (0.35 mol y^{-1}). In this case, some amount of CO_2 derived from magma would be trapped by water in soil or groundwater during its ascent, so the true ^{3}He flux is underestimated and should be higher than the estimate. Marrero et al. [52] estimates through a CO_2 mass balance that 17.5×10^8 mol y^{-1} (211 t d^{-1}) of CO_2 is discharged by the groundwaters of Las Cañadas aquifer (144 km^2) (Figure 6). That means that there is a large amount of magmatic CO_2 that is trapped in the aquifer during its ascent to the atmosphere, suggesting that ^{3}He emission calculated using the second assumption is clearly subestimated.

These summit-cone wide values are consistent with the crater-only value which was reported by Hernández et al. [53] to be 0.51 mol y^{-1} (after correction of an error observed in the original calculation).

This work provides one more of the few values reported to date related to ^{3}He global emission, of which volcanic systems are highly significant. Other hot spot-type volcanic systems have shown similar (Piton de la Fournaise, La Réunion island, 1.1 mol y^{-1}) or higher emission values (Kilauea, Hawaii, 9-14 mol y^{-1}) [54], using fumarolic data. Other studies of soil ^{3}He emission in volcanic areas are rare. Padrón et al. [51] estimated a total output of ^{3}He in Cumbre Vieja volcano (La Palma, Canary Islands) of 0.6-0.7 mol y^{-1} considering a pure diffusive transport mechanism for an area of 220 km^2.

4.4. Heat Flow. The computed thermal energy released by degassing of 1.26×10^{12} J d^{-1} corresponds to a total heat flow of 2.21 MW. We obtained a value of 8.1 ± 0.97 MW using the Dawson method. In the interpolation map, the areas with the highest heat flow occurred at the fumarolic areas inside the crater, the crater rim, and the NE flank (Figure 7). The fumarolic area in the crater of Teide volcano has an average temperature of 83.5°C that it is constant since it began to register in 1993. The major component of these fumaroles is the water vapour, which originates from the vaporization of the rainfall water [33] followed by CO_2, N_2, H_2, H_2S, Ar, CH_4, and CO, a composition typical of hydrothermal fluids [34, 35]. These data suggest that the fumarolic effluents are made by endogenous gases which cross the aquifer located somewhere in the postcaldera structure close to the surface [33]. At the same time, the heat flux in the crater of Teide volcano has been registered since 2009 and no significant changes have been detected. Most of the heat flow measured in Teide volcano is the result of the emitted heat by the phase change of water from gas to liquid in the condensation zone.

The difference between the heat emission calculations among two different methods is because the method proposed by Chiodini et al. [46] assumes that the H_2O/CO_2 molar ratio measured in the fumarolic discharges is the same for the whole hydrothermal system. In this study, we are comparing areas with higher convective component at the

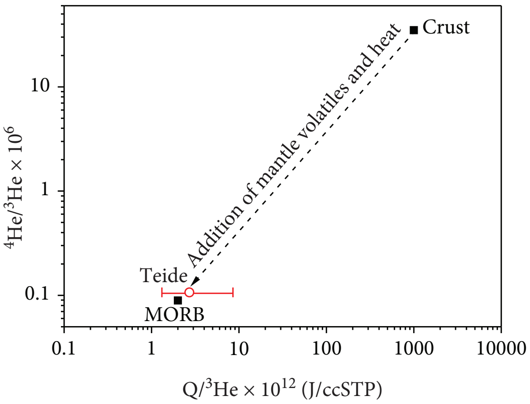

Figure 8: Schematic representation of the coherence between heat and helium.

crater with areas typified mainly by diffusive component at the flanks of the volcano, where there are no surface evidences of hydrothermal alteration.

To compare our data with other volcanic systems, Hernández et al. [3] estimated a total heat flow of 1.24 MW for the Hengill volcanic system; Chiodini et al. [2] reported the energy released by other volcanic areas as Campi Flegrei 100.8 MW, Ischia 40.1 MW, Vesuvio cone 16.6 MW, Vulcano crater 21 MW, and Comalito cinder cone 0.9 MW, and Dionis et al. [21] estimated a value of 10.3 MW released from the summit crater of Pico do Fogo volcano.

4.5. ^3He/Heat Ratio. Following from the end-member assumptions used to calculate the ^3He and heat flux, we calculated a plausible ^3He/heat ratio range from 0.117×10^{-12} to 0.764×10^{-12} cm^3 STP J^{-1}, with an average value of 0.370×10^{-12} cm^3 STP J^{-1}. This value is close to the 0.5×10^{-12} cm^3 STP J^{-1} calculated for the ^3He/heat ratio for hydrothermal activity from the upper mantle [19, 20]. Figure 8 shows the relationship between heat and helium emissions, following the model of Kennedy et al. [17], which demonstrate that Teide volcano is a useful window to take measurements of volatiles and heat from the upper mantle of the Earth to the atmosphere. By extension, future studies that focus upon the temporal evolution of heat and volatile emission from Teide and similar windows to the mantle will improve understanding of mantle dynamics and the link between lithosphere and atmosphere.

5. Conclusions

Most of the volcano-hydrothermal fluid discharges occurring at the summit cone of Teide volcano occur in the crater area; yet, other important emission rates were measured along the north and north-east flanks. These extracrater emissions are suggestive of a strong structural control in the degassing process of Teide volcano. Given the prevalence of structural controls on the expression of volcanic systems worldwide, we can suggest that other important, yet not as obvious, emissions are likely to be encountered at other volcanic systems.

The estimated global volcanic emission of ^3He is 1250 ± 250 mol y^{-1} [54]. The contribution to this estimate emission obtained by Teide volcano in this work is about 0.62 mol y^{-1}, for an area of 0.5 km^2, 0.05% of the total global emission. This study provides the first estimation of ^3He/heat from the Teide volcanic system and supports theoretical estimates at a global scale. The calculation of flux supports the presence of an important mantle source of volatiles and heat to the atmosphere.

Data Availability

The raw geochemical data used to support the findings of this study are stored on servers at ITER and can be made available by reasonable arrangement with the corresponding author.

Conflicts of Interest

The authors declare that there is no conflict of interest regarding the publication of this paper.

Acknowledgments

This research was financially supported by the projects (i) VOLRISKMAC from MAC 2014-2020, (ii) TFvolcano and TFinnova from the Cabildo Insular de Tenerife (Spain), and (iii) the Ministry of Science and Innovation from Spanish Government from DI-16-08974. We thank Iván Cabrera Pérez and Matthew James Pankhurst for their contribution to improve the quality of this paper and also Teleférico del Teide and Teide National Park for their assistance during the field work and for the logistic support.

Supplementary Materials

Supplementary materials 1: ambient and soil temperatures and CO_2 flux measured in each sampling site, and heat and ^4He fluxes calculated using the methodology described in the manuscript. Supplementary materials 2: data obtained from the analysis of the soil gases recollected in each sampling site. *(Supplementary Materials)*

References

[1] T. A. Mather, "Volcanoes and the environment: lessons for understanding Earth's past and future from studies of present-day volcanic emissions," *Journal of Volcanology and Geothermal Research*, vol. 304, pp. 160–179, 2015.

[2] G. Chiodini, D. Granieri, R. Avino, S. Caliro, A. Costa, and C. Werner, "Carbon dioxide diffuse degassing and estimation of heat release from volcanic and hydrothermal systems," *Journal of Geophysical Research*, vol. 110, no. B8, pp. 2156–2202, 2005.

[3] P. A. Hernández, N. M. Pérez, T. Fridriksson et al., "Diffuse volcanic degassing and thermal energy release from Hengill volcanic system, Iceland," *Bulletin of Volcanology*, vol. 74, no. 10, pp. 2435–2448, 2012.

[4] L. A. Pogorsky and G. S. Quirt, "Helium emanometry in exploring for hydrocarbons: part I," in *Unconventional Methods in Exploration for Petroleum and Natural Gas II-South*, pp. 124–135, Methodist University Press, 1981.

[5] D. M. Thomas and J. J. Naughton, "Helium/carbon dioxide ratios as premonitors of volcanic activity," *Science*, vol. 204, no. 4398, pp. 1195-1196, 1979.

[6] Y. Sano, Y. Nakamura, H. Wakita, A. Urabe, and T. Tominaga, "Helium-3 emission related to volcanic activity," *Science*, vol. 224, no. 4645, pp. 150-151, 1984.

[7] E. Padrón, N. M. Pérez, P. A. Hernández et al., "Diffusive helium emissions as a precursory sign of volcanic unrest," *Geology*, vol. 41, no. 5, pp. 539–542, 2013.

[8] W. B. Clarke, W. J. Jenkins, and Z. Top, "Determination of tritium by mass spectrometric measurement of ^{3}He," *International Journal of Applied Radiation and Isotopes*, vol. 27, no. 9, pp. 515–522, 1976.

[9] D. W. Graham, "Noble gas isotope geochemistry of mid-ocean ridge and ocean island basalts: characterization of mantle source reservoirs," *Reviews in Mineralogy and Geochemistry*, vol. 47, no. 1, pp. 247–317, 2002.

[10] M. Sakamoto, Y. Sano, and H. Wakita, "^{3}He/^{4}He ratio distribution in and around the Hakone volcano," *Geochemical Journal*, vol. 26, no. 4, pp. 189–195, 1992.

[11] N. M. Pérez, S. Nakai, H. Wakita, P. A. Hernández, and J. M. Salazar, "Helium-3 emission in and around Teide volcano, Tenerife, Canary Islands, Spain," *Geophysical Research Letters*, vol. 23, no. 24, pp. 3531–3534, 1996.

[12] N. M. Pérez, S. Nakai, H. Wakita, Y. Sano, and S. N. Williams, "^{3}He/^{4}He isotopic ratios in volcanic-hydrothermal discharges from the Canary Islands, Spain: implications on the origin of the volcanic activity," *Mineralogical Magazine*, vol. 58A, no. 2, pp. 709-710, 1994.

[13] D. R. Hilton, C. G. Macpherson, and T. R. Elliot, "Helium isotope ratios in mafic phenocrysts and geothermal fluids from La Palma, the Canary Islands Spain: implications for HIMU mantle sources," *Geochimica et Cosmochimica Acta*, vol. 64, no. 12, pp. 2119–2132, 2000.

[14] J. M. D. Day and D. R. Hilton, "Origin of ^{3}He/^{4}He ratios in HIMU-type basalts constrained from Canary Island lavas," *Earth and Planetary Science Letters*, vol. 305, no. 1-2, pp. 226–234, 2011.

[15] T. Torgersen and W. J. Jenkins, "Helium isotopes in geothermal systems: Iceland, The Geysers, Raft River and Steamboat Springs," *Geochimica et Cosmochimica Acta*, vol. 46, no. 5, pp. 739–748, 1982.

[16] Y. Sano and H. Wakita, "Geographical distribution of ^{3}He/^{4}He ratios in Japan: implications for arc tectonics and incipient magmatism," *Journal of Geophysical Research*, vol. 90, no. B10, pp. 8729–8741, 1985.

[17] B. M. Kennedy, T. P. Fischer, and D. L. Shuster, "Heat and helium in geothermal systems," *Twenty-Fifth Workshop on Geothermal Reservoir Engineering Stanford University*, 2000, Stanford, CA, USA, January 2000, 2000.

[18] K. Umeda, Y. Sakagawa, A. Ninomiya, and K. Asamori, "Relationship between helium isotopes and heat flux from hot springs in a non-volcanic region, Kii Peninsula, southwest Japan," *Geophysical Research Letters*, vol. 34, no. 5, article L05310, 2007.

[19] J. E. Lupton, E. T. Baker, and G. J. Massoth, "Variable ^{3}He/heat ratios in submarine hydrothermal systems: evidence from two plumes over the Juan de Fuca ridge," *Nature*, vol. 337, no. 6203, pp. 161–164, 1989.

[20] H. Elderfield and A. Schultz, "Mid-ocean ridge hydrothermal fluxes and the chemical composition of the ocean," *Annual Review of Earth and Planetary Sciences*, vol. 24, no. 1, pp. 191–224, 1996.

[21] S. M. Dionis, G. Melián, F. Rodríguez et al., "Diffuse volcanic gas emission and thermal energy release from the summit crater of Pico do Fogo, Cape Verde," *Bulletin of Volcanology*, vol. 77, no. 2, p. 10, 2015.

[22] T. Fridriksson, B. R. Kristjánsson, H. Ármannsson, E. Margrétardóttir, S. Ólafsdóttir, and G. Chiodini, "CO_2 emissions and heat flow through soil, fumaroles and steam heated mud pools at the Reykjanes geothermal area, SW Iceland," *Applied Geochemistry*, vol. 21, no. 9, pp. 1551–1569, 2006.

[23] J. C. Carracedo, E. R. Badiola, H. Guillou et al., "Eruptive and structural history of Teide volcano and rift zones of Tenerife, Canary Islands," *Geological Society of America Bulletin*, vol. 119, no. 9-10, pp. 1027–1051, 2007.

[24] F. Anguita and F. Hernán, "The Canary Islands origin: a unifying model," *Journal of Volcanology and Geothermal Research*, vol. 103, no. 1-4, pp. 1–26, 2000.

[25] H. Guillou, J. C. Carracedo, R. Paris, and F. J. Pérez Torrado, "Implications for the early shield-stage evolution of Tenerife from K/Ar ages and magnetic stratigraphy," *Earth and Planetary Science Letters*, vol. 222, no. 2, pp. 599–614, 2004.

[26] E. Ancochea, J. M. Fuster, E. Ibarrola et al., "Volcanic evolution of the island of Tenerife (Canary Islands) in the light of new K.Ar data," *Journal of Volcanology and Geothermal Research*, vol. 44, no. 3-4, pp. 231–249, 1990.

[27] J. Martí, J. Mitjavila, and V. Araña, "Stratigraphy, structure and geochronology of the Las Cañadas caldera (Tenerife, Canary Islands)," *Geological Magazine*, vol. 131, no. 6, pp. 715–727, 1994.

[28] J. Martí and A. Gudmundsson, "The Las Cañadas caldera (Tenerife, Canary Islands); an overlapping collapse caldera generated by magma-chamber migration," *Journal of Volcanology and Geothermal Research*, vol. 103, no. 1-4, pp. 161–173, 2000.

[29] M. J. Huertas, N. O. Arnaud, E. Ancochea, J. M. Cantagrel, and J. M. Fúster, "^{40}Ar/^{39}Ar stratigraphy of pyroclastic units from the Cañadas Volcanic edifice (Tenerife, Canary Islands) and their bearing on the structural evolution," *Journal of Volcanology and Geothermal Research*, vol. 115, no. 3-4, pp. 351–365, 2002.

[30] J. Martí, M. Hurlimann, G. J. Ablay, and A. Gudmundsson, "Vertical and lateral collapses on Tenerife (Canary Islands) and other volcanic ocean islands," *Geology*, vol. 25, no. 10, pp. 879–882, 1997.

[31] J. Dóniz, C. Romero, E. Coello et al., "Morphological and statistical characterisation of recent mafic volcanism on Tenerife (Canary Islands, Spain)," *Journal of Volcanology and Geothermal Research*, vol. 173, no. 3-4, pp. 185–195, 2008.

[32] G. J. Ablay and J. Martí, "Stratigraphy, structure, and volcanic evolution of the Pico Teide-Pico Viejo formation, Tenerife, Canary Islands," *Journal of Volcanology and Geothermal Research*, vol. 103, no. 1-4, pp. 175–208, 2000.

[33] J. F. Albert-Beltrán, V. Araña, J. L. Diez, and A. Valentin, "Physical-chemical conditions of the Teide volcanic system (Tenerife, Canary Islands)," *Journal of Volcanology and Geothermal Research*, vol. 43, no. 1-4, pp. 321–332, 1990.

[34] N. M. Pérez, N. C. Sturchio, S. N. Williams, J. C. Carracedo, and J. Coello, "Geochemical characteristics of the volcanic-hydrothermal gases in Teide, Timafaya, Taburiente, and

Teneguia volcanoes, Canary Islands, Spain," in *Proceedings of the Scientific Sessions: III Geological Congress of Spain, Volume 1*, pp. 463–467, Graficas Varona, Salamanca, 1992.

[35] G. Melián, F. Tassi, N. Pérez et al., "A magmatic source for fumaroles and diffuse degassing from the summit crater of Teide volcano (Tenerife, Canary Islands): a geochemical evidence for the 2004–2005 seismic–volcanic crisis," *Bulletin of Volcanology*, vol. 74, no. 6, pp. 1465–1483, 2012.

[36] T. Mori, P. A. Hernández, J. M. L. Salazar, N. M. Pérez, and K. Notsu, "An in situ method for measuring CO_2 flux from volcanic-hydrothermal fumaroles," *Chemical Geology*, vol. 177, no. 1-2, pp. 85–99, 2001.

[37] N. M. Pérez, P. A. Hernández, E. Padrón et al., "An increasing trend of diffuse CO_2 emission from Teide volcano (Tenerife, Canary Islands): geochemical evidence of magma degassing episodes," *Journal of the Geological Society*, vol. 170, no. 4, pp. 585–592, 2013.

[38] K. J. Parkinson, "An improved method for measuring soil respiration in the field," *Journal of Applied Ecology*, vol. 18, no. 1, pp. 221–228, 1981.

[39] W. F. Giggenbach and R. L. Goguel, *Collection and Analysis of Geothermal and Volcanic Water and Gas Discharges*, Unpublished report, Chemistry Division, DSIR-Petone, New Zealand, 1989.

[40] H. Sumino, K. Nagao, and K. Notsu, "Highly sensitive and precise measurement of helium isotopes using a mass spectrometer with double collector system," *Journal of the Mass Spectrometry Society of Japan*, vol. 49, no. 2, pp. 61–68, 2001.

[41] J. Matsuda, T. Matsumoto, H. Sumino et al., "The $^3He/^4He$ ratio of the new internal He standard of Japan (HESJ)," *Geochemical Journal*, vol. 36, no. 2, pp. 191–195, 2002.

[42] H. Craig and J. E. Lupton, "Primordial neon, helium and hydrogen in oceanic basalts," *Earth and Planetary Science Letters*, vol. 31, no. 3, pp. 369–385, 1976.

[43] G. Etiope and G. Martinelli, "Migration of carrier and trace gases in the geosphere: an overview," *Physics of the Earth and Planetary Interiors*, vol. 129, no. 3-4, pp. 185–204, 2002.

[44] M. G. Schaap and I. Lebron, "Using microscope observations of thin sections to estimate soil permeability with the Kozeny-Carman equation," *Journal of Hydrology*, vol. 251, no. 3-4, pp. 186–201, 2001.

[45] M. L. Carapezza and D. Granieri, "CO_2 soil flux at Vulcano (Italy): comparison between active and passive methods," *Applied Geochemistry*, vol. 19, no. 1, pp. 73–88, 2004.

[46] G. Chiodini, F. Frondini, C. Cardellini, D. Granieri, L. Marini, and G. Ventura, "CO_2 degassing and energy release at Solfatara volcano, Campi Flegrei, Italy," *Journal of Geophysical Research*, vol. 106, no. B8, pp. 16213–16221, 2001.

[47] F. Frondini, G. Chiodini, S. Caliro, C. Cardellini, D. Granieri, and G. Ventura, "Diffuse CO_2 degassing at Vesuvio, Italy," *Bulletin of Volcanology*, vol. 66, no. 7, pp. 642–651, 2004.

[48] J. H. Keenan, F. G. Keyes, P. G. Hill, and J. G. Moore, *Steam Tables Thermodynamic Properties of Water Including Vapor, Liquid and Solid Phases. International edition metric units*, Wiley, New York, NY, USA, 1969.

[49] G. B. Dawson, "The nature and assessment of heat flow from hydrothermal areas," *New Zealand Journal of Geology and Geophysics*, vol. 7, no. 1, pp. 155–171, 1964.

[50] C. Deutsch and A. Journel, *GSLIB: Geostatistical Software Library and Users Guide*, Oxford University Press, New York, NY, USA, 2nd edition, 1998.

[51] E. Padrón, N. M. Pérez, P. A. Hernández et al., "Helium emission at cumbre Vieja volcano, La Palma, Canary Islands," *Chemical Geology*, vol. 312-313, pp. 138–147, 2012.

[52] R. Marrero, D. L. López, P. A. Hernández, and N. M. Pérez, "Carbon dioxide discharged through the las Cañadas aquifer, Tenerife, Canary Islands," *Pure and Applied Geophysics*, vol. 165, no. 1, pp. 147–172, 2008.

[53] P. A. Hernández, N. M. Pérez, J. M. Salazar, S. Nakai, K. Notsu, and H. Wakita, "Diffuse emission of carbon dioxide, methane and helium-3 from Teide volcano, Tenerife, Canary Islands," *Geophysical Research Letters*, vol. 25, no. 17, pp. 3311–3314, 1998.

[54] P. Allard, "Global emissions of Helium-3 by subaerial volcanism," *Geophysical Research Letters*, vol. 19, no. 14, pp. 1479–1481, 1992.

[55] R. Marrero-Díaz, D. López, N. M. Pérez et al., "Carbon dioxide and helium dissolved gases in groundwater at Central Tenerife Island, Canary Islands: chemical and isotopic characterization," *Bulletin of Volcanology*, vol. 77, no. 10, p. 86, 2015.

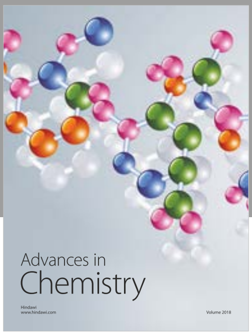
Advances in
Chemistry

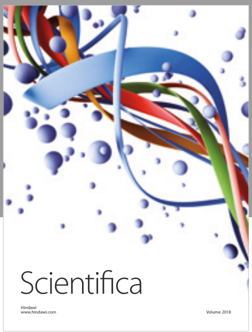
Scientifica

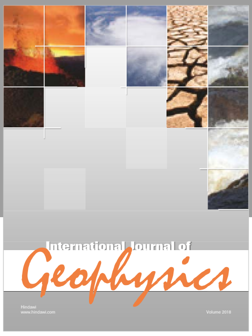
International Journal of
Geophysics


The Scientific
World Journal

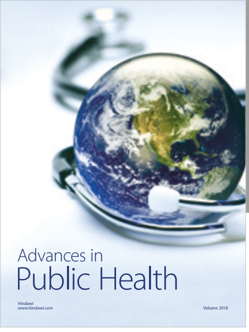
Advances in
Public Health

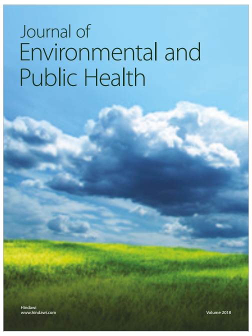
Journal of
Environmental and
Public Health

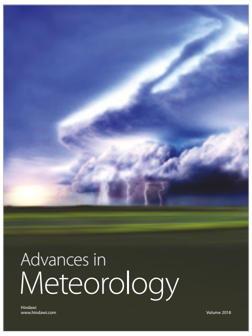
Advances in
Meteorology

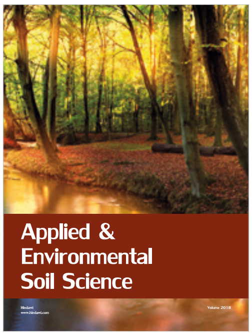
Applied &
Environmental
Soil Science


Journal of
Geological Research


International Journal of
Forestry Research

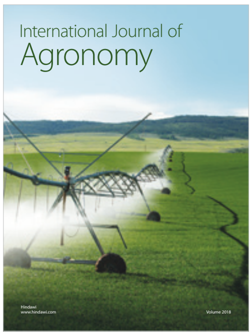
International Journal of
Agronomy


International Journal of
Microbiology


International Journal of
Ecology

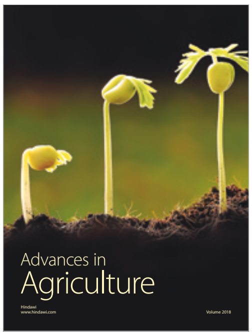
Advances in
Agriculture


International Journal of
Biodiversity

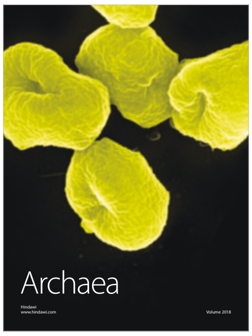
Archaea

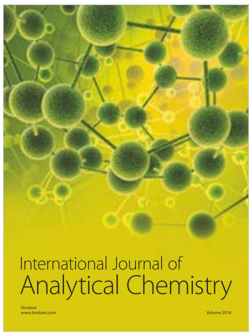
International Journal of
Analytical Chemistry


Journal of
Chemistry


Journal of
Marine Biology

Journal of Volcanology and Geothermal Research 416 (2021) 107271

Contents lists available at ScienceDirect

Journal of Volcanology and Geothermal Research

journal homepage: www.elsevier.com/locate/jvolgeores

Changes in the thermal energy and the diffuse ^{3}He and ^{4}He degassing prior to the 2014–2015 eruption of Pico do Fogo volcano, Cape Verde

Mar Alonso [a,b,*], Nemesio M. Pérez [a,b,c], Eleazar Padrón [a,b,c], Pedro A. Hernández [a,b,c], Gladys V. Melián [a,b,c], Hirochika Sumino [d], Germán D. Padilla [a,b], José Barrancos [a,b], Fátima Rodríguez [a], Samara Dionis [a,1], María Asensio-Ramos [a], Cecilia Amonte [b,c], Sonia Silva [e], Jose Manuel Pereira [f]

[a] *Instituto Volcanológico de Canarias (INVOLCAN), 38320, San Cristóbal de la Laguna, Tenerife, Canary Islands, Spain*
[b] *Instituto Tecnológico y de Energías Renovables (ITER), 38600 Granadilla de Abona, Tenerife, Canary Islands, Spain*
[c] *Agencia Insular de la Energía de Tenerife (AIET), 38600 Granadilla de Abona, Tenerife, Canary Islands, Spain*
[d] *Department of General Systems Studies, Graduate School of Arts and Sciences, The University of Tokyo, 3-8-1 Komaba, Meguro-ku, Tokyo 153-0041, Japan*
[e] *Universidade de Cabo Verde (UNICV), Praia, Santiago, Cape Verde*
[f] *Laboratório de Engenharia Civil of Cape Verde (LEC) Tira - Chapéu, Santiago, Praia, Cape Verde*

ARTICLE INFO

Article history:
Received 21 September 2020
Received in revised form 26 April 2021
Accepted 27 April 2021
Available online 30 April 2021

Keywords:
Pico do Fogo volcano
Helium isotopes
Helium-3
Heat flux
Thermal energy released

ABSTRACT

We report the temporal evolution of helium isotopes emission and thermal energy release in the period 2007–2018 at the summit crater of Pico do Fogo volcano, Cape Verde. ^{3}He/^{4}He ratio measured in a fumarolic discharge, ranged from 6.69 to 8.63 R_A, being the maximum mantle-derived composition measured in November 2013, one year before the eruption onset in 23 November 2014, and confirm the beginning of a possible magmatic intrusion four years and eight months before the 2014–2015 eruption. ^{3}He and mantle ^{4}He emission rates showed similar trends in temporal evolution. Thermal energy release calculated for the study period ranged from 1 up to 72 MW, being the maximum values linked to maximum ^{3}He (1.7×10^{-2} and 1.5×10^{-3} mol d^{-1} using the first and the second approach respectively), confirming a close relationship between both parameters. After the eruptive event, a simultaneous decrease in R_A, ^{4}He and ^{3}He emissions is observed due to the rapid degassing of the magma responsible of the 2014–2015 eruptive process.

1. Introduction

The chemical composition of volcanic gases depends on the origin and type of magma involved, which is linked to the geodynamic setting (Pepin and Porcelli, 2002). However, many magma-derived gases are modified from their original composition. Dilution by surface processes, including biological and meteorological processes, and solubility-controlled fractionation in groundwaters play a role in re-defining the gas species and affecting the fluxes between the magma and the surface (Federico et al., 2002; Marini and Gambardella, 2005; Tassi et al., 2007). Helium, as a noble gas, experiences little chemical interaction during its ascent from the mantle reservoir to the atmosphere, and therefore can be considered an ideal geochemical tracer of the characteristics of the source (Sano et al., 1984, Marty et al., 1989, Hernández et al., 1998, Padrón et al., 2013).

There are two naturally occurring isotopes of helium: ^{4}He and ^{3}He, that occur in the modern atmosphere in a ^{3}He/^{4}He ratio (R_A) of 1.384×10^{-6} (Clarke et al., 1976). The most important and almost unique terrestrial source of ^{3}He is mantle degassing (Graham, 2002). ^{3}He is primordial helium trapped during Earth's formation, and the mantle shows higher ^{3}He/^{4}He ratios than the atmosphere (Lupton and Craig, 1975; Lupton, 1983; Pepin and Porcelli, 2002). ^{4}He in the Earth's crust is produced by radioactive decay of ^{238}U, ^{235}U and ^{232}Th, and as these elements become increasingly enriched over geological time (Graham, 2002), the ratio of ^{3}He/^{4}He from this source is lower. Thus, the ^{3}He/^{4}He ratio is a simple and 'clean' measure of mantle vs. crustal degassing, due to the stark difference between reservoirs. The efficiency of He isotopes as tracers of volcanic activity has been demonstrated in numerous studies performed in different volcanic systems (Sano et al. 1991, 1997 and 2015; Capasso et al., 2005; Rizzo et al., 2006), in which significant increases in the ^{3}He/^{4}He ratios in natural fluids have been observed prior to eruptive events. Changes in helium isotopic composition are therefore a useful geochemical tool to detect episodes of volcanic unrest, and they can contribute to an eruption prediction

---

[*] Corresponding authors at: Instituto Volcanológico de Canarias (INVOLCAN), 38320, San Cristóbal de la Laguna, Tenerife, Canary Islands, Spain, Instituto Tecnológico y de Energías Renovables (ITER), 38600 Granadilla de Abona, Tenerife, Canary Islands, Spain.
E-mail address: mar@iter.es (M. Alonso).

[1] Now at: Instituto Tecnológico de Canarias (ITC), 35,199 Pozo Izquierdo, Las Palmas de Gran Canaria, Canary Islands, Spain.

https://doi.org/10.1016/j.jvolgeores.2021.107271

early warning system (Padrón et al., 2013; Sano et al., 2015; McMurtry et al., 2019; Kagoshima et al., 2019). Other studies have highlighted a positive relationship between ^{3}He emission and heat flux (Kennedy et al., 2000; Umeda et al., 2007; Alonso et al., 2019). Degassing processes, coupled with thermal energy release from the volcanic-hydrothermal system, provide valuable information about volcanic systems' energy balance, activity, and connection to the mantle.

Volcanoes dissipate most of their thermal energy through hot soils and soil degassing. There is a direct connection between hydrothermal discharge and variations in local magmatic activity (Baker and Lupton, 1990). Temporal evolution of ^{3}He emission together with thermal energy release studies have proven a powerful tool that helps understanding of mantle dynamics, and the link between the mantle and the atmosphere (Alonso et al., 2019).

A previous work in Pico do Fogo volcanic system, Cape Verde, published by Dionis et al. (2015a) constrains the highest gas emissions and ground temperatures close to the fumarolic field inside the crater, assuming convection as the main transport mechanism for the gases. In this work, the thermal energy released by the diffuse degassing process was also calculated, which together with gas emissions, provided insights into the dynamics of the volcano.

The isotopic composition of helium in olivine and clinopyroxene phenocrysts of Fogo Island lavas have previously been reported up to R/R_A value of 12.1 ± 0.9, (where R is the measured ^{3}He/^{4}He ratio and R_A is that in air; 1.384×10^{-6}; Clarke et al., 1976), interpreted as evidence of deep mantle component which is more enriched in ^{3}He compared to the MORB-source convecting mantle having ^{3}He/^{4}He of 8.1 ± 1 R_A (Christensen et al., 2001). Doucelance et al. (2003) reported a maximum value of 9.54 R_A in a similar study on Fogo basalts, and interpreted these values as reflecting mixing between recycled oceanic crust and deep mantle, with addition of subcontinental lithospheric material.

We herein report the temporal evolution of He isotopes and thermal energy released from Pico do Fogo volcano between March 2007 and November 2018.

2. Geological setting

The Cape Verde archipelago is a cluster of volcanic islands located in the Atlantic Ocean between 550 and 800 km west of the coast of Senegal, West Africa. It is formed by ten major islands and some smaller islets arranged in a westward-opening horseshoe shape. The islands are built upon oceanic crust, and lie on the Cape Verde Rise, a ~ 2 km high and ~ 700 km diameter hotspot swell formed by the activity of a Miocene mantle plume (Knudsen and Abrahamsen, 2000; Duprat et al., 2007; Holm et al., 2008; Pim et al., 2008; Dyhr and Holm, 2010). The archipelago is divided into two alignments. The Barlovento (windward) alignment is located in the north, with the Islands of Santo Antão, São Vicente, Santa Luzia, São Nicolau, Sal and Boa Vista defining a SE-NW orientation. The Sotavento (leeward) alignment includes Maio, Santiago, Fogo and Brava, which together define an ENE-WSW orientation and are located in the southern area of the archipelago (Fig. 1a).

While the oldest islands including Sal, Boa Vista, Santiago, São Nicolau and São Vicente have highly eroded surfaces, all the major islands, except Maio, display well-preserved volcanic edifices. The youngest islands, including Santo Antão, Fogo and Brava are characterized by young volcanic morphology. The highest elevation in the archipelago is Pico do Fogo in Fogo Island, whose summit is 2829 m.a.s.l. (Holm et al., 2008).

Fogo Island (476 km^2) is located in the southwest of the archipelago and its main geological feature is a 9-km-north-to-south wide collapse caldera opened toward the east. This caldera is partially delimited by vertical rim walls (Bordeira, Fig. 1b) rising ~1000 m from the bottom of the caldera (Chã das Caldeiras), within which Pico do Fogo is situated.

Pico do Fogo is one of the world's most active volcanoes, with 27 historical eruptions since its discovery in 1460 by Portuguese sailors (Day et al., 2000). The summit crater of Pico do Fogo is characterized by the existence of a fumarole field located in the NW sector, composed of low and moderate-temperature gas discharges, from 95 °C to ~315 °C (Fig. 1c), with an emission of ~1060 tons/day of CO$_2$, being a huge contribution of volatiles to the atmosphere (Aiuppa et al., 2020). Some historical eruptions occurred at the summit area, but since 1785 the activity has migrated to the lower flanks (Worsley, 2015). The last eruption took place also in the lower flank between November 23, 2014 and February 7, 2015 (Barrancos et al., 2015; Capello et al., 2016; González et al., 2015; Perez et al., 2015; Silva et al., 2015). Perez et al., 2015 observed two anomalous periods prior to this eruptive event. In the first period, a rapid increase was measured in the diffuse CO$_2$ emission of and on the δ^{13}C-CO$_2$ signature, indicating an enrichment in the magmatic component of CO$_2$. In the second period a greater increase in diffuse CO$_2$ emission and a continuous increase in the measurement of heat flow was observed 8 months before the eruption, suggesting a second magmatic intrusion, this time ending in an eruptive event. These observations are evident as clear precursor signals of the2014–2015 Pico do Fogo eruption. During this episode, four eruptive vents appeared, through which gases, pyroclastic rocks and lava were emitted, destroying the villages of Portela and Bangaeira. The volume of magma emitted during the eruptive period was $47.7 \pm 5.2 \times 10^6$ m^3 (Richter et al., 2016) and the eruptive column reached 6000 m high, scattering ashes that reached Brava Island, 17 km from Fogo Island (Silva et al., 2015).

3. Sampling procedures and analytical methods

From March 2007 to November 2018, sixteen surveys were conducted inside the summit crater of Pico do Fogo. Sixty-three measurements were performed in each survey, covering an area of 0.142 km^2. The average distance between the sampling points was 30 m, creating a sampling grid that serves to maximise coverage and density of points (Fig. 1c), which means a useful level of inter-survey consistency was maintained. At each sampling point, surface gas was collected by means of a metallic probe inserted 40 cm depth into the ground. The gas was extracted into a 60 cc syringe and stored in 12 cc preevacuated glass vials, ensuring that the vial is completely filled with soil gas. The ^{4}He concentration in the soil gases was analysed in ITER's laboratory (Instituto Tecnológico y de Energías Renovables, Tenerife, Spain) by means of a quadrupole mass spectrometer (Pfeiffer Omnistar 422), with an accuracy of ±300 ppb. Ambient and ground (15 and 40 cm depth) temperatures were measured at each sampling site using a portable Type-K thermocouple.

The active low-temperature-fumarole was sampled in each survey. Gas discharge from the fumarolic field situated in the NW section of the crater (Fig. 1c) was sampled with pre-evacuated glass flasks following the method described by Giggenbach and Goguel (1989). The glass flask was partially filled with 50 mL of 4 N KOH in water into which the acidic gases were dissolved; the inert and non-condensable gases accumulated in the empty space of the flask and the H$_2$O vapour condensed. Non-condensable gases (He, H$_2$, O$_2$, N$_2$, CH$_4$, CO) were analysed by a gas chromatograph (Varian 3800) with an analytical errors of <5% and < 10% for the main gas components and for minor gas compounds respectively. An aliquot of the alkaline liquid phase was oxidized with H$_2$O$_2$ under gentle heat for the determination of CO$_2$ and then analysed by titration with diluted HCl using an automatic titration system (Metrohm 716 DMS Titrino, Metrohm). Analytical precision was <1%.

High-vacuum lead-glass containers were filled with the fumarolic gas discharge for the measurements of He isotopes. The ^{3}He/^{4}He isotopic ratio was analysed following the procedure of Sumino et al. (2001) using a high-precision noble gas mass spectrometer (Isotech modified VG-5400). The analytical error for R_A was <2% and the correction factor for the He isotope ratio was determined by measurements of the inter-laboratory helium standard named HESJ, with an established ^{3}He/^{4}He value of 20.63 ± 0.10 R_A (Matsuda et al., 2002). ^{4}He/^{20}Ne ratio was used as a correction factor for atmospheric contamination assuming

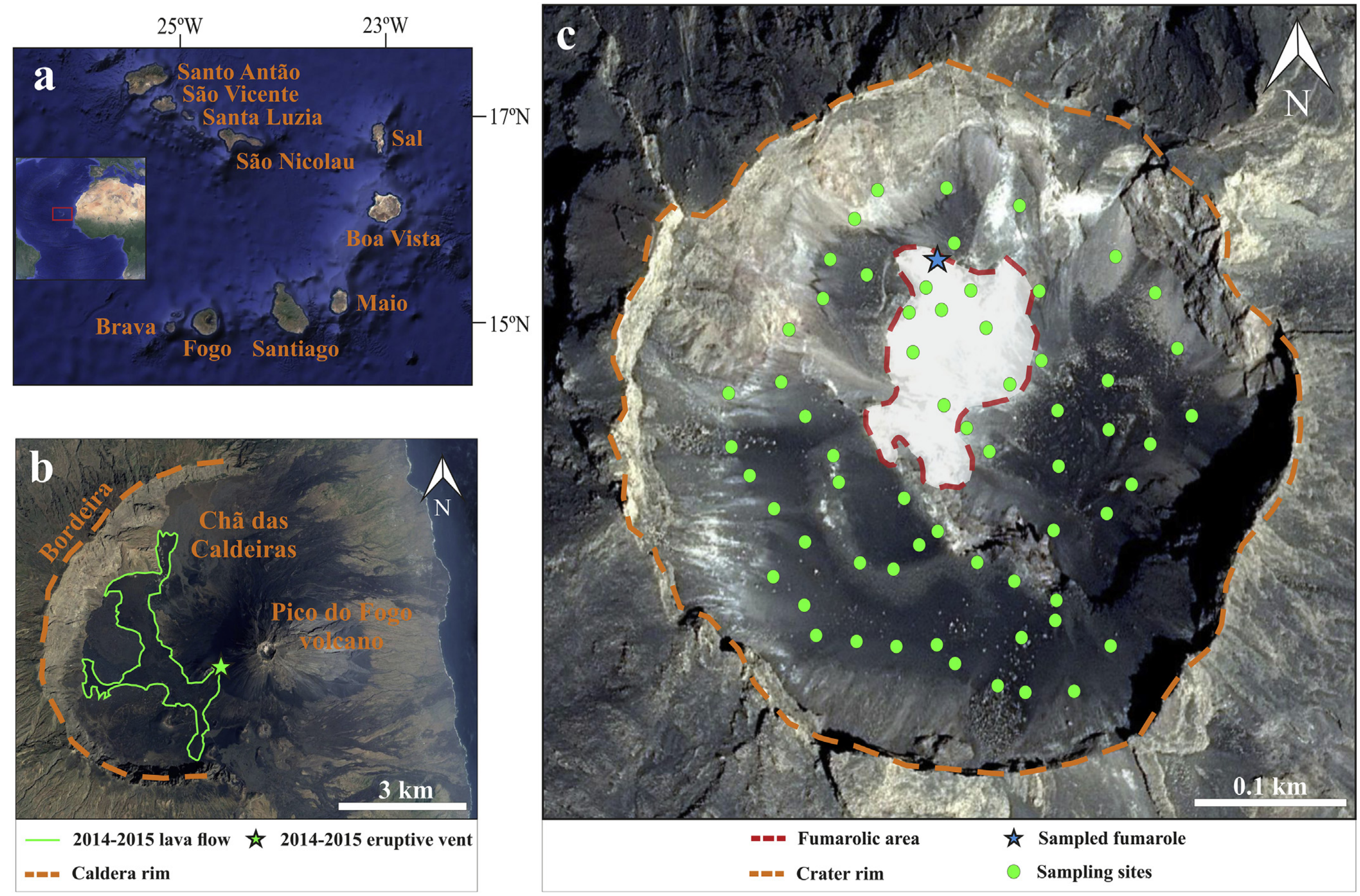

Fig. 1. a) Geographic location of the Cape Verde archipelago. b) Portion of Fogo island showing Pico do Fogo volcano and its caldera (Chã das Caldeiras). The 2014–2015 eruptive vent is marked by a green star, and the emitted lava flow for that period by a green line (Richter et al., 2016; Cappello et al., 2016; Jenkins et al., 2017; Calvari et al., 2018). c) Summit crater of Pico do Fogo volcano showing, the location of sampling sites (green dots) and sampled fumarole (blue star). The red and orange lines delimit the fumarolic area and the crater rim respectively, during November 2018. (For interpretation of the references to colour in this figure legend, the reader is referred to the web version of this article.)

that all the Ne has an atmospheric origin (Craig and Lupton, 1976). The ^{4}He/^{20}Ne ratios were calibrated by the measurements of an atmospheric standard. The error in the reported ^{4}He/^{20}Ne ratios are 14%, which is estimated from stability of sensitivity of the mass spectrometer during repeated measurements of the air standard. The error in the reported air-corrected ^{3}He/^{4}He ratios are 1 sigma, including errors of the measured raw ^{3}He/^{4}He ratio, measured raw ^{3}He/^{4}He ratio of HESJ, that of the recommended ^{3}He/^{4}He ratio of HESJ, and that of ^{4}He/^{20}Ne ratio.

3.1. ^{4}He emission determination

Helium-4 (^{4}He) concentration from samples collected at each of the 63 surface sites in the summit crater were used to estimate the diffusive and advective ^{4}He fluxes calculated by means of Fick and Darcy's laws respectively, following the procedure described in Alonso et al. (2019). The gas content at 40 cm depth was used to estimate the diffusive and advective gas fluxes (Φ), using the general equation of gas transport shown by Etiope and Martinelli (2002).

$$\Phi_i = -nD_m \frac{dC}{dz} + \nu C \quad (1)$$

n: effective porosity of the soils; D_m: molecular diffusion coefficient (m^2/s); *dC/dz*: concentration gradient in one-dimensional form; ν: velocity (m/s) of the gas; C: gas concentration (kg/m^3). According to Etiope and Martinelli (2002), the apparent diffusion coefficient (D) was used:

$$D = D_m \cdot n^2 \quad (2)$$

The diffusive emission values ($-nD_m \cdot dC/dz$) for He in Eq. (1) were calculated using a soil porosity value of 0.35, as has been used in similar volcanic areas (Carapezza and Granieri, 2004), and a molecular diffusion coefficient of 7×10^{-3} (Etiope and Martinelli, 2002).

Assuming that the advective component was mainly governed by convection, the following equation was used to calculate the convective component of the flux (F_i) (Alonso et al., 2019):

$$F_i = -C_i \frac{K_s \cdot P_{amb}}{\rho \cdot g \cdot Z}\left(1 - \frac{T_{soil,40}}{T_{air}}\right) \quad (3)$$

C_i: gas concentration (kg·m^{-3}); K_s: hydraulic permeability (m·s^{-1}); T_{soil} and T_{amb}: soil and ambient temperatures; P_{amb}: ambient pressure (Pa); ρ: density of the gas (kg·m^{-3}); *g*: gravitational acceleration (m·s^{-2}); *Z*: depth of the soil gas sample (m). The hydraulic permeability was estimated by means of direct measurements of ambient and ground temperatures.

3.2. ^{3}He emission determination

To calculate ^{3}He output released from the summit crater of Pico do Fogo volcano we used two approaches (Alonso et al., 2019). The first assumes that the ^{3}He/^{4}He isotopic ratio measured in the fumarolic gases is also applicable to the surface gas environment of the summit crater.

Once the ^{4}He flux (Φ_{4He}) is calculated at each sampling site following the procedure explained before, the ^{3}He flux (Φ_{3He}) can be calculated as follows:

$$\Phi_{3He} = (^3He/^4He) \times \Phi_{4He}.$$

The second approach assumes that the CO_2 measured from the Pico do Fogo volcanic system derives from a deep-seated source, and travels along with ^{3}He during its ascent from the mantle source. The calculated CO_2 emission and $CO_2/^4He$ and $^3He/^4He$ measured in the fumarole discharge can be used to estimate ^{3}He output using the following equations:

$$(CO_2/^4He)/(^3He/^4He) = CO_2/^3He;$$

$$\Phi_{3He} = \Phi_{CO2}/(CO_2/^3He).$$

Diffuse CO_2 emission was obtained following the accumulation chamber method (Parkinson, 1981; Chiodini et al., 1998) using a West System portable non-dispersive infrared (NDIR) LICOR LI-820 and L-840 CO_2 analysers equipped with a 20,000 ppm optical path. The portable efflux meter was previously calibrated using several flows with known CO_2 concentrations to be sure of the reliability of the method. The equipment was interfaced to a handheld computer running Flux Manager-data-acquisition-software, where the increase of CO_2 concentration as a function of time was recorded (Chiodini et al., 1996).

3.3. Thermal energy released

CO_2 and H_2O measured in fumarolic gas discharge were used as a tracer of hydrothermal fluids following the method described by Chiodini et al. (2001). In brief, the thermal energy release is computed by adding the following contributions: i) the enthalpy of condensation at 100 °C given by the total amount of steam condensed in one day, multiplied by the enthalpy of evaporation at 100 °C (2,260 $J \cdot g^{-1}$); and ii) the heat loss by liquid water on cooling from 100 °C to the average seasonal value of 14 °C, given by the product of the enthalpy lost by 1 g of water (398.71 $J \cdot g^{-1}$) times the mass of the water. Diffuse CO_2 emission values were used to estimate the emitted H_2O (steam condensed), assuming the CO_2/H_2O ratio in the fumarolic discharge of Pico do Fogo. In addition, the enthalpy of the vapour must be considered in instances where the soil temperature is higher than the steam condensation temperature.

3.4. Geochemical mapping

Sequential Gaussian simulations (sGs) (Deutsch and Journel, 1998; Cardellini et al., 2003) were used to obtain the CO_2 and ^{4}He emissions and to construct the ^{4}He spatial emission maps by WinGslib software. The simulation is conditional and sequential, i.e., the variables (CO_2 and ^{4}He) are simulated at the non-sampled areas by random sampling of a Gaussian conditional cumulative distribution function defined on the basis of original data and of previously simulated data within its neighbourhood (Cardellini et al., 2003). One hundred simulations were performed in order to quantify model uncertainty.

4. Results and discussion

4.1. $^3He/^4He$ ratios in gas samples

Fumarolic $^3He/^4He$ ratios were obtained from 13 samples collected between March 2007 and November 2018, always in the same fumarole (Fig. 1c). The air corrected $^3He/^4He$ $(R/R_A)_{cor}$ ratio ranged from 6.69 to 8.63 R_A (Table 1). The temporal evolution of the $^3He/^4He$ $(R/R_A)_{cor}$ ratio shows two main peaks, with an increase of ~0.7 R_A in the isotopic ratio (Fig. 2), in February 2010 and November 2013, the latter followed by a continuous decrease in the isotopic ratio until the end of the study period. The decreasing slope represents degassing of the magmatic melts that were responsible of the 2014–2015 eruptive process.

Tedesco and Scarsi, 1999 studied long-term isotopic variations of $^3He/^4He$ isotopic ratios collected from Vulcano Island since 1987, and obtained values between 4.9 and 6.0–6.2 R/R_A. The authors suggested that variations in the isotopic ratio through time were due to pressure variations in a deep gas reservoir, and that therefore these variations did not represent a period of volcanic unrest. This explanation cannot be ruled out in the variations observed in R_A measured at the Pico do Fogo volcanic system during the period comprised between end 2008 and 2010. Other geophysical and geochemical data would be necessary to support the statement of the occurrence of a magmatic intrusion in that period. One observation supporting this statement is that the variations in R_A (~0.7) are similar for both 2009–2010 and 2012–2014 periods, because the magmatic intrusion of the second period was evident due to the occurrence of the subsequent volcanic eruption.

4.2. Estimation of He isotopes emission

The results of ^{4}He emission estimations from each survey ranged from 249 ± 42 to 1997 ± 290 $mol \cdot d^{-1}$ (Table 1 and Fig. 3). Similar to

Table 1

Corrected $^3He/^4He$ (R/RA), $^4He/^{20}Ne$, calculated ^{4}He emission ($mol\ d^{-1}$), ^{3}He emissions ($mol\ d^{-1}$) by the different approaches:*^{3}He emission calculated by multiplying the ^{4}He emission by $^3He/^4He$ molar ratio measured in the fumarole, **^{3}He emission calculated by multiplying the diffuse CO_2 emission by the $^3He/CO_2$ ratio measured in the fumarolic gas, H_2O/CO_2 mass ratio measured in the fumarolic gas and thermal energy released (MW). One sigma error in the corrected $^3He/^4He$ ratios is reported. n.m.: not measured.

Date	$(^3He/^4He)_{cor}$ (R/R_A)	$^4He/^{20}Ne$	^{4}He emission (mol/d)	^{3}He emission* (mol/d)	^{3}He emission** (mol/d)	H_2O/CO_2 mass ratio	Diffuse CO_2 emission (t/d)	Thermal energy released (MW)
30/03/2007	8.09 ± 0.08	123	n.m.	n.m.	2.8×10^{-4}	0.8	71.1 ± 19.3	1.6
06/11/2008	8.22 ± 0.09	362	n.m.	n.m.	4.5×10^{-6}	5	41.8 ± 10.6	6.4
10/05/2009	7.81 ± 0.09	23	975 ± 401	$1.1 \times 10^{-2} \pm 4.5 \times 10^{-5}$	1.7×10^{-4}	0.4	146. 9 ± 34.7	1.7
21/02/2010	8.53 ± 0.09	228	1046 ± 227	$1.2 \times 10^{-2} \pm 2.8 \times 10^{-5}$	4.3×10^{-4}	1.2	219.1 ± 36.2	7.9
08/12/2010	8.23 ± 0.07	94	570 ± 104	$6.5 \times 10^{-3} \pm 1.3 \times 10^{-5}$	2.4×10^{-4}	0.6	88. 9 ± 16.0	1.7
24/02/2011	8.23 ± 0.15	42	361 ± 66	$4.1 \times 10^{-3} \pm 8.3 \times 10^{-6}$	2.0×10^{-4}	0.2	127.5 ± 23.9	0.9
24/02/2012	7.93 ± 0.12	194	298 ± 31	$3.3 \times 10^{-3} \pm 3.9 \times 10^{-6}$	1.5×10^{-4}	1.2	44.9 ± 8.8	1.7
27/04/2013	8.20 ± 0.08	18	580 ± 72	$6.6 \times 10^{-3} \pm 9.0 \times 10^{-6}$	1.1×10^{-4}	7.6	22.9 ± 4.5	4.8
07/10/2013	n.m.	n.m.	318 ± 41	n.m.	n.m.	n.m.	152.9 ± 26.4	n.m.
06/11/2013	8.63 ± 0.10	406	n.m.	n.m.	n.m.	5.1	n.m.	n.m.
22/03/2014	8.37 ± 0.09	110	1432 ± 412	$1.7 \times 10^{-2} \pm 5.0 \times 10^{-5}$	1.5×10^{-3}	7.1	326.6- ±54.5	71.6
14/01/2015	n.m.	n.m.	1997 ± 290	n.m.	n.m.	0.3	166.0 ± 19.1	n.m.
16/02/2015	8.33 ± 0.08	36	783 ± 188	$9.0 \times 10^{-3} \pm 2.2 \times 10^{-5}$	n.m.	n.m.	182.7 ± 25.8	n.m.
22/11/2015	n.m.	n.m.	595 ± 152	n.m.	n.m.	n.m.	219.5 ± 43.4	n.m.
30/10/2016	7.66 ± 0.02	106	249 ± 42	$2.6 \times 10^{-3} \pm 4.4 \times 10^{-6}$	5.3×10^{-4}	0.3	179.9 ± 42.6	2.4
13/11/2018	6.69 ± 0.04	16	430 ± 213	$4.0 \times 10^{-3} \pm 2.0 \times 10^{-5}$	2.2×10^{-4}	0.6	106.1 ± 25.8	2.2

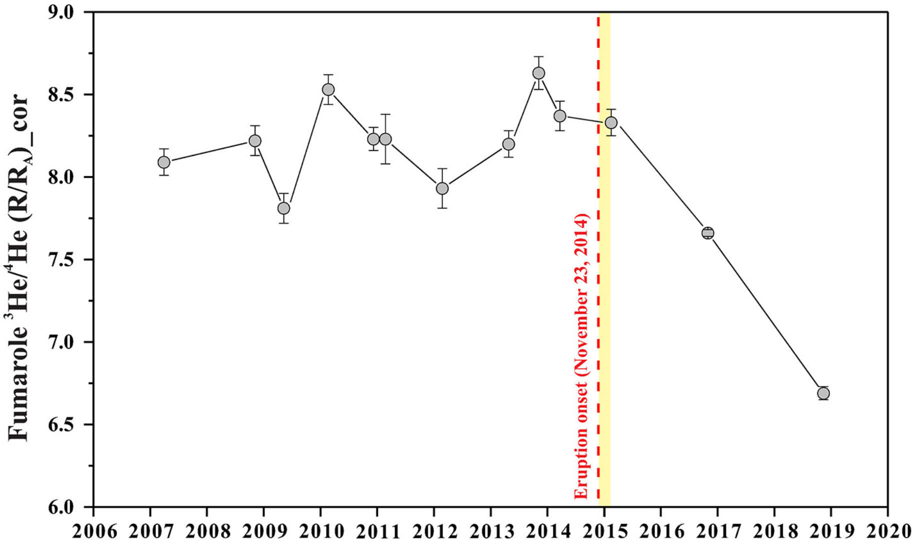

Fig. 2. Temporal evolution of the ^{3}He/^{4}He isotopic ratio measured in fumarolic gas from March 2007 to November 2018. The red dashed line indicates the eruption onset on November 23, 2014, and the yellow bar represents the eruptive period (November 23, 2014 to February, 72,015). (For interpretation of the references to colour in this figure legend, the reader is referred to the web version of this article.)

the ^{3}He/^{4}He $(R/R_A)_{cor}$ ratio, the temporal evolution of ^{4}He emission from Pico do Fogo volcano shows two peaks. The first peak (1046 ± 227 $mol \cdot d^{-1}$) coincides with the February 2010 ^{3}He/^{4}He $(R/R_A)_{cor}$ peak. The other peak in ^{4}He was measured in January 2015 (1997 ± 290 mol d^{-1}), and the continuous decrease in the emission was observed after the eruptive period (Fig. 3). Although the maximum value was measured in January 2015, the steepest increase in the ^{4}He emission was observed in March 2014, reaching a value of 1432 ± 412 mol d^{-1}.

In order to estimate the different contributions to the ^{4}He emission, radiogenic (crustal) and mantle (magmatic), ^{3}He/^{4}He ratios and ^{4}He emissions from each survey were considered, following the method described by Ballentine et al. (2002). Although the highest He isotopic value measured in Fogo is 12.1 R_A (Christensen et al., 2001), we decided to use the second highest value of 9.54 R_A (Doucelance et al., 2003), both were measured in olivine and clinopyroxene phenocryst of Fogo Island lavas, since it is closer to values obtained in this work for the diffuse degassing of Fogo volcanic system. Our results suggest a low crustal contribution, with a mean value of ~100 mol d^{-1}, while mantle He is much higher, ranging between 200 and 1256 mol d^{-1} (Fig. 3).

The spatial distribution of ^{4}He emission inside the summit crater of Pico do Fogo volcano (Fig. 4) shows maximum ^{4}He values closest to the fumarolic field of the crater, well-correlated with ground hydrothermal alteration and suggesting that advection is the dominant emission mechanism. The increase observed in ^{4}He emission from October 2013 to January 2015 can be considered a clear precursory geochemical signal of the 2014–2015 eruption (warmer colours in Fig. 4). The first pulse in ^{4}He emissions (observed in 2010) suggest intrusion of a less degassed magma to a shallower position beneath the Pico do Fogo volcanic system, between the end of 2009 and early 2010, although this intrusion did not end in an eruptive process.

^{3}He emission values using two approaches during each survey are presented in Table 1. The values calculated in the first approach ranged

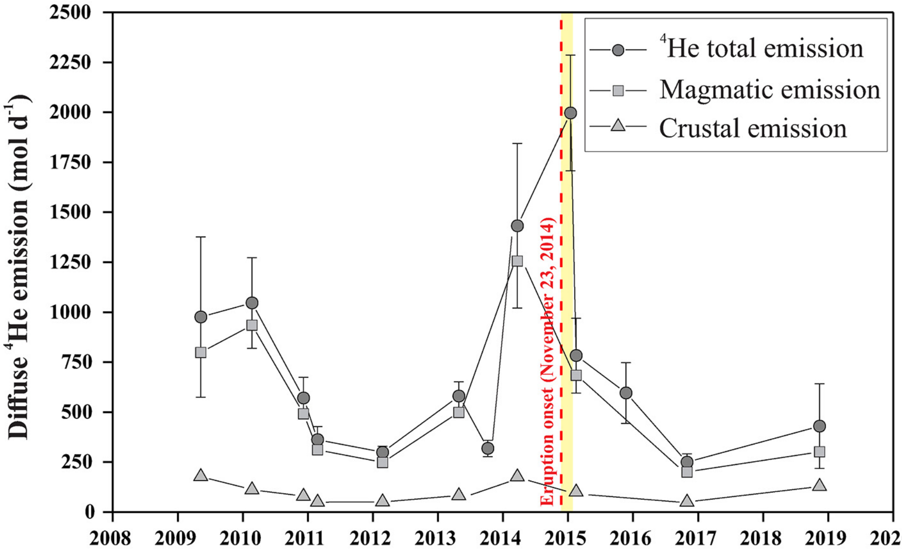

Fig. 3. Time series of diffuse ^{4}He output from March 2007 to November 2018 (dark grey circles). Estimated magmatic (light grey squares) and crustal (light grey triangles) helium emission during the study period are also present. Eruption onset and eruptive period shown as in Fig. 2.

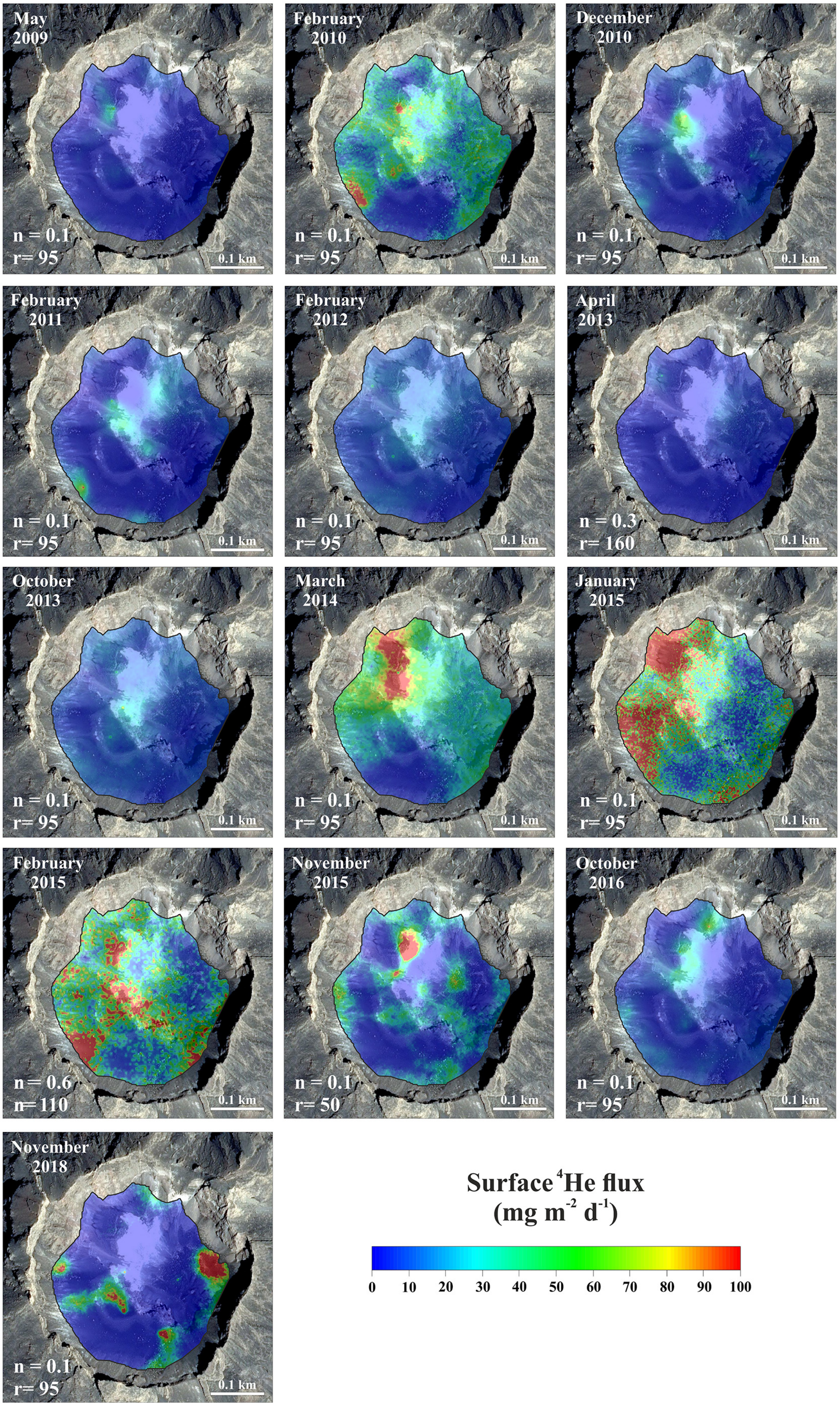

Fig. 4. Spatial distribution of ^{4}He emission inside the main crater of Pico do Fogo volcano from May 2009 to November 2018. The range (r) and the nugget (n) of the variogram are indicated in each spatial distribution map.

from 2.6 × 10^{-3} to 1.7 × 10^{-2} mol d^{-1} (surveys performed in October 2016 and March 2014, respectively), with a mean value of 7.58 × 10^{-3} mol d^{-1}. Emission values calculated with the second approach ranged from 4.5 × 10^{-6} to 1.5 × 10^{-3} mol d^{-1} (November 2008 and March 2014 surveys, respectively), with a mean value of 3.5 × 10^{-4} mol d^{-1}. Both calculation methodologies agree that the highest ^{3}He emission value was measured seven months before the eruption onset, which can be interpreted as an early warning signal that an eruptive process may have started. The observed differences between the methodologies calculating the ^{3}He emissions (resulting in higher values in the first approach), may be due to scrubbing processes that limit the amount of measured CO_2 released from deep sources to the atmosphere, yet do not affect the He emission: gas scrubbing by groundwaters, interaction with rocks, etc. (Marini and Gambardella, 2005). Thus, the second calculation approach which takes into account diffuse CO_2 emissions from the surface of Pico do Fogo volcano should provide underestimated values, as has been observed in Teide volcanic system (Alonso et al., 2019). Therefore, ^{3}He emission calculated using the diffuse CO_2 emission should be underestimated. Despite the different results, temporal evolution of ^{3}He emission shows some similarities in the observed trend (Fig. 5). As seen in Fig. 5a and b, two peaks in ^{3}He can be differentiated: one in February 2010 and another in March 2014, with each peak followed by a continuous decrease in emissions. Both approaches confirm the occurrence of a significant increase in the mantle He released several months before the eruption onset, together with another important mantle contribution in 2010. The rapid decrease in the parameters after the eruptive event may be due to the drop in the gas pressure within the volcanic body, and as a result, a decrease in the diffuse degassing through the volcanic edifice and in the magmatic component of the gas that feeds the fumarole activity (Notsu et al. 2006).

A relatively good correlation was obtained between the ^{3}He and ^{4}He emission values and the calculated CO_2 emission (Fig. 6), as those surveys in which higher CO_2 emission were measured, higher emission rates of both He isotopes was also observed.

4.3. Thermal energy released

The fumarolic H_2O/CO_2 ratio at each survey and the diffuse CO_2 output from the summit crater of Pico do Fogo were used to calculate the thermal energy released following the method proposed by Chiodini et al. (2001) (Table 1). The thermal energy released ranged from a minimum of 1 MW (February 2011) to a maximum of 72 MW (March 2014), with an average of 9 MW. In the temporal evolution (Fig. 7),

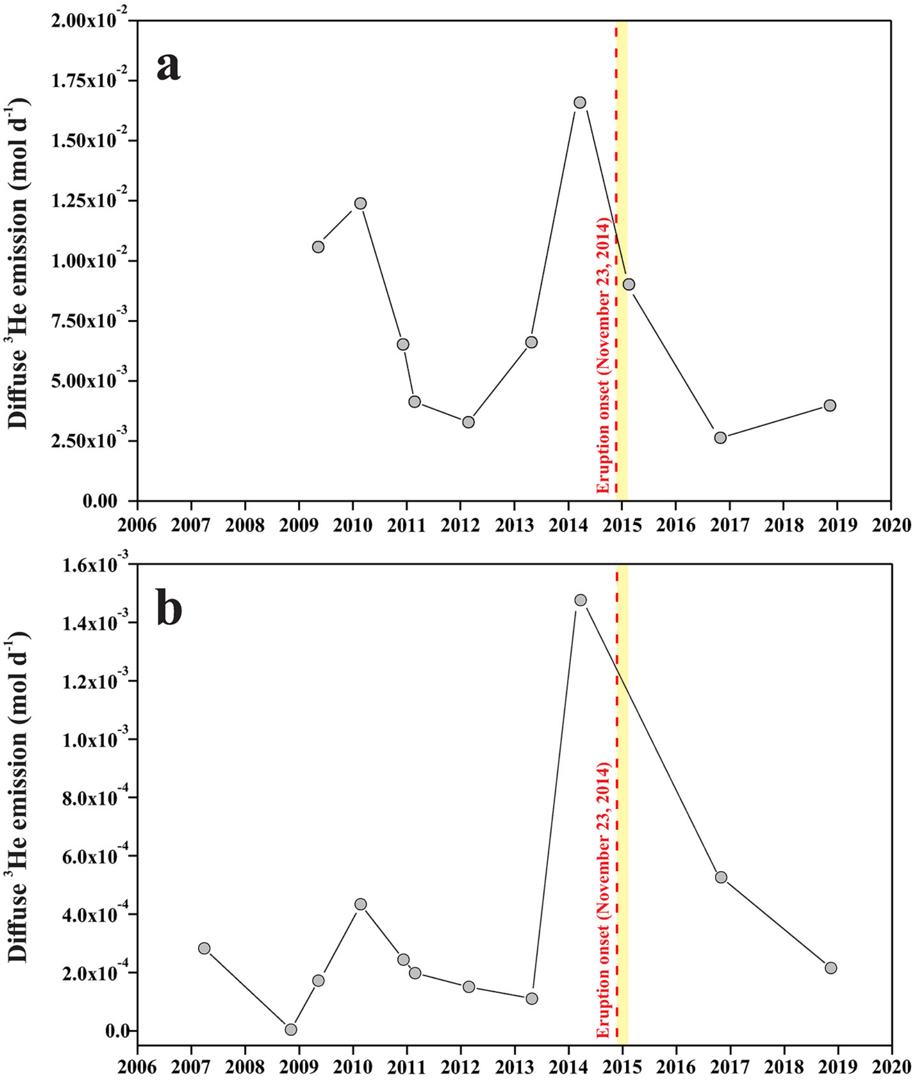

Fig. 5. a) Temporal evolution of ^{3}He emission calculated by multiplying the ^{4}He emission by $^3He/^4He$ molar ratio measured in the fumarole, and b) temporal evolution of ^{3}He emission calculated by multiplying the diffuse CO_2 emission by the $^3He/CO_2$ ratio measured in the fumarole. Eruption onset and eruptive period shown as in Fig. 2.

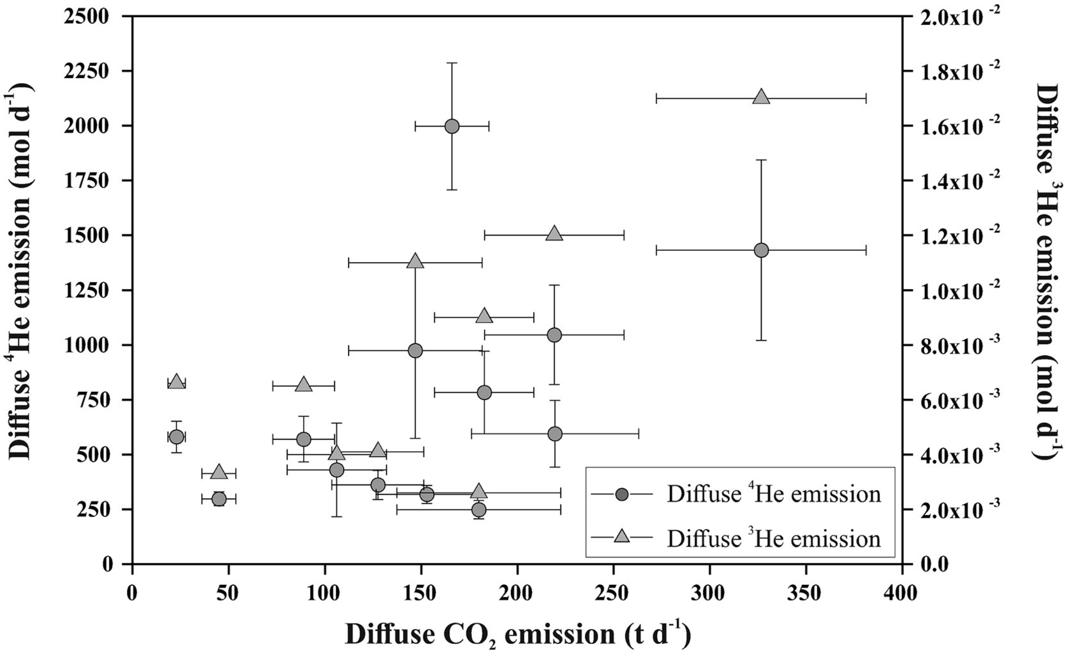

Fig. 6. Correlation between the diffuse CO$_2$ (t d^{-1}) and diffuse ^{4}He and diffuse ^{3}He emission rates measured at Pico do Fogo during the study period.

three peaks are evident, November 2008, February 2010 and March 2014, with values of 6, 8 and 72 MW, respectively. The change in trend from 4.8 MW measured in April 2012 to 71.6 MW measured during March 2014, several months prior to the eruption, is due to the rise of magma to the surface, resulting in an increase in the heat released by the volcanic system.

Coeval variations in the magmatic He emission and thermal energy output in 2010 and 2014 are shown. The magnitude of the precursory signals was different: while the ^{3}He, magmatic ^{4}He, and emission rates in 2010 and 2014 were similar, there was a marked difference of one order of magnitude in the thermal energy released (8 and 72 MW for 2010 and 2014, respectively). This observation suggests the relationship between these parameters (i.e. ^{3}He/heat ratio) in volcanic systems could provide a discriminating indicator between magmatic intrusions that will have the enough energy to produce a volcanic eruption. In volcanoes that present an active crater with significant surface volcanic-hydrothermal manifestations, precursory changes in the ^{3}He emission should be accompanied by a significant increase in the thermal energy released, resulting in a volcanic eruption.

During the study period, the trend in the temporal evolution of the measured parameters is similar to observed by Perez et al., 2015 in the diffuse emission of CO$_2$, δ^{13}C-CO$_2$ signature and heat flow, corresponding to precursory signals of the 2014–2015 Pico do Fogo eruption.

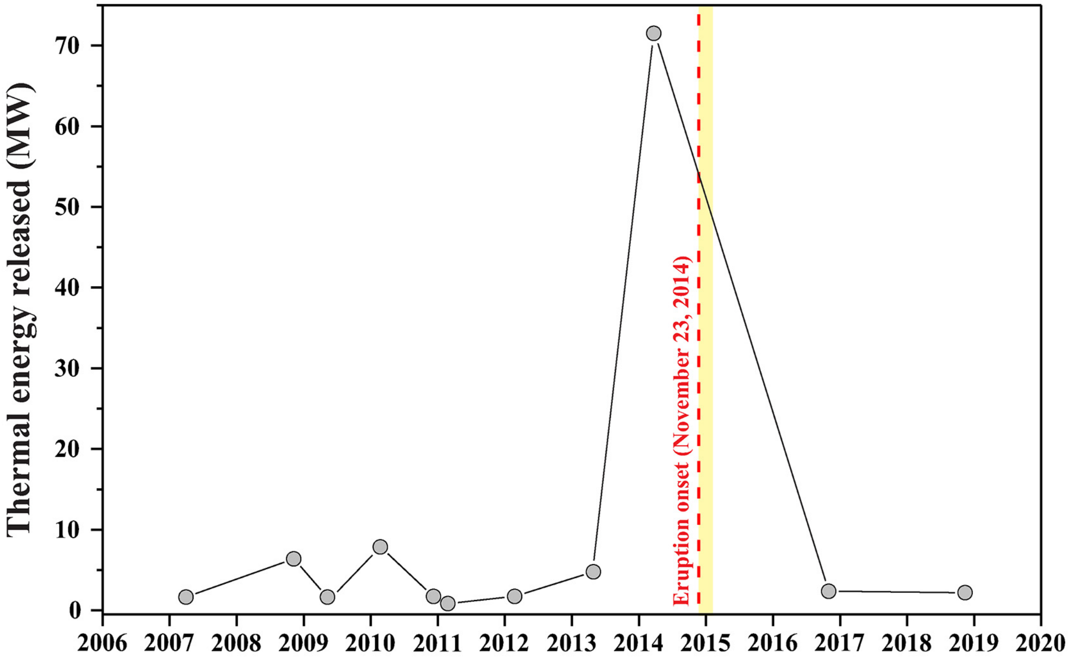

Fig. 7. Time series of thermal energy released (MW) from March 2007 to November 2018. Eruption onset and eruptive period shown as in Fig. 2.

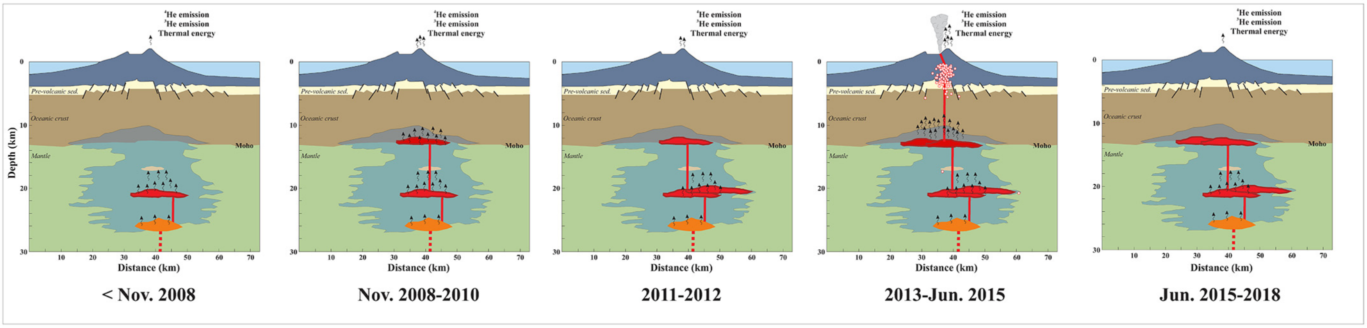

Fig. 8. Conceptual model of the observed changes in ^{3}He and ^{4}He emissions and thermal energy during the study period for Pico do Fogo volcanic system. Modified from Klugel et al. 2020.

4.4. Model for He emission and thermal energy temporal evolutions in Fogo volcanic system

We present a conceptual model for the evolution of He and thermal energy in the Pico do Fogo volcanic system during the study period, which we divide into five phases. The model explains observations in the years leading-up to, through, and after, the eruptive event (Fig. 8):

1. The Fogo volcanic system is in an inter-eruptive period during which no anomalous geochemical signals were observed (pre-Nov. 2008). The source of magmatic gas was located in a magma reservoir in the uppermost mantle at 24–30 km depth, according to geochemical data measured from erupted rocks (Klügel et al., 2020).
2. During Nov. 2008–2010 period, a significant increase was observed in the ^{4}He and ^{3}He emissions, ^{3}He/^{4}He isotopic ratio, and in the thermal energy released. These signals suggest the reactivation of the volcanic system accompanied by a magmatic intrusion hosted in an area close to the MOHO at ~12–13 km depth, which Klügel et al., 2015 call the magma accumulation zone.
3. A significant, and simultaneous, decrease in all three parameters was observed during the period 2011–2012, which suggests that the intrusion of magma of phase 2 ended.
4. Resumption of primitive magma input, again accumulating close to the MOHO (period 2013 - Jun 2015). During this second ascent the magma broke through a complex storage region, possibly an interconnected network of dikes/sills where part of the magma passed through, and part was stored (Klügel et al., 2020). The size of the MOHO-magma-accumulation zone had increased due to an increasing number of emplaced intrusions (Klügel et al., 2015). After breaking through the storage region, the magma rise rapidly through the crust and reached the surface on November 23, 2014. Prior to the eruptive period (November 23 to February 7) maximum values during the study period of 8.63 R_A; 1.7×10^{-2} mol/d; 1.5×10^{-3} mol/d, and; 71.6 MW were observed for ^{3}He/^{4}He isotopic ratio; ^{3}He emissions, and; thermal energy released, respectively. Although ^{4}He emission maximum value (1997 mol/d) was observed during the eruptive period, the biggest increase in the rate of change was observed prior to the eruptive event, in agreement with the other measured parameters.
5. After the eruptive period (from June 2015), a dramatic decrease was observed in all parameters simultaneously, beginning what can now be considered the next inter-eruptive period. This radical decrease is due to efficient degassing of the magma responsible for the eruption.

5. Conclusions

We have observed clear ^{3}He/^{4}He isotopic ratio and ^{3}He emission increases at Pico do Fogo, four years and eight months before the 2014–2015 eruption. Significant increases were also observed in both the total and magmatic ^{4}He emission from the surface of Pico do Fogo summit crater, confirming an increase in mantle He contribution several months before eruption onset (an earlier mantle contribution is also recorded in 2010). Our results are consistent with an input of less degassed magma to the Pico do Fogo volcanic system between the end of 2009 and early 2010. However, other geophysical and geochemical data would be necessary to confirm such statement and to rule out other possible processes such as pressure variations in a deep gas reservoir. This explanation cannot be ruled out in the variations in R_A measured at the Pico do Fogo volcanic system during the period comprised between end 2008 and 2010.The ^{3}He/^{4}He ratio measured in fumarolic gases after the eruption show a decrease, due to the rapid degassing of the magma responsible of the 2014–2015 eruptive process.

The link between ^{3}He and released thermal energy provides a robust discriminator for magmatic intrusions with the enough energy to produce a volcanic eruption. We propose that, at those volcanoes with an active crater and established surface hydrothermal manifestations, changes in ^{3}He emissions should be accompanied by a significant increase in thermal output if the system is in an eruptive cycle. Long-term gas emission and heat flux data may reveal patterns that allow a more thorough understanding of the timing of deep volatile release, and constitute a powerful tool to monitor the activity of volcanic areas around the world.

Data availability statements

The geochemical data that support the findings of this study are stored on servers at ITER and can be made available by reasonable arrangement with the corresponding author.

Declarations

Not applicable.

Declaration of Competing Interest

The authors declare that they have no known competing financial interests or personal relationships that could have appeared to influence the work reported in this paper.

Acknowledgments

This work has been funded in part by the projects (i) MAKAVOL (MAC/3/C161) of the European Union Transnational Cooperation Programme MAC 2007-2013, ii) CABOVERDE (08-CAP2-1202) of the Spanish Agency for International Cooperation & Development, AECID, iii) UNICV of the Servicio de Acción Exterior del Cabildo Insular de Tenerife (Canary Islands, Spain), iv) VOLRISKMAC (MAC/3.5b/124) financed by the Program INTERREG V A Spain-Portugal MAC 2014-2020 of the European Comission, v) TFassistance, TFinnova Program of the Cabildo

Insular de Tenerife and vi) Doctorados Industriales Program (DI-16-08974) financed by Spanish National Plan for Scientific and Technical Research and Innovation 2013-2016. We thank Paulo Teixeira and all the people from Chã das Caldeiras for the support and help during the field work, as well as Dr. Beverley Coldwell and Dr. Matthew James Pankhurst for improving the quality of this paper. Thanks also to the two anonymous reviewers for their constructive comments.

References

Aiuppa, A., Bitetto, M., Rizzo, A.L., Viveiros, F., Allard, P., Frezzotti, M.L., Valenti, V., Zanon, V., 2020. The fumarolic output from Pico do Fogo Volcano (Cape Verde). Ital. J. Geosci. 139 (3), 325–340. https://doi.org/10.3301/IJG.2020.03.

Alonso, M., Padrón, E., Sumino, H., Hernández, P.A., Melián, G.V., Asensio-Ramos, M., Rodríguez, F., Padilla, G., García-Merino, M., Amonte, C., Pérez, N.M., 2019. Heat and Helium-3 fluxes from Teide Volcano, Canary Islands, Spain. Geofluids 2019. https://doi.org/10.1155/2019/3983864 ID 3983864.

Baker, E.T., Lupton, J.E., 1990. Changes in submarine hydrothermal ^{3}He/heat ratios as an indicator of magmatic/tectonic activity. Nature 346, 556–558. https://doi.org/10.1038/346556a0.

Ballentine, C.J., Burgess, R., Marty, B., 2002. Tracing fluid origin, transport and interaction in the crust. Rev. Mineral. Geochem. 47 (1), 539–614. https://doi.org/10.2138/rmg.2002.47.13.

Barrancos, J., Dionis, S., Quevedo, R., Fernandes, P., Rodríguez, F., Pérez, N.M., Silva, S.V., Cardoso, N., Hernández, P.A., Melián, G.V., Padrón, E., Padilla, G., Asensio-Ramos, M., Calvo, D., Semedo, H., 2015. AlfamaV (2015). Sulphur dioxide (SO_2) emissions during the 2014-15 Fogo eruption, Cape Verde. Geophys. Res. Abstr. 17, EGU2015–11263.

Calvari, S., Ganci, G., Silva, S.V., Hernández, P.A., Pérez, N.M., Barrancos, J., Alfama, V., Dionis, S., Cabral, J., Cardoso, N., Fernandes, P., Melian, G., Pereira, J.M., Semedo, H., Padilla, G., Rodríguez, F., 2018. Satellite and ground remote sensing techniques to trace the hidden growth of a lava flow field: the 2014-2015 effusive eruption at Fogo Volcano (Cape Verde). Remote Sens. 10, 1115. https://doi.org/10.3390/rs10071115.

Capasso, G., Carapezza, M.L., Federico, C., Inguaggiato, S., Rizzo, A., 2005. Geochemical monitoring of the 2002-2003 eruption at Stromboli volcano (Italy): precursory changes in the carbon and helium isotopic composition of fumarole gases and thermal waters. Bull. Volcanol. 68, 118–134. https://doi.org/10.1007/s00445-005-0427-5.

Capello, A., Ganci, G., Calvari, S., Pérez, N.M., Hernández, P.A., Silva, S.V., Cabral, J., Del Negro, C., 2016. Lava flow hazard modelling during the 2014–2015 Fogo eruption, Cape Verde. J. Geophys. Res. Solid Earth 121, 2290–2303. https://doi.org/10.1002/2015JB012666.

Carapezza, M.L., Granieri, D., 2004. CO_2 soil flux at Vulcano (Italy): comparison between active and passive methods. Appl. Geochem. 19 (1), 73–88. https://doi.org/10.1016/S0883-2927(03)00111-2.

Cardellini, C., Chiodini, G., Frondini, F., 2003. Application of stochastic simulation to CO_2 flux from soil: Mapping and quantification of gas release. J. Geophys. Res. 108, 2425. https://doi.org/10.1029/2002JB002165.

Chiodini, G., Frondini, F., Raco, B., 1996. Diffuse emission of CO_2 from the Fossa Crater, Vulcano Island (Italy). Bull. Volcanol. 58, 41–50. https://doi.org/10.1007/s004450050124.

Chiodini, G., Cioni, R., Guidi, M., Raco, B., Marini, L., 1998. Soil CO_2 flux measurements in volcanic and geothermal areas. Appl. Geochem. 13 (5), 543–552. https://doi.org/10.1016/S0883-2927(97)00076-0.

Chiodini, G., Frondini, F., Cardellini, C., Granieri, D., Marini, L., Ventura, G., 2001. CO_2 degassing and energy release at Solfatara volcano, Campi Flegrei, Italy. J. Geophys. Res. 106 (B8), 16213–16221. https://doi.org/10.1029/2001JB000246.

Christensen, B.P., Holm, P.M., Jambon, A., Wilson, J.R., 2001. Helium, argon and lead isotopic composition of volcanics from Santo Antao and Fogo, Cape Verde Islands. Chem. Geol. 178 (1–4), 127–142. https://doi.org/10.1016/S0009-2541(01)00261-3.

Clarke, W.B., Jenkins, W.J., Top, Z., 1976. Determination of tritium by mass spectrometric measurement of ^{3}He. Int. J. Appl. Radiat. Isot. 27 (9), 515–522. https://doi.org/10.1016/0020-708X(76)90082-X.

Craig, H., Lupton, J.E., 1976. Primordial neon, helium and hydrogen in oceanic basalts. Earth Planet. Sci. Lett. 31 (3), 369–385. https://doi.org/10.1016/0012-821X(76)90118-7.

Day, S.J., Carracedo, J.C., Guillou, H., Pais Pais, F.J., Badiola, E.R., Fonseca, J.F.B.D., Heleno, S.I.N., 2000. Comparison and cross-checking of historical, archaeological and geological evidence for the location and type of historical and sub-historical eruptions of multiple-vent oceanic island volcanoes. Geol. Soc. Lond. Spec. Publ. 171 (1), 281–306.

Deutsch, C., Journel, A., 1998. GSLIB: Geostatistical Software Library and Users Guide. 2nd edn. Oxford University Press, New York, p. 369.

Dionis, S.M., Melián, G., Rodríguez, F., Hernández, P.A., Padrón, E., Pérez, N.M., Barrancos, J., Padilla, G., Sumino, H., Fernandes, P., Bandomo, Z., Silva, S., Pereira, J.M., Semendo, H., 2015. Diffuse volcanic gas emission and thermal energy release from the summit crater of Pico do Fogo, Cape Verde. Bull. Volcanol. 77, 10. https://doi.org/10.1007/s00445-014-0897-4.

Doucelance, R., Escrig, S., Moreira, M., Gariépy, C., Kurz, M.D., 2003. Pb-Sr-he isotope and trace element geochemistry of the Cape Verde Archipelago. Geochim. Cosmochim. Acta 67 (19), 3717–3733. https://doi.org/10.1016/S0016-7037(03)00161-3.

Duprat, H.I., Friis, J., Holm, P.M., Grandvuinet, T., Sørensen, R.V., 2007. The volcanic and geochemical development of São Nicolau, Cape Verde Islands: constraints from field and ^{40}Ar/^{39}Ar evidence. J. Volcanol. Geotherm. Res. 162 (1–2), 1–19. https://doi.org/10.1016/j.jvolgeores.2007.01.001.

Dyhr, C.T., Holm, P.M., 2010. A volcanological and geochemical investigation of Boa Vista, Cape Verde Islands; ^{40}Ar/^{39}Ar geochronology and field constraints. J. Volcanol. Geotherm. Res. 189 (1–2), 19–32. https://doi.org/10.1016/j.jvolgeores.2009.10.010.

Etiope, G., Martinelli, G., 2002. Migration of carrier and trace gases in the geosphere: an overview. Phys. Earth Planet. Inter. 129 (3–4), 185–204. https://doi.org/10.1016/S0031-9201(01)00292-8.

Federico, C., Aiuppa, A., Allard, P., Bellomo, S., Jean-Baptiste, P., Parello, F., Valenza, M., 2002. Magma-derived gas influx and water-rock interactions in the volcanic aquifer of Mt. Vesuvius, Italy. Geochim. Cosmochim. Acta 66 (6), 963–981. https://doi.org/10.1016/S0016-7037(01)00813-4.

Giggenbach, W.F., Goguel, R.L., 1989. Collection and analysis of geothermal and volcanic water and gas discharges. Unpublished report. Chemistry Division, DSIR-Petone, New Zealand, p. 81.

González, P.J., Bagnardi, M., Hooper, A., Larsen, Y., Marinkovic, P., Samsonov, S.V., Wright, T.J., 2015. The 2014-2015 eruption of Fogo volcano: Geodetic modelling of Sentinel-1 TOPS Interferometry. Geophys. Res. Lett. 42, 9239–9246. https://doi.org/10.1002/2015GL066003.

Graham, D.W., 2002. Noble gas isotope geochemistry of mid-ocean ridge and ocean island basalts: Characterization of mantle source reservoirs. Rev. Mineral. Geochem. 47 (1), 247–317. https://doi.org/10.2138/rmg.2002.47.8.

Hernández, P.A., Pérez, N.M., Salazar, J.M., Nakai, S., Notsu, K., Wakita, H., 1998. Diffuse emission of carbon dioxide, methane, and helium-3 from Teide Volcano, Tenerife, Canary Islands. Geophys. Res. Lett. 25 (17). https://doi.org/10.1029/98GL02561.

Holm, P.M., Grandvuinet, T., Friis, J., Wilson, J.R., Barker, A.K., Plesner, S., 2008. An ^{40}Ar–^{39}Ar study of the Cape Verde hot spot: temporal evolution in a semistationary plate environment. J. Geophys. Res. 113, B08201. https://doi.org/10.1029/2007JB005339.

Jenkins, S.F., Day, S.J., Faria, B.V.E., Fonseca, J.F.B.D., 2017. Damage from lava flows: insights from the 2014-2015 eruption of Fogo, Cape Verde. J. Appl. Volcanol. 6 (6). https://doi.org/10.1186/s13617-017-0057-6.

Kagoshima, T., Sano, Y., Takahata, N., Lee, H., Lan, T., Ohba, T., 2019. Secular variations of helium and nitrogen isotopes related to the 2015 volcanic unrest of Mt. Hakone, Central Japan. Geochem. Geophys. Geosyst. 20, 4710–4722. https://doi.org/10.1029/2019GC008544.

Kennedy, B.M., Fischer, T.P., Shuster, D.L., 2000. Heat and helium in geothermal systems. Twenty-Fifth Workshop on Geothermal Reservoir Engineering Stanford University SGP-TR-165.

Klügel, A., Longpré, M.A., García-Cañada, L., Stix, J., 2015. Deep intrusions, lateral magma transport and related uplift at ocean island volcanoes. Earth Planet. Sci. Lett. 431, 140–149. https://doi.org/10.1016/j.epsl.2015.09.031.

Klügel, A., Day, S., Schmid, M., Faria, B., 2020. Magma Plumbing during the 2014–2015 Eruption of Fogo (Cape Verde Islands). Front. Earth Sci. 8. https://doi.org/10.3389/feart.2020.00157.

Knudsen, M.F., Abrahamsen, N., 2000. Magnetostratigraphy of Young Pliocene Volcanics at Santo Antão, Cape Verde Islands: the Escabecada and Chã de Morte profiles. Phys. Chem. Earth 25 (5), 461–467. https://doi.org/10.1016/S1464-1895(00)00071-5.

Lupton, J.E., 1983. Terrestrial inert gases: isotope tracer studies and clues to primordial components in the mantle. Annu. Rev. Earth Planet. Sci. 11, 371–414. https://doi.org/10.1146/annurev.ea.11.050183.002103.

Lupton, J.E., Craig, H., 1975. Excess ^{3}He in oceanic basalts: evidence for terrestrial primordial helium. Earth Planet. Sci. Lett. 26 (2), 133–139. https://doi.org/10.1016/0012-821X(75)90080-1.

Marini, L., Gambardella, B., 2005. Geochemical modeling of magmatic gas scrubbing. Ann. Geophys. 48, 739–753. https://doi.org/10.4401/ag-3230.

Marty, B., Jambon, A., Sano, Y., 1989. Helium isotopes and CO_2 in volcanic gases of Japan. Chem. Geol. 76 (1–2), 25–40. https://doi.org/10.1016/0009-2541(89)90125-3.

Matsuda, J., Matsumoto, T., Sumino, H., Nagao, K., Yamamoto, J., Miura, Y., Kaneoka, I., Takahata, N., Sano, Y., 2002. The ^{3}He/^{4}He ratio of the new internal he Standard of Japan (HESJ). Geochem. J. 36 (2), 191–195. https://doi.org/10.2343/geochemj.36.191.

McMurtry, G.M., Dasilveira, L.A., Horn, E.L., DeLuze, J.R., Blessing, J.E., 2019. High ^{3}He/^{4}He ratios in lower East Rift Zone steaming vents precede a new phase of Kilauea 2018 eruption by 8 months. Sci. Rep. 9, 11860. https://doi.org/10.1038/s41598-019-48268-0.

Notsu, K., Mori, T., Vale, S., Kagi, H., Ito, T., 2006. Monitoring Quiescent Volcanoes by Diffuse CO_2 Degassing: Case Study of Mt. Fuji, Japan. Pure Appl. Geophys. 163, 825–835. https://doi.org/10.1007/s00024-006-0051-0.

Padrón, E., Pérez, N.M., Hernández, P.A., Sumino, H., Melián, G., Barrancos, J., Nolasco, D., Padilla, G., Dionis, S., Rodríguez, F., Hernádez, I., Calvo, D., Peraza, M.D., Nagao, K., 2013. Diffusive helium emissions as a precursory sign of volcanic unrest. Geology 41 (5), 539–542. https://doi.org/10.1130/G34027.1.

Parkinson, K.J., 1981. An improved method for measuring soil respiration in the field. J. Appl. Ecol. 18, 221–228. https://doi.org/10.2307/2402491.

Pepin, R.O., Porcelli, D., 2002. Origin of noble gases in the terrestrial planets. Rev. Mineral. Geochem. 47 (1), 191–246. https://doi.org/10.2138/rmg.2002.47.7.

Perez, N.M., Dionis, S., Fernandes, P., Barrancos, J., Rodríguez, F., Bandomo, Z., Hernández, P.A., Melián, G.V., Silva, S.V., Padilla, G., Padrón, E., Cabral, J., Calvo, D., Asensio-Ramos, M., Pereira, J.M., Gonçalves, A.A., 2015. Barros I and Semedo H (2015). Precursory signals of the 2014-15 Fogo eruption (Cape Verde) detected by surface CO_2 emission and heat flow observations. Geophys. Res. Abstr. 17 EGU2015–10644.

Pim, J., Peirce, C., Watts, A.B., Grevemeyer, I., Krabbenhoeft, A., 2008. Crustal structure and origin of the Cape Verde rise. Earth Planet. Sci. Lett. 272 (1–2), 422–428. https://doi.org/10.1016/j.epsl.2008.05.012.

Richter, N., Favalli, M., Zeeuw-van Dalfsen, E., Fornaciai, A., da Silva Fernandes, R.M., Pérez, N.M., Levy, J., Silva, S.V., Walter, T.R., 2016. Lava flow hazard at Fogo Volcano, Cabo Verde, before and after the 2014-2015 eruption. Nat. Hazards Earth Syst. Sci. 16, 1925–1951. https://doi.org/10.5194/nhess-16-1925-2016.

Rizzo, A., Caracausi, A., Favara, R., Martelli, M., Paonita, A., Paternoster, M., 2006. New insights into magma dynamics during last two eruptions of Mount Etna as inferred by geochemical monitoring from 2002 to 2005. Geochem. Geophys. Geosyst. 7, Q06008. https://doi.org/10.1029/2005GC001175.

Sano, Y., NakamuraY, Wakita H., Urabe, A., Tominaga, T., 1984. Helium-3 emission related to volcanic activity. Science 224 (4645), 150–151. https://doi.org/10.1126/science.224.4645.150.

Sano, Y., Notsu, K., Ishibashi, J., Igarashi, G., Wakita, H., 1991. Secular variations in helium isotope ratios in an active volcano: Eruption and plug hypothesis. Earth Planet. Sci. Lett. 107 (1), 95–100. https://doi.org/10.1016/0012-821X(91)90046-K.

Sano, Y., Gamo, T., Williams, S.N., 1997. Secular variations of helium and carbon isotopes at Galeras volcano, Colombia. J. Volcanol. Geotherm. Res. 77 (1–4), 255–265. https://doi.org/10.1016/S0377-0273(96)00098-4.

Sano, Y., Kagoshima, T., Takahata, N., Nishio, Y., Roulleau, E., Pinti, D.L., Fischer, T.P., 2015. Ten-year helium anomaly prior to the 2014 Mt Ontake eruption. Sci. Rep. 5, 13069. https://doi.org/10.1038/srep13069.

Silva, S., Cardoso, N., Alfama, V., Cabral, J., Semedo, H., Pérez, N.M., Dionis, S., Hernández, P.A., Barrancos, J., Melián, G., Pereira, J.M., Rodríguez, F., 2015. Chronology of the 2014 Volcanic Eruption on the Island of Fogo, Cape Verde. Geophysical Research Abstracts EGU General Assembly, Vienna, Austria ID13378.

Sumino, H., Nagao, K., Notsu, K., 2001. Highly sensitive and precise measurement of helium isotopes using a mass spectrometer with double collector system. J. Mass Spectr. Soc. Japan 49 (2), 61–68. https://doi.org/10.5702/massspec.49.61.

Tassi, F., Vaselli, O., Capaccioni, B., Montegrossi, G., Barahona, F., Caprai, A., 2007. Scrubbing process and chemical equilibria controlling the composition of light hydrocarbons in natural gas discharges: An example from the geothermal fields of El Salvador. Geochem. Geophys. Geosyst. 8, Q05008. https://doi.org/10.1029/2006GC001487.

Tedesco, D., Scarsi, P., 1999. Intensive gas sampling of noble gases and carbon at Vucano Island (southern Italy). Geophys. Res. 104 (B5), 10499–10510. https://doi.org/10.1029/1998JB900066.

Umeda, K., Sakagawa, Y., Ninomiya, A., Asamori, K., 2007. Relationship between helium isotopes and heat flux from hot springs in a non-volcanic region, Kii Peninsula, Southwest Japan. Geophys. Res. Lett. 34, L05310. https://doi.org/10.1029/2006GL028975.

Worsley, P., 2015. Physical geology of the Fogo volcano (Cape Verde Islands) and its 2014-2015 eruption. Geol. Today 31, 153–159. https://doi.org/10.1111/gto.12102.

Renewable Energy 182 (2022) 17–31

Contents lists available at ScienceDirect

Renewable Energy

journal homepage: www.elsevier.com/locate/renene

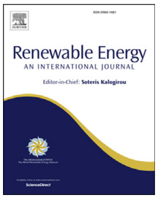

Thermal energy and diffuse ^{4}He and ^{3}He degassing released in volcanic-geothermal systems

Mar Alonso [a, b, *], Nemesio M. Pérez [a, b, c], Pedro A. Hernández [a, b, c], Eleazar Padrón [a, b, c], Gladys Melián [a, b, c], Fátima Rodríguez [a], Germán Padilla [a, b], José Barrancos [a, b], María Asensio-Ramos [a], Thráinn Fridriksson [d], Hirochika Sumino [e]

[a] *Instituto Volcanológico de Canarias (INVOLCAN), 38320, San Cristóbal de La Laguna, Tenerife, Canary Islands, Spain*
[b] *Instituto Tecnológico y de Energías Renovables (ITER), 38600, Granadilla de Abona, Tenerife, Canary Islands, Spain*
[c] *Agencia Insular de La Energía de Tenerife (AIET), 38600, Granadilla de Abona, Tenerife, Canary Islands, Spain*
[d] *Reykjavic Energy, Baejarhals 1, 110 Reykjavík, Iceland*
[e] *Department of General Systems Studies, Graduate School of Arts and Sciences, The University of Tokyo, 3-8-1 Komaba, Meguro-ku, Tokyo 153-0041, Japan*

ARTICLE INFO

Article history:
Received 14 May 2021
Received in revised form
17 September 2021
Accepted 4 October 2021
Available online 8 October 2021

Keywords:
Helium isotopes
Diffuse 4-He degassing
Diffuse 3-He degassing
Thermal energy
Geothermal exploration

ABSTRACT

Active/recent volcanism indicates the presence of high-enthalpy resources at depth, but sometimes there is not any evidence of endogenous fluids manifestations at surface, that confirms the presence of an active geothermal system. In this study we present an extensive study of published and new diffuse ^{4}He and ^{3}He emission and thermal energy released data from fifteen volcanic systems, confirming a direct relationship between diffuse helium emissions and thermal energy released associated with the rise of mantle fluids. The results are useful to infer the existence of deep and/or hidden geothermal resources and to estimate roughly its potential at those areas without obvious geothermal manifestations at the surface, but with measureable anomalous emissions of ^{4}He and ^{3}He. Tracing diffuse He emission anomalies at the surface environment of volcanic systems provides very important information for the exploration and discovery of geothermal resources at those areas where the resources are either hidden or lie at great depth.

1. Introduction

Geothermal resources are considered a valuable component of a low-carbon future energy mix. Active/recent volcanism indicates the presence of high-enthalpy resources at depth, but often no obvious shallow manifestations are present. Geothermal energy has its ultimate origin in the difference in temperature between the Earth's core and crust, which causes a continuous heat flux from the interior to the surface. This flux is spatially heterogeneous, and regions of high flux may be economic to exploit as a source of energy. However, without a targeting guide, the investment risk in expensive exploration drilling projects is prohibitive. Deep geothermal systems with no visible surface heat anomalies (blind geothermal systems) may be substantial and economically viable to exploit, even if require innovative approaches to detect and quantify potential resources.

The Earth's mantle constitutes a huge reservoir of gaseous compounds as water, carbon dioxide and noble gases, either captured during planet formation, added later by nuclear reactions, or recycled from the surface. The main path of mantle degassing is through volcanic activity, accompanied by large amounts of thermal energy. Gases can be emitted as visible emanations (fumaroles, solfataras and plumes) and as invisible emanations (diffuse degassing) as a result of advective and diffusive transport mechanisms [1,2].

In volcanic areas where significant blind resources are plausible, non-visible or diffuse CO_2 degassing surveys have been carried out to help locate targets for focussed geothermal exploration [3–8]. Normally, and in addition to the absence of thermal anomalies, this type of geothermal reservoirs show with very low gas flows which hinder target definition. Confirmation by other geochemical techniques such as studies of CO_2 isotopic composition to determine the source of the CO_2 emission [6–9] support larger scale investments in exploration, but due to the reactivity of CO_2 through

---

[*] Corresponding author. Instituto Volcanológico de Canarias (INVOLCAN), 38320, San Cristóbal de la Laguna, Tenerife, Canary Islands, Spain.
E-mail address: mar@iter.es (M. Alonso).

https://doi.org/10.1016/j.renene.2021.10.016
0960-1481/